INFORMATION TO USERS

This manuscript has been reproduced from the microfilm master. UMI films the text directly from the original or copy submitted. Thus, some thesis and dissertation copies are in typewriter face, while others may be from any type of computer printer.

The quality of this reproduction is dependent upon the quality of the copy submitted. Broken or indistinct print, colored or poor quality illustrations and photographs, print bleedthrough, substandard margins, and improper alignment can adversely affect reproduction.

In the unlikely event that the author did not send UMI a complete manuscript and there are missing pages, these will be noted. Also, if unauthorized copyright material had to be removed, a note will indicate the deletion.

Oversize materials (e.g., maps, drawings, charts) are reproduced by sectioning the original, beginning at the upper left-hand corner and continuing from left to right in equal sections with small overlaps.

ProQuest Information and Learning
300 North Zeeb Road, Ann Arbor, MI 48106-1346 USA
800-521-0600

UMI®

University of Alberta

Hydrometeorology of a High Arctic Glacier

by

Sarah M.H. Boon ©

A thesis submitted to the Faculty of Graduate Studies and Research in partial fulfillment of the

requirements for the degree of Doctor of Philosophy

Department of *Earth and Atmospheric Sciences*

Edmonton, Alberta

Spring 2005

to be nobody-but-yourself -- in a world which is doing its best, night and day, to make you everybody else -- means to fight the hardest battle which any human being can fight: and never stop fighting.

e e cummings

Abstract

Field studies of John Evans Glacier (JEG). Ellesmere Island. (79° 40' N. 74° 30' W) were used to investigate Arctic glacier melt. runoff and mass balance (MB) response to climate change. Seasonal development of glacier drainage is driven by a hydrofracture process: meltwater-filled crevasses propagate from the glacier surface to the bed. forcing a connection between the supra- and subglacial drainage systems. Given the importance of surface meltwater in this process. the melt response of a high wind/high air temperature event (28-30 July. 2000) was examined. Results show that this event produced 30% of total seasonal melt. strongly contributing to negative MB conditions in 2000. The timing and frequency of such events therefore critically impacts both seasonal drainage development and interannual variability in Arctic glacier MB.

Field measurements at JEG highlight problems inherent in current MB models. Models assume constant negative summer air temperature lapse rates (STLR) and positive winter accumulation lapse rates (WALR) over glacier surfaces. Results show that STLR and WALR are highly spatially and temporally variable: STLR is often positive. and WALR is negative due to snow redistribution/sublimation from wind scour events. Models also do not incorporate summer snowfall events. which significantly reduce melt: and summer wind events that. while rare. substantially reduce MB. Results are significant for the high Arctic where annual MB is relatively small. and minor changes in annual ablation/accumulation can significantly impact MB.

Model parameterization sensitivity was determined using parameter values selected from field observations. Degree-day model (DDM) output is most sensitive to values of STLR and summer ALR. and the variable degree-day factor. These input parameters

must therefore be verified by field measurements to increase confidence in model predictions.

Perturbation of the DDM with global circulation model predictions of future (2000-2029) air temperature/precipitation show that increased air temperatures will have the greatest impact on net annual MB at JEG. and are hardly mitigated by a concurrent predicted winter precipitation increase. This results in enhanced melt/runoff production and superimposed ice formation. likely causing more extensive seasonal development of the glacier drainage system. and potentially impacting the dynamic response of JEG to climate change.

Acknowledgements

Thanks to Martin Sharp for taking me on as a research assistant way back in 1998, and still agreeing to be my supervisor a year later: he always pushed my work to be better, and then some.

Many thanks to Anthony Arendt for always taking the time to answer my modeling questions and fine-tune the degree-day model. Thanks to Rob Stefaniuk for creating outstanding custom field equipment, and to Bea Alt for discussing various meteorological problems with me. Thanks to Dave Lewis, Rob Bingham, Michelle Hanson, and Dave Burgess for a good laugh (and help) both in and out of the field. Thanks to Joel Barker, Maya Bhatia, Karen Heppenstall, and Pete Nienow for additional field assistance.

The Natural Sciences and Engineering Research Council, Steve and Elaine Antoniuk, and the University of Alberta awarded the scholarships that enabled me to complete this degree: the Geological Society of America, Northern Scientific Training Program, American Alpine Club, and Circumpolar-Boreal Alberta Research funded my field research. The University of Alberta's Institute for Geophysical Research provided funding that allowed me to present my research at several key conferences.

Thanks to the people of Resolute Bay and Grise Fjord for permission to conduct research in the area, and to the Polar Continental Shelf Project, without whose superb logistical support this research couldn't have been done.

Thanks to my parents, for putting up with my complaints and threats to quit on more occasions than I care to remember, and still believing that I would finish. But the greatest thanks goes to my husband, Dave Lewis, for always being there to talk, tell a joke, take me out for dinner, or just listen. I know you're glad it's all over!

Table of Contents

List of Tables

List of Figures

CHAPTER 1.

INTRODUCTION

1.1. Thesis goal and objectives

The goal of this thesis is to use field studies of a polythermal high Arctic glacier (John Evans Glacier (JEG), Ellesmere Island, 79° 40' N, 74° 30' W) to investigate Arctic glacier melt, runoff, and mass balance response to climate change.

My research objectives are:

(a) to determine the importance of surface meltwater storage and subsequent drainage system evolution in modulating the relationship between water entering and exiting the glaciohydrological system;

(b) to determine glacier melt response to local meteorological conditions by assessing the role of extreme events in overall melt and mass balance, and identifying the role of specific seasonal conditions in enhancing/suppressing melt; and,

(c) to use the information from (b) in a degree-day model (DDM) to investigate glacier melt, runoff, and mass balance response to climate change.

1.2. Background

Anthropogenic climate warming on the scale predicted by global circulation models will have the largest impact on Arctic regions (Boer et al., 2000; Houghton et al., 2001; Holland and Bitz, 2003). Recent studies indicate that Arctic warming is already occurring (Morison et al., 2000; Serreze et al., 2000). Warming is predicted to increase runoff from glaciated areas, enhancing freshwater inputs to the global ocean system and raising sea level (Meier, 1990). Such changes could alter sea ice formation (Chapman and Walsh, 1993; Johannessen et al., 1999; Kerr, 1999) and ocean circulation in the North Atlantic (Manabe and Stouffer, 1997; Broecker, 1999; Siedov et al., 2001), affecting global climate through feedback mechanisms involving surface albedo and global atmospheric circulation.

1

However, there are several areas of uncertainty in this scenario. including: (1) the relative contribution of small glaciers such as John Evans Glacier to sea level rise (Meier. 1984; 1990; Oerlemans and Fortuin. 1992); (2) the role of meltwater refreezing and surface meltwater storage (processes specific to Arctic glaciers) in absorbing a portion of the increased meltwater production. thereby limiting meltwater input to the ocean system (Pfeffer et al.. 1991; Woodward et al.. 1997; Janssens and Huybrecht. 2000); (3) the relationship between increased air temperature and increased precipitation. and whether an increase in precipitation will offset higher temperatures and mitigate glacier response to climate change (Oerlemans et al.. 1998; van der Veen. 2002); and. (4) the dynamic response of glaciers to climate change. and whether this will accelerate or decelerate the climate change response (Zwally et al.. 2002; Bingham. 2003). A better understanding of glacier hydrometeorological response to climate change is therefore necessary to determine the impacts of climate change on melt and runoff production. and glacier mass balance.

Due to the remoteness of Arctic glaciers and the high cost of long-term fieldwork. numerical modelling studies are often used to determine climate change impacts on melt. runoff and glacier mass balance (MB) (e.g.. Bøggild et al.. 1994; Fleming et al.. 1997; Jóhannesson. 1997; Braithwaite and Zhang. 1999; Greuell and Genthon. 2004). As most modelling studies have been conducted on temperate (Alpine) glaciers or large Arctic ice caps (i.e.. Greenland). our understanding of melt-runoff processes on smaller Arctic glaciers. and the response of these processes to climate change. remains limited. In addition. models created for Alpine glaciers cannot readily be transferred to Arctic glaciers given: (a) differences in local meteorological conditions: with a relatively short melt season. meteorological events such as summer snowfalls have a significant impact on Arctic glacier melt and MB. but are often poorly represented in numerical models: and. (b) substantial differences in glacier thermal regime (Blatter and Hutter. 1991; Ødegård et al.. 1992). which result in significant refreezing (Schytt. 1949; Pfeffer and Humphrey. 1996; Woodward et al.. 1997) and surface water storage (Liestol et al.. 1980; Flowers and Clarke. 2002). and differences in the ability of surface water to penetrate to the glacier bed (Hodgkins. 1997; Hodgkins. 2001; van der Veen. 1998; Zwally et al.. 2002).

2

1.2.1. Role of meteorology and thermal regime in glacier melt and hydrology

While largely temperate glaciers have been studied extensively in terms of their hydrometeorology and drainage system development (e.g.. Haut Glacier d'Arolla. Switzerland: Arnold et al.. 1998: Willis et al.. 2002: Storglaciären. Sweden: Hock et al.. in press: South Cascade Glacier. Washington: Tangborn. 1999). few such studies have been conducted on polar/subpolar glaciers (e.g.. Svalbard glaciers: Vatne et al.. 1995: Hodgkins. 2001: Wadham et al.. 2001: White Glacier. Canadian Arctic: Adams. 1966).

Temperate glaciers experience a relatively long melt season with marked diurnal cycles of incoming radiation. and associated high-amplitude diurnal cycles of meltwater production (Collins. 1987: Lawson. 1993: Fountain and Walder. 1998). In contrast. Arctic glaciers experience a short but intense melt season with 24-hour daylight. which results in lower-amplitude diurnal meltwater cycles over a relatively short time period (Wolfe and English. 1995: Hodson et al.. 1998). Thus even small changes in summer surface albedo on an Arctic glacier can have a significant impact on total melt – and subsequently runoff (Alt. 1987: Oerlemans and Klok. 2003) – and can therefore be a significant source of error in Arctic glacier modelling studies.

Surface meltwater plays a key role in glacier drainage system development. However. the drainage systems of temperate and Arctic glaciers differ significantly. due not only to differences in the production of meltwater that feeds these systems. but also to their different thermal regimes.

Temperate glaciers are at the pressure melting point throughout. so surface meltwater can penetrate the ice through both small- and large-scale features. including intergranular veins (Nye and Frank. 1973: Mader. 1992). crevasses (Röthlisberger and Lang. 1987: Hooke. 1989: Fountain and Walder. 1998). and moulins (Iken. 1972: Holmlund and Hooke. 1983). Temperate glaciers undergo extensive drainage system development during the summer melt season. with the subglacial system expanding in an up-glacier direction as the snowline retreats and meltwater enters moulins higher up on the glacier (Nienow et al.. 1998). These systems constrict in winter when surface meltwater inputs cease (Fountain and Walder. 1998).

In contrast. most high Arctic glaciers are either cold-based (all ice is below the pressure melting point: e.g.. Scott Turnerbreen. Svalbard (Hodgkins et al.. 1998)). or

3

predominantly cold polythermal (a core of temperate ice at the glacier bed is surrounded by ice below the pressure melting point: e.g., McCall Glacier, Alaska (Rabus and Echelmeyer, 1997); White Glacier, Canadian Arctic (Blatter, 1987)). They may also be largely temperate with a perennial cold surface layer: e.g., Erikbreen, Svalbard (Etzelmüller et al., 1993). Meltwater penetration into cold surface ice is limited, and refreezing often occurs when waters contact the cold glacier surface (Pfeffer and Humphrey, 1996). Water enters the glacier only through large-scale features such as crevasses and moulins, which are often rare due to generally low deformation rates and crevassing in cold ice (Hodgkins, 1997).

The limited opportunities for meltwater to enter the glacier result in the development of large stream channels and many storage locations on the glacier surface, including crevasses, moulins, and supraglacial lakes (Liestol et al., 1980; Odegård et al., 1992; Vatne et al., 1995; Hodgkins et al., 1998; Hodson et al., 1998). En- and subglacial drainage development may be limited, and connections between these drainage systems and the surface close each winter and must be re-opened in summer (Skidmore and Sharp, 1999; Bingham, 2003). When water does penetrate to the glacier bed it must open new pathways to the glacier snout, where flow is often impeded by the presence of a cold ice dam caused by a combination of glacier thermal regime and meltwater refreezing near the outlets of subglacial drainage channels in late summer and fall (Rabus and Echelmeyer, 1997; Hodgkins, 2001; Wadham et al., 2001; Skidmore and Sharp, 1999; Copland and Sharp, 2001; Bingham, 2003).

These specific meteorological and thermal characteristics may alter the melt-runoff response on Arctic glaciers, resulting in substantial differences in the timing of melt and runoff production, and the sequence and extent of drainage system evolution, between temperate and Arctic glaciers.

1.3. Study site: John Evans Glacier

John Evans Glacier (JEG) is a large valley glacier located at 79° 40' N and 74° 30' W, on the east coast of Ellesmere Island, Arctic Canada. It covers approximately 75% of a 220 km² catchment, is 15 km long and spans an elevation range from 100-1500 m a.s.l. (Skidmore and Sharp, 1999). Ice reaches a maximum thickness of ~400 m near the long-

4

term (1963-1998) equilibrium line (750 m a.s.l.). The glacier is cold-based in the accumulation area and at the glacier margins where ice is thin: the glacier is warm-based (at the pressure melting point) over much of the ablation zone (Copland and Sharp. 2001). Ice temperature at 15 m depth ranges from -15.1°C at 1173 m a.s.l. to -10.9°C at ~615 m a.s.l. For this thesis. three years of hydrological data (2000-2002) and six years of meteorological data (1996-2002) were analysed.

1.3.1. Hydrology

The following summary is based on three years of field observations at JEG. At the beginning of the melt season. initial melt percolates into the snowpack and firn as on a temperate glacier (Fountain. 1996). However. internal refreezing (meltwater refreezing within the snow/firn (Colbeck. 1982)) and formation of superimposed ice (SI: Pfeffer and Humphrey. 1991) delay runoff response to melt production. Model studies (for 1997) suggest that approximately 47% of the snow water equivalent (SWE) of the winter snowpack refreezes (Arendt. 1997).

Melt produced following refreezing flows either directly off the glacier to bulk runoff. or to supraglacial storage. which occurs in either surface lakes. or initially closed basins within supraglacial stream channels. As the melt season progresses. these basins interconnect. either by surface overflow or the development of englacial linkages: they also connect with ice-marginal lakes that develop at glacier confluences and may spill over onto the glacier surface. It is hypothesized that englacial interconnections are driven by pressure head differences between adjacent basins.

Progressive interconnection of supraglacial storage locations develops supraglacial stream channels with continuous throughflow. At the downstream end of these channels. meltwater either drains directly off the glacier. or ponds above a crevasse. In the latter case. continued input of surface meltwater may increase the pressure above the crevasse. eventually causing it to propagate to the glacier bed (van der Veen. 1998). This may allow englacial drainage to develop. provided that surface meltwater inputs are sustained.

Although the mechanism behind the transfer of supraglacial meltwater to the subglacial system is unclear. hydrochemical studies of subglacial outflow indicate that surface waters eventually access the glacier bed (Skidmore. 1995: Heppenstall. 2001).

5

The en-/subglacial system initially contains a volume of water stored from the previous melt season, which increases with surface meltwater input, thereby increasing subglacial water pressure. Once sufficient pressure is reached, the cold ice dam at the glacier terminus is breached and subglacial outflow initiated (Skidmore and Sharp, 1999). This breach may form either through fracturing of the cold ice to the glacier surface, forming an artesian fountain (e.g., Baranowski, 1973; Skidmore and Sharp, 1999; Copland et al., 2003), or through glacier uplift which allows stored meltwater to flow underneath the glacier toe (Jarvis and Clarke, 1975; Goodwin, 1988). Initial outflow appears to consist of solute-rich waters that have been stored beneath the glacier over winter, but solute concentrations fall rapidly within ~4 days as the new season's runoff begins to emerge from the glacier snout (Skidmore, 1995; Heppenstall, 2001).

As the melt season progresses and the size and significance of each drainage system component changes, the melt-runoff delay is reduced. The snowpack thins and retreats (Fountain, 1996), more glacier ice is exposed (Nienow et al., 1998), supraglacial storage times are reduced as sub-basins merge, and the en-/subglacial system becomes more channelised and begins to transmit water more efficiently (Bingham, 2003).

While it is clear that the evolution of the glacial hydrological system on JEG is driven largely by meltwater inputs from the surface, how surface meltwater accesses the glacier bed remains unclear. As this is a crucial stage in the seasonal development of the glacial hydrological system, it is necessary to determine the mechanism behind this connection.

1.3.2. Hydrometeorology

Glacial hydrological development is driven by meltwater production, which is highly sensitive to interannual variations in meteorological variables such as the end-of-winter (spring; EOW) snow distribution, summer air temperature and summer snowfalls (Alt, 1979; Collins, 1987; Röthlisberger and Lang, 1987; Wolfe and English, 1995; Fountain and Walder, 1998).

The high-albedo EOW snowpack must be removed prior to exposure of the lower-albedo ice surface. With a thicker EOW snowpack, there is a longer delay between melt onset and ice surface exposure, and total seasonal melt is reduced given the shorter duration of ice exposure (Röthlisberger and Lang, 1987; Fountain, 1996; Fountain and

6

Walder. 1998). With a thin snowpack. however. the reverse is true. and total seasonal melt is higher. In the summer of 2000. a relatively thin spring snowpack. combined with an extreme melt event in late July. resulted in substantial melt. and contributed to extensive up-glacier development of the subglacial drainage system (Bingham. 2003). Total seasonal meltwater inputs to the subglacial drainage system were relatively high. thereby increasing the cross-sectional area of subglacial drainage. and possibly precluding complete over-winter closure of the subglacial outflow channel (Bingham. 2003). The high level of hydraulic development also significantly decreased the lag between melt production and runoff response (Bingham. 2003).

Summer air temperature is the main driver of melt production (Braithwaite. 1984: Braithwaite and Oleson. 1987: Hock. 1999: Ohmura. 2001). which subsequently feeds internal accumulation and SI formation. surface meltwater storage. subglacial storage. and eventually runoff. In the cool summers of 1994. 1996 and 2001. proglacial outflow (runoff) at JEG occurred as a series of outburst floods. and the subglacial drainage system appeared to shut down during the cold weather periods between floods (Skidmore and Sharp. 1999: Bingham. 2003). In the warmer summers of 1998-2000. however. outflow was continuous once initiated (Sharp. pers. comm.). This suggests that constriction of en- and/or subglacial components of the system can occur relatively rapidly if meltwater production decreases under poor weather (i.e.. low air temperature) conditions. and high water throughputs are not sustained.

Summer snowfalls can reduce melt production by increasing surface albedo (Tronov. 1962: Alt. 1987: Röthlisberger and Lang. 1987: Oerlemans and Klok. 2003). In 2002. for example. small (< 5 cm) snowfalls throughout the melt season at JEG delayed glacier drainage system development. while a 50 cm snowfall in late July completely shut down both supra- and subglacial drainage. resulting in a late-season episode of SI formation.

Given the strong connection between meteorological conditions and glaciohydrological response. it is necessary to determine the general meteorological setting of JEG. as well as the relative impact of EOW snowpack. summer air temperature. and summer snowfalls on glacier melt. runoff. and MB.

7

1.3.3. Potential climate change impacts on hydrology and hydrometeorology

It is clear that melt on Arctic glaciers is driven by meteorological conditions, and that the melt-runoff relationship is modulated by internal accumulation and the formation of SI (Pfeffer et al., 1991; Janssens and Huybrecht, 2000; Wadham and Nuttall, 2002), and meltwater storage within the snowpack (Colbeck, 1983; Fountain, 1996), in supraglacial lakes and crevasses (Hodgkins, 1997; Flowers and Clarke, 2002), and at the glacier bed (Skidmore and Sharp, 1999; Copland and Sharp, 2001; Heppenstall, 2001; Bingham, 2003). This relationship, and thus the timing and magnitude of peak runoff and the magnitude of total seasonal runoff, may be altered under climate change conditions (Houghton et al., 2001).

While models predict increases in total glacier melt, resulting in increased glacier runoff (e.g., Jóhannesson, 1997), the specifics of the melt response are unclear. Will the melt season be longer, more intense, or both? If winter precipitation increases (Mayo and March, 1990), will it offset the impact of increased air temperature by increasing meltwater storage in the snowpack at the onset of the melt season, delaying the exposure of the ice surface, and trapping meltwater through refreezing at the end of the melt season (much like firn; Fountain, 1996)? Or will runoff increase due to the greater amount of snowpack melted, thereby offsetting the delay in ice surface exposure (Lawson, 1993)? Will meltwater storage in SI, as well as in glacier surface features, mitigate the impacts of climate warming on runoff production (e.g., Pfeffer et al., 1991; Woodward et al., 1997; Janssens and Huybrechts, 2000)?

If peak runoff increases and occurs earlier, the glacier drainage system may develop more quickly and extensively, affecting glacier dynamics and possibly impacting glaciohydrological conditions the following year (Bingham, 2003). An increase in total runoff could also impact the ecology of glacier-fed rivers, as water temperature, sediment concentrations, and discharge volumes may be altered (McGregor et al., 1995). Increased runoff may subsequently increase freshwater input to the global ocean system, which may impact sea ice formation (Chapman and Walsh, 1993) and ocean circulation (Broecker, 1999).

The impact of climate change on the melt-runoff relationship on Arctic glaciers has not been studied in detail; our understanding of this interaction remains limited. As

8

numerical models are widely used in determining glacier response to climate change. accurate model parameterizations of EOW snow distribution and air temperature are critical in order to increase confidence in model output. In addition, summer wind and snowfall events, which have a significant impact on Arctic glacier melt and MB, are often poorly simulated by numerical models due both to their rare occurrence, and to the fact that most models utilise only air temperature as input data.

It is therefore necessary to examine the sensitivity of numerical models to parameterization of EOW snow distribution, air temperature, and summer snowfall events, in order to increase confidence in model tests of glacier response to climate change.

1.4. Thesis outline

Given our current knowledge of hydrological and hydrometeorological conditions at JEG, it is evident that several areas require closer study: (1) what is the mechanism whereby surface meltwater accesses the glacier bed and initiates subglacial outflow; (2) how do glacier melt and runoff respond to extreme events (e.g., high wind and high air temperature); (3) what is the relationship between glacier melt and local meteorological conditions (i.e., EOW snowpack, summer air temperature, summer snowfalls); and, (4) how well do numerical models represent those meteorological events that significantly impact mass balance at JEG, and what is the sensitivity of JEG melt, runoff and mass balance to predicted future climate change.

This thesis is presented in paper format, with each of the four main chapters written as a standalone manuscript. As of 1 September, 2004, Chapters 2 and 3 have been published, and Chapter 4 is in review. The full titles and publication details are:

Chapter 2: Boon, S., M. Sharp. 2003. The role of hydrologically-driven ice fracture in drainage system evolution on an Arctic glacier. *Geophysical Research Letters* 30(18): 1916. DOI: 10.1029/2003GL018034.

9

Chapter 3: Boon, S., M.J. Sharp, P.W. Nienow. 2003. Impact of an extreme melt event on the hydrology and runoff of a high Arctic glacier. *Hydrological Processes* 17(6): 1051-1072.

Chapter 4: Boon, S., M. Sharp. In review. A 6-year meteorological record from a high Arctic glacier: implications for mass balance modelling. *Global and Planetary Change.*

Chapter 5: Modelled response of the melt, runoff and mass balance of an Arctic glacier to climate change.

Several of these papers are co-authored, as field data were collected as part of a collaborative research project at John Evans Glacier. This includes meteorological data (A.A. Arendt, D.H. Lewis, M.J. Sharp, T.M. Wohlleben), snowpack data (D.H. Lewis), field observations of the extreme melt event (P.W. Nienow), and a degree-day melt model (A.A. Arendt). In addition, all co-authors provided critiques of manuscript drafts. However, all data analysis and interpretation, and writing of chapters/papers, is entirely my own work.

Chapter 2 uses field records of water level measured in a supraglacial crevasse/channel system to describe a hydrofracture mechanism whereby meltwater produced at the glacier surface can access the glacier bed. This paper indicates that surface meltwater storage, and subsequent catastrophic meltwater drainage through hydrofracture, significantly impacts the melt-runoff relationship on Arctic glaciers. Chapter 3 involves an energy balance analysis of a high wind/high air temperature event in July 2000 that contributed significantly to glacier melt and runoff in that year, and discusses the implications of such an event for glacier hydrology and long-term mass balance. Chapter 4 describes the temporal and spatial distribution of meteorological conditions at JEG over a six-year period (1996-2002), and discusses the implications of these findings for modelling glacier mass balance. Finally, Chapter 5 examines the impact of the issues discussed in Chapter 4 on melt model output by determining the model sensitivity to parameterization. The chapter then discusses the sensitivity of JEG melt, runoff and mass balance to future climate change, taking into consideration model

10

output errors caused by parameterization sensitivities. The thesis summary, conclusions and suggestions for further work are presented in Chapter 6.

1.5. References

Adams, P.W. 1966. Ablation and run-off of the White Glacier, Axel Heiberg Island, Canadian Arctic Archipelago. McGill University: Axel Heiberg Research Reports, Glaciology 177: 77 pp.

Alt, B.T. 1979. Investigation of summer synoptic climate controls on the mass balance of Meighen Ice Cap. Atmosphere-Ocean 17(3): 181-199.

Alt, B.T. 1987. Developing synoptic analogs for extreme mass balance conditions on Queen Elizabeth Island ice caps. Journal of Climate and Applied Meteorology 26(12): 1605-1623.

Arendt, A.A. 1997. Approaches to modelling the mass balance of high Arctic glaciers. M.Sc. thesis, University of Alberta. 221 pp.

Arnold, N., K. Richards, I. Willis, M. Sharp. 1998. Initial results from a distributed, physically based model of glacier hydrology. Hydrological Processes 12(2): 191-219.

Baranowski, S. 1973. Geyser-like water spouts at Werenskioldbreen, Spitsbergen. International Association of Hydrological Sciences 95: 131-133.

Bingham, R.G. 2003. The hydrology and dynamics of a high Arctic glacier. Ph.D. thesis, University of Glasgow. 254 pp.

Blatter, H. 1987. On the thermal regime of an Arctic valley glacier: a study of White Glacier, Axel Heiberg Island, NWT, Canada. Journal of Glaciology 33(114): 200-210.

11

Blatter. H.. K. Hutter. 1991. Polythermal conditions in Arctic glaciers. Journal of Glaciology 37(126): 261-269.

Boer. G.J.. G. Flato. D. Ramsden. 2000. A transient climate change simulation with greenhouse gas and aerosol forcing: projected climate to the 21st century. Climate Dynamics 16: 427-450.

Bøggild. C.E.. N. Reeh. H. Oerter. 1994. Modelling ablation and mass-balance sensitivity to climate change of Storstrømmen. Northeast Greenland. Global and Planetary Change 9: 79-90.

Braithwaite. R.J. 1984. Calculation of degree-days for glacier-climate research. Zeitschrift fur Gletscherkunde und Glazialgeologie 20: 1-8.

Braithwaite. R.J.. O.B. Olesen. 1987. Calculation of glacier ablation from air temperature. West Greenland. In Glacier Fluctuations and Climatic Change. J. Oerlemans. ed. Dordrecht: Kluwer Academic Publishers. p. 219-233.

Braithwaite. R.J.. Y. Zhang. 1999. Modelling changes in glacier mass balance that may occur as a result of climate changes. Geografiska Annaler 81A(4): 489-496.

Broecker. W.S. 1999. What if the conveyor were to shut down? Reflections on the possible outcome of the great global experiment. GSA Today 9(1): 1-7.

Chapman. W.L.. J.E. Walsh. 1993. Recent variations of sea ice and air temperature in high latitudes. Bulletin of the American Meteorological Society 74(1): 33-47.

Colbeck. S.C. 1982. An overview of seasonal snow metamorphism. Reviews of Geophysics 20(1): 45-61.

Colbeck. S.C. 1983. Theory of metamorphism of dry snow. Journal of Geophysical Research – Oceans and Atmospheres **88**(C9): 5475-5482.

Collins. D.N. 1987. Hydrometeorological conditions. mass balance and runoff from alpine glaciers. In Glacier Fluctuations and Climatic Change. J. Oerlemans. ed. Dordrecht: Kluwer Academic Publishers. p. 235-260.

Copland. L.. M. Sharp. 2001. Mapping thermal and hydrological conditions beneath a polythermal glacier with radio-echo sounding. Journal of Glaciology **47**(157): 232-242.

Copland. L.. M.J. Sharp. P.W. Nienow. R.G. Bingham. 2003. The distribution of basal motion beneath a High Arctic polythermal glacier. Journal of Glaciology **49**(166): 407-414.

Etzelmüller. B.. G. Vatne. R.S. Ødegård. J.L. Sollid. 1993. Dynamics of two subpolar valley glaciers - Erikbreen and Hannabreen. Liefdefjorden. Northern Spitsbergen. Geografiska Annaler **75A**(1-2): 41-54.

Fleming. K.M.. J.A. Dowdeswell. J. Oerlemans. 1997. Modelling the mass balance of northwest Spitsbergen glaciers and responses to climate change. Annals of Glaciology **24**: 203-210.

Flowers. G.E.. G.K.C. Clarke. 2002. A multicomponent coupled model of glacier hydrology: 2. Application to Trapridge Glacier. Yukon. Canada. Journal of Geophysical Research – Solid Earth **107**(B11): 2288. DOI:10.1029/2001JB001124

Fountain. A.G. 1996. Effect of snow and firn hydrology on the physical and chemical characteristics of glacial runoff. Hydrological Processes **10**: 509-521.

Fountain. A.G.. J.S. Walder. 1998. Water flow through temperate glaciers. Reviews of Geophysics **36**(3): 299-328.

13

Goodwin. I.D. 1988. The nature and origin of a jökulhlaup near Casey Station. Antarctica. Journal of Glaciology 34(116): 95-101.

Greuell. W., C. Genthon. 2004. Modelling land ice surface mass balance. In Mass balance of the cryosphere: Observations and modelling of contemporary and future changes. J. L. Bamber and A. J. Payne. eds. Cambridge: Cambridge University Press. p. 117-168.

Heppenstall. K.E. 2001. Chemical Weathering in a Glaciated Carbonate Catchment. Canadian High Arctic: Implications for Subglacial Hydrology. M.Sc. thesis. University of Alberta. 118 pp.

Hock. R. 1999. A distributed temperature-index ice- and snowmelt model including potential direct solar radiation. Journal of Glaciology 45(149): 101-111.

Hock. R., P. Jansson. L.N. Braun. (in press). Modelling the response of mountain glacier discharge to climate warming. In Global Change and Mountain Regions - Advances in Global Change Research. M. Beniston. ed. Dordrecht: Kluwer Academic Publishers.

Hodgkins. R. 1997. Glacier hydrology in Svalbard. Norwegian High Arctic. Quaternary Science Reviews 16: 957-973.

Hodgkins. R. 2001. Seasonal evolution of meltwater generation. storage and discharge at a non-temperate glacier in Svalbard. Hydrological Processes 15(3): 441-460.

Hodgkins. R., M. Tranter. J.A. Dowdeswell. 1998. The hydrochemistry of runoff from a 'cold-based' glacier in the High Arctic (Scott Turnerbreen. Svalbard). Hydrological Processes 12: 87-103.

14

Hodson, A., A. Gurnell, M. Tranter, J Bogen, J.O. Hagen, M. Clark. 1998. Suspended sediment yield and transfer processes in a small High-Arctic glacier basin. Svalbard Hydrological Processes 12: 73-86.

Holland, M.M., C.M. Bitz. 2003. Polar amplification of climate change in coupled models. Climate Dynamics 21: 221-232.

Holmlund, P., R.L. Hooke. 1983. High water-pressure events in moulins, Storglaciären, Sweden. Geografiska Annaler 65A(1-2): 19-25.

Hooke, R.L. 1989. Englacial and subglacial hydrology: a qualitative review. Arctic and Alpine Research 21(3): 221-233.

Houghton, J. T., Y. Ding, D.J. Griggs, M. Noguer, P.J. van der Linden, D. Xiaosu, eds. 2001. Climate Change 2001: The Scientific Basis. Contribution of Working Group I to the Third Assessment Report of the Intergovernmental Panel on Climate Change (IPCC). Cambridge: Cambridge University Press. 944 pp.

Iken, A. 1972. Measurements of water pressure in moulins as part of a movement study of the White Glacier, Axel Heiberg Island, Northwest Territories, Canada. Journal of Glaciology 11(61): 53-58.

Janssens, I., P. Huybrechts. 2000. The treatment of meltwater retention in mass-balance parameterizations of the Greenland ice sheet. Annals of Glaciology 31: 133-140.

Jarvis, G.T., G.K.C. Clarke. 1975. The thermal regime of Trapridge Glacier and its relevance to glacier surging. Journal of Glaciology 14(71): 235-250.

Johannessen, O.M., E.V. Shalina, M.W. Miles. 1999. Satellite evidence for an Arctic sea ice cover in transformation. Science 286: 1937-1939.

15

Jóhannesson. T. 1997. The response of two Icelandic glaciers to climatic warming computed with a degree-day glacier mass-balance model coupled to a dynamic glacier model. Journal of Glaciology 43(143): 321-327.

Kerr. R.A. 1999. Will the Arctic Ocean lose all its ice? Science 286: 1828.

Lawson. D.E. 1993. Glaciohydrologic and glaciohydraulic effects on runoff and sediment yield in glacierized basins. U.S. Army Corps of Engineers: Cold Regions Research and Engineering Laboratory Monograph 93-2, 123 pp.

Liestol. O.. K. Repp. B. Wold. 1980. Supra-glacial lakes in Spitsbergen. Norsk Geografiska Tidsskrift 34: 89-92.

Mader. H.M. 1992. The thermal behaviour of the water-vein system in polycrystalline ice. Journal of Glaciology 38(130): 359-374.

Manabe. S.. R.J. Stouffer. 1997. Coupled ocean-atmosphere model response to freshwater input: Comparison to Younger Dryas event. Paleoceanography 12(2): 321-336.

Mayo. L.R.. R.S. March. 1990. Air temperature and precipitation at Wolverine Glacier. Alaska: Glacier growth in a warmer. wetter climate. Annals of Glaciology 14: 191-194.

McGregor. G.R.. G.E. Petts. A. Gurnell. A.M. Milner. 1995. Sensitivity of alpine stream ecosystems to climate change and human impacts. Aquatic Conservation: Marine and Freshwater Ecosystems 5: 233-247.

Meier. M. 1984. Contribution of small glaciers to global sea level. Science 226: 1418-1421.

Meier, M. 1990. Role of Land Ice in Present and Future Sea-Level Change. In <u>Sea-Level Change</u>. M.A.R. Geophysics Study Committee - Commission on Physical Sciences. Washington: National Academy Press. p. 171-184.

Morison, J., K. Aagaard, M. Steele. 2000. Recent environmental changes in the Arctic: a review. Arctic **53**(4): 359-371.

Nienow, P.W., M.J. Sharp, I.C. Willis. 1998. Seasonal changes in the morphology of the subglacial drainage system, Haut Glacier d'Arolla, Switzerland. Earth Surface Processes and Landforms **23**(9): 825-843.

Nye, J.F., F.C. Frank. 1973. Hydrology of the intergranular veins in a temperate glacier. International Association of Hydrological Sciences **95:** 157-161.

Ødegård, R.S., S.-E. Hamran, P.H. Bø, B. Etzelmüller, G. Vatne, J.L. Sollid. 1992. Thermal regime of a valley glacier, Erikbreen, northern Spitsbergen. Polar Research **11**(2): 69-79.

Oerlemans, J., J.P.F. Fortuin. 1992. Sensitivity of glaciers and small ice caps to greenhouse warming. Science **258**(5079): 115-117.

Oerlemans, J., B. Anderson, A. Hubbard, P. Huybrechts, T. Jóhannesson, W.H. Knap, M. Schmeits, A.P. Stroeven, R.S.W. van de Wal, J. Wallinga, Z. Zuo. 1998. Modelling the response of glaciers to climate warming. Climate Dynamics **14**(4): 267-274.

Oerlemans, J., E.J. Klok. 2003. Effect of summer snowfall on glacier mass balance. Annals of Glaciology **38,** in press.

Ohmura, A. 2001. Physical basis for the temperature-based melt-index method. Journal of Applied Meteorology **40**(4): 753-761.

Pfeffer, W.T., M.F. Meier, T.H. Illangasekare. 1991. Retention of Greenland runoff by refreezing: implications for projected future sea level change. Journal of Geophysical Research – Oceans 96(C12): 22,117-22,124.

Pfeffer, W.T., N.F. Humphrey. 1996. Determination of timing and location of water movement and ice-layer formation by temperature measurements in sub-freezing snow. Journal of Glaciology 42: 292-304.

Rabus, B.T., K.A. Echelmeyer. 1997. The flow of a polythermal glacier: McCall Glacier, Alaska, USA. Journal of Glaciology 43(145): 522-536.

Röthlisberger, H., H. Lang. 1987. Glacial hydrology. In Glacio-Fluvial Sediment Transfer. A. Gurnell and M. Clark, eds. Toronto: John Wiley and Sons, p. 207-284.

Schytt, V. 1949. Re-freezing of the melt-water on the surface of glacier ice. Geografiska Annaler 31A(1-4): 222-227.

Seidov, D., E. Barron, B.J. Haupt. 2001. Meltwater and the global ocean conveyor: northern versus southern connections. Global and Planetary Change 30(3-4): 257-270.

Serreze, M.C., J.E. Walsh, F.S. Chapin III, T. Osterkamp, M. Dyurgerov, V. Romanovsky, W.C. Oechel, J. Morison, T. Zhang, R.G. Barry. 2000. Observational evidence of recent change in the northern high-latitude environment. Climatic Change 46: 159-207.

Skidmore, M.L. 1995. The hydrochemistry of a high Arctic glacier. M.Sc. thesis, University of Alberta, 114pp.

Skidmore, M.L., M.J. Sharp. 1999. Drainage system behaviour of a high Arctic polythermal glacier. Annals of Glaciology 28: 209-215.

Tangborn. W. 1999. A mass balance model that uses low-altitude meteorological observations and the area-altitude distribution of a glacier. Geografiska Annaler 81A(4): 753-765.

Tronov. M.V. 1962. On the role of summer snowfall in glacier variations. International Association of Hydrological Sciences 58: 262-269.

van der Veen. C.J. 1998. Fracture mechanics approach to penetration of surface crevasses on glaciers. Cold Regions Science and Technology 27: 31-47.

van der Veen. C.J. 2002. Polar ice sheets and global sea level: how well can we predict the future? Global and Planetary Change 32: 165-194.

Vatne. G., B. Etzelmuller. J.L. Sollid. R.S. Odegard. 1995. Hydrology of a polythermal glacier. Erikbreen. Northern Spitsbergen. Nordic Hydrology 26: 169-190.

Wadham. J.L., A.-M. Nuttall. 2002. Multiphase formation of superimposed ice during a mass-balance year at a maritime high-Arctic glacier. Journal of Glaciology 48(163): 545-551.

Wadham. J.L., R. Hodgkins. R.J. Cooper. M. Tranter. 2001. Evidence for seasonal subglacial outburst events at a polythermal glacier. Finsterwalderbreen. Svalbard. Hydrological Processes 15: 2259-2280.

Willis. I., N. Arnold. B. Brock. 2002. Effect of snowpack removal on energy balance. melt and runoff in a small supraglacial catchment. Hydrological Processes 16(14): 2721-2749.

Wolfe. P.M., M.C. English. 1995. Hydrometeorological relationships in a glacierized catchment in the Canadian High Arctic. Hydrological Processes 9: 911-921.

19

Woodward. J.. M.J. Sharp. A. Arendt. 1997. The influence of superimposed-ice formation on the sensitivity of glacier mass balance to climate change. Annals of Glaciology **24**: 186-190.

Zwally. H.J.. W. Abdalati. T. Herring. K. Larson. J. Saba. K. Steffen. 2002. Surface melt-induced acceleration of Greenland ice-sheet flow. Science **297**: 218-222.

20

CHAPTER 2.

THE ROLE OF HYDROLOGICALLY-DRIVEN ICE FRACTURE IN DRAINAGE SYSTEM EVOLUTION ON AN ARCTIC GLACIER*

2.1. Introduction

Variations in the rate of surface meltwater delivery to the beds of temperate glaciers induce seasonal fluctuations in glacier velocity and shorter-term rapid motion events (Iken, 1972; Iken and Bindschadler, 1986). Recently, seasonal velocity variations have been observed on the Greenland Ice Sheet in a region where ice is over 1200 m thick (Zwally et al., 2002). This suggests that surface waters can penetrate very thick ice at sub-freezing temperatures, reach the glacier bed, and affect rates of basal motion. The mechanisms by which penetration takes place, however, are not well understood. Here we present observations from a predominantly sub-temperate glacier on Ellesmere Island, which suggest that the penetration mechanism may involve water-pressure-induced ice fracturing.

2.2. Study site and methods

John Evans Glacier (JEG) is a large valley glacier located at 79° 40' N and 74° 30' W, on the east coast of Ellesmere Island, Arctic Canada (Fig. 2.1). It covers approximately 75% of a 220 km^2 catchment, and is 15 km long with an elevation range of 100-1500 m a.s.l. (Skidmore and Sharp, 1999). Ice reaches a maximum thickness of ~400 m near the long-term equilibrium line (750 m a.s.l.). The glacier is cold-based in the accumulation area and at the glacier margins where ice is thin; basal ice reaches the pressure melting point over much of the ablation zone (Copland and Sharp, 2001). Ice temperature at 15 m depth is recorded annually, and ranges from -15.1°C at 1173 m a.s.l. to -10.9°C in the area where observations were made (~615 m a.s.l.).

The drainage system was monitored at the downstream limit of a 3 km long supraglacial stream where it enters the glacier via a crevasse oriented perpendicular to the stream (Fig. 2.1). This location is 5 km from the glacier terminus, and the local ice thickness is ~150 m (Copland and Sharp, 2001). A Druck 1830 pressure transducer connected to a Campbell Scientific CR10 datalogger was installed in the stream, 2 m

21

from the crevasse. to monitor water level half-hourly from 1600 on 16 June. to 1730 on 21 July. 2002 (Fig. 2.2). Additional observations were provided by thrice-daily time-lapse photography. and regular site visits.

Meteorological variables were measured every ten seconds at a weather station located at 824 m a.s.l. (MWS. Fig. 2.1). and hourly averages were recorded. A point-based energy balance melt model (EBM) was used to compute hourly rates of surface melt from these data (Fig. 2.2) (Brock and Arnold. 2000).

A linear reservoir model was used to simulate the role of the snowpack in delaying the transfer of melt calculated with the EBM to the supraglacial channel (Oerter et al.. 1981; Appendix A). The results of a windowed cross-correlation analysis. and field observations of changing snowpack thickness and saturation. were used to generate temporally variable values of the model storage coefficient (k). Values of k were varied to obtain an optimum fit between normalized (by maxima) time series of modelled reservoir outflow. which drives water level (WL) change in a closed basin. and measured WL change (final $r^2 = 0.87$. $p < 0.05$). This approach maximizes the proportion of the variance in water level that is attributed to surface melt and runoff processes. The difference between the two standardized time series thus highlights events that may be attributable to other processes. such as drainage into newly formed fractures.

2.3. Results

When observations began on 16 June. water was flowing into the crevasse at the monitoring site (Fig. 2.3a). Within three days. the crevasse had filled and meltwater had begun to pond within the stream channel. Water level continued to rise for 11 days. reaching a maximum of 6.9 m above the channel floor and creating a pond that extended ~200 m upstream of the crevasse (Fig. 2.3b). At this time. the snowline was at ~500 m a.s.l.. and supraglacial streams were flowing on the lower glacier. During the period of ponding. crevasses at the pond margins widened by ~0.03 m. Deep cracking noises were often heard. and air bubbles were observed rising from fractures in the channel bed.

The rate of measured WL change fell below zero on four occasions from 16-18 June. indicating that drainage was taking place (Fig. 2.4). A plot of the difference between the normalized time series of modeled reservoir outflow and measured WL change identifies

these same periods. It also identifies a further four periods between 19-23 June when the rate of WL change was less than expected given the modeled transfer of surface melt to the channel (Fig. 2.4). This suggests the occurrence of eight events during which drainage was initiated. but not sustained.

Starting at 0100 on 29 June. the monitored pond drained completely within one hour (Figs. 2.2. 2.3c). Following drainage. six new crevasses ~0.20 m wide and oriented perpendicular to the direction of water flow were observed (Fig. 2.3c). Although they were not monitored continuously. similar drainage events occurred in three other supraglacial streams in the same area in the period 27-28 June. These four drainage events were followed at 1800 on June 30 by the appearance of a slightly turbid. solute-rich upwelling at the glacier toe (electrical conductivity (EC) = 0.065 S m^{-1}). Subsequently. an artesian fountain. also fed by solute-rich water (EC = 0.050 S m^{-1}). formed on the ice surface ~200 m from the glacier terminus at 0800 on July 1 (Fig. 2.1).

2.4. Discussion

Field data indicate that multiple. relatively abrupt. drainage events occurred while the crevasse was water-filled or overfilled. These events culminated in a major drainage event that established a permanent hydrological connection between the surface and subglacial drainage systems. and initiated subglacial outflow at the terminus. The abruptness of these events suggests hydrologically-driven ice fracture as the most likely means of drainage development. This is supported by the deep fracturing noises heard. the widening of existing crevasses during the ponding period. and the creation of new crevasses during the drainage event. The occurrence of ice fracture in this situation is consistent with the results of previous theoretical analyses of the process. They concluded that. so long as the tensile stress acting normal to the crevasse is ≥100 kPa. water-filled crevasses will penetrate to the glacier bed regardless of ice thickness or crevasse spacing within a crevasse field (van der Veen. 1998).

Our observation of multiple premonitory drainage events raises two significant questions: what limited the development of the first eight fractures into drainage connections. and why was a permanent drainage connection with the bed established during the ninth and final event?

23

The development of the first fractures was likely initially limited by the elastic nature of the fracture process. which results in almost immediate closure of the fracture in the absence of an opposing force (van der Veen. 1998). These fractures would likely have been thin. with a large surface area to volume ratio. resulting in inefficient water penetration. As 15 m ice temperature measurements indicate that the fracture walls were likely at -5°C to -10°C. the first meltwater to penetrate the fracture may have refrozen on contact with this cold ice. re-sealing the fracture. Water that was able to reach the glacier bed may have experienced significant flow resistance within the subglacial drainage system. especially since dye tracing experiments indicate that this system had contracted substantially during the previous winter (Bingham. 2003). This would have slowed drainage from the fracture and reduced the rate of turbulent heating of water descending into the fracture. thus limiting the potential for fracture enlargement by wall melting and causing the fracture to re-seal by freezing.

Eventually. however. fracturing allowed the development of a drainage system capable of transmitting a sustained flux of water. Several factors may have allowed this to happen. The release of latent heat from refreezing during the previous events would have warmed the ice walls. allowing water to penetrate deeper into the ice during successive fracture events. In addition. the continued filling of the surface pond increased the water pressure acting on the crevasse tip. making it easier for the fracture to penetrate to the bed (van der Veen. 1998). Surface ponding also increased the availability of water to drain into the fracture. thus increasing the potential for both turbulent heating of falling water. and rapid enlargement of the fracture through wall melt (Nye. 1976). Thus fracture closure was no longer limited by the elastic response or refreezing. but by ice deformation. which was offset by both water pressure and turbulent heating.

Successive episodes of water input to the glacier bed may have driven progressive development of the subglacial drainage system. reducing the resistance to surface inputs and allowing more continuous inflow. Water reaching the bed would have increased water pressures in the subglacial drainage system downstream from the crevasse. causing subglacial cavity growth and basal uplift. and reducing basal shear traction. resulting in local acceleration of ice flow (Iken et al.. 1983: Kamb and Engelhardt. 1986: Kavanaugh and Clarke. 2001). The longitudinal velocity gradient and tensile stress in the vicinity of

24

the crevasse would have increased, resulting in a feedback between crevasse widening, increased drainage of ponded water, and fracture enlargement due to wall melting. This is supported by ice velocity measurements from 2000 and 2001, which indicate that both horizontal and vertical ice velocities downstream of the crevasse region increased prior to major high velocity events in late June and early July (Bingham et al., 2003). These events were also associated with the drainage of water ponded on the glacier surface and the seasonal onset of subglacial outflow at the glacier terminus.

2.5.   Conclusions

Field observations of the seasonal development of a drainage connection between the surface and bed of a predominantly cold glacier provide insights into the rapid response of cold glacier flow dynamics to changes in surface melt rate. Propagation of water-filled crevasses to the glacier bed seems to play a major role in seasonal establishment of the surface-bed connection, but is not the sole process responsible for establishing a sustained drainage connection.

In temperate glaciers, fracture propagation alone may be sufficient to develop seasonal drainage, as ice is everywhere at the pressure melting point and water penetrating fractures is unlikely to refreeze. In cold glaciers, however, refreezing of percolating meltwater, which may be facilitated by flow restrictions in the subglacial drainage system, likely impedes drainage development along fractures. As a result, formation of a sustained connection is preceded by a number of premonitory drainage events. Warming of glacier ice due to initial refreezing events increases the likelihood of a permanent surface-bed connection developing during subsequent events. In addition, surface water ponding raises the water pressure at the crevasse tip: this stored water contributes to crevasse enlargement by wall melting when it eventually drains.

Drainage may also be facilitated by a positive feedback involving ice flow dynamics. The rate of ice flow downstream from the fracture increases once water penetrates to the bed, increasing the tensile stress in the ice surrounding the fracture, widening the fracture and increasing water delivery to the bed. This mechanism likely plays an important role in the seasonal development of glacier drainage systems (e.g. Flowers and Clarke, 2000; Bingham et al., 2003), provides a means by which the flow of large ice sheets may

25

respond rapidly to climatically-induced changes in surface melt rates (e.g. Arnold and Sharp. 2002: Zwally et al.. 2002), and may also contribute to ice shelf break-up and tidewater glacier calving (van der Veen. 1998: Scambos et al.. 2000).

2.6. References

Arnold. N.. M. Sharp. 2002. Flow variability in the Scandinavian ice sheet: modelling the coupling between ice sheet flow and hydrology. Quaternary Science Reviews **21**: 485-502.

Bingham. R.G.. P.W. Nienow. M.J. Sharp. 2003. Short-term variations in glacier dynamics in the ablation zone of a High Arctic polythermal glacier: relation to seasonal changes in subglacial drainage system structure. EGS/AGU/EUG Joint Assembly. Nice. France. 6-11 April.

Brock. B.W.. N.S. Arnold. 2000. A spreadsheet-based (Microsoft Excel) point surface energy balance model for glacier and snow melt studies. Earth Surface Processes and Landforms **25**: 649-658.

Copland. L.. M. Sharp. 2001. Mapping hydrological and thermal conditions beneath a polythermal glacier with radio-echo sounding. Journal of Glaciology **47**: 232-242.

Flowers. G.E.. G.K.C. Clarke. 2000. An integrated modelling approach to understanding subglacial hydraulic release events. Annals of Glaciology **31**: 222-228.

Iken. A. 1972. Measurements of water pressure in moulins as part of a movement study of the White Glacier. Axel Heiberg Island. NWT. Canada. Journal of Glaciology **11**: 53-58.

Iken. A.. H. Röthlisberger. A. Flotron. W. Haeberli. 1983. The uplift of Unterargletscher at the beginning of the melt season - a consequence of water storage at the bed? Journal of Glaciology **20**: 28-47.

Iken. A.. R.A. Bindschadler. 1986. Combined measurements of subglacial water pressure and surface velocity of Findelengletscher. Switzerland: conclusions about drainage system and sliding mechanism. Journal of Glaciology 32: 101-119.

Kamb. B.. H. Engelhardt. 1987. Waves of accelerated motion in a glacier approaching surge: the mini-surges of Variegated Glacier. Alaska. U.S.A. Journal of Glaciology 33: 27-46.

Kavanaugh. J.L.. G.K.C. Clarke. 2001. Abrupt glacier motion and reorganization of basal shear stress following the establishment of a connected drainage system. Journal of Glaciology 47: 472-480.

Nye. J.F. 1976. Water flow in glaciers: jökulhlaups. tunnels and veins. Journal of Glaciology 17: 181-207.

Oerter. H.. D. Baker. H. Moser. O. Rienwarth. 1981. Glacial-hydrological investigations at the Vernagtferner Glacier as a basis for a discharge model. Nordic Hydrology 12: 335-348.

Scambos. T.A.. C. Hulbe. M. Fahnestock. J. Bohlander. 2000. The link between climate warming and break-up of ice shelves in the Antarctic Peninsula. Journal of Glaciology 46: 516-530.

Skidmore. M.L.. M.J. Sharp. 1999. Drainage system behaviour of a high Arctic polythermal glacier. Annals of Glaciology 28: 209-215.

van der Veen. C.J. 1998. Fracture mechanics approach to penetration of surface crevasses on glaciers. Cold Regions Science and Technology 27: 31-47.

Zwally. H.J.. W. Abdalati. T. Herring. K. Larson. J. Saba. K. Steffen. 2002. Surface melt-induced acceleration of Greenland ice-sheet flow. Science 297: 218-222.

2.7. Figures

Figure 2.1. Location of John Evans Glacier (inset): location of monitored and adjacent crevasse/moulins (open circles), meteorological station (MWS), and artesian fountain (asterisk).

28
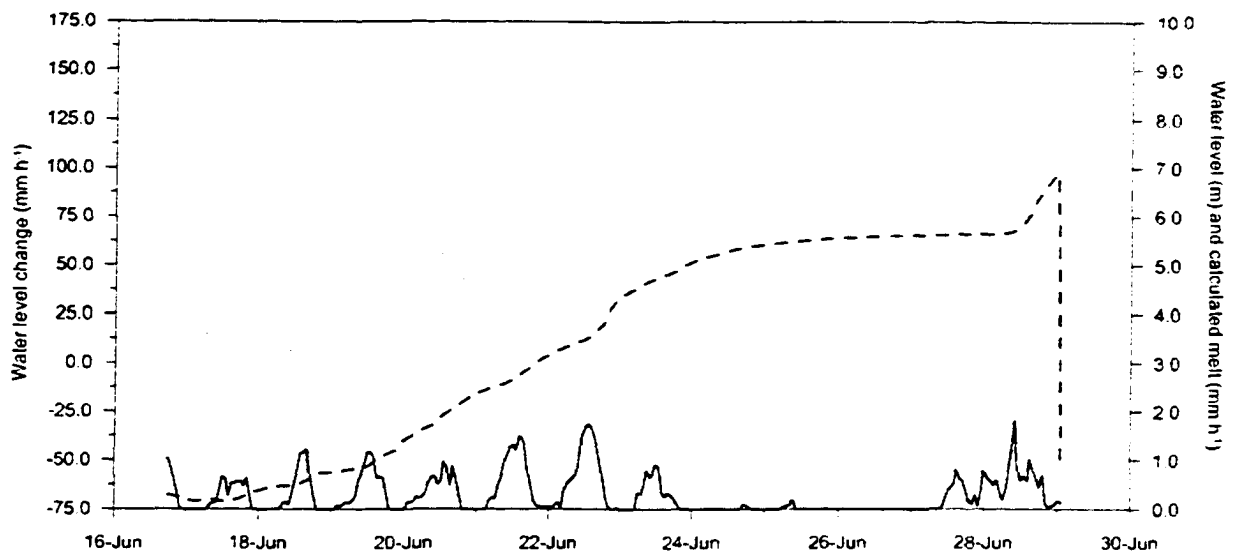
Figure 2.2. Water level (dashed black) and rate of water level change (grey) in the moulin, and melt calculated with EBM (black). Note the magnitude of the final drainage event.

29

Figure 2.3 Sequence of moulin development: (a) initial water-filled crevasse and supraglacial stream (16 June); (b) maximum fill depth (28 June); and, (c) following drainage (30 June). Fresh crevasses marked with an `x`.
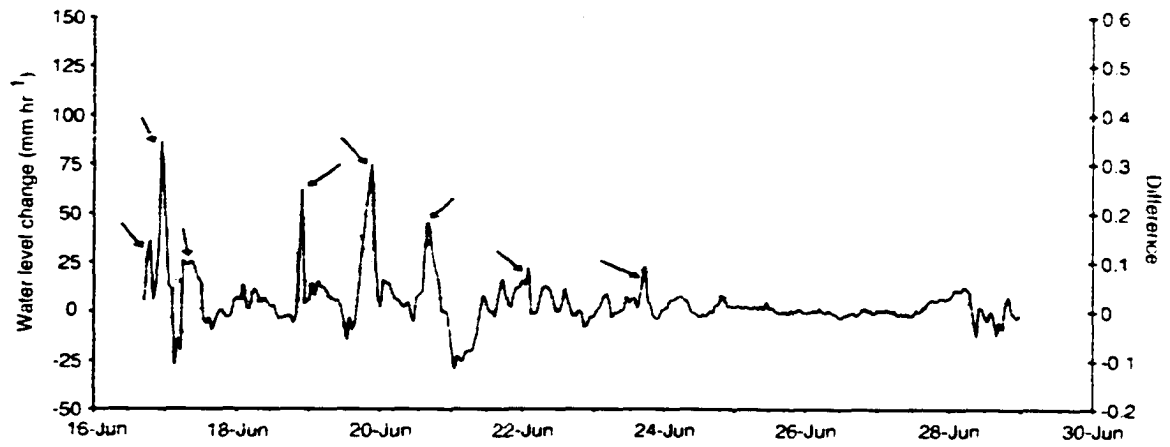
Figure 2.4. Rate of water level change (grey). and difference between standardized time series of modelled reservoir outflow and water level change (black). Premonitory drainage events marked with arrows.

31

CHAPTER 3.

IMPACT OF AN EXTREME MELT EVENT ON THE HYDROLOGY AND RUNOFF OF A HIGH ARCTIC GLACIER*

3.1. Introduction

An extreme melt event occurred on John Evans Glacier. Ellesmere Island. Nunavut. Canada (Fig. 3.1) in the period 28-30 July 2000. This event was characterised by significant increases in air temperature and wind speed, and by a concurrent decrease in relative humidity. Over the three days of the event, average rates of surface lowering at 1183 m a.s.l. increased significantly, from $\sim$13 mm d^{-1} to 56 mm d^{-1}, and supra- and proglacial discharges reached peak melt-season values. Rapid surface melting removed the cryoconite layer on the glacier surface. It thus appears that the event contributed disproportionately to summer ablation and runoff, and that it may have had a significant influence on the annual mass balance of the glacier. This raises the possibility that variations in the incidence of such events may contribute in a major way to inter-annual variability and longer term changes in runoff and mass balance at high Arctic glaciers, where summer melt is typically very low.

To evaluate this possibility, this paper attempts to quantify the impact of the event on summer ablation and runoff. It also seeks to identify the synoptic conditions associated with the event, to determine the mechanisms by which melt was enhanced, and to evaluate the frequency with which such events have occurred within the period of instrumental record. Although several similar events have been recorded in the Canadian high Arctic (see Courtin and Labine. 1977: Doran et al.. 1996). there has been no previous systematic study of their incidence or impact on glacier runoff and mass balance. It has, however, been recognised that synoptically driven extreme melt events may be significant drivers for change in glacier hydrological systems (Gordon et al.. 1998: Nienow et al.. 1998).

3.2. Study Site

John Evans Glacier (JEG) is a large valley glacier located at 79° 40' N and 74° 00' W, on the east coast of Ellesmere Island, Nunavut, Canada (Fig. 3.1). It covers approximately 75% of a 220 km² catchment, with a length of 15 km and an elevation range of 100 - 1500 m a.s.l. (Skidmore and Sharp, 1999). The glacier is polythermal, with cold-based ice in the accumulation area and at the glacier margins where ice is thin, and warm-based ice throughout the remainder of the ablation zone (Copland and Sharp, 2001). Ice thickness reaches a maximum of ~400 m close to the equilibrium line, and 100-200 m in the lower 4 km of the glacier. During the period 1997-2000, mean annual air temperature at the equilibrium line (~850 m a.s.l.) was -15.1°C.

3.3. Hydrology of John Evans Glacier

At the onset of summer melt, the drainage system of JEG consists of disconnected supraglacial lakes and streams, and there is no subglacial outflow. As surface melt progresses, snowmelt is routed both into storage in ice-marginal lakes and supraglacial channel systems (e.g., Nunatak and Ridge Lakes and Streams: Fig. 3.1), and directly to ice-marginal streams. Eventually (late June to early July), the supraglacial Ridge and Nunatak Streams (and others in the same area) become connected to moulins located in a major crevasse field approximately 4 km from the glacier terminus (Lower Crevasse Field: Fig. 3.1). The opening of these moulins allows water to drain from the surface to the glacier bed. Pro-glacial outflow of subglacially routed waters is usually initiated within 24 hours of the moulins opening. Initially, outflow consists of extremely solute-rich waters that have probably been stored beneath the glacier over winter, but solute concentrations fall rapidly within 3 to 4 days as these "old" waters are diluted by the new season's melt (Skidmore and Sharp, 1999: Heppenstall, 2001). Subglacial outflow emerges from one large portal at the centre of the glacier snout (Fig. 3.1), but the resulting stream channel regularly changes course. In the cooler summers of 1994 and 1996, subglacial outflow occurred as a series of outburst floods, and the subglacial drainage system shut down between floods (Skidmore and Sharp, 1999). However, in the warmer summers of 1998-2000, outflow was continuous once initiated.

33

Most runoff that does not enter the Lower Crevasse Field is routed across the glacier surface to ice-marginal channels. In the summers of 1999-2001 (and possibly also in other summers). however. additional connections between surface channels and the en- and subglacial drainage systems developed at the Crevasse Lake and Upper Crevasse Field (Fig. 3.1) later in the season. resulting in englacial/subglacial drainage of ~40% of supraglacially derived meltwater.

3.4. Methods

3.4.1. Synoptic conditions

Charts detailing synoptic conditions for 28-30 July. 2000. were obtained from the National Centre for Environmental Prediction's (NCEP) Climate Data Assimilation System (CDAS) daily reanalysis datasets (1000 mb geopotential heights. and 1000 mb zonal wind speed). and from the Meteorological Service of Canada (MSC) Northern Hemisphere daily analyses (500 mb geopotential heights).

3.4.2. Local meteorological data

Meteorological data have been collected year-round at JEG since May 1996. Three on-ice automatic weather stations are deployed along the glacier centreline at 1183 m a.s.l. (Upper Weather Station - UWS). 824 m a.s.l. (Middle Weather Station - MWS) and 261 m a.s.l. (Lower Weather Station - LWS) (Fig. 3.1). The LWS is located in the ablation zone. the MWS near the equilibrium line. and the UWS in the accumulation zone. During the summer melt season. hourly and daily averages of 10 second readings of air temperature. relative humidity (RH). net all-wavelength radiation (Q^*). incoming and reflected solar radiation (K_{in}. K_{out}). wind speed and direction. and rates of surface lowering are recorded at each station (Table 3.1). Measured solar radiation includes both direct and diffuse components.

Only data from the UWS and MWS are used in this study. Malfunction of the anemometer at the LWS precluded use of data from that station. Accurate measurements of surface lowering over the entire season (including the event) are available only from the UWS. as the masts supporting the ultra-sonic depth gauges (UDG) at both the MWS and LWS began to tilt during the melt event due to the high rates of surface lowering.

34

Tilting also caused errors in Q* values from the MWS for 28 July to 1 August. Data from 9 June - 1 August were used in this study, as this is the period during which both meteorological stations were recording hourly average values. These data cover the majority of the melt season. which lasted from approximately 9 June to 10 August 2000.

The MWS was serviced four times during the field season. On each occasion. instrument heights were adjusted and masts were re-drilled. Due to its distance from base camp. the UWS was serviced only twice: once at the beginning and once at the end of the field season. This is not considered problematic. as there was insufficient melt at this station to cause the masts to tilt. As net lowering at this site was < 0.3 m over the whole season. no attempt is made to correct for the effect of changing instrument heights on melt calculations.

3.4.3. Melt calculations

Surface melt rates at the UWS and the MWS were calculated using the following energy balance equation:

$$Q_m = Q^* + LHF + SHF - GHF \tag{1}$$

where Q_m is the total energy available for melt. Q^* is the net radiation. LHF is the latent heat flux. SHF is the sensible heat flux. and GHF is the ground heat flux (Brock and Arnold. 2000). All terms were calculated in W m^{-2}. then converted to millimetres of water equivalent (mm w.e.) by multiplying by the latent heat of fusion (3.33 x 10^5 J kg^{-1}). Resulting values were summed to determine total melt at each meteorological station. Melt rates were output as both hourly and daily totals.

Calculations were performed using measured values of Q*. and thus take account of diurnal variations in albedo. which are significant for melt at this latitude (Arendt. 1999). As the radiation sensors were aligned parallel to the slope. the effects of slope and aspect are also taken into account in the measured data. Erroneous Q* values recorded at the MWS between 28 July and 1 August were replaced by Q* values calculated using a point surface energy balance model (EBM) (Brock and Arnold. 2000). This model requires inputs of hourly values of air temperature. pressure and wind speed from a local

35

meteorological station of known elevation. and a value for the aerodynamic roughness length at the point for which melt is being calculated. To calculate Q^*. the model required additional inputs of latitude. longitude. slope. aspect. elevation and albedo. as well as measured incoming solar radiation. The EBM assumes that: (1) cloud cover increases linearly as the ratio of measured K_{in} to theoretical clear-sky maximum K_{in} decreases: (2) the ice surface is constantly at $0°C$. and energy is not required to return the surface to $0°C$ after a cold spell (which is likely incorrect for both sites at some points in the season): (3) vapour pressure just above the melting glacier surface is 611 Pa: and (4) the bulk aerodynamic method. incorporating the Monin-Obukhov similarity theory. is appropriate for this situation. When tested in an alpine setting. the model was found to approximate measured melt amounts very well. despite shading differences between the meteorological station and the modelled point (Brock and Arnold. 2000). In this study melt is calculated only for those locations at which meteorological data are collected. and the effect of shading is taken into account by the measurements used to drive the model. For a more detailed description of the model. see Brock and Arnold (2000).

Comparison of hourly melt rates at the MWS. derived from both calculated and measured values of Q^*. shows that

$$Q_{m(calc)} = Q_{m(meas)} + 0.25 \text{ mm w.e. h}^{-1} \ (r^2 = 0.85 : p < 0.05) \tag{2}$$

for the period 9 June to 27 July. where $Q_{m(calc)}$ is melt determined using Q^* values calculated by the EBM. and $Q_{m(meas)}$ is melt determined using Q^* values measured at the meteorological station. Given the good relationship between the two values. substituting calculated for measured values during the period in question is justified. As calculated values are used for five days (28 July – 1 August). melt during this period may be over-estimated by as much as ~ 30 mm.

The turbulent flux terms (LHF and SHF) were also calculated using the EBM. Positive LHF indicates energy being directed into the glacier surface (condensation). Negative LHF indicates energy being released from the glacier surface (evaporation/sublimation). At both the UWS and the MWS. SHF and LHF were calculated using data from 9 June – 1 August 2000 and the parameter values in Table 3.2

36

as model inputs. Due to the uncertainty involved in assigning values for roughness length (z_0). sensitivity tests were performed to determine the impact of varying z_0. Values for z_0 were obtained from Paterson (1994. p. 63). using measured albedo as a basis for characterising surface conditions. The first sensitivity experiment involved comparing results from a simulation that used a constant value of z_0 for the entire melt season. with one that used different values of z_0 for sub-periods defined on the basis of observed variations in surface albedo. The constant value chosen was a weighted average of the values used for the different sub-periods. Given the possible error in the selection of z_0 values. a second constant z_0 sensitivity test was performed using extreme high and low estimates of z_0 applied over the entire melt season. Tables 3.3 and 3.4 list the z_0 values used in each sensitivity experiment.

Partitioning the melt season into sub-periods with different z_0 values resulted in only minor differences in predicted seasonal melt (3 and 8 mm w.e. at the MWS and UWS. respectively) from the simulation using constant z_0. Differences in seasonal melt predictions using maximum and minimum estimates of z_0 are only 23 mm w.e. at the MWS and 15 mm w.e. at the UWS. Given the relatively small sensitivity of the EBM to variations in z_0. a single value for this parameter was used in subsequent simulations.

GHF was assigned a value of 17.6 W m^{-2} (based on the work of Konzelmann and Braithwaite (1995). in northeast Greenland). as heat conduction into the underlying ice is significant on non-temperate glaciers.

It is important to note that on high Arctic glaciers not all melt (Q_m) goes directly to runoff. Refreezing of meltwater that percolates into the cold snowpack plays a large role in delaying runoff at the start of the season. In 2001. for example. the delay between the onset of melt and the onset of runoff was approximately 12 days on the lower glacier. and 24 days on the upper glacier (D. Lewis. pers. comm). Reeh (1991) suggested that an amount of water equivalent to approximately 60% of the winter snowpack might refreeze before runoff begins. This value was therefore used to determine seasonal runoff from calculated melt. The initial snow water equivalent (SWE) at the start of the 2000 melt season was 83.8 mm at the MWS. and 93.8 mm at the UWS.

Total summer melt at the MWS and UWS was calculated by summing modelled daily melt totals. The proportion of summer *melt* that occurred during the extreme melt event

37

was determined by dividing the total melt from 28-30 July by the seasonal total (9 June – 1 August). The proportion of summer *runoff* contributed by the melt event was estimated by dividing the total melt from 28-30 July by the estimated total runoff (total melt minus 60% of initial SWE at each weather station).

3.4.4. Glacier hydrology

Water levels in supraglacial streams were monitored throughout the melt season. Keller 169-L pressure transducers connected to Campbell Scientific CR10 dataloggers were placed in the Nunatak Lake, Ridge Stream, and Crevasse Lake (Fig. 3.1). Relative stage values were recorded every 10 seconds, and an average reading was output every 15 minutes. Due to frequent channel aggradation and migration, the record from a transducer placed in the proglacial stream was unreliable. Observations of proglacial drainage system development over the melt season were therefore also used to qualitatively assess changes in runoff. Proglacial discharge volumes were estimated to reach ~30 m^3 s^{-1} during the melt event, but reliable measurements were difficult to obtain by the velocity-area method when discharge was in excess of ~5 m^3 s^{-1}.

3.4.5. Past events

Frequency distributions of mean daily summer (June, July, August – JJA) air temperature, wind speed, and relative humidity, were derived from the 5-year JEG climate record (1996-2000) to determine where the days of the melt event fall within these distributions. In addition, a 50-year record of daily synoptic conditions (Keimig, unpublished) was searched to determine the frequency of occurrence of days with synoptic conditions similar to those associated with the event. The database constitutes a 7x28 grid (7 grid points of latitude by 28 grid points of longitude), spanning 90°N - 75°N and 110°W - 42.5°W. The size of each grid box is 2.5° x 2.5°.

3.5. Results

3.5.1. Synoptic conditions

MSC 500 mb geopotential height maps for the period of the melt event show a low over north-west Greenland that deepened and moved into Baffin Bay. A stationary low

38

was located over the Barents Sea, a weak high was located over the Arctic Ocean, and a second high was moving northwards from the Queen Elizabeth Islands (Fig. 3.2). This high reached its most northerly position on 29 July. By the end of 30 July, it had disappeared, and the low over Greenland had moved south-westwards, over Baffin Island.

NCEP 1000 mb height maps show a weak low over western Greenland, which intensified during the course of the event (28-30 July) to encompass most of Baffin Bay (Fig. 3.3). NCEP 1000 mb zonal wind charts show an area of peak wind strength over north-west Greenland, extending into central Ellesmere Island (Fig. 3.4).

3.5.2. Local meteorology

The onset of the melt event was marked by a shift in wind direction to NE at 0100 h on 28 July (Fig. 3.5). This shift was recorded at both the MWS and the UWS, suggesting that it dominated over local wind patterns, which vary greatly between stations throughout the melt season. At each station, the shift in wind direction was accompanied by a ~5 m s^{-1} increase in wind speed, and a 3-5°C increase in air temperature (Figs. 3.5 and 3.6). Initially, RH dropped to 45% at each station, but by 29 July it had returned to background values of 70-75% (Fig. 3.6). Hourly wind speeds reached a maximum of 13.5 m s^{-1} at the MWS and 11.5 m s^{-1} at the UWS: hourly air temperatures peaked at 10°C at the MWS and 8°C at the UWS, and remained high overnight, displaying only weak diurnal variation. By 30 July, winds at the MWS had shifted to the N-NW, and wind speeds had diminished. By 31 July, the air temperature had returned to seasonal background values. Winds at the UWS did not return to N-NW until 1200 h on 1 August.

UDG measurements at the UWS indicate surface lowering rates of 80 mm d^{-1} on 28 July, with lower rates of 57 and 30 mm d^{-1} on 29 and 30 July, respectively, giving an average lowering rate of 56 mm d^{-1} over the period of the event (Fig. 3.7). These were the highest rates recorded during the melt season, and are significantly higher than the 13 mm d^{-1} average for the three days immediately prior to the event (24 – 27 July).

39

3.5.3. Verification of EBM output

The UDG data were collected over a melting snow surface. Since the density of the melting snow is unknown, the UDG data cannot be used for quantitative validation of the performance of the EBM. Since internal re-freezing of initial melt causes snowpack densification, rather than runoff, the calculated melt likely exceeds the amount of water actually removed from the snowpack. In addition, the effects of summer snowfalls, which raise surface elevation, are not included in the model simulations, as accurate measurements of snowfall amounts and densities are not available.

Despite these limitations, there is good qualitative correspondence between the EBM calculations and recorded rates of surface lowering at both stations (Fig. 3.8). EBM output captures the main periods of high and low lowering rate detected by the UDG, and the significant difference in total lowering between the two sites. Calculated early-season melt is mirrored by a gradual decrease in surface height at both sites. Low calculated melt during a relatively cool period in early-mid July coincides with a period of surface height increases due to snowfall. The extreme melt event is marked by a sudden increase in calculated melt, and a corresponding rapid decline in surface height at the UWS.

Total melt at the UWS over the melt season was calculated as 404 mm w.e., while total surface lowering recorded by the UDG was approximately 350 mm. At the MWS, the UDG and EBM records correspond well until the period of the melt event (after which the UDG record is unreliable due to tilting of the mast). Total melt calculated by the EBM between 9 June – 27 July was approximately 711 mm w.e., while total surface lowering in this time period was 560 mm. This reflects the differences between the UDG and the EBM records outlined above.

3.5.4. Surface energy balance

During the melt event, Q* and SHF were the most significant energy sources at both the MWS and the UWS, while LHF was less important. LHF was, however, a strong source of melt energy during the latter part of the event, as opposed to the energy sink it represented for the remainder of the melt season (Fig. 3.9).

At the MWS, values of Q* during the melt event were similar to those reached under clear sky conditions earlier in the summer. At the UWS, Q* reached a seasonal peak

40

during the event. SHF, while positive for most of the melt season, increased significantly during the event, from <0.5 mm w.e. h^{-1} to 3 mm w.e. h^{-1} at the MWS, and to 1.6 mm w.e. h^{-1} at the UWS (Fig. 3.9). The period of high SHF lasted longer at the UWS than the MWS, however. SHF returned to seasonal background values by 31 July at the MWS, and a day later at the UWS. At both the MWS and the UWS, LHF became strongly negative on 28 July, and then switched to strongly positive on 29 July (Fig. 3.9). It remained positive until 31 July. During most of the remainder of the season, LHF was negative, except during a rainy period on 7 July. While LHF at the onset of the event was more negative at the UWS than at the MWS, it reached a similar maximum at both stations (~0.4 and 0.6 mm w.e. h^{-1}) during the event.

3.5.5. Melt rates

Hourly melt rates at both stations were commonly < 0.5 mm w.e. h^{-1} (Fig. 3.10). Such rates occurred 55% of the time at the MWS, and 74% of the time at the UWS. By contrast, melt rates during the event reached 6.1 mm w.e. h^{-1} at the MWS, and 3.7 mm w.e. h^{-1} at the UWS, values which lie above the 96th percentile of the melt rate distribution for the season.

The melt event (28-30 July) was responsible for 17% and 30% of total seasonal *melt* at the MWS and UWS respectively, even though the event occupied only 6% of the melt season (Fig. 3.11). Assuming that an amount of melt equivalent to 60% of the winter snowpack refroze within the snowpack (Reeh, 1991), the contribution of the event to total seasonal *runoff* is estimated as approximately 18% at the MWS and 35% at the UWS. Since runoff is equivalent to summer ablation, these results underline the potential impact of events such as this on the mass balance of glaciers in the Canadian high Arctic, where ablation totals are low and inter-annual variability in mass balance is largely attributable to variations in summer balance (Paterson, 1994).

3.5.6. Hydrological records

High melt rates during the event produced a clear response in the pressure transducer records from the Nunatak Lake and Ridge Stream, which experienced the second-highest water levels of the season during this period (Fig. 3.12). In the Nunatak Lake, stage was

41

higher only at the beginning of the season before the lake connected to the supraglacial drainage system. In the Ridge Stream. peak water levels earlier in the season resulted from the drainage of the Ridge Lake. which occurred after a connection was established between the Ridge Stream and the englacial/subglacial system.

Water levels in the Nunatak Lake began to increase rapidly on 28 July. rising 3 m in 24 hours to peak at 3.5 m on 29 July. The amplitude of this rise was at least 5 times that of the normal daily stage cycle during the pre-event period. In the Ridge Stream. water levels also increased on 28 July. rising 0.5 m in 36 hours to peak at 0.8 m on 29 July. This rise was approximately 1.5 times the normal daily rise during the pre-event period. Although water level in the Crevasse Lake had been decreasing steadily in the days prior to the event it increased rapidly by ~0.5 m on 29 July. before beginning to drop again. As melt rates remained high throughout the night the normal diurnal runoff cycle was overridden and water levels remained high overnight only dropping to values typical of daily minima during the pre-event period on the final day of the melt event. The Crevasse Lake drained abruptly 2 days after the extreme melt event.

Numerous observations confirm that the high melt rates during the event resulted in large volumes of water being routed through the englacial/subglacial drainage system. The surface layer of the glacier. in which cryoconite holes up to 0.2 m in depth were developed. was removed by melting. and the resulting bare ice surface was covered with a thin film of water. Water exiting the glacier covered a significantly larger area of the proglacial outwash plain than in the pre-event period. A standing wave ~1 m high appeared 5 m downstream from the proglacial outlet. and boulders up to 50 cm in diameter were entrained during peak discharge.

3.5.7. Historical climate record

Except in 2000. daily mean air temperatures greater than 8°C were not recorded at either the MWS or the UWS during the five years of record (Fig. 3.13). Thus. conditions during the event constitute the 100th percentile of the air temperature distribution. Wind speeds greater than 5 m s^{-1} at the MWS are in the 98th percentile of the distribution. while at the UWS they are in the 97th percentile. RH lower than 45% is in the 99.96[th] percentile at the MWS. and the 90th percentile at the UWS. Further examination of the local

42

meteorological record indicates that the specific combination of conditions that occurred during the event (high wind speed. high air temperature. and reduced relative humidity) did not occur at JEG on any other occasion in the period 1996-2000.

A search of Keimig's (unpublished) synoptic database indicated that conditions similar to these occurred on only 0.1% of days between 1948-2000. These synoptic conditions occurred during the summer season (JJA) on 61% of days. with the majority occurring in June and July (Fig. 3.14). 1987 had the greatest number of days with similar conditions. and many years had none at all (Fig. 3.15). Occurrence of similar synoptic conditions was generally highest during the 1950s and 1980s. and low during the 1960s. 1970s and 1990s.

3.6. Discussion

3.6.1. Synoptic, meteorological and energy balance conditions

The synoptic conditions during the period 28-30 July. 2000. created a large-scale pressure gradient between the low over NW Greenland and the high over the Arctic Ocean. forcing air to rise orographically over the north-eastern region of the Greenland Ice Sheet. The descent of this air on the lee (NW) side of the ice sheet likely led to adiabatic warming. causing the resulting north-east winds to feed warm air into the study area (Barry. 1992). This is indicated by the shift in wind direction to NE at both the UWS and MWS. as well as by the increases in air temperature and wind speed.

EBM results indicate an increase in sensible heat transfer at the onset of the event. as warm air was advected into the study area. The initial increase in SHF. however. was partly offset by the strongly negative LHF. which directed melt energy out of the glacier surface through evaporation/sublimation. The equilibration of the melting surface with the overlying atmosphere. which is indicated by the return of RH to background values. resulted in a positive peak in LHF. and peak melt rates on 29 July.

3.6.2. Differences between stations

The differences in the relative contributions to melt of each energy balance component. especially Q*. between the MWS and the UWS suggest that altitude has a significant impact. Air temperatures at the UWS are generally lower than at the MWS.

43

especially during periods of colder weather (Fig. 3.6). Surface albedo is also higher at the UWS. as melt rates are lower and summer snowfalls are more frequent than at the MWS (Fig. 3.16). Air temperatures at the UWS remained close to 0°C for a period of ~ 2 weeks in early to mid-July. Albedo thus remained high following fresh snowfalls in early July (Fig. 3.16) as there was insufficient energy to produce melt (Fig. 3.9c). During the melt event. however. melt driven initially by increases in Q^* and SHF lowered the surface albedo sufficiently through alteration of snowpack properties that Q^* made a larger contribution to melt generation later in the event. when LHF was also a source of melt energy (Figs. 3.9 and 3.16).

At the MWS. however. air temperatures remained above freezing through most of July (Fig. 3.6) and melt occurred through most of this period (Fig. 3.7). This was driven largely by Q^*. with a small and intermittent contribution from SHF. Snowfall around 12 July was less significant than at UWS (Fig. 3.8). and although it resulted in a short-term increase in albedo (Fig. 3.16). this was quickly reversed when melt resumed. As a result. surface albedo was lower for most of the season than at UWS (Fig. 3.16). and the enhancement of Q^* by snow-albedo feedback during the melt event was less marked than at UWS. Thus. the relative importance of the extreme event at MWS (17% of seasonal melt) was less than at UWS (30% of seasonal melt).

3.6.3. Implications for glacier hydrology

The event described above occurred relatively late in the melt season at JEG. when drainage connections had been established between the glacier surface and glacier bed. and outflow of subglacially routed runoff had begun. Although the event made a very significant contribution to total surface melt and runoff in the 2000 melt season. it probably did not play a major role in the seasonal development of the glacier drainage system. Keimig's (unpublished) synoptic analysis. however. showed that conditions similar to those that created the melt event occur most frequently in June. July and August. i.e.. throughout the summer melt season (Fig. 3.14). It thus seems likely that the nature and magnitude of the impact of such events may vary depending on the stage of the melt season at which they occur.

44

Several researchers have suggested that such extreme runoff events could have a significant impact on subglacial drainage system development (Gordon et al., 1998, Nienow et al., 1998). At JEG, the major event in the seasonal development of the glacier's drainage system is the establishment of a drainage connection between the glacier surface and glacier bed, and the ensuing initiation of subglacial outflow. During the period 1994-2001, this event occurred between 22 June and 12 July. The possible hydrological impacts of extreme melt events are therefore considered for periods prior to the initiation of subglacial outflow (early season, early-mid June), around the time when subglacial outflow is initiated (mid-season, late June-early July), and when subglacial outflow is occurring (late season, mid-July to early August).

Given the normally low rates of early-season melt, especially at the UWS, extreme melt events at this time may increase the rate of snowline retreat on the lower glacier, lowering the snow albedo and possibly exposing the underlying ice surface. This would result in increased total seasonal melt, as the period for which low albedo ice was exposed would be increased. The impact of an early-season event on drainage development would, however, be limited by the need to warm the snowpack to 0°C before melt can occur, and by the refreezing of meltwater within the snowpack, which delays runoff response (Fountain, 1996). Nevertheless, early season events may have the effect of advancing the dates on which runoff and subglacial outflow are initiated.

By contrast, an event in late June or early July, when the snowpack had ripened and the surface albedo had dropped, could provide a major impetus for the establishment and initial growth of englacial and subglacial drainage passageways. This is significant because July has the highest incidence of synoptic conditions similar to those that produced the event (Fig. 3.14). The impact of such events on runoff may, however, be limited by the existence of a cold snowpack over much of the upper glacier at this time of year.

Late-season events would have a much stronger impact on runoff than events earlier in the season, but their influence on the development of englacial and subglacial drainage might be more limited. Low albedo glacier ice melts rapidly under conditions such as those described, and the reduced snowpack later in the season would permit a more rapid runoff response (Fountain, 1996). It is, however, likely that englacial and subglacial

45

channels would already have formed in response to runoff earlier in the season. so the impact of large melt events could be limited to enlargement of pre-existing channels. In some cases. however. creation of new englacial connections between the supraglacial and subglacial systems might occur. resulting in upglacier expansion of the subglacial network (Nienow et al.. 1998: Flowers and Clarke. 2002).

In addition to their contribution to the development of drainage systems within glaciers. such events could play an important role in the ecology of subglacial and proglacial environments. The removal of the cryoconite layer could have important implications for the maintenance of life within and beneath glaciers. Cryoconites typically contain sediment. microbial populations. organic carbon. and nutrients (Vincent et al.. 2000). On JEG. the organic carbon content of cryoconite sediment is typically 8 - 10% by weight. Thus. when transferred to the glacier bed. the contents of cryoconites could represent a source of innoculum. energy. and nutrients for subglacial microbial ecosystems. which are typically carbon and nutrient limited (Sharp et al.. 1999: Skidmore et al.. 2001). Sudden increases in the contribution of meltwater runoff to the discharge of glacier-fed rivers could result in noticeable lowering of stream temperatures. and expansion of the subglacial drainage network could enhance sediment transport. both of which may impact riverine ecology and benthic communities (McGregor et al.. 1995).

3.6.4. Past events

The results presented above show that extreme events of short duration can make a disproportionate contribution to total summer melt. especially at high elevation sites that would normally be located in the accumulation area of the glacier. Although such events are rare. and no others occurred at JEG in the period 1996-2001. Keimig's (unpublished) synoptic database provides some evidence for clustering of similar events during some periods of the recent past. For instance. 6 days with similar synoptic conditions occurred in the 1950s and 9 in the 1980s. but only 6 in the 1960s. 1970s and 1990s combined (Fig. 3.15). Such changes in the occurrence of extreme melt events may contribute to both inter-annual variability and longer-term trends in seasonal runoff. drainage development. and glacier mass balance. The effect of such events is likely to be especially marked in the high Arctic. where both winter accumulation and summer melt are low. and inter-

46

annual variability in summer mass balance is large. On the Devon and Meighen ice caps for instance. the coefficient of variation in summer mass balance is ~ 70% (R.M. Koerner. unpublished data).

If major atmospheric oscillations (such as the Arctic Oscillation or North Atlantic Oscillation) or greenhouse-gas induced climate warming resulted in systematic changes in the incidence of such events. this could be an important factor in determining the sensitivity of glacier mass balance to such changes. It is therefore important to establish whether there is a relationship between the incidence of synoptic configurations similar to those seen during the event. and larger scale patterns of climate change and variability.

3.7. Conclusions

An extreme melt event occurred on John Evans Glacier on 28-30 July 2000. As a result of the synoptic conditions associated with the event. airflow was routed over the northern sections of the Greenland ice sheet. resulting in strong north-easterly winds on the east coast of Ellesmere Island. Increased air temperatures and a sudden drop in relative humidity accompanied the strong winds at JEG.

The event had a significant impact on glacier melt. accounting for approximately 15% of total seasonal melt at the MWS. and 30% at the UWS. Enhancement of the melt rates was attributable largely to an increase in the turbulent heat fluxes. but at the UWS the contribution of net radiation to melt energy also increased due to snow-albedo feedback. The extreme melt event generated peak seasonal runoff. and removed the cryoconite layer from the surface of the glacier. Depending on the time of year at which such events occur. they may have a major impact on the timing and magnitude of summer ablation and runoff. the development of the englacial/subglacial component of glacier drainage systems. and the ecology of subglacial environments and glacially-fed rivers. Variability in the occurrence of such events may also be a significant factor in the inter-annual variability and longer-term changes in the mass balance of high Arctic glaciers. and needs to be considered when evaluating the likely response of mass balance to climate change.

The synoptic conditions that created the event are rare. occurring on only 0.1% of days within the 1948-2000 record. They are. however. most common during the summer melt season. and were apparently more frequent in the 1950's and 1980's than in other

47

recent decades. Given that such events can account for a large fraction of summer melt in a relatively short period, they may play an important role in determining the sensitivity of mass balance and runoff to climate changes. It is therefore important to investigate the relationship between the incidence of such events, longer-term climate trends and characteristic modes of climate variability.

3.8. References

Arendt, A. 1999. Approaches to modelling the surface albedo of a high Arctic glacier. Geografiska Annaler 81A(4): 477-487.

Barry, R.G. 1992. Mountain Weather and Climate. New York: Routledge Publishers. 402 pp.

Brock, B.W., N.S. Arnold. 2000. A spreadsheet-based (Microsoft Excel) point surface energy balance model for glacier and snow melt studies. Earth Surface Processes and Landforms 25: 649-658.

Copland, L., M. Sharp. 2001. Mapping hydrological and thermal conditions beneath a polythermal glacier with radio-echo sounding. Journal of Glaciology 47: 232-242.

Courtin, G.M., C.L. Labine. 1977. Microclimatological studies on Truelove Lowland. In Truelove Lowland, Devon Island, Canada: A High Arctic Ecosystem. L.C. Bliss, ed. Edmonton: University of Alberta Press, p. 73-106.

Doran, P.T., C.P. McKay, W.P. Adams, M.C. English, R.A. Wharton, M.A. Meyer. 1996. Climate forcing and thermal feedback of residual lake-ice covers in the high Arctic. Limnology and Oceanography 4(15): 839-848.

Flowers, G.E., G.K.C. Clarke. 2002. A multicomponent coupled model of glacier hydrology: 2. Application to Trapridge Glacier, Yukon, Canada. Journal of Geophysical Research – Solid Earth 107(B11): 2288. DOI:10.1029/2001JB001124

Fountain. A.G. 1996. Effect of snow and firn hydrology on the physical and chemical characteristics of glacial runoff. Hydrological Processes 10: 509-521.

Gordon. S.. M. Sharp. B. Hubbard. C.C. Smart. B. Ketterling. I. Willis. 1998. Seasonal reorganization of subglacial drainage inferred from measurements in boreholes. In Glacier Hydrology and Hydrochemistry. M. Sharp. K. Richards. and M. Tranter. eds. Chichester: John Wiley and Sons. p. 239-267.

Heppenstall. K.E. 2001. Chemical Weathering in a Glaciated Carbonate Catchment. Canadian High Arctic: Implications for Subglacial Hydrology. M.Sc. thesis. University of Alberta: 118 pp.

Konzelmann. T.. R. Braithwaite. 1995. Variations of ablation. albedo and energy balance at the margin of the Greenland ice sheet. Kronprins Christian Land. eastern north Greenland. Journal of Glaciology 41(137): 174-182.

McGregor. G.R.. G.E. Petts. A. Gurnell. A.M. Milner. 1995. Sensitivity of alpine stream ecosystems to climate change and human impacts. Aquatic Conservation: Marine and Freshwater Ecosystems 5: 233-247.

Nienow. P.. M. Sharp. I. Willis. 1998. Seasonal changes in the morphology of the subglacial drainage system. Haut Glacier D'Arolla. Switzerland. Earth Surface Processes and Landforms 23: 825-843.

Paterson. W.S.B. 1994. The Physics of Glaciers. Oxford: Pergamon Press. 480 pp.

Reeh. N. 1991. Parameterization of melt rate and surface temperature on the Greenland Ice Sheet. Polarforschung 59(3): 113-128.

49

Sharp. M.. J. Parkes. B. Cragg. I.J. Fairchild. H. Lamb. M. Tranter. 1999. Widespread bacterial populations at glacier beds and their relationship to rock weathering and carbon cycling. Geology 27: 107-110.

Skidmore. M.L.. M.J. Sharp. 1999. Drainage system behaviour of a high Arctic polythermal glacier. Annals of Glaciology 28: 3-12.

Skidmore. M.L.. J.M. Foght. M.J. Sharp. 2000. Microbial life beneath a High Arctic glacier. Applied and Environmental Microbiology 66: 3214-3220.

Vincent. W.F.. J.A.E. Gibson. R. Pieniitz. V. Villeneuve. P.A. Broady. P.B. Hamilton. C. Howard-Williams. 2000. Ice shelf microbial ecosystems in the high Arctic and implications for life on Snowball Earth. Naturwissenschaften 87(3): 137-141.

3.9. Tables

Table 3.1. Meteorological station setup on John Evans Glacier.

Instrument	Location on Mast
LI200s Li-Cor Pyranometer	Mast 1: on vertical pole on south end of crossarm. 1.80 m above snow. parallel to slope and pointed up
Kipp and Zonen Pyranometer	Mast 1: on vertical pole on south end of crossarm. 0.8 m above snow. parallel to slope and pointed down
HMP 35CF Vaisala RH/Temperature	Mast 1: housed in RM Young 12-Plate Gill radiation shield (1.25 m)
RM Young 05103 Wind Monitor	Mast 1: on vertical pole on north end of crossarm (1.75 m above snow)
Vaisala PTB101 Barometric Pressure (MWS only)	Mast 1: in peli-case datalogger enclosure
REBS Q7 net radiometer	Mast 2: 0.80 m above snow. facing south
Campbell Scientific UDG01	Mast 2: 0.91 m above snow (MWS). 1.45 m above snow (LWS): mounted at end of crossarm

51

Table 3.2. Input parameters for each run of the energy balance model.

Parameter	MWS	UWS
Latitude	79.67	79.71
Longitude	-74.35	-74.56
Reference longitude	-75	-75
Summertime (hrs)	1	1
Elevation	824 m	1183 m
Roughness length	0.001 m	0.0005 m
Met stn elevation	824 m	1183 m

Table 3.3. Input parameters for the first roughness sensitivity test. Note that albedo values are shown only to indicate the basis for selected roughness values, and are not used in the model. Roughness values from Paterson (1994: p. 63).

MWS			UWS		
	Albedo			**Albedo**	
sub-period (JD)	**(≥0.6 = snow; <0.6 = ice)**	**roughness (m)**	**sub-period (JD)**	**(≥0.6 = snow; <0.6 = ice)**	**roughness (m)**
161-170	0.60	0.0007	161-170	0.79	0.00055
171-192	0.52	0.001	171-184	0.66	0.0008
193-194	0.76	0.0005	185-206	0.86	0.0001
195-202	0.62	0.00075	207-209	0.76	0.0005
203-209	0.54	0.001	210-214	0.56	0.001
210-214	0.42	0.002		**WEIGHTED AVG 0.0005**	
	WEIGHTED AVG 0.001				

52

Table 3.4. Input parameters for second roughness sensitivity test. Note that albedo values are shown only to indicate the basis for selected roughness values, and are not used in the model. Roughness values from Paterson (1994; p. 63).

MAXIMUM ROUGHNESS VALUES

MWS			UWS		
sub-period (JD)	albedo (≥0.6 = snow; <0.6 = ice)	MAX roughness (m)	sub-period (JD)	albedo (≥0.6 = snow; <0.6 = ice)	MAX roughness (m)
161-170	0.60	0.007	161-209	0.74	0.007
171-192	0.52	0.06	210-214	0.56	0.06
193-202	0.69	0.007		WEIGHTED AVG 0.012	
203-214	0.48	0.06			
	WEIGHTED AVG 0.041				

MINIMUM ROUGHNESS VALUES

MWS			UWS		
sub-period (JD)	albedo (≥0.6 = snow; <0.6 = ice)	MIN roughness (m)	sub-period (JD)	albedo (≥0.6 = snow; <0.6 = ice)	MIN roughness (m)
161-170	0.60	0.001	161-209	0.74	0.001
171-192	0.52	0.01	210-214	0.56	0.01
193-202	0.69	0.001		WEIGHTED AVG 0.002	
203-214	0.48	0.01			
	WEIGHTED AVG 0.007				

53

3.10. Figures
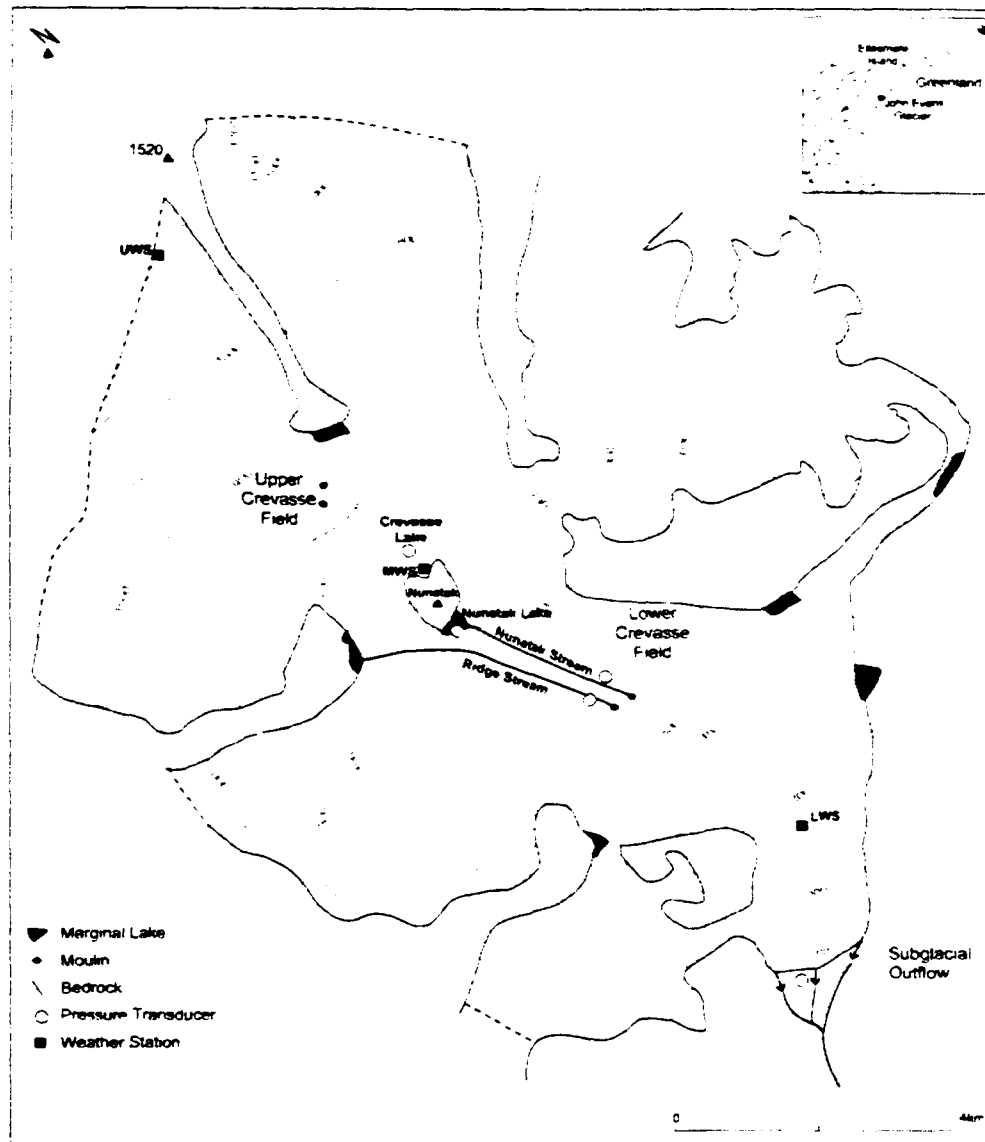
Figure 3.1. Site map of John Evans Glacier. Inset map shows study site location: main map indicates location of meteorological and hydrological stations. and of supraglacial streams that connect to the englacial/subglacial drainage system via crevasses.

54
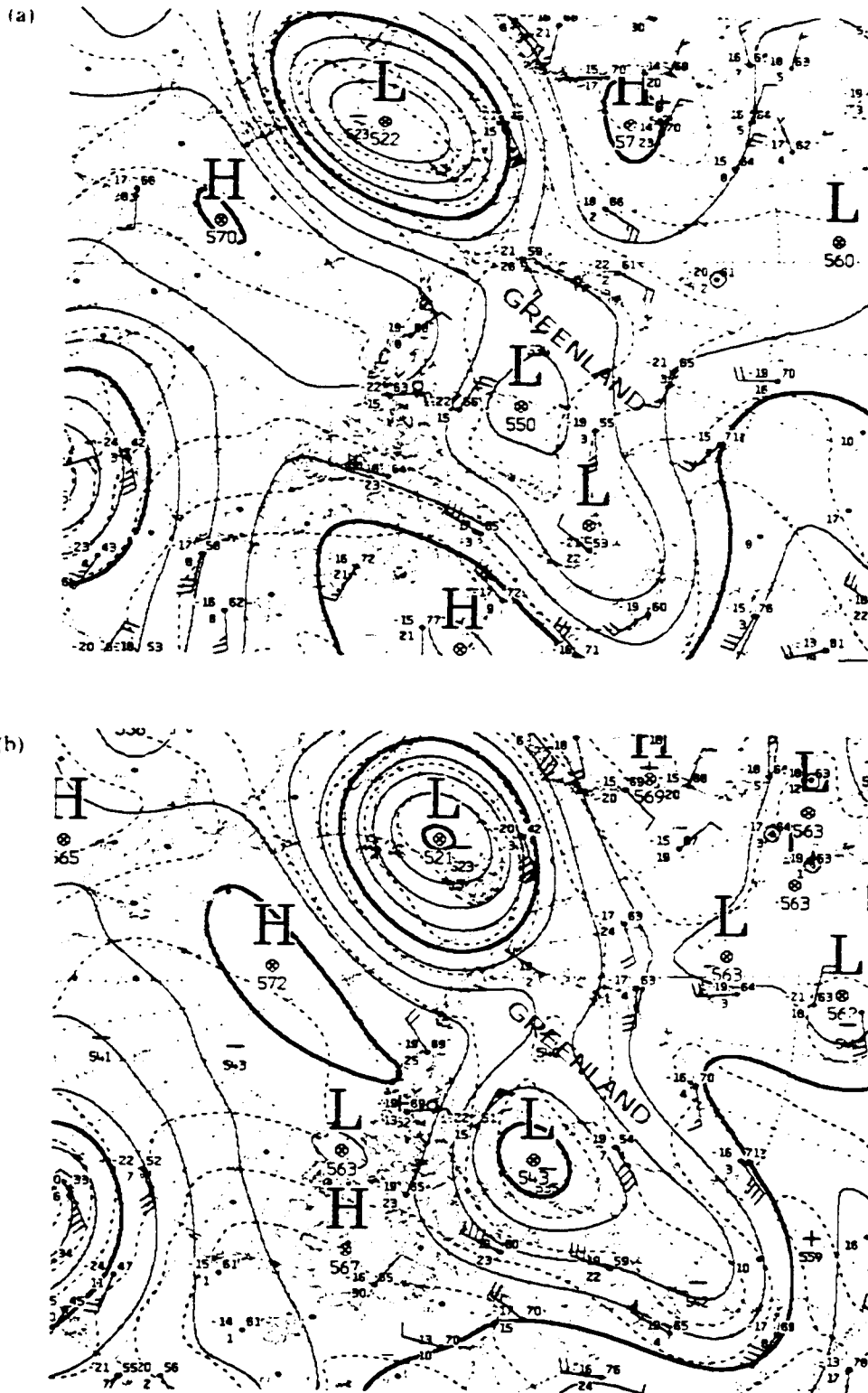
Figure 3.2. 500 mb geopotential heights on (a) 28 July and (b) 29 July. 2000 from the Meteorological Service of Canada. Greenland is labelled: John Evans Glacier is marked with a dot.

(a)

(b)

(c)
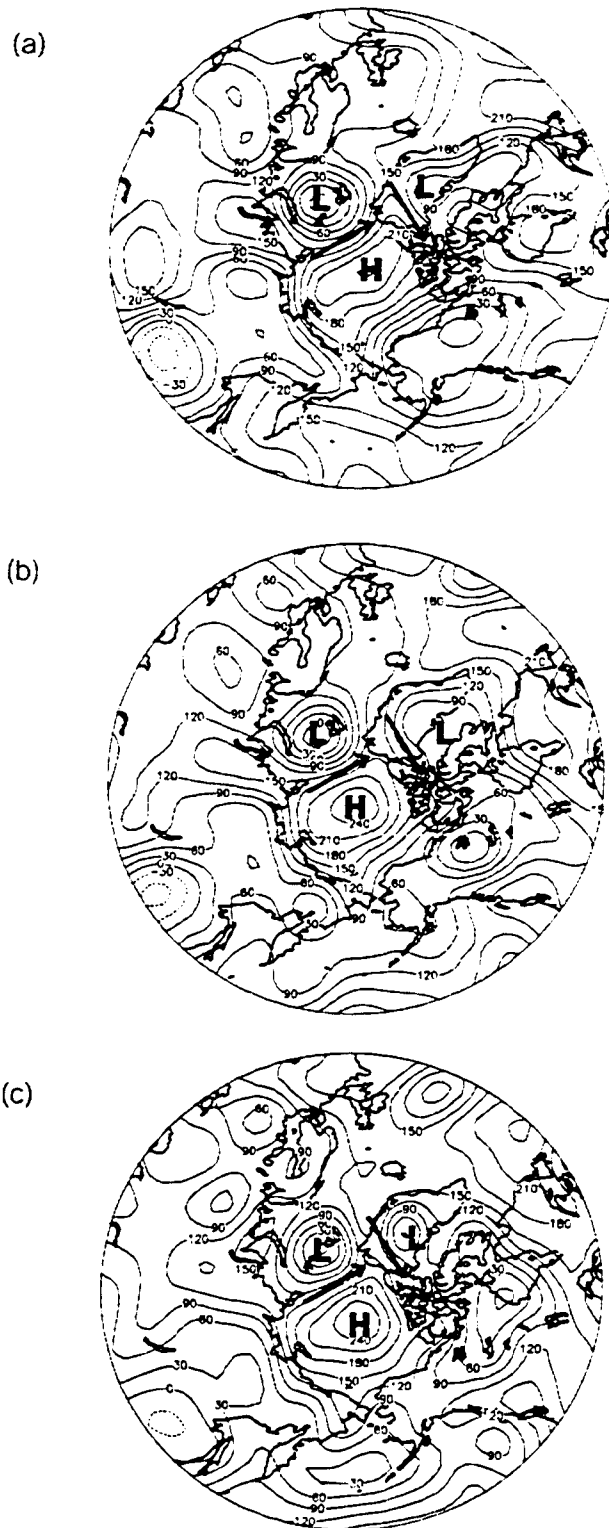
Figure 3.3. 1000 mb geopotential heights on (a) 28 July, (b) 29 July, and (c) 30 July, 2000 from the NCEP Re-analysis. Pressure centres are labelled: L=low, H=high; direction of flow is marked by the arrows.

56
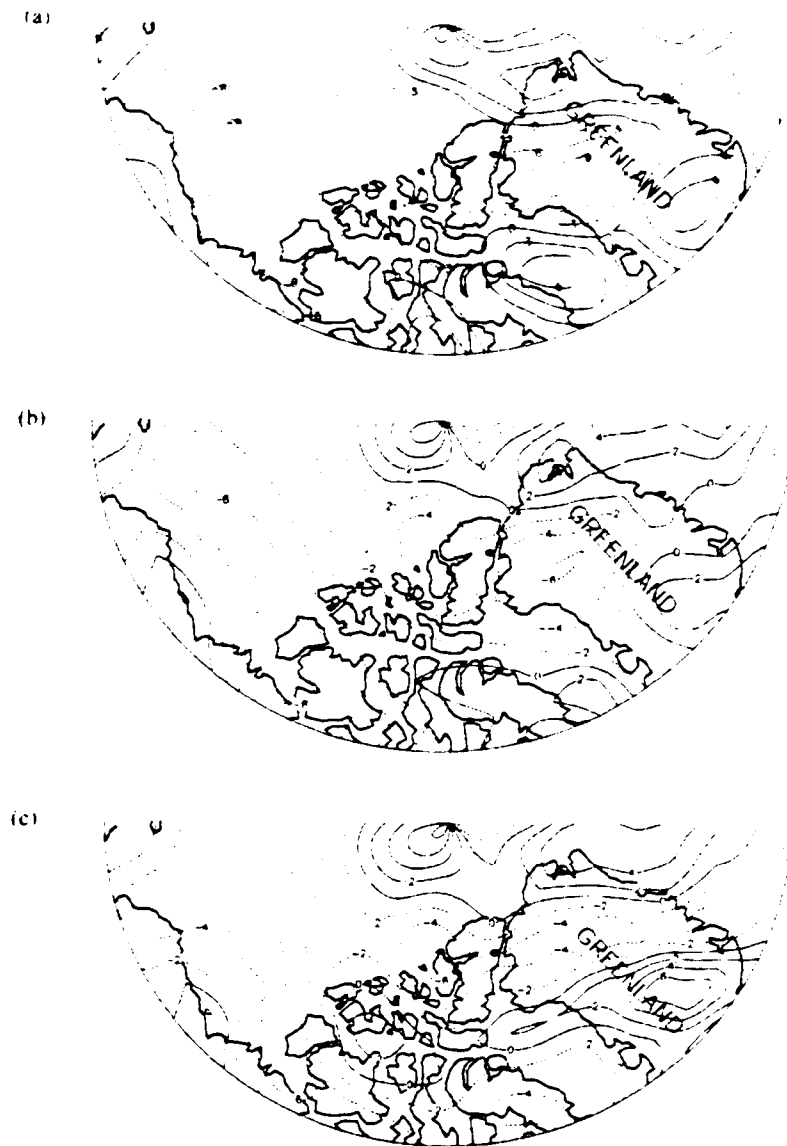
Figure 3.4. Surface u (E-W component of the wind) wind speed (m s^{-1}) on (a) 28 July, (b) 29 July, and (c) 30 July, 2000 from the NCEP Re-analysis. Negative values indicate easterly winds; positive values indicate westerly winds. Greenland is labelled; John Evans Glacier is marked with a dot.

57
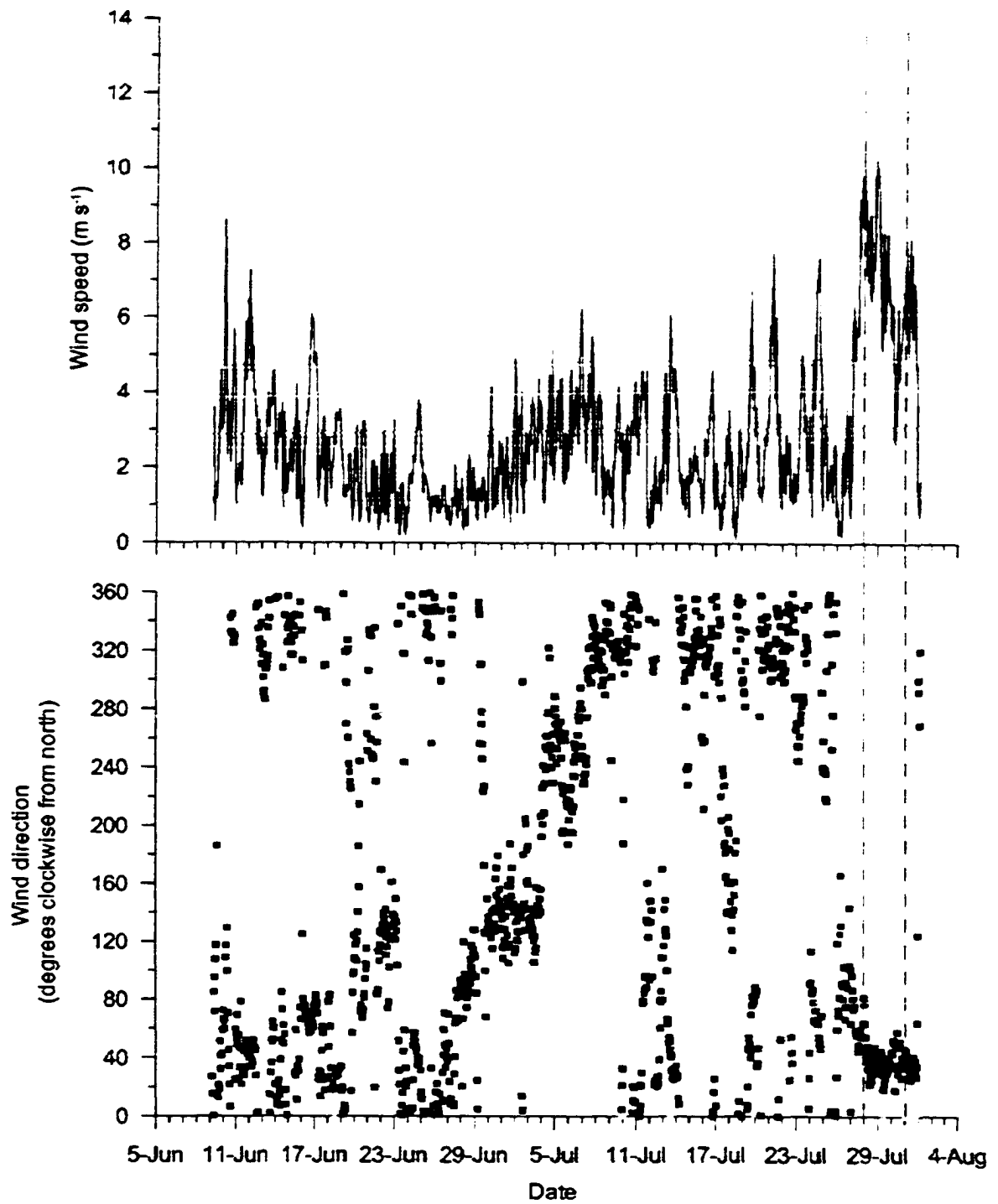
Figure 3.5. Wind speed (m s^{-1}) and direction at the MWS (grey) and the UWS (black). The dashed lines mark the period of the event.
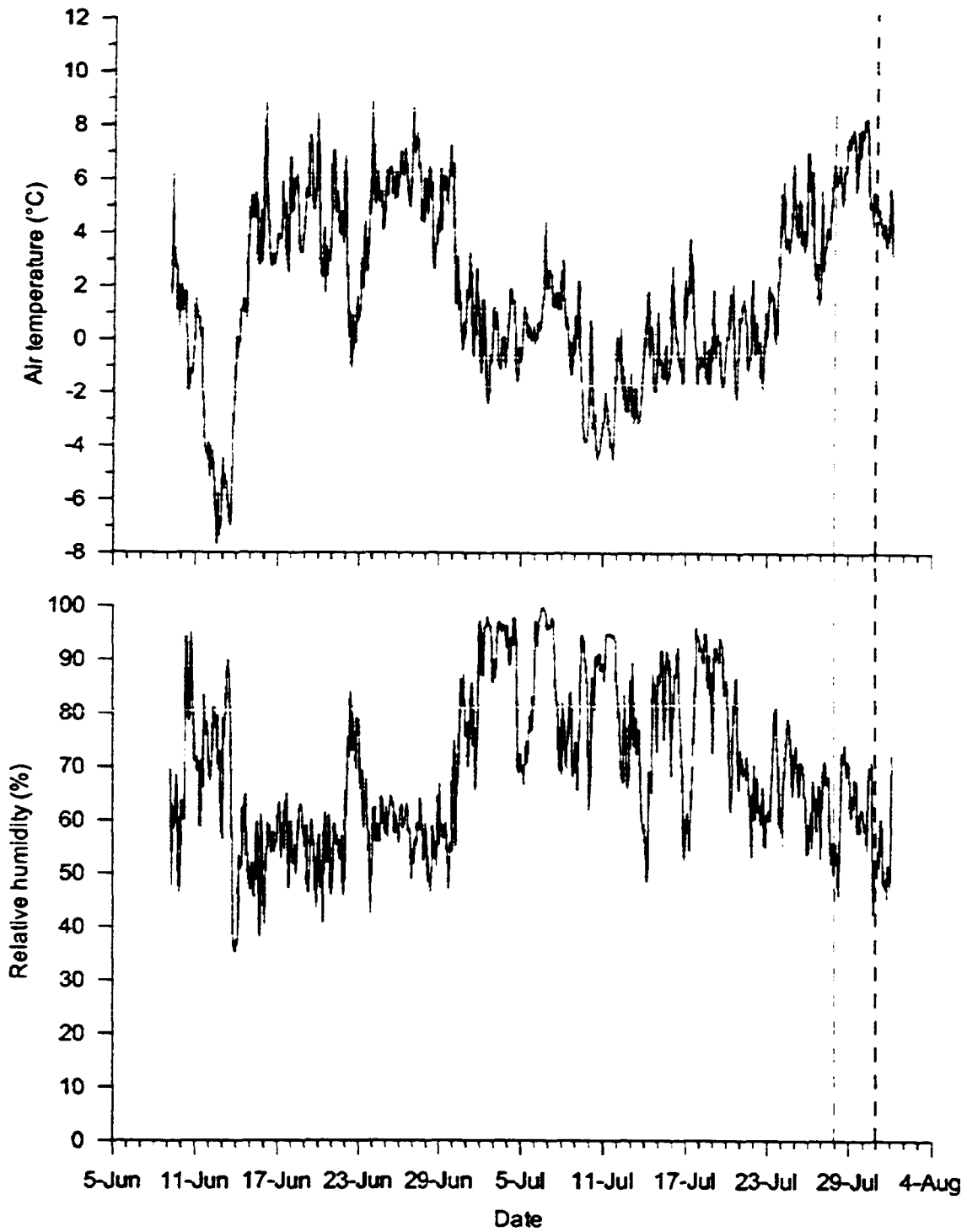
Figure 3.6. Temperature (°C) and relative humidity (%) at the MWS (grey) and the UWS (black). The dashed lines mark the period of the event.
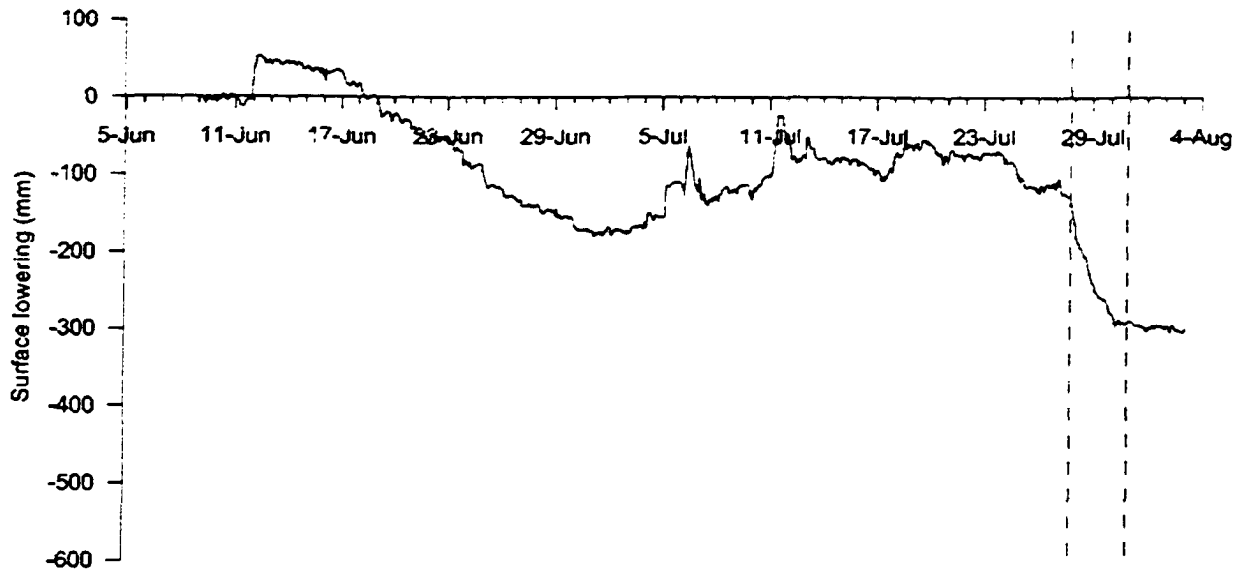
Figure 3.7. Ultrasonic depth gauge (UDG) records of surface lowering (mm) at the MWS (grey) and the UWS (black). The dashed lines mark the period of the event.

60
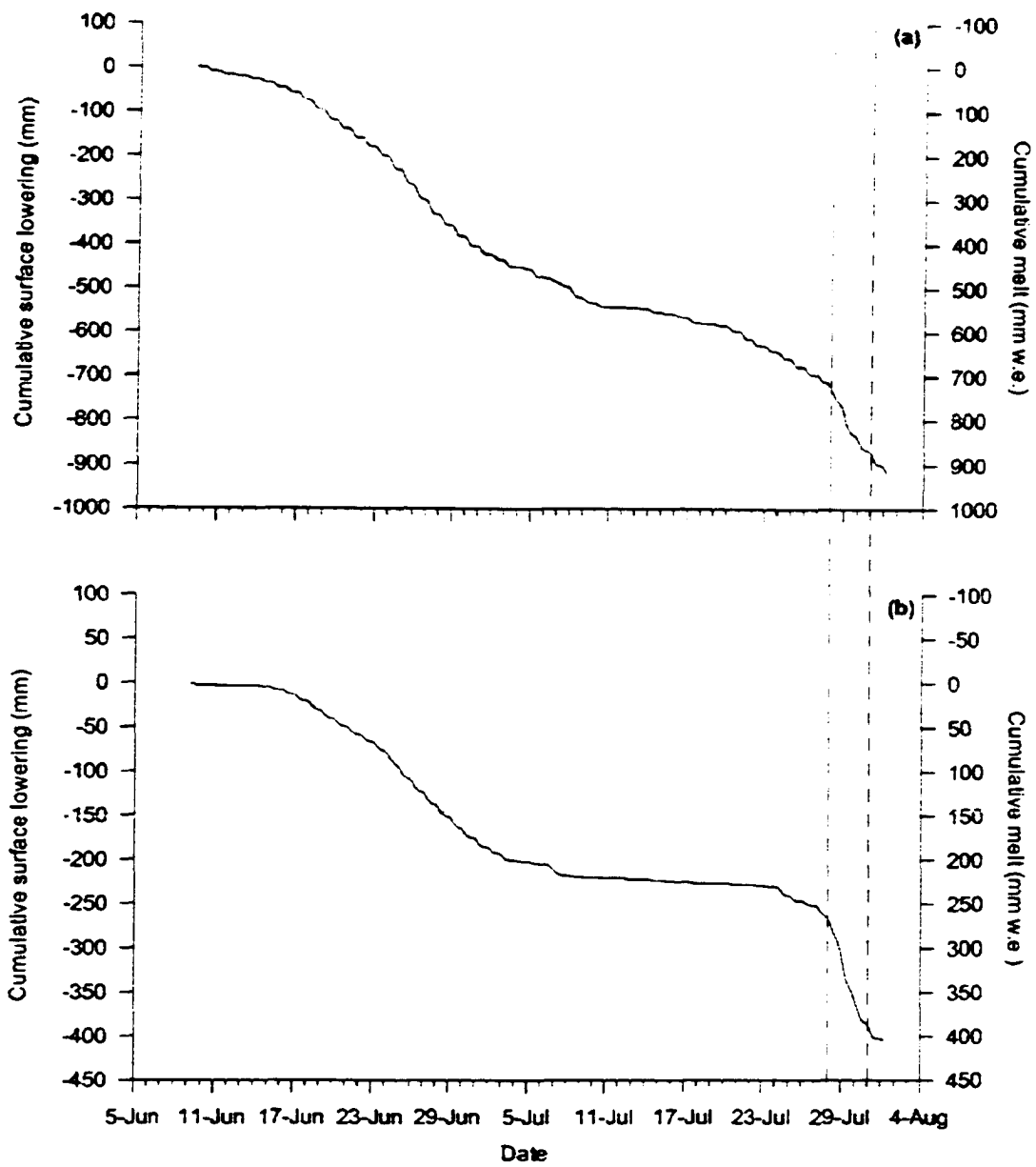
Figure 3.8. Surface lowering (grey) and calculated cumulative melt (black) at the (a) MWS and (b) UWS. The dashed lines mark the period of the event.

61

SHF (mm w.e. hr⁻¹)

3
2.5
2
1.5
1
0.5
0
-0.5
-1

(a)

0.8
0.6
0.4
0.2
0
-0.2
-0.4
-0.6
-0.8
-1

LHF (mm w.e. hr⁻¹)

(b)

3

2

1

0

-1

-2

Q* (mm w.e. hr⁻¹)

(c)

5-Jun 11-Jun 17-Jun 23-Jun 29-Jun 5-Jul 11-Jul 17-Jul 23-Jul 29-Jul 4-Aug

Date
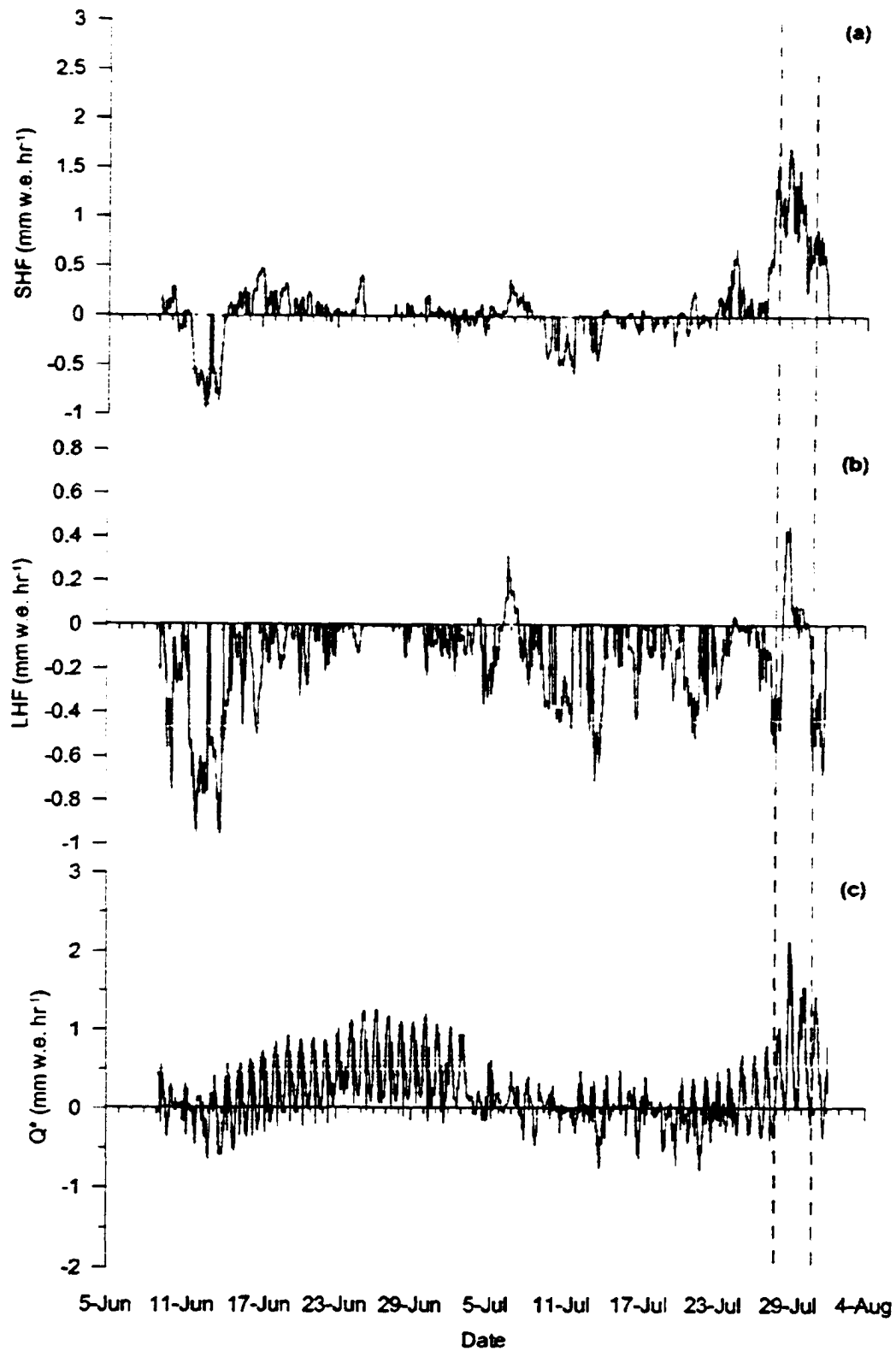
Figure 3.9. Contributions of (a) SHF. (b) LHF. and (c) Q* to melt at the MWS (grey) and the UWS (black). The dashed lines mark the period of the event.

62
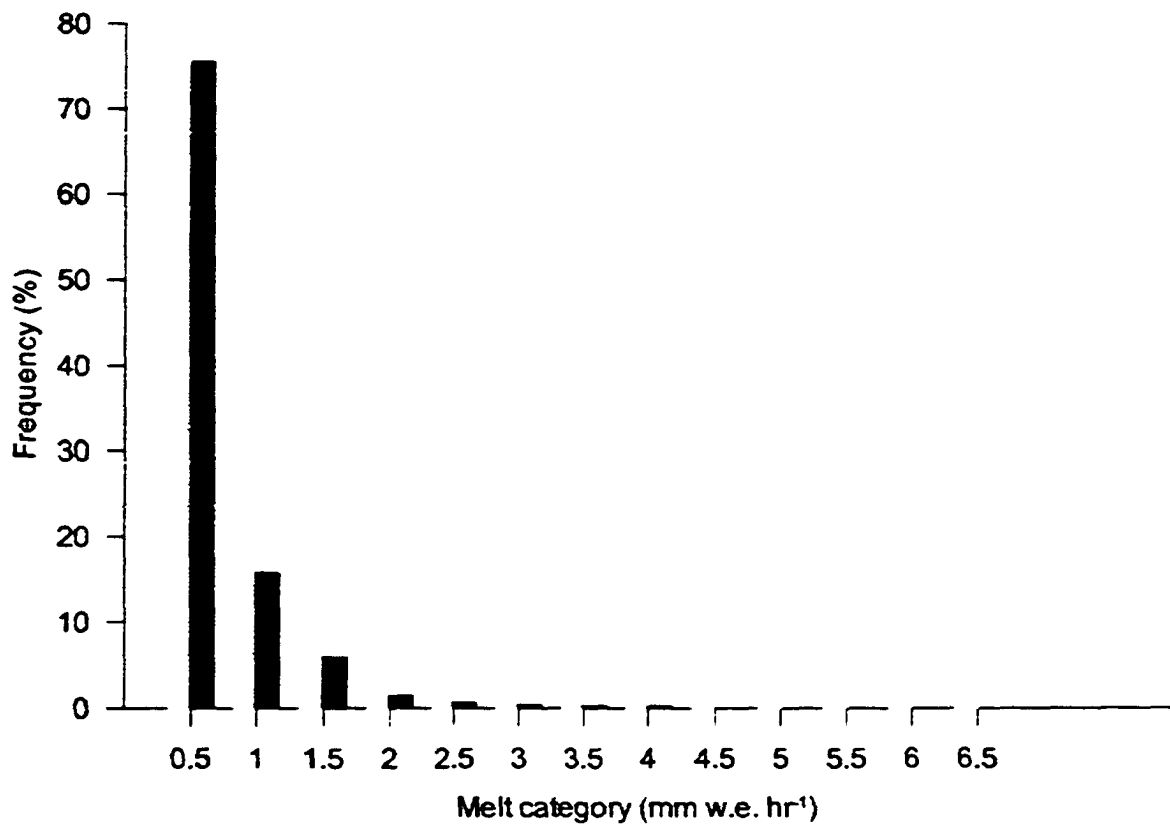
Figure 3.10. Frequency distribution of calculated hourly melt amounts in 2000 for the MWS (grey) and the UWS (black).
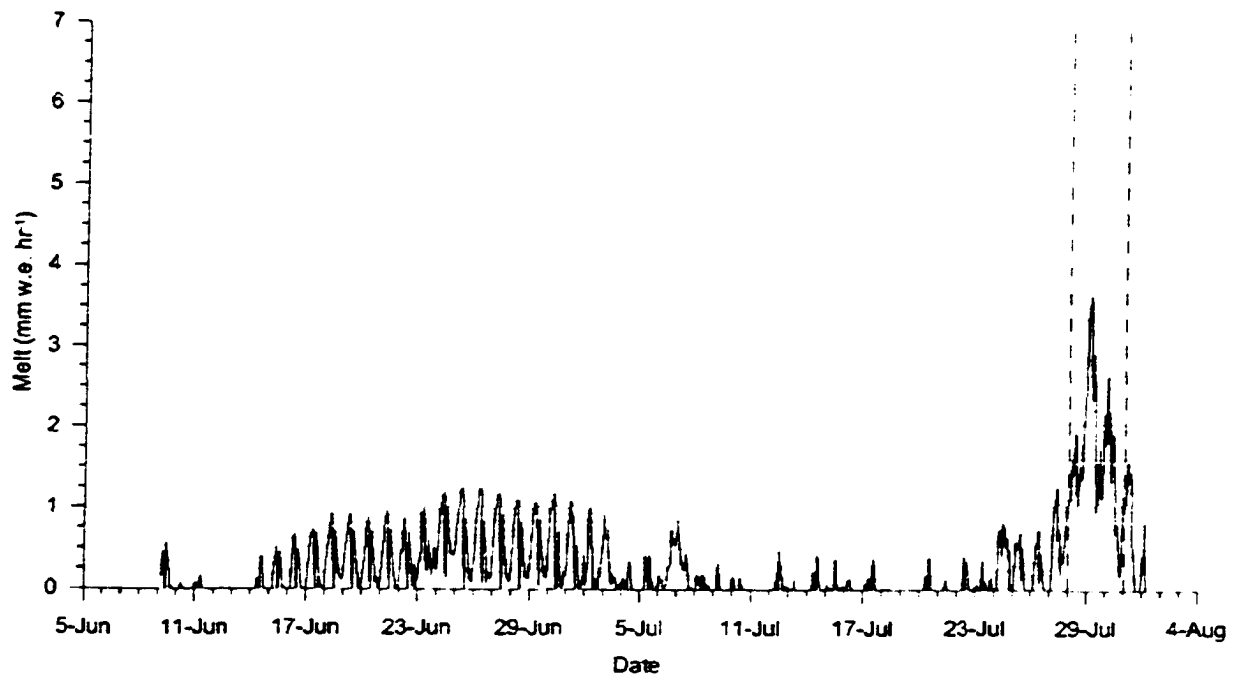
Figure 3.11. Calculated total-season melt at the MWS (grey) and the UWS (black). The dashed lines mark the period of the event.
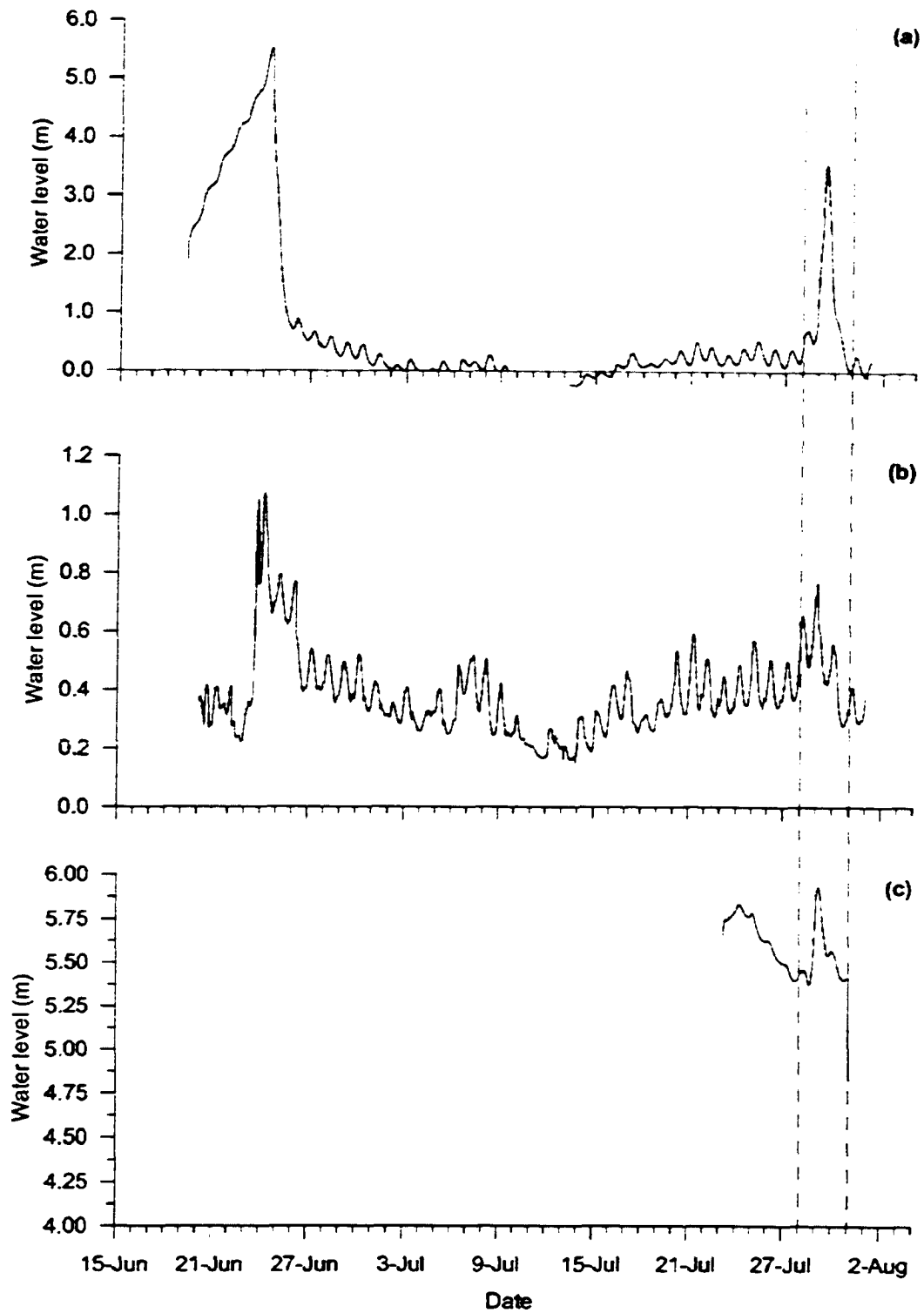
Figure 3.12. Water level (transducer) records from the (a) Nunatak Lake. (b) Ridge Stream. and (c) Crevasse Lake. The dashed lines mark the period of the event.

65
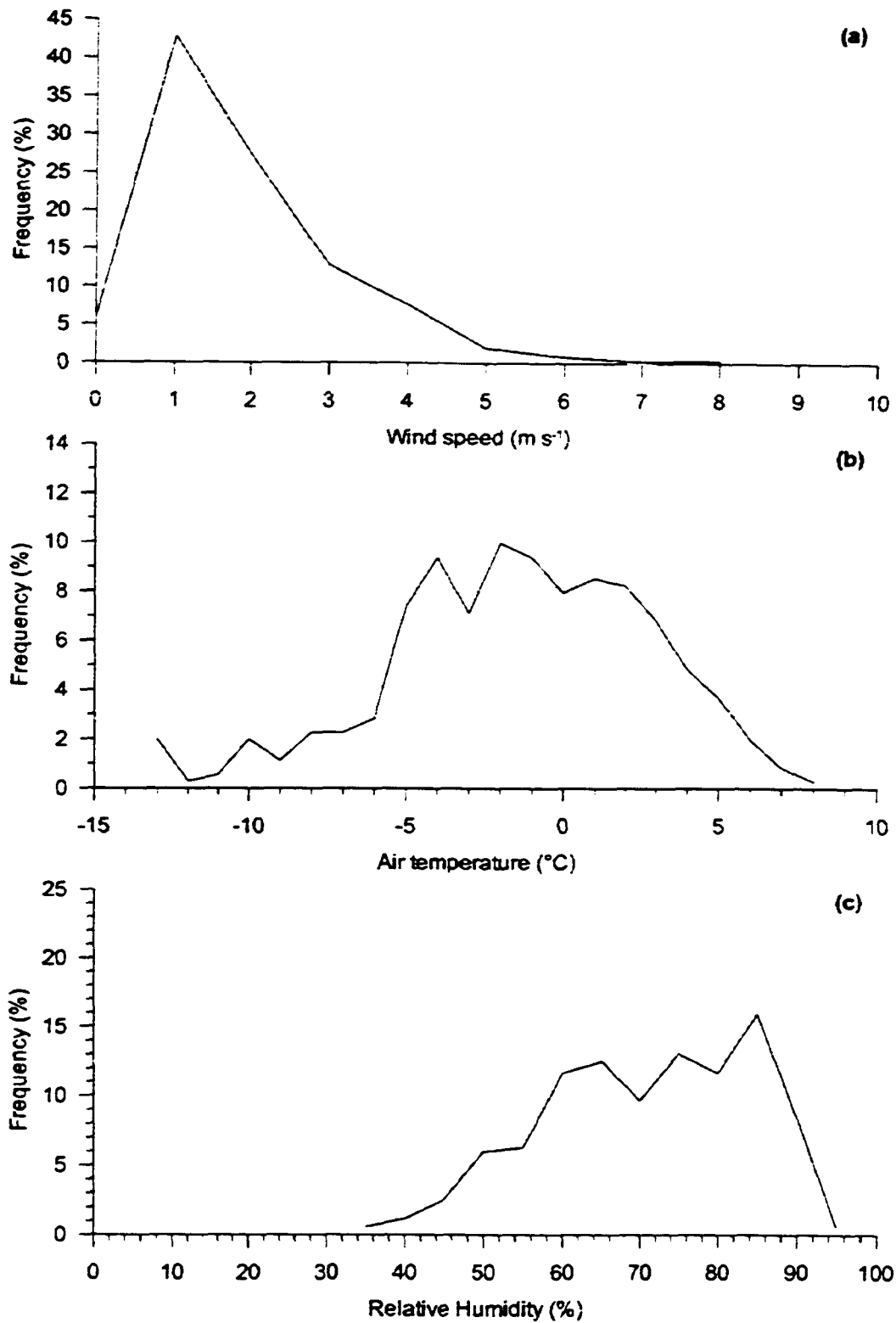
Figure 3.13. Frequency distribution of mean daily (a) wind speed. (b) temperature. and (c) relative humidity. calculated from MWS (grey) and UWS (black) data collected at the study site between 1996-2000.

66
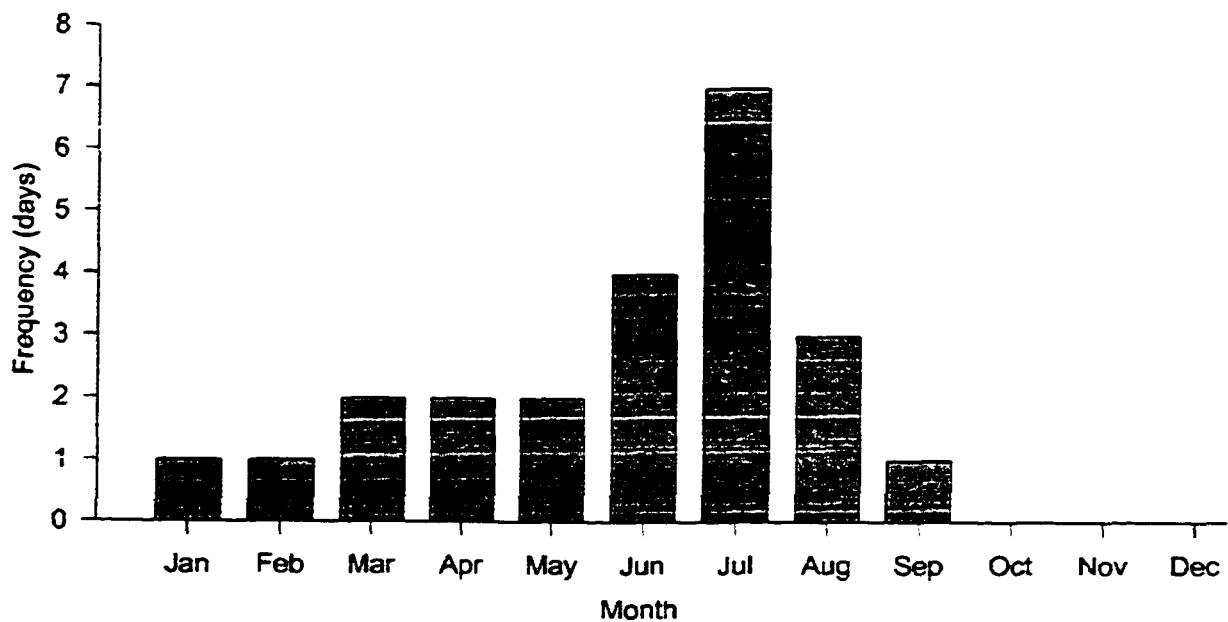
Figure 3.14. Monthly frequency distribution of synoptic conditions for the period 1948-2001 similar to those which generated the extreme melt event, based on Keimig's (unpub. data) synoptic classification.
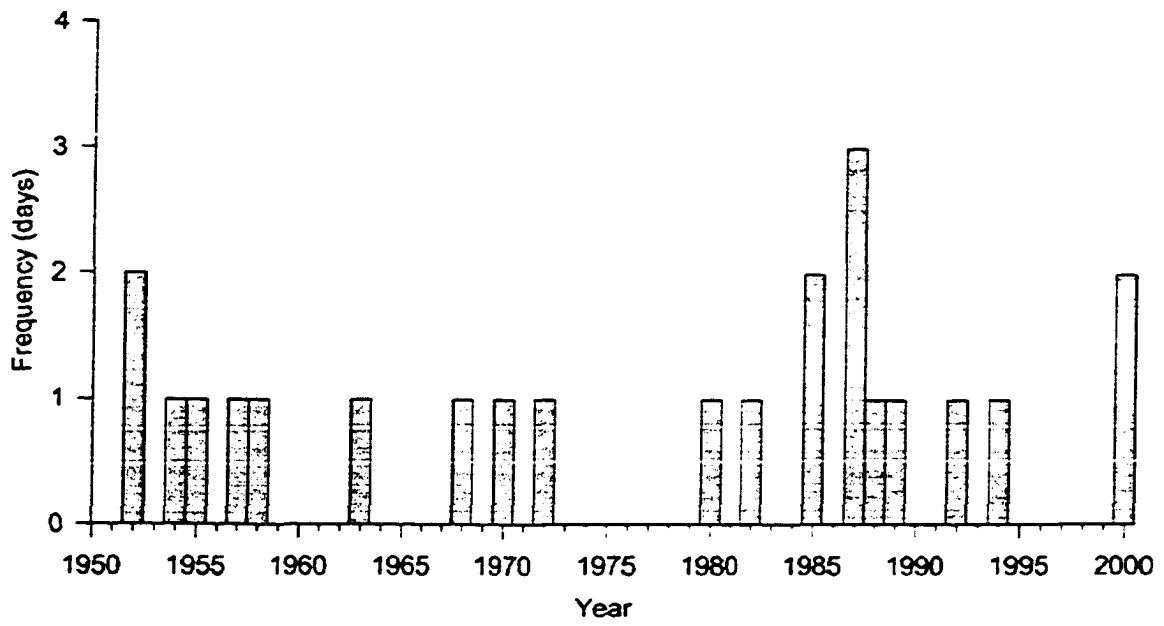
Figure 3.15. Annual frequency distribution of synoptic conditions for the period 1948-2001 similar to those that generated the extreme melt event, based on Keimig's (unpub. data) synoptic classification.
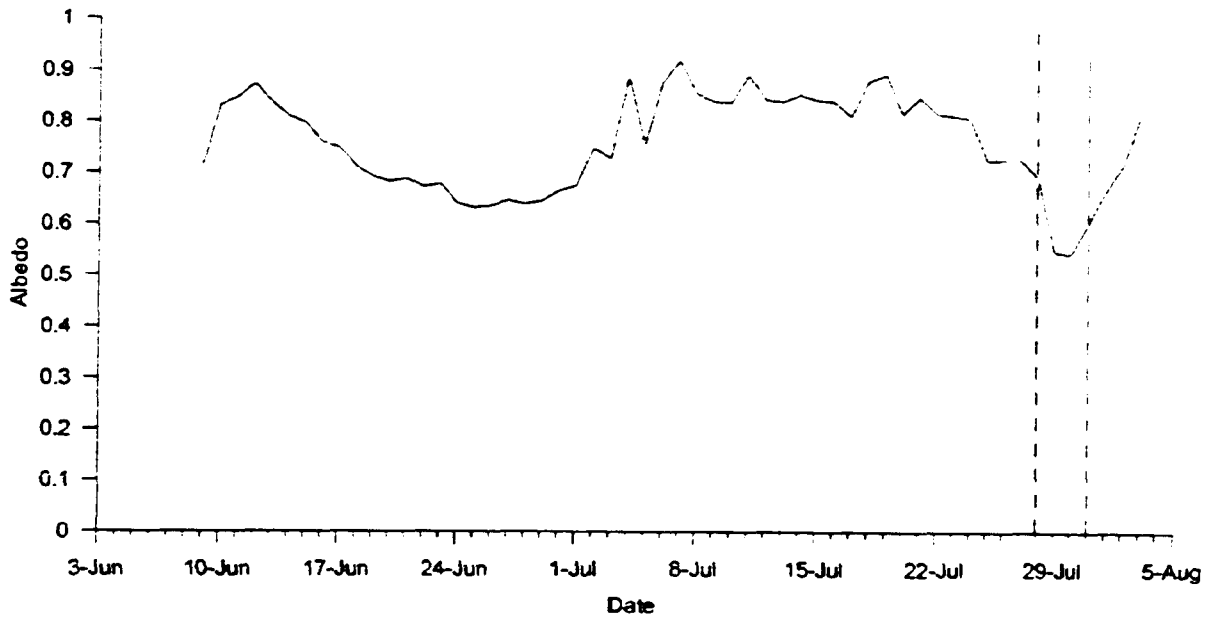
Figure 3.16. Calculated albedo at the MWS (grey) and the UWS (black). 2000. The dashed lines mark the period of the event.

CHAPTER 4.

A 6-YEAR METEOROLOGICAL RECORD FROM A HIGH ARCTIC GLACIER: IMPLICATIONS FOR MASS BALANCE MODELLING*

4.1. Introduction

Climate models predict that anthropogenic climate warming will be greatest in northern high latitudes (Boer et al., 2000; Holland and Bitz, 2003), and there is an increasing amount of evidence to indicate that changes similar to those predicted are already occurring (Serreze et al., 2000; Morison et al., 2000; Moritz et al., 2002). The projected warming will likely have a significant impact on the mass balance (MB) of Arctic glaciers (Dowdeswell et al., 1997).

While the MB response of alpine glaciers to climate change is relatively well understood (e.g., Braun et al., 2000), the processes controlling the MB response of Arctic glaciers are more complex (Pfeffer et al., 1991; Rabus and Echelmeyer, 1998; van der Veen, 2002). The Arctic experiences a very short but intense melt season that is offset by a long and relatively cold winter, resulting in low absolute values of both melt and accumulation. Arctic glacier net MB is therefore highly sensitive to relatively small changes in rates of winter accumulation and summer melt.

Glacier MB response to climate is often investigated using degree-day models (DDMs) (Bøggild et al., 1994; Jóhannesson, 1997; Braithwaite and Zhang, 1999), which are most useful when available meteorological datasets are limited, and/or where MB must be determined on a large scale (i.e., for a large glacier, ice cap, or ice sheet). DDMs rely on a simple linear relationship between air temperature and ablation (Braithwaite, 1984; Braithwaite, 1995; Ohmura, 2001; Hock, 2003), where the factor of proportionality is the degree-day factor (DDF: in m WE d^{-1} °C), which varies according to surface type (snow or ice) (Hock, 1999; Singh et al., 2000). At the beginning of a model run, the end-of-winter snowpack measured at a single meteorological station is distributed across the glacier surface. Air temperature is extrapolated across the glacier from the same meteorological station, melting the snowpack at the specified rate for snow (DDF_{snow}).

70

Once the snow is removed. the surface is melted at the specified rate for ice (DDF_{ice}). The process continues until air temperature becomes negative. and the summer melt and EOW snowpack are summed to determine the annual MB.

Two aspects of DDMs. however. remain problematic. First. they follow two basic assumptions that may not hold true at a given study site: (a) a constant air temperature lapse rate exists between a meteorological station and all points on a glacier (usually the moist adiabatic lapse rate (MALR): -6°C km^{-1}) (Jóhannesson. 1997: Greuell and Böhm. 1998: Braithwaite and Zhang. 2000): and. (b) a constant accumulation lapse rate exists between a meteorological station and all points on a glacier (usually increasing with elevation) (Jóhannesson. 1997: Hock. 2003). Second. variables other than air temperature are important in the climate-MB relationship (Greuell and Genthon. 2004). Several modelling studies have attempted to improve DDM output by incorporating solar radiation (Hock. 1999) or surface albedo (Arendt and Sharp. 1999). but wind (Hock. 2003) or summer snowfalls (Fujita and Ageta. 2000) may also be important.

Given the high sensitivity of Arctic glacier MB to relatively small changes in absolute accumulation and ablation. therefore. these problems must be addressed prior to conducting modelling studies. Field data are therefore required to determine: (a) the validity of specific model assumptions at Arctic glaciers: and. (b) whether all meteorological conditions that significantly impact seasonal MB on Arctic glaciers are adequately incorporated in DDMs. However. the scarcity of long-term climate records for Arctic glaciers results in a lack of detailed meteorological data with which to answer these questions.

We use a 6-year (1996-2002) meteorological record from three automated weather stations situated on a single glacier in the Canadian high Arctic to investigate spatial and temporal variability in net annual surface elevation change. Variability in wind speed and air temperature. and related derived variables (i.e.. winter wind scour events: summer wind and snowfall events: melt season length. strength and intensity). are examined in terms of their relative impact on net annual surface elevation change. We then examine the role of seasonal synoptic conditions in driving surface processes. Finally. we discuss the implications of our results for basic DDM assumptions. and examine how well DDMs represent those processes that significantly impact net annual surface elevation change.

71

4.2.   Study site

John Evans Glacier (JEG) is a large valley glacier on the east coast of Ellesmere Island (79° 40' N and 74° 00' W: Fig. 4.1). It is 15 km in length. covers approximately 75% of a 220 km^2 catchment. and ranges in elevation from 100 to 1500 m a.s.l. (Skidmore and Sharp. 1999). The glacier is polythermal. with cold-based ice in the accumulation area and at the glacier margins where ice is thin. and warm-based ice throughout much of the ablation zone (Copland and Sharp. 2001). Ice thickness reaches a maximum of ~400 m close to the long-term equilibrium line (~750-800 m a.s.l.). and is ~100-200 m in the lower 4 km of the glacier.

Meteorological data have been collected year-round at JEG since June 1996 at three on-ice automatic weather stations (Fig. 4.1). The upper weather station (UWS) is at 1183 m a.s.l. on an exposed plateau in the accumulation zone: the middle weather station (MWS) is at 824 m a.s.l. on a col in an area of diverging glacier flow. and is in the transition area between the long-term mean ablation and accumulation areas: and the lower weather station (LWS) is at 261 m a.s.l. in a confined valley in the ablation area.

4.3.   Methods

4.3.1. Synoptic data

The National Centre for Environmental Prediction's (NCEP) Climate Data Assimilation System (CDAS) daily reanalysis datasets (Kalnay et al.. 1996) from 1968-1996 were used to examine seasonally averaged synoptic conditions over the Arctic region. Seasonal average values of 1000 mb geopotential height were calculated to examine surface conditions. while 500 mb geopotential heights were calculated to examine regional conditions unaffected by surface topography. Seasonal average values of 1000 mb wind speed and direction were also calculated to determine flow directions. and surface air temperature and surface precipitable water were calculated to relate surface conditions with conditions at the 500 mb level. Maps of annual (1996-2002) JJA 500 mb geopotential height anomalies (relative to the 1968-1996 mean) were also plotted to determine the impact of large-scale atmospheric conditions on annual surface conditions.

72

4.3.2. Local meteorological data

During summer field seasons (~21 May – 3 August: 1996-2002). hourly and daily averages of 10-second readings of rates of surface elevation change (UDG). wind speed and direction. air temperature (T). relative humidity (RH). incoming and reflected radiation (K_{in} and K_{out}). net radiation (Q^*). and air pressure (MWS only). were recorded at each station (Table 4.1). The standard deviation of wind direction was also monitored. During the rest of the year (~3 August – 20 May). daily averages of 10-second readings of these variables (except Q^*) were recorded.

The LWS was serviced approximately six times per melt season. the MWS four times. and the UWS twice. Differences in servicing frequency are due to differences in rates of surface lowering at the three stations. Instrument heights were adjusted to maintain an approximately constant height above the melting ice surface (Table 4.1). and generally deviated no more than 0.30 to 0.40 m from the preferred height between servicings. Although adjusting sensor heights may affect air temperature measurements. we assume that the impact is minimal. but we have no data on air temperature variation with elevation above the glacier surface that could be used to correct the air temperature record.

All stations malfunctioned for some portion of the 6-year period between 1996-2002. resulting in incomplete datasets (Table 4.2). During the summer period at the UWS. missing daily data were re-calculated from recorded hourly values. Comparison of measured daily values with daily values calculated from hourly data showed good correspondence in years for which both datasets were available. with the exception of wind direction and standard deviation of wind direction. These variables were therefore not used.

Missing UDG data from 2001 and 2002 were supplemented with snow depths measured in the field (D. Lewis. pers. comm.). Point-based density measurements from the beginning of each melt season were used to determine whether observed EOW snowpack thickness is a good indicator of actual snow water equivalence (SWE). In the absence of continuous density measurements. however. UDG measurements in perennially snow-covered regions of the glacier cannot be converted to direct measurements of mass gain and loss due to the effects of internal refreezing. They do.

73

however, allow determination of the length and magnitude of the accumulation and ablation seasons, and identification of major snowfalls, wind redistribution events, and melt events. These values give some indication of the sign and relative magnitude of annual mass change at each station, and are used to determine the general relationship between annual mass change and specific meteorological events (snowfalls, wind events, etc.).

Winter surface elevation change was calculated from the last day of surface lowering in the previous year to the first day of surface lowering in the present year. Summer surface elevation change was calculated for the period between the first and last day of lowering each year. The effect of wind scour on selection of the onset of summer surface lowering was removed by ensuring correspondence between the first and last lowering dates and the first and last days of positive air temperatures. These values could not be calculated for years for which end-of-season UDG data were unavailable. Net annual surface elevation change was calculated as the sum of summer and preceding winter surface elevation change at each station.

While albedo data are available for the LWS and UWS, K_{out} values at the MWS are problematic from 1999-2002. Albedo data are therefore used in combination with written meteorological observations from each summer field season to identify summer snowfalls. Summer snowfalls could not be determined in 1997 and the beginning of 1998, however, when only daily averages of meteorological data were available, and no researchers were on site to provide visual observations.

Snowfalls were classified as 'summer' if they fell within the bounds of the melt season as defined by the first and last positive degree-day (PDD). In some cases, therefore, a snowfall that occurred at all stations may only be classified as 'summer' at the LWS, as the other stations had not yet had a PDD. This excludes snowfalls that do not interrupt the melt process, by ignoring any snowfalls that occurred before melt began.

Recovery time was calculated as the time required for surface albedo to return to pre-snowfall values, while non-recovery snowfalls were defined as snowfalls from which surface albedo did not recover prior to the next new snowfall. Summer days with elevated albedo were calculated as the sum of all snowfall durations and recovery periods, while

74

the percentage of elevated albedo days was calculated as the total number of summer days with elevated albedo divided by annual melt season length.

Wind speed data from the LWS are not available from 1999-2001 due to a malfunction of the anemometer. At the UWS, winter rime accumulation on the wind sensor is a significant problem. To exclude readings impacted by rime, all UWS wind speed values for periods when the standard deviation of wind direction was between 0 and 10 degrees and the wind speed was less than 1 m s^{-1} were removed. This accounted for 2.2% of all days over the 6-year period for which wind data were available.

Winter wind scour events were defined as decreases in surface elevation (>0.01 m) occurring simultaneously with strong winds (>3 m s^{-1}). Cumulative elevation drop due to wind scour was calculated as the sum of all surface elevation drops during scour events in each winter. Winter wind events are also associated with snowpack thickening due to redistribution from surrounding locations (Winstral et al., 2002). However, wind speed and UDG records are insufficient to differentiate these events from winter blizzards, which cause additional accumulation, rather than redistributing accumulation that is already present. Therefore, winter wind-driven accumulation events were not extracted from the meteorological records. Summer wind events were defined as periods in which wind speeds increased to ≥4 m s^{-1} in combination with either a decrease in surface height, or an increase in air temperature. The threshold wind speed value is one standard deviation greater than the monthly mean July wind speed at the UWS, thus ensuring that only extreme values are selected at each station.

As the deviations of monthly mean air temperature from the 6-year monthly mean are similar at each station, they were combined into a single averaged record to facilitate interannual comparisons. Melt season strength was calculated as the sum of all positive daily mean air temperatures (positive degree-days: PDDs). Melt season length was calculated as the time between the first and last PDD each year. In cases where the final PDD followed the previous PDD by more than three days, the previous PDD was taken as the last of the melt season. This removes slightly positive air temperatures on days following a period of negative air temperature, which likely have no impact on melt. Melt season intensity was calculated as the PDD total divided by melt season length.

4.4. Results

4.4.1. Regional synoptic setting

Maps of 1000 mb geopotential height indicate that JEG is located in a zone of diverging flow caused by the position and strength of pressure systems over both Greenland and the Baffin region, and the western Arctic and Arctic Ocean (Fig. 4.2). In summer (JJA), a low over Greenland interacts with a low over Baffin Island and a high over the western Arctic to create airflow generally from the east. In the fall (SON), a high forms over Greenland and interacts with the Icelandic low to create south-to-north flow along the west coast of Greenland, and flow from the southeast over JEG. Over winter (DJF), the Greenland high remains strong while the Icelandic low deepens, shifting flow slightly from the east-southeast over JEG. In spring (MAM), both the Icelandic low and the Greenland high weaken substantially, but flow over JEG remains from the east.

Mean surface winds extracted from the NCEP Reanalysis, and mean flow directions inferred from the geopotential height maps, indicate that winds flow generally from the southeast over northern Ellesmere Island and from the northeast over southern Ellesmere Island, but are weaker and highly variable over the JEG region.

At the 500 mb geopotential height level, the dominant feature is the low-pressure centre of the Polar Vortex (Fig. 4.3). The Vortex is at its weakest in summer, when it is centred over the Arctic Ocean. Pressure gradients are relatively weak, and flow is generally from the southwest over JEG. A deep trough develops along the west side of the Baffin Bay area, and a weak ridge stretches from southeast to northwest Greenland. In fall, the Vortex intensifies: pressure gradients increase, but flow remains from the southeast over JEG. The trough deepens and moves west, over the western QEI, while the ridge weakens. The Vortex is at its deepest during the winter months, when it moves south and is centred over northern Baffin Island, with very strong pressure gradients, and flow from the south over JEG. The trough remains in the same location, although slightly weakened, while the ridge doesn't change. The Vortex weakens in the spring: pressure gradients are not as intense, and the Vortex centre moves northward. Flow remains from the south over JEG. The trough moves slightly east again while the ridge remains the same.

76

Seasonal average surface air temperature and precipitable water follow a seasonal cycle related to the shifting position of the Polar Vortex (Table 4.3). Winter experiences the lowest temperatures and minimum precipitable water in association with the maximum extent of the Vortex. Summer experiences the highest temperatures and greatest amount of precipitable water in association with the minimum extent of the Vortex.

The study site is also affected by cyclonic activity in the Baffin Bay region. Cyclones formed in this area occasionally move northwards, through Nares Strait along the east coast of Ellesmere Island. Air masses from Baffin Bay often cross the Thule peninsula (Greenland) prior to reaching JEG, thereby warming at the dry adiabatic lapse rate as they descend into the JEG area. and bringing little precipitation. Cyclonic activity is greatest in winter. and decreases in the summer (Maxwell. 1980).

Surface pressure at JEG is highest (~942 mb at the MWS) between mid-May and the end of July. Pressure drops from August to December. reaching a minimum (~910 mb at the MWS) in January and February. This pressure cycle corresponds closely with that recorded in Baffin Bay (Barber et al.. 2001. their Fig. 3b).

4.4.2. Spatial variability in local meteorological conditions

4.4.2.1. Surface elevation change

Annual surface elevation change is greatest at the LWS (Fig. 4.4a). Between June 1996 and July 2002. the glacier surface dropped ~8.7 m at the LWS. ~3.1 m at the MWS. and ~0.4 m at the UWS. Although the UWS is normally located in the accumulation zone. it experienced net surface lowering due mainly to substantial net lowering in 1998 and 1999.

The LWS has the most winter surface elevation gain. while the UWS has the least (Fig. 4.4b). At the LWS. September-October and March-April are the main periods of surface elevation gain. Winter accumulation at the LWS is generally unaffected by strong winds. as surface elevation continues to increase from December-February. At the MWS and UWS. however. surface elevation gain begins earlier (August). and ends later (May) than at the LWS. Minimal surface elevation gain and/or surface lowering between January and March likely reflect wind reworking and compaction of the fall snowpack.

77

and coincide with the period during which these stations experience the greatest wind speeds (Fig. 4.5).

Summer surface lowering amounts are the greatest at the LWS (Fig. 4.4b), which also has the longest lowering period and sees the most substantial changes in surface albedo (0.30-0.80: Fig. 4.6). Surface lowering occurs from May-August with an average lowering period of 74 d. Snowmelt begins around the third week of May, and the ice surface is exposed in the 2nd or 3rd week of July. Albedo changes most rapidly in July, as the snowpack ripens and the snowline retreats quickly from the lower part of the glacier.

At the MWS, lowering occurs mainly during June and July, with an average lowering period of 62 d beginning in the first week of June. Field observations indicate that the surface typically remains snow-covered until the 3rd week of July. Superimposed ice, rather than glacier ice, is often exposed at this location. Given the higher albedo of superimposed ice, albedo at the MWS likely does not fall as low as at the LWS, where superimposed ice is thinner and is removed more quickly.

At the UWS, lowering is also concentrated in June and July, with an average lowering period of 53 d beginning in the second week of June. As this station is in the accumulation zone, the rare retreat of the snowline to this location exposes firn, and not ice. Thus the albedo at the UWS remains relatively high (~0.75: Fig. 4.6), and does not vary substantially over the melt season. Variability in the monthly mean rate of summer surface elevation change is highest in May at the LWS and August at the UWS, due to variations in the timing of melt season onset and end (Fig. 4.4b).

On average, the LWS has more summer snowfalls than the MWS and UWS, as it has the longest melt season in which they can occur (Table 4.4). However, the number of non-recovery snowfalls is greatest at the UWS and lowest at the LWS. The average number of summer days with elevated albedo due to summer snow is greatest at the LWS, and lowest at the MWS. As a percentage of total melt season length, however, the number of summer days with elevated albedo is greatest at the UWS.

4.4.2.2. Wind speed and direction

Few wind speed data are available for the LWS. At the MWS and UWS, wind speed follows an annual cycle, with lower monthly mean values from April to October and

78

higher monthly means from November to March (Fig. 4.5). Mean annual wind speed at both stations is 2.4 m s^{-1}. Day-to-day wind speed variability is consistently higher at the UWS than at the MWS, and has a more pronounced annual cycle. Variability reaches a maximum in March at the MWS and April at the UWS, with minima in June at the UWS, and January at the MWS (Fig. 4.5).

Wind direction is least variable at the LWS and most variable at the UWS. Monthly average fall through spring wind direction at the LWS parallels the local valley direction, and is predominantly from the north. Summer directions vary more, with additional winds from the northeast, and from the southeast to southwest.

Wind directions at the MWS vary more than at the LWS, as the station is located near the confluence of several surrounding valleys (Fig. 4.1). As at the LWS, monthly average wind direction is predominantly from the northwest to northeast from fall to spring, but westerly winds occur in spring and summer. Summer wind directions also include southerly and southwesterly components.

The UWS experiences the greatest variety in wind direction of all stations. Located at the head of the glacier on an exposed plateau, it is largely free of topographic influences, and responds more to synoptic-scale conditions. Monthly average wind direction is mainly from the northeast to east in all seasons. Spring and summer show the greatest range in wind direction, with secondary peaks from the south to southeast and the northwest.

4.4.2.3. Air temperature

During the study period (1996-2002), mean annual air temperature was highest at the LWS and lowest at the MWS, and the 6-year range in mean daily air temperature decreased with elevation (Table 4.5). Monthly mean air temperatures at all stations are lowest in January and February, and highest in July (Fig. 4.7). The standard deviation of mean daily air temperature at all stations is highest during the winter months, due to an inversion in air temperatures measured immediately above the glacier surface, which results in higher mean monthly air temperatures at the UWS than at the other stations (Fig. 4.7). Summer (JJA) standard deviations are much lower, likely due to the formation of a stable melting boundary layer directly above the glacier surface.

Air temperature lapse rates are generally larger in the upper part of the glacier than the lower (Fig. 4.7). Lapse rates between the LWS and the MWS are negative for the majority of the year, with the exception of February and March. Lapse rates between the MWS and the UWS, however, are positive from October to April. Summer lapse rates between the LWS and UWS range from 2 to 4°C lower than the constant often assumed in modelling studies (-6.0°C km^{-1}). When calculating monthly average lapse rates from daily averages, it was apparent that daily lapse rates vary significantly over short timescales, often even changing sign.

The melt season is longest, strongest, and most intense at the LWS, and decreases with elevation (Table 4.6). At all stations, the maximum number of melt season PDDs occurs in July, and the minimum in May. The PDD total is most variable during the transition months of May and August at all stations, and least variable in July, as positive air temperatures dominate the middle of the melt season.

4.4.3. Temporal variability in local meteorological conditions

4.4.3.1. Surface elevation change

Snow water equivalent (SWE) is strongly related to snow depth at the end of winter in years for which density measurements are available (Table 4.7). The deepest end-of-winter (EOW) snowpack formed during the winter of 1996-1997, and the shallowest snowpack during the winter of 1999-2000 at all stations (Fig. 4.8). The MWS and LWS had the second deepest snowpack in 2000-2001, while the UWS had an equally deep snowpack to 1996-1997 in the winters of both 1997-1998 and 1998-1999. The elevation gradient of snow depth is highly variable: snow depth (and SWE) increased between the LWS and the UWS only in 1998 and 1999. In the other years, snow depth (and SWE) generally decreased with increasing elevation, or remained relatively similar at all stations. Inter-annual variability in winter surface elevation change is fairly similar at all stations (Table 4.8).

Minimum summer surface lowering occurred in 1996 and 2002 (Fig. 4.8). Maximum lowering occurred in 1998 at the UWS, 2000 at the MWS, and 2001 at the LWS. 1998 and 1999 also produced high rates of lowering at the LWS. In all years, the amount of surface lowering decreased with increasing elevation, although the LWS experienced

substantially greater lowering than the other two stations in most years. with the exception of 1996 and 2000. Summer surface lowering shows the greatest inter-annual variability at the UWS. and the least at the LWS (Table 4.8).

All stations had the most summer snowfalls and non-recovery snowfalls in 2002 (Table 4.4). The fewest summer snowfalls occurred in 1996 at the LWS and MWS. and in 1999 at the UWS. while the fewest non-recovery snowfalls occurred in 1996 at all stations. As a percentage of melt season length. 2002 had the most elevated albedo days at the LWS and MWS. while 1996 had the most at the UWS. 1999 had the lowest percentage of elevated albedo days at all stations. Information from 1997 and 1998 was not available. as only daily average meteorological data were recorded. and no manual observations of meteorological conditions were taken.

Net surface elevation change was positive at the MWS and UWS in 1997. 2001 and 2002. At the LWS. 1997 and 2002 had reduced net surface elevation loss (Fig. 4.8). 1998 was a year of net surface elevation loss at all stations. and the 6-year maximum net surface elevation loss at the LWS and UWS. The MWS. however. had maximum net surface elevation loss in 2000.

4.4.3.2. Wind events

Snow removal due to wind scour is rare at the LWS. At the UWS. however. wind scour occurs throughout the fall. winter and spring. From 1996-1999. the UWS lost the majority of its snowpack in the fall. but in 2001-2002. it had almost equal snow loss in all seasons (Table 4.9). The UWS experienced a greater number of scour events per winter than the MWS. and had larger positive monthly deviations from the 6-year monthly mean wind speed than the MWS. The winters of 1998-99 and 1999-2000 were the windiest at the UWS (Fig. 4.9a). with the greatest number of scour events and significant cumulative winter surface elevation drop (Fig. 4.9b). The springs of 1997 and 1998 were the least windy periods. and had the least number of scour events.

At the MWS. the pattern of snow removal is more seasonally variable (Table 4.9). As at the UWS. the winter of 1999-2000 was one of the windiest (Fig. 4.9a). with the greatest number of wind scour events. and the maximum cumulative drop in winter surface elevation due to wind scour (Fig. 4.9b). 2000-2001 was also windy. Although the

81

total number of individual scour events was lowest during this winter. the cumulative elevation drop from these events was relatively high. Scour events also occurred in 1996-1997. but resulted in little cumulative elevation drop. This may relate to the relatively low monthly deviations of wind speed from the 6-year monthly mean. Cumulative surface elevation drop was high at the MWS in 1998-1999. which corresponds with the high wind speeds and scour events at the UWS. but does not appear in the record of wind speed deviations at the MWS.

At the UWS. the total number of scour events each winter relates broadly to deviations of wind speed from the 6-year mean. In 1998-1999. a high number of scour events from September-March corresponds with high deviations of monthly wind speed during the same period; the same is true of spring (but not winter) events in 1999-2000. However. plots of monthly wind speed deviations against the monthly number of scour events or the monthly amount of cumulative surface elevation drop due to wind scour at the MWS and UWS show a poor relationship. as scour events occur on so few days within each month that they often have little impact on monthly mean wind speeds.

Snowpack loss due to scour events at each station can be offset by additional snowfalls. In 1996-1997. fall and winter scour events at both stations were offset by significant accumulation events in April-June. resulting in the deepest annual snowpack in the 6-year record. The high number of scour events during September-March 1998-1999 was offset by snowfalls that continued well into May and June. The high number of scour events at both the UWS and MWS in the winter and spring of 1999-2000. however. was not offset by additional snowfall. resulting in a minimal snowpack at the onset of the melt season.

Summer wind events are generally associated with summer snowfalls. rather than enhanced lowering. Daily wind speed. air temperature. UDG. and albedo data indicate only three occasions when summer winds likely reduced surface albedo and/or enhanced melt: 16-17 July and 31 July. 1999. and 28-30 July. 2000 (Table 4.10). Despite the occurrence of these events. however. monthly summer wind speed deviations remained within ± 0.5 m s^{-1} of the 6-year monthly mean in all summer months (Fig. 4.9a).

82

4.4.3.3.   Air temperature

1998 was the warmest year of the six at JEG, and the warmest year on record in the Canadian Arctic (1950-2001: Atkinson et al., 2004), with a maximum monthly deviation from the 6-year monthly mean temperature of +3.2°C (Fig. 4.10a). 2001 was the second warmest year of the six, with a maximum monthly deviation of +3.7°C. The coldest year for which a full record was available was 1997, with a minimum monthly deviation of -2.6°C. 1996 and 2002 were also relatively cold, but lack a full annual record.

The longest melt season was 1998 at all stations, while the shortest was 1996 (Fig. 4.10b). However, there is considerable variability in melt season strength and intensity (Fig. 4.10b). At the LWS, the greatest number of PDDs occurred in 2001, at the MWS in 1999, and at the UWS in 1998. The least number of PDDs occurred in 1996 at all stations. Melt season intensity was greatest in 1999 at all stations, and lowest in 2002 at the MWS and UWS, and in 1996 at the LWS. Inter-annual variability in melt season length and total PDDs is greatest at the UWS, and lowest at the LWS (Table 4.8).

4.5.   Discussion

4.5.1.   Winter spatial variability

Winter air temperatures generally increase with elevation due to a temperature inversion near the glacier surface: this inversion results in a stable atmosphere with low winter air temperature variability.

Cyclonic systems bring winter precipitation to JEG from the Baffin Bay region. EOW snowpack at lower elevations is likely closely related to these synoptically generated snowfall events. At higher elevations, however, EOW snowpack is more related to wind events. Snowpack thins with elevation on the glacier, due to winter wind scour events at higher elevations that result in snow sublimation (Box and Steffen, 2001) and redistribution (Winstral et al., 2002). Scour events are the result of high wind speeds (>3 m s^{-1}), which are greater in winter than summer.

The change of snow pack thickness with elevation varies interannually, however, depending on the cumulative wind scour over winter, and whether or not scour losses are replaced prior to melt season onset. Losses due to fall scour events are often offset by snowfall events in the spring (e.g., 1996-1997). In years when only a portion of the spring

83

snowpack is removed by wind scour. the loss may be offset by late spring snowfalls (e.g.. 1998-1999). In years when scour continues into late spring. however. losses cannot be recovered (e.g.. 1999-2000). In years with reduced scour or sufficient additional precipitation to offset scour losses. the gradient of snowpack with elevation is more likely to be positive (e.g.. 1997-1998. 1998-1999).

4.5.2. Summer spatial variability

Summer air temperature is highly variable. While the summer air temperature lapse rate is negative. it varies daily. and does not reach the commonly assumed -6.0°C km^{-1}. Air temperatures are higher on the lower glacier. resulting in higher PDD totals and longer melt seasons. The maximum PDD total across the glacier occurs in July: PDD totals in May and August are most variable due to significant interannual differences in melt season onset and end.

The high air temperature and PDD totals on the lower glacier result in faster snowpack removal. and longer ice surface exposure. resulting in maximum summer surface lowering at low elevations (Hoinkes. 1968: Collins. 1987: Alt. 1979). Summer surface lowering generally decreases with elevation. although the gradient with elevation is non-linear. In some years the LWS has substantially greater lowering than the MWS and UWS (e.g.. 2001). Interannual variability in summer surface elevation change is greatest on the upper glacier. as it is dependent on melt season length. total PDDs (also most variable at high elevations) and melt season intensity.

Summer snowfalls occur most frequently on the lower glacier due to the longer melt season in which they can occur. but they last the longest on the upper glacier due to the lower air temperatures. Note that a snowfall will often occur at one station but not the others. indicating either that the precipitation falls as rain on the lower glacier (most years). or that the air mass bringing the snowfalls moves up- rather than down-glacier (e.g.. 1999). Summer snowfalls have the greatest impact on surface elevation change if they are followed by a period of inclement weather. when air temperature does not recover sufficiently to remove the snow (e.g.. 1999 vs. 2002) (Tronov. 1962: Alt. 1987: Oerlemans and Klok. 2003). Snowfalls that take longer to reach peak thickness are also important. as melt is suppressed not only following. but also during. these snowfalls (e.g..

2000). Summer wind events significantly impact summer surface lowering (e.g., 2000), but are rare, having occurred only three times during the 6-year period (e.g., Boon et al., 2003).

4.5.3. Net surface elevation change – interannual variability

Different combinations of specific meteorological conditions (winter wind scour, EOW snowpack, summer air temperature, summer snowfalls) can result in a similar degree of net surface elevation change.

The greatest net surface elevation gain occurred in 2001-2002, and was due mainly to a combination of low summer air temperatures, with low PDDs, a short melt season, and a high number of summer snowfalls. Net surface elevation gain in 1996-1997 at the MWS and UWS, however, is attributed to the fact that the 1996-1997 snowpack was the deepest of the 6-year record, with few winter scour events that were offset by spring snowfalls, and the 1997 summer was one of the coldest of the 6-year record, with a short melt season and relatively few PDDs. Net surface elevation gain in 2000-2001 at the MWS and UWS was due to a combination of a relatively deep snowpack (despite significant winter wind scour at the MWS) and significant summer snowfalls. At the LWS, however, net surface elevation change in 2000-2001 was strongly negative, due to the high number of PDDs and long melt season at this station.

The greatest net surface elevation loss occurred in 1997-1998, and is attributed to the fact that, although the snowpack was relatively thick, 1998 was the warmest summer of the record, with the longest melt season and maximum PDDs at the UWS. The second greatest amount of net surface elevation loss occurred in 1998-1999, despite a deep winter snowpack that accumulated in spite of significant winter wind scour. Although the melt season was relatively short and had a relatively high number of summer snowfalls, it was the most intense of the 6-year record, and included two short summer wind events. Net surface elevation loss in 1999-2000 was due to a combination of a shallow snowpack caused by significant winter wind scour, and the occurrence of a strong summer wind event.

Statistically, multiple regression of summer surface elevation change on EOW snowpack and total PDDs indicates that summer elevation change at all stations is driven

85

mainly by PDDs, while EOW snowpack also plays a role at the LWS and UWS (Table 4.11). However, summer surface elevation change at the LWS and UWS becomes more negative as EOW snowpack increases, suggesting that deeper snowpacks result in more summer surface elevation change. This indicates that surface elevation change cannot be used as a proxy for MB without density corrections, as unit changes in surface elevation are assumed equivalent for snow and ice surfaces, which is not true in terms of water equivalency (w.e.). Thus a thick snowpack results in large surface elevation changes that mean less in terms of w.e. than if the same elevation change were to occur, for example, half over snow and half over ice. While it is feasible to compare interannual variations at a single station, we cannot compare stations with each other.

Given that EOW snowpack and summer surface elevation change are not independent variables, a multiple regression of net surface elevation change on PDDs and EOW snowpack was done to determine the relative impact of summer and winter conditions. Results show that net surface elevation change at all stations is driven mainly by PDDs (Table 4.12), confirming the impact of summer conditions on annual surface elevation change determined in previous studies (Koerner, 2001). At the MWS, however, EOW snowpack also impacts net surface elevation change. This is likely because, at the LWS ice melt is always much greater than snowmelt, and at the UWS the melting surface is always snow-covered. At the MWS, however, either variable can dominate depending on the altitude of the seasonal snow line.

4.5.4. Synoptic controls on meteorological conditions

It is apparent that there is high interannual variability in the specific meteorological conditions affecting net annual surface elevation change, although summer conditions are the main driver behind net annual surface elevation change. As JEG is located in a zone of diverging flow, the fluctuating positions of the Polar Vortex, the Baffin trough and the Greenland ridge in the summer season (JJA) may drive local meteorological conditions. It may therefore be possible to use large-scale synoptic conditions to select the appropriate air temperature lapse rate for a given day. A change in the relative frequency of different synoptic types would result in a change in the frequency distribution of air

86

temperature lapse rates. which would affect total glacier melt resulting from a given sea level air temperature history.

We examine annual plots of JJA 500 mb geopotential height anomalies (from the 1968-1996 average) (Fig. 4.11), in combination with annual plots of average JJA 500 mb geopotential height (Fig. 4.12). They show that 1997 was a relatively average year, with a slight negative height anomaly over the northern QEI corresponding with southward extension of the Polar Vortex.

In cool years like 1996 and 2002, a strong negative height anomaly occurs over the northern QEI, indicating southward extension of the Polar Vortex. The trough in the Baffin Bay region also deepens and moves to the east. In 1996 the Vortex was far enough south to maintain flow from the west-southwest over JEG, but in 2002 it was slightly northwest, resulting in strong south-southwest flow up from Baffin Bay. This likely accounts for the high number of summer snowfalls seen in 2002.

In warmer years like 1998, 2000, and 2001, strong positive height anomalies occur over the JEG region, although they are the result of differing synoptic configurations. In 1998, the positive height anomalies were caused by a weak Polar Vortex situated on the Asian side of the Arctic Ocean, and significant weakening of the Baffin trough. In 2001, positive anomalies were caused by the development of a strong ridge over western Greenland, and the concurrent weakening of the Baffin trough as it shifted west. In 2000, positive anomalies are attributed to the Vortex moving to the east and the Baffin trough weakening. In each of these three summers, flow over JEG was from the southwest to west-southwest.

1999, however, represents an outlier year, with height anomalies of a completely different pattern. The Vortex weakened significantly and moved south into Baffin Bay, deepening the Baffin trough and resulting in strong positive height anomalies in the Arctic Ocean and slight negative anomalies over the Baffin region.

While we can generally conclude that warm years are associated with positive height anomalies over the JEG region, and cool years with negative height anomalies, these results could be improved by examining monthly – rather than seasonal – scale plots. This would provide increased detail when examining years such as 1998, when the melt season lasted into September but cannot be seen on a JJA plot; or 1999, which had a hot

87

July and August, although a relatively cold June likely had a strong impact on the seasonal average synoptic configuration.

4.5.5. Implications for degree-day modelling

As stated previously, DDMs often rely on two basic assumptions. First is the constant air temperature lapse rate (MALR). Field data indicate that the air temperature lapse rate is highly variable. thus corroborating the results of previous studies (e.g.. Arendt and Sharp. 1999: Marshall et al., in review). Summer lapse rates can be up to 4°C km^{-1} lower. varying monthly and even daily; on a daily scale. lapse rates often fluctuate between positive and negative values. Use of the MALR in modelling studies. when extrapolating upwards from low elevation meteorological stations. will underestimate melt at higher elevations. subsequently impacting MB predictions. Second is the constant accumulation lapse rate (usually assumed to be positive). Results show that winter wind scour events at higher elevations often result in a decrease of EOW snowpack (and subsequently SWE) with elevation. This assumption could thus result in overestimation of EOW snowpack. subsequently impacting simulations of melt and MB.

Also stated previously. DDMs rely solely on a linear relationship between air temperature and melt. the factor of proportionality being the DDF (m WE d^{-1} °C^{-1}). which varies for different surface types (i.e.. snow or ice). Results of the study indicate that other factors are important in the climate-MB relationship. however. such as summer snowfalls. When the model is run. the EOW snowpack is removed using a snow DDF. and once the ice surface is exposed it is melted using an ice DDF (e.g.. Bugnion. 1999). Summer snowfalls are not incorporated. as the model does not take precipitation events as input. Thus both melt amounts and MB may be overestimated. A simple way to incorporate summer snowfalls (where field data are available) is to set the DDF to the snow value during the known snowfall duration. then reset it to the ice DDF. Alternatively. models could be set to either read input summer precipitation data. or to automatically revert to the snow DDF when air temperature reaches a given threshold (e.g.. 0°C).

A second problem involves incorporating the effect of summer wind events on melt and MB. Study results indicate that summer wind events can significantly impact net

annual mass balance. However, when using only air temperature input data, enhanced melt due to wind events is not represented in DDMs. While some researchers argue against it (Ohmura, 2001), others have suggested that incorporating wind speed into the DDF parameterization may be useful in areas where warm wind events - such as the event observed at JEG in 2000 - occur (Hock, 2003).

4.6. Conclusions

Study results shows that meteorological conditions on an Arctic glacier are highly spatially and temporally variable, with conditions that affect net annual surface elevation change (winter wind scour: summer snowfall and wind events: summer PDDs) varying in significance both spatially and interannually. In general, snowpack decreases with elevation on the glacier due to increased wind speeds and wind scour events at higher elevations. Summer surface and net annual elevation drop are greatest lower on the glacier, and decrease with elevation. Air temperature decreases with elevation in the summer months, although not at a constant lapse rate, and not at the MALR. In the winter months, however, an inversion often occurs. Air temperature thus increases with elevation, with more positive lapse rates on the upper part of the glacier than the lower.

Although the UWS is usually located in the accumulation area, it experienced net elevation loss over the recording interval due to the anomalously warm years of 1998 and 1999. The MWS experienced net surface elevation loss in 1998-2000, while the LWS experienced net surface elevation loss in all years. Net surface elevation change at the UWS and LWS is driven mainly by summer conditions. The position of the MWS near the fluctuating equilibrium line results in net elevation change being affected by both winter and summer conditions.

Examination of synoptic maps indicates that years with net surface elevation loss are generally associated with positive geopotential height anomalies in the JEG region, while years with net surface elevation gain are associated with negative height anomalies.

These results are significant for Arctic glacier modelling studies. Basic DDM assumptions require closer consideration: (a) snowpack cannot be assumed to increase with elevation at a specified accumlation lapse rate: and, (b) summer air temperatures cannot be assumed to decrease with elevation at the MALR (-6.0°C km^{-1}). Additionally,

89

DDM performance could be improved by incorporating the effects of summer snow and wind events. Degree-day factors for the summer melt season could be varied to incorporate the reduction of melt due to increased surface albedo both during and following summer snowfalls, the duration of which is highly dependent on local meteorological conditions. Finally, the role of summer winds in enhancing melt must also be considered in regions where warm summer wind events occur. Arctic glacier MB and its sensitivity to climate change cannot be accurately modelled without taking these issues into consideration.

4.7. References

Alt, B. 1979. Investigation of summer synoptic climate controls on the mass balance of Meighen Ice Cap. Atmosphere-Ocean 17(3): 181-199.

Alt, B. 1987. Developing synoptic analogs for extreme mass balance conditions on Queen Elizabeth Island ice caps. Journal of Climatology and Applied Meteorology 26 (12): 1605-1623.

Arendt, A., M.J. Sharp. 1999. Energy balance measurements on a Canadian high Arctic glacier and their implications for mass balance modelling. International Association of Hydrological Sciences 256: 165-172.

Atkinson, D., R. Brown, B. Alt, T. Agnew, J. Bourgeois, M. Burgess, C. Duguay, G. Henry, S. Jeffers, R. Koerner, A.G. Lewkowicz, S. McCourt, H. Melling, M. Sharp, S. Smith, A. Walker, K. Wilson, S. Wolfe, M-k. Woo, K. Young. 2004. Canadian cryospheric response to an anomalous warm summer. Atmosphere-Ocean. in press.

Barber, D.G., J.M. Hanesiak, W. Chan, J. Piwowar. 2001. Sea-ice and meteorological conditions in Northern Baffin Bay and the North Water Polynya between 1979 and 1996. Atmosphere-Ocean 39(3): 343-359.

Boer. G.J.. G. Flato. D. Ramsden. 2000. A transient climate change simulation with greenhouse gas and aerosol forcing: projected climate change in the 21st century. Climate Dynamics 16: 427-450.

Bøggild. C.E.. N. Reeh. H. Oerter. 1994. Modelling ablation and mass-balance sensitivity to climate change of Storstrømmen. Northeast Greenland. Global and Planetary Change 9: 79-90.

Boon. S.. M.J. Sharp. P.W. Nienow. 2003. Impact of an extreme melt event on the runoff and hydrology of a High Arctic glacier. Hydrological Processes 17(6): 1051-1072.

Box. J.E.. K. Steffen. 2001. Sublimation on the Greenland ice sheet from automated weather station observations. Journal of Geophysical Research – Atmospheres 106(D24): 33.965-33.981.

Braithwaite. R.J. 1984. Calculation of degree-days for glacier-climate research. Zeitschrift fur Gletscherkunde und Glazialgeologie 20: 1-8.

Braithwaite. R.J. 1995. Positive degree-day factors for ablation on the Greenland ice sheet studied by energy-balance modelling. Journal of Glaciology 41: 153-160.

Braithwaite. R.J.. Y. Zhang. 1999. Modelling changes in glacier mass balance that may occur as a result of climate changes. Geografiska Annaler 81A(4): 489-496.

Braithwaite. R.J.. Y. Zhang. 2000. Sensitivity of mass balance of five Swiss glaciers to temperature changes assessed by tuning a degree-day model. Journal of Glaciology 46: 7-14.

Braun. L.N.. M. Weber. M. Schulz. 2000. Consequences of climate change for runoff from alpine regions. Annals of Glaciology 31: 19-25.

Bugnion. V. 1999. Model estimates of the mass balance of the Greenland and Antarctic ice sheets. MIT Joint Program on the Science and Policy of Global Change 54: 36 pp.

Collins. D.N. 1987. Hydrometeorological conditions. mass balance and runoff from alpine glaciers. In Glacier Fluctuations and Climatic Change. J. Oerlemans. ed. Dordrecht: Kluwer Academic Publishers. p. 235-260.

Copland. L.. M. Sharp. 2001. Mapping hydrological and thermal conditions beneath a polythermal glacier with radio-echo sounding. Journal of Glaciology 47(157): 232-242.

Dowdeswell. J.A.. J.O. Hagen. H. Bjornsson. A.F. Glazovsky. W.D. Harrison. P. Holmlund. J. Jania. R.M. Koerner. B. Lefauconnier. C.S.L. Ommanney. R.H. Thomas. 1997. The mass balance of circum-Arctic glaciers and recent climate change. Quaternary Research 48: 1-14.

Fujita. K.. Y. Ageta. 2000. Effect of summer accumulation on glacier mass balance on the Tibetan Plateau revealed by mass-balance model. Journal of Glaciology 46(153): 244-252.

Greuell. W.. R. Böhm. 1998. 2 m temperatures along melting mid-latitude glaciers. and implications for the sensitivity of the mass balance to variations in temperature. Journal of Glaciology 44(146): 9-20.

Greuell. W.. C. Genthon. 2004. Modelling land ice surface mass balance. In Mass balance of the cryosphere: Observations and modelling of contemporary and future changes. J. L. Bamber and A. J. Payne. eds. Cambridge: Cambridge University Press. p. 117-168.

Hock. R. 2003. Temperature index melt modelling in mountain areas. Journal of Hydrology 282(1-4): 104-115.

Hock. R. 1999. A distributed temperature-index ice- and snowmelt model including potential direct solar radiation. Journal of Glaciology 45(149): 101-111.

Hoinkes. H.C. 1968. Glacier variation and weather. Journal of Glaciology 7(49): 3-19.

Holland. M.M.. C.M. Bitz. 2003. Polar amplification of climate change in coupled models. Climate Dynamics 21: 221-232.

Jóhannesson. T. 1997. The response of two Icelandic glaciers to climatic warming computed with a degree-day glacier mass-balance model coupled to a dynamic glacier model. Journal of Glaciology 43(143): 321-327.

Kalnay. E.. M. Kanamitsu. R. Kistler. W. Collins. D. Deaven. L. Gandin. M. Iredell. S. Saha. G. White. J. Woollen. Y. Zhu. M. Chelliah. W. Ebisuzaki. W Higgins. J. Janowiak. K.C. Mo. C. Ropelewski. J. Wang. A. Leetmaa. R. Reynolds. R. Jenne. D. Joseph. 1996. The NCEP/NCAR 40-year reanalysis project. Bulletin of the American Meteorological Society 77: 437-471.

Koerner. R.M. 2001. Glacier mass balance in the Canadian Arctic: placing the summer of 1998 in long-term context. In The state of the Arctic cryosphere during the extreme warm summer of 1998: documenting cryospheric variability in the Canadian Arctic. CCAF Summer 1998 Project Team. CCAF Final Report. Available at http://www.socc.ca.

Maxwell. J.B. 1980. The Climate of the Canadian Arctic Islands and Adjacent Waters. Ottawa: Atmospheric Environment Service. 300 pp.

Morison. J.. K. Aagaard. M. Steele. 2000. Recent environmental changes in the Arctic: a review. Arctic 53(4): 359-371.

Moritz. R.E.. C.M. Bitz. E.J. Steig. 2002. Dynamics of recent climate change in the Arctic. Science 297: 1497-1502.

93

Oerlemans, J., E.J. Klok. 2003. Effect of summer snowfall on glacier mass balance. Annals of Glaciology **38**, in press.

Ohmura, A. 2001. Physical basis for the temperature-based melt-index method. Journal of Applied Meteorology **40**(4): 753-761.

Pfeffer, W.T., M.F. Meier, T.H. Illangasekare. 1991. Retention of Greenland runoff by refreezing: implications for projected future sea level change. Journal of Geophysical Research – Oceans **96**(C12): 22,117-22,124.

Rabus, B.T., K.A. Echelmeyer. 1998. The mass balance of McCall Glacier, Brooks Range, Alaska, U.S.A.: its regional relevance and implications for climate change in the Arctic. Journal of Glaciology **44**(147): 333-351.

Serreze, M.C., J.E. Walsh, F.S. Chapin III, T. Osterkamp, M. Dyurgerov, V. Romanovsky, W.C. Oechel, J. Morison, T. Zhang, R.G. Barry. 2000. Observational evidence of recent change in the northern high-latitude environment. Climatic Change **46**: 159-207.

Singh, P., N. Kumar, M. Arora. 2000. Degree-day factors for snow and ice for Dokriani Glacier, Garhwal Himalayas. Journal of Hydrology **235**: 1-11.

Skidmore, M.L., M.J. Sharp. 1999. Drainage system behaviour of a high Arctic polythermal glacier. Annals of Glaciology **28**: 209-215.

Tronov, M.V. 1962. On the role of summer snowfall in glacier variations. International Association of Hydrological Sciences **58**: 262-269.

van der Veen, C.J. 2002. Polar ice sheets and global sea level: how well can we predict the future? Global and Planetary Change **32**: 165-194.

94

Winstral, A., K. Elder, R.E. Davis. 2002. Spatial snow modeling of wind-redistributed snow using terrain-based parameters. Journal of Hydrometeorology 3(5): 524-538.

95

4.8. Tables

Table 4.1. Instruments, heights, and accuracy at each meteorological station.

Instrument	Location on station*	Accuracy
LI200s Li-Cor Pyranometer	1.80 m. pointed up	±5%
Kipp & Zonen Pyranometer	0.8 m. pointed down	±2%
HMP35CF Vaisala RH/Temperature	1.25 m	±2% RH (0-90%) ±3% RH (90-100%)
RM Young 05103 Wind Monitor	1.75 m: oriented north	1.0 m s^{-1} threshold sensitivity
Vaisala PTB101 Barometric Pressure (MWS only)	~1.00 m	±4 mb (@ -20°C)
REBS Q7 net radiometer	0.80 m. facing south	wind speed dependent
Campbell Scientific UDG01	0.85 m (LWS): 0.91 m (MWS). 1.45 m (UWS)	±1 cm or 0.4% of distance to target (whichever is greatest)

all heights are above snow surface

Table 4.2. Missing data at each meteorological station.

LWS	MWS	UWS
All data:	*All data:*	*All data:*
14 Nov 2000 – 19 May 2001	28 Jul 2001 – 31 Dec 2001	3 Aug 2000 – 9 Apr 2001
25 Dec 2001 – 25 May 2002	7 Mar 2002 – 8 May 2002	
Daily average wind speed:	*Daily average air pressure:*	*All daily average data:*
22 May 1999 – 30 May 2001	7 Jun 2001 – 18 May 2002	9 Jun 2000 – 25 May 2001
Daily average wind dir:		*Daily average UDG:*
3 Aug 1999 – 30 May 2001		25 May 2001 – 1 Aug 2001

Table 4.3. Seasonal average surface air temperature and surface precipitable water at JEG (derived from NCEP data).

Season	Average surface air temperature (°C)	Average surface precipitable water (kg m^{-2})	Extent of 5200 hgt Polar Vortex (°N)
Winter (DJF)	-30	1-2	52
Spring (MAM)	-20	2-3	69
Summer (JJA)	0	8-9	Non-existent
Fall (SON)	-20	3-4	80

Table 4.4. Summer snowfalls at each meteorological station.

	Total snowfalls			Total non-recovery snowfalls			% elevated albedo days*		
	LWS	MWS	UWS	LWS	MWS	UWS	LWS	MWS	UWS
1996	4	3	3	0	0	0	27.7	35.1	79.2
1997	-	-	-	-	-	-	-	-	-
1998	-	-	-	-	-	-	-	-	-
1999	6	5	2	0	1	0	20.0	21.7	17.3
2000	4	5	7	1	1	3	32.5	23.9	36.4
2001	6	6	5	1	3	3	29.7	27.1	59.0
2002	7	7	8	4	3	4	53.0	53.9	43.8
AVG	5.4	5.2	5.0	1.2	1.6	2.0	32.6	32.3	47.1

*calculated as total elevated albedo days/melt season length

Table 4.5. Mean annual air temperature and range all stations.

	LWS	MWS	UWS
Mean annual air temperature (°C)	-12.3	-14.6	-13.8
Annual range of mean daily temperature (°C)	-28.3°C to 3.5°C	-28.1°C to 2.6°C	-26.8°C to 1.2°C

Table 4.6. Average melt season characteristics at each station.

	PDD total	Length (days from first to last PDD)	Intensity (PDDs/length)	PDD coefficient of variation (%)			
				May	Jun	Jul	Aug
LWS	212	75	2.9	156	41	27	80
MWS	153	68	2.4	196	54	42	107
UWS	119	57	2.1	185	82	63	104

Table 4.7. Relationship between end-of-winter snow depth and SWE in years for which data were available.

	1997	2000	2001	2002
r	0.87	0.80	0.87	0.90
n	20	18	45	11

Table 4.8. Inter-annual coefficient of variation of winter and summer surface elevation change, melt season length, and PDD total at each station.

	CV of winter surface elevation change (%)	CV of summer surface elevation change (%)	CV of melt season length (%)	CV of PDD total (%)
LWS	35	36	22	34
MWS	30	44	24	39
UWS	32	53	33	42

Table 4.9. Percentage of annual total amount of snow moved by wind scour.

	1996-1997	1997-1998	1998-1999	1999-2000	2000-2001	2001-2002
MWS						
Fall	73.3	60.3	37.2	17.0	93.9	-
Winter	21.8	35.4	36.8	45.4	6.1	-
Spring	5.0	4.3	26.0	37.6	0.0	-
UWS						
Fall	49.6	55.5	53.8	10.9	-	39.3
Winter	37.1	29.2	22.5	50.9	-	22.1
Spring	13.3	15.3	23.8	38.1	-	38.6

Table 4.10. Summary of summer wind events.

	MWS				UWS			
Dates	Wind speed (m s⁻¹)	Temp (°C)	Net surface change (mm)	Albedo change	Wind speed (m s⁻¹)	Temp (°C)	Net surface change (mm)	Albedo change
16-17 Jul 1999	6.0	5.1	-52	-18	5.8/6.1	1.2/3.6	-18	-17
31 Jul 1999	-	-	-	-	4.8	3.7	-16	-10
28-29 Jul 2000	5.5/8.0	7.0/7.9	-400	-16	8.4/7.8	5.8/7.8	-120	-23

98

Table 4.11. Role of PDDs and snowpack in summer surface elevation change. Negative relationships result from the use of negative values for summer surface elevation drop.

	LWS	MWS	UWS
R^2	0.80	0.56	0.90
PDD coefficient	-0.96	-0.75	-0.64
Snowpack coefficient	-0.47	n.s.	-0.63

*n.s. = no score: p< 0.05 for all values

Table 4.12. Role of PDDs and snowpack in net annual surface elevation change. Negative relationships results from the use of negative values for summer surface elevation drop.

	LWS	MWS	UWS
R^2	0.82	0.71	0.80
PDD coefficient	-0.91	-0.64	-0.90
Snowpack coefficient	n.s.	0.58	n.s.

*n.s. = no score: p < 0.05 for all values

99

4.9. Figures
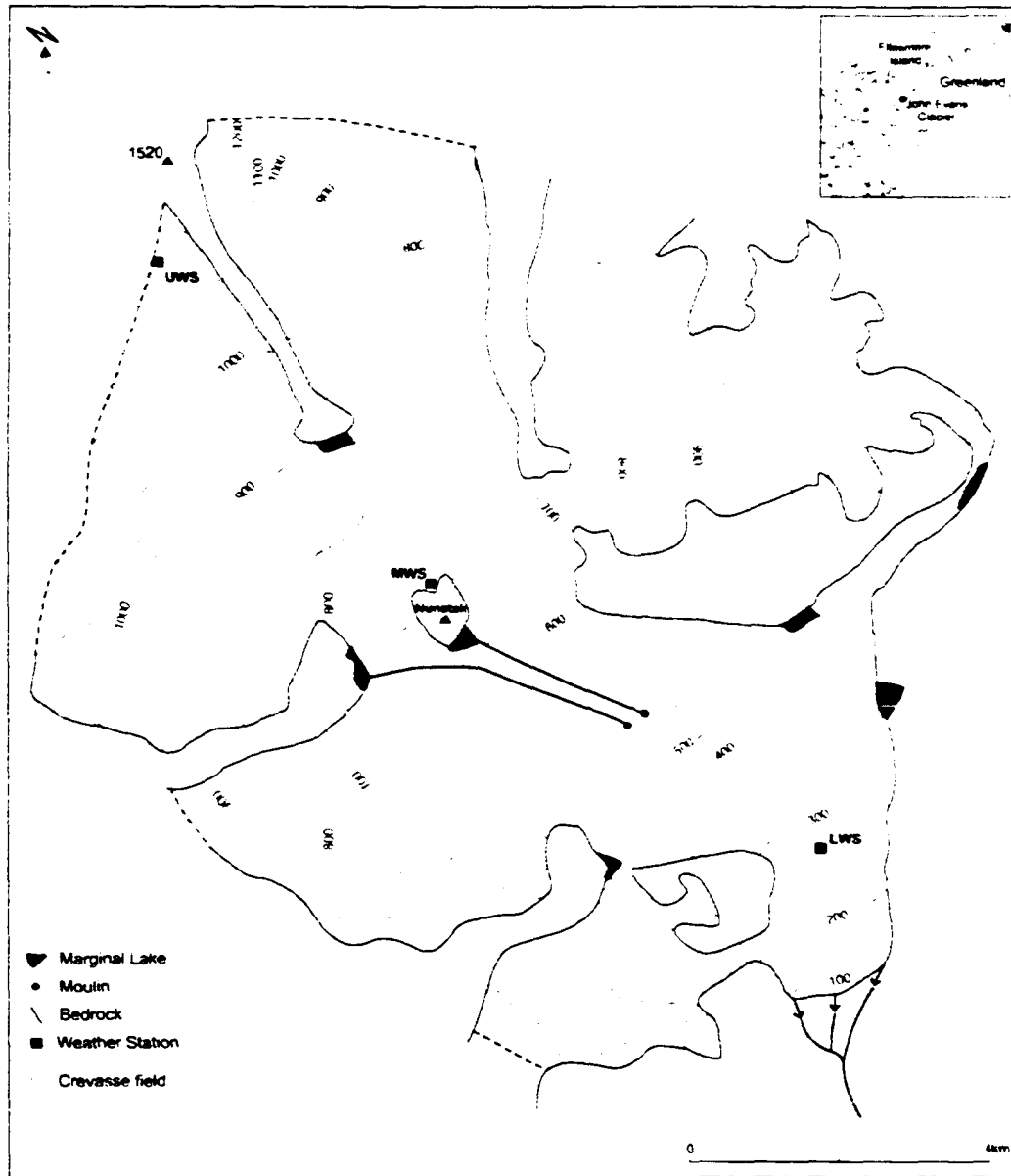
Figure 4.1. Study site location and location of meteorological stations.
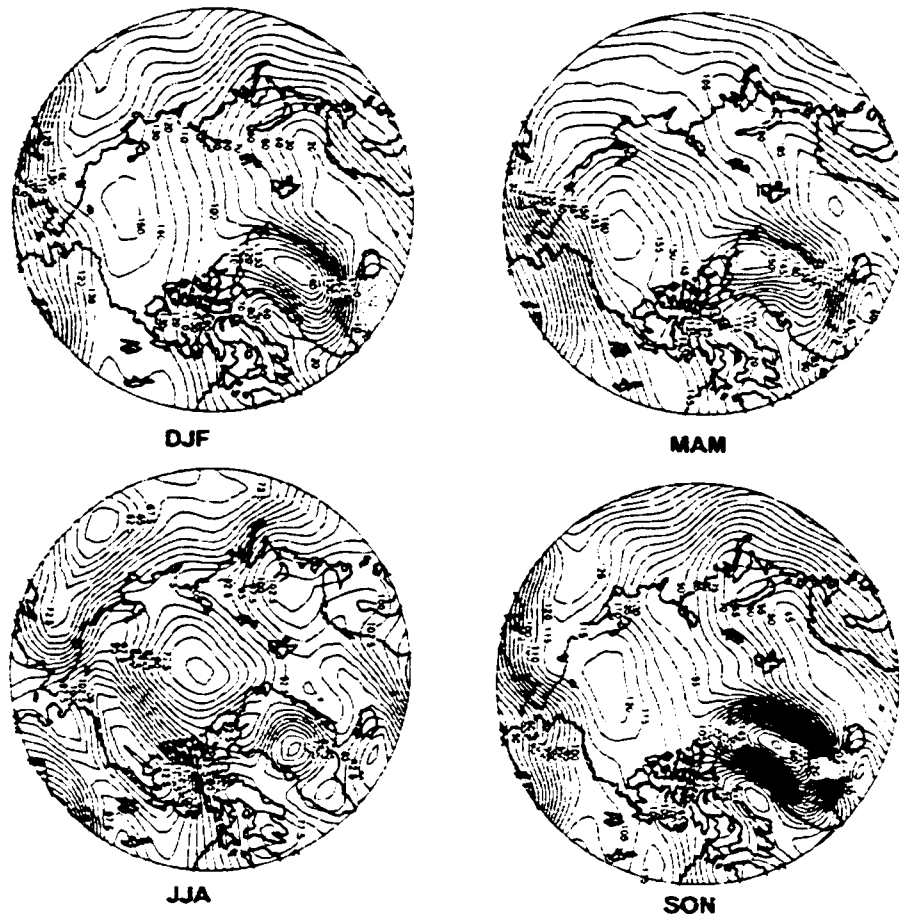
Figure 4.2. Polar stereographic projections (60°N to 90°N) of seasonal long term (1968-1999) averages of 1000 mb geopotential height.

101
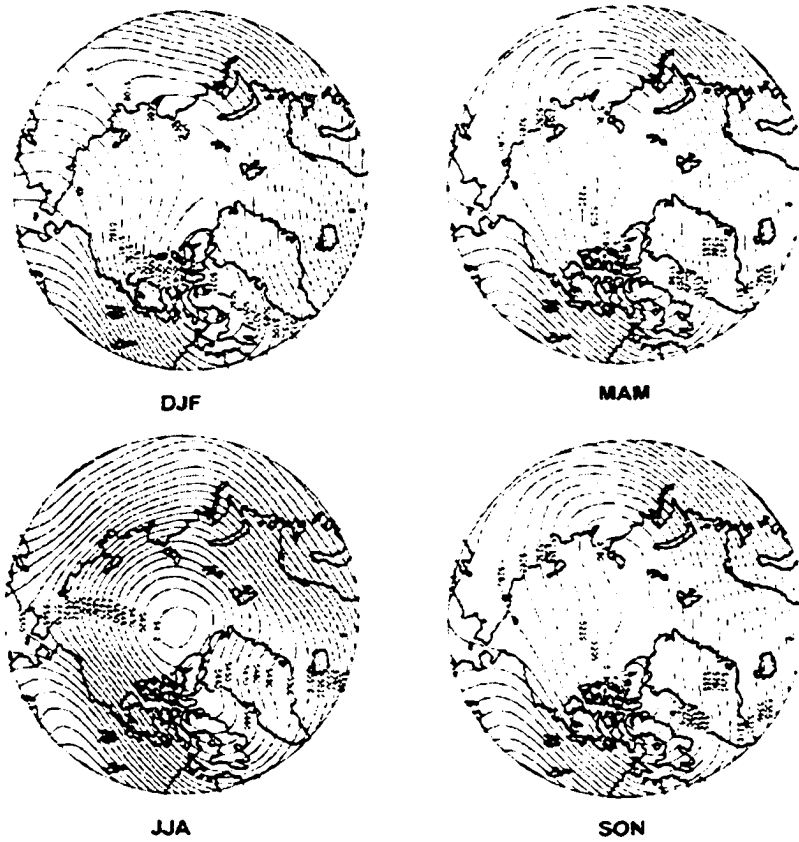
Figure 4.3. Polar stereographic projections (60°N to 90°N) of seasonal long term (1968-1999) averages of 500 mb geopotential height.

102
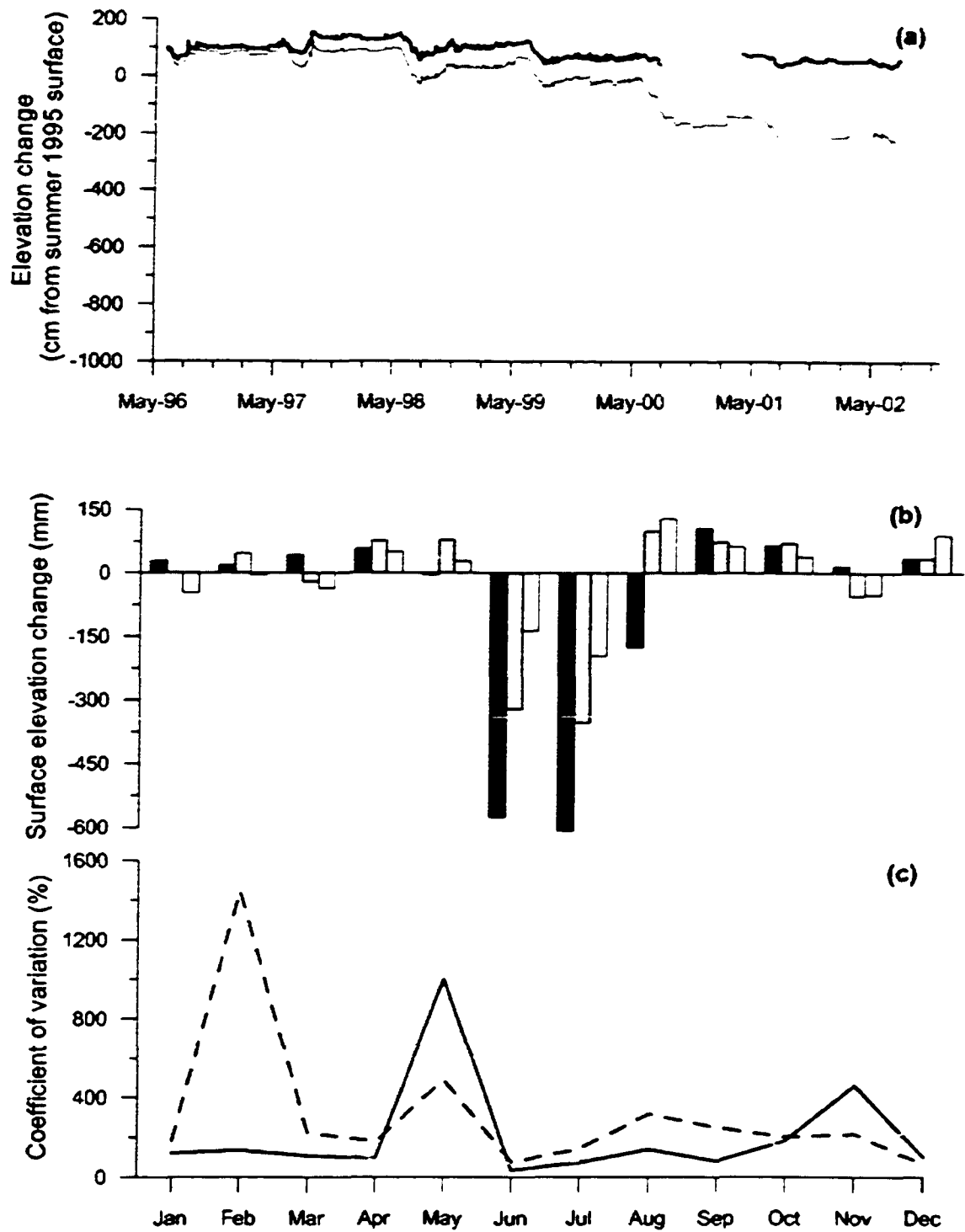
Figure 4.4. (a) Surface elevation change from 1996-2002 at the LWS (light grey). MWS (dark grey), and UWS (black): (b) monthly average (1996-2002) surface elevation change at the LWS (solid black). MWS (grey) and UWS (white): (c) coefficient of variation of monthly average (1996-2002) surface elevation change at the LWS (solid black). MWS (grey). and UWS (dashed black).

103
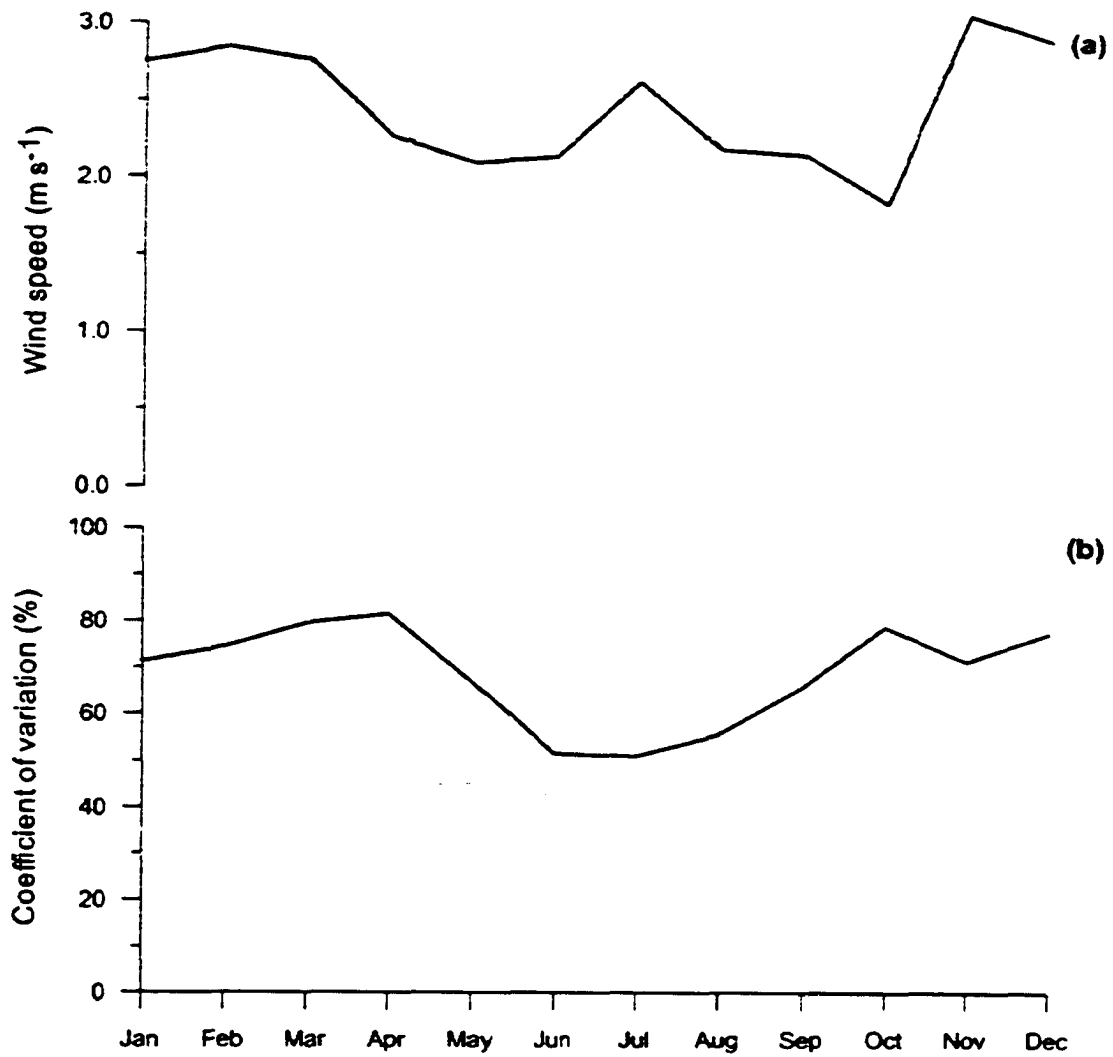
Figure 4.5. (a) Monthly average (1996-2002) wind speed: (b) coefficient of variation of monthly average (1996-2002) wind speed. MWS: grey. UWS: black. Note that data from the LWS are not available due to anemometer malfunction.

104
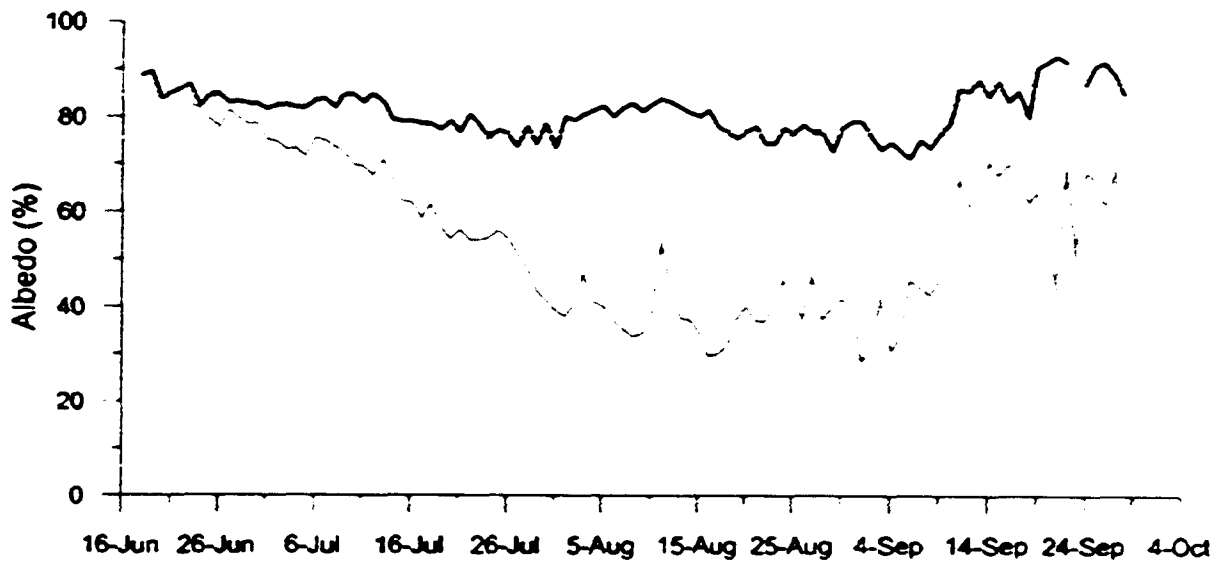
Figure 4.6. Daily average (1996-2002) summer albedo at the LWS (grey) and UWS (black). Note that data from the MWS were unavailable due to malfunction of the K_{in} sensor.

105
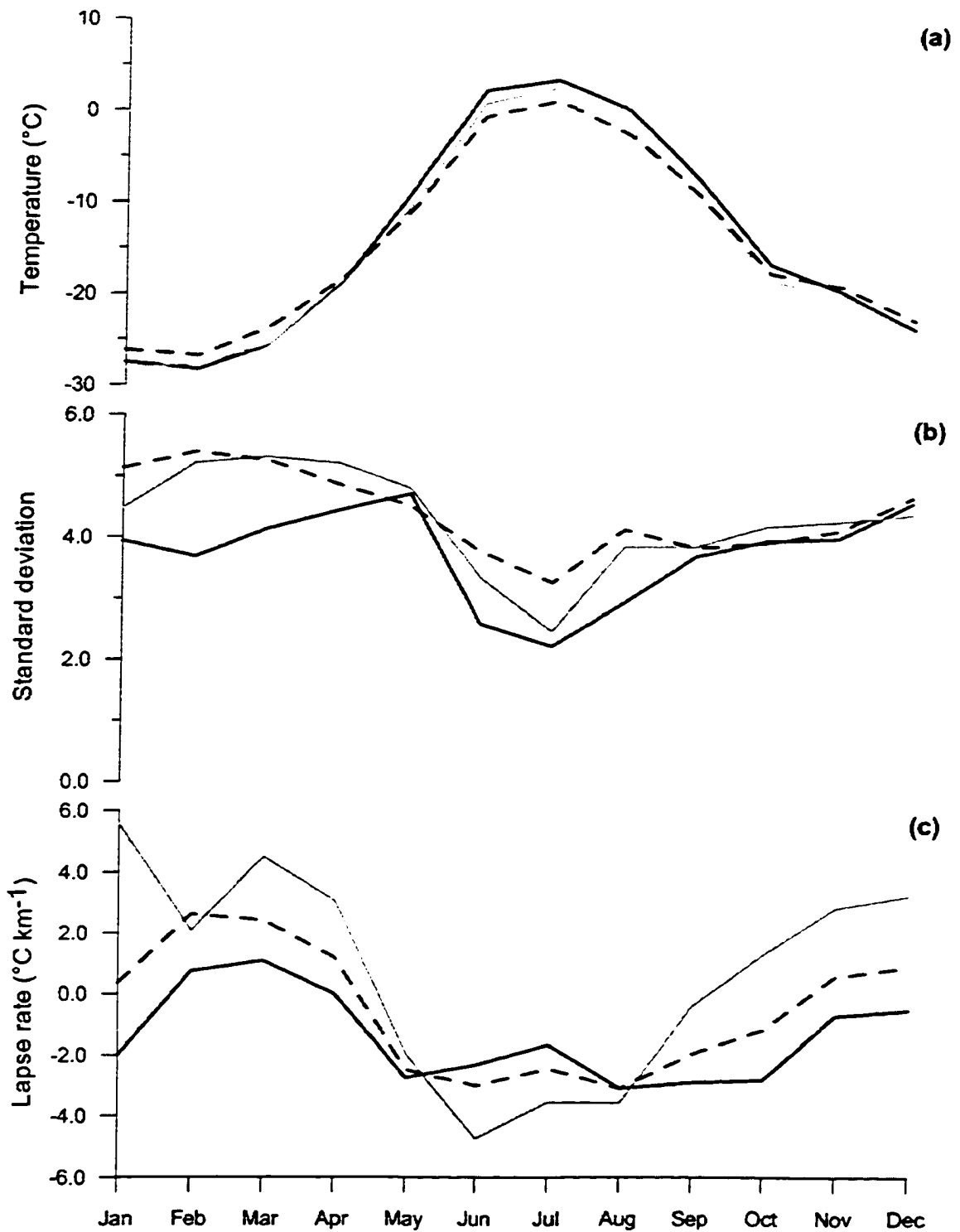
Figure 4.7. (a) Monthly average (1996-2002) air temperature: (b) standard deviation of monthly average (1996-2002) air temperature. LWS: black. MWS: grey. UWS: dashed black: (c) monthly average (1996-2002) air temperature lapse rates between the LWS-MWS (black). MWS-UWS (grey). and LWS-UWS (dashed black). Note that the moist adiabatic lapse rate is -6.0°C km^{-1}.

106
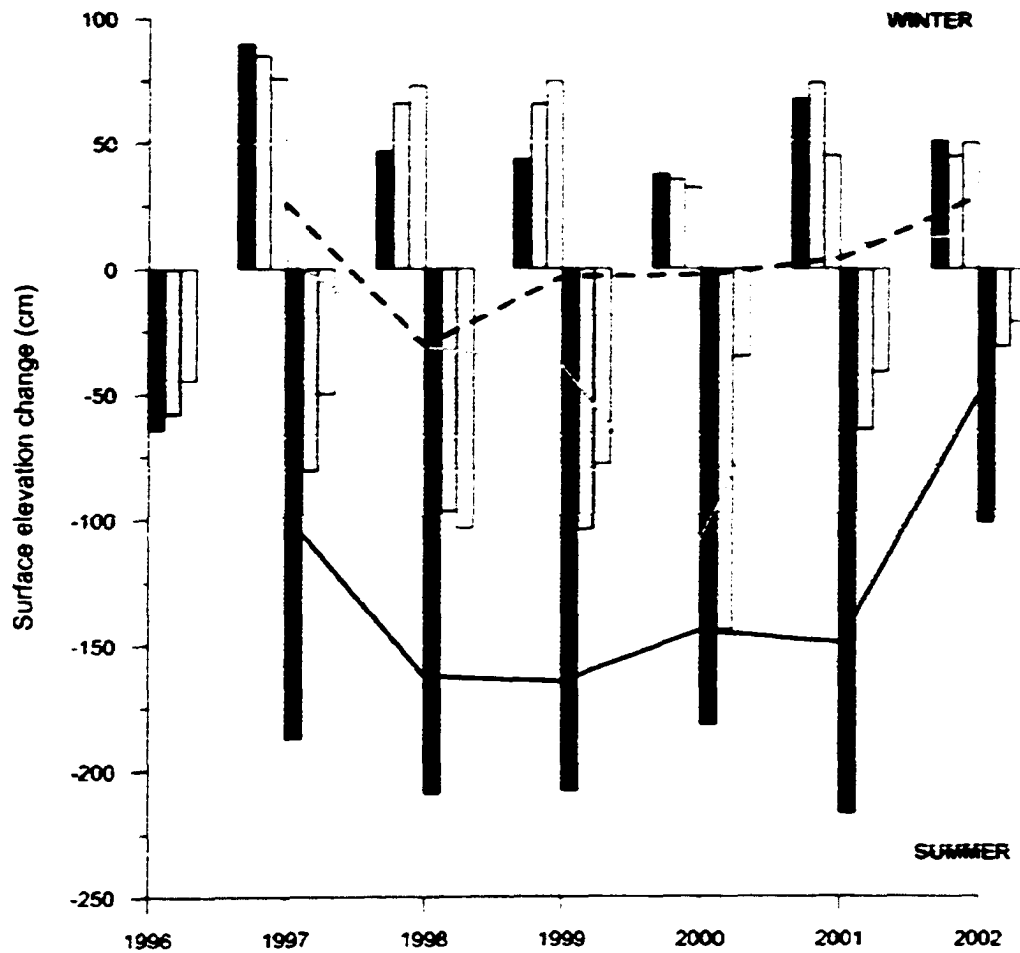
Figure 4.8. Annual winter and summer surface elevation change at the LWS (black). MWS (grey) and UWS (white). Line graphs indicate annual net surface elevation change at the LWS (black). MWS (grey). and UWS (dashed black).
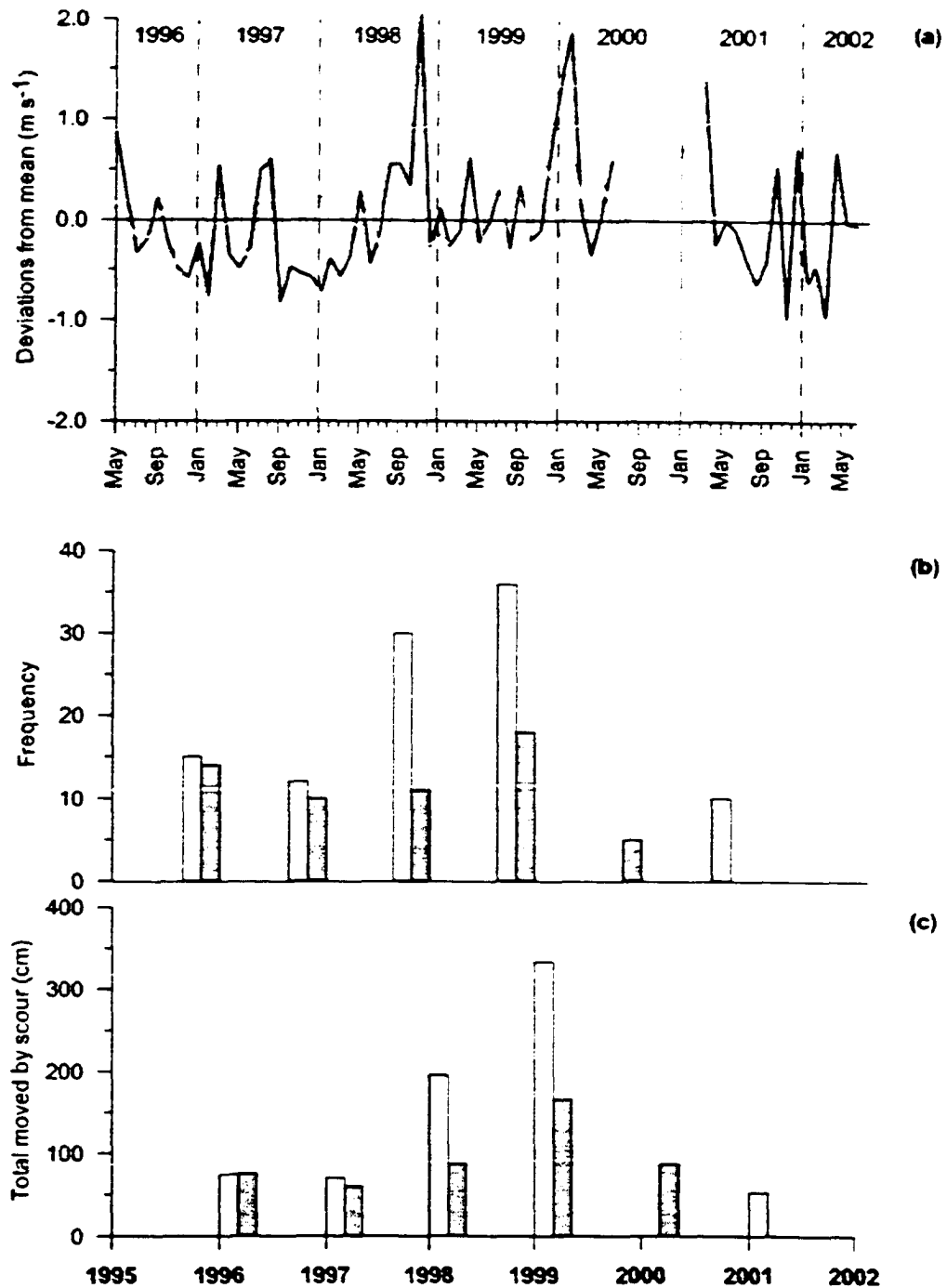
Figure 4.9. (a) Average monthly deviation of wind speed from the monthly (1996-2002) mean at the MWS (grey) and UWS (black); (b) annual frequency of winter wind scour events; (c) annual cumulative surface elevation drop due to winter wind scour events. MWS: grey, UWS: white.
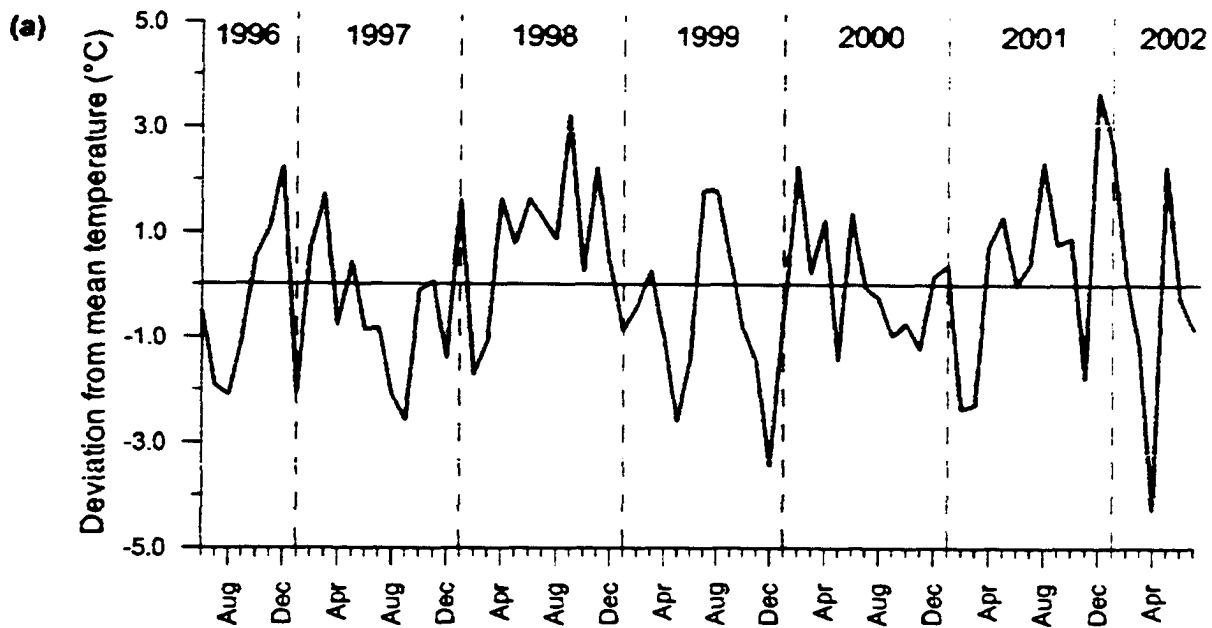
Figure 4.10a. Average monthly deviation of air temperature from the monthly (1996-2002) mean. all stations combined.

109
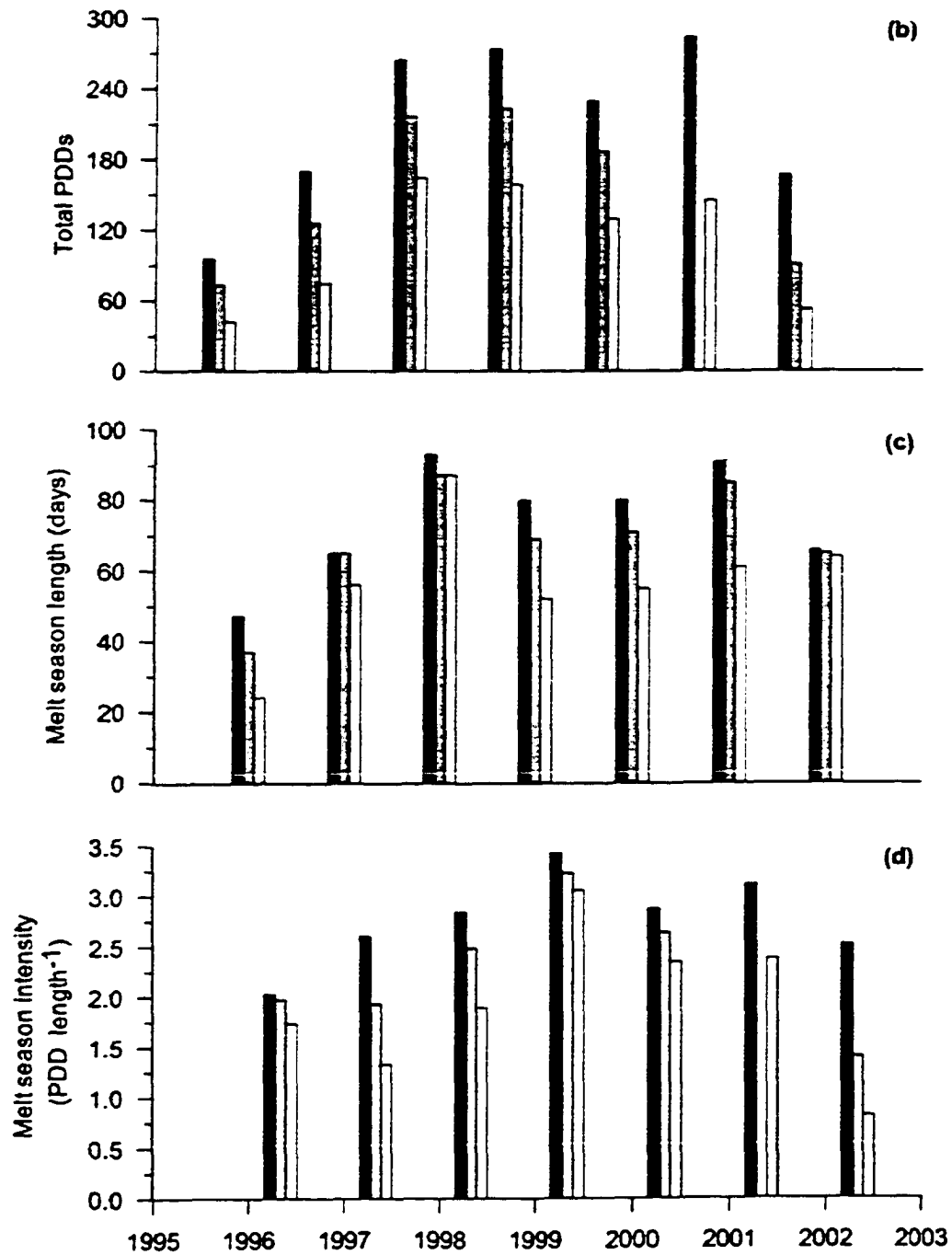
Figure 4.10b. Annual PDD total: (c) melt season length from first to last positive degree-day: (d) melt season intensity. LWS: black. MWS: grey. UWS: white.

110
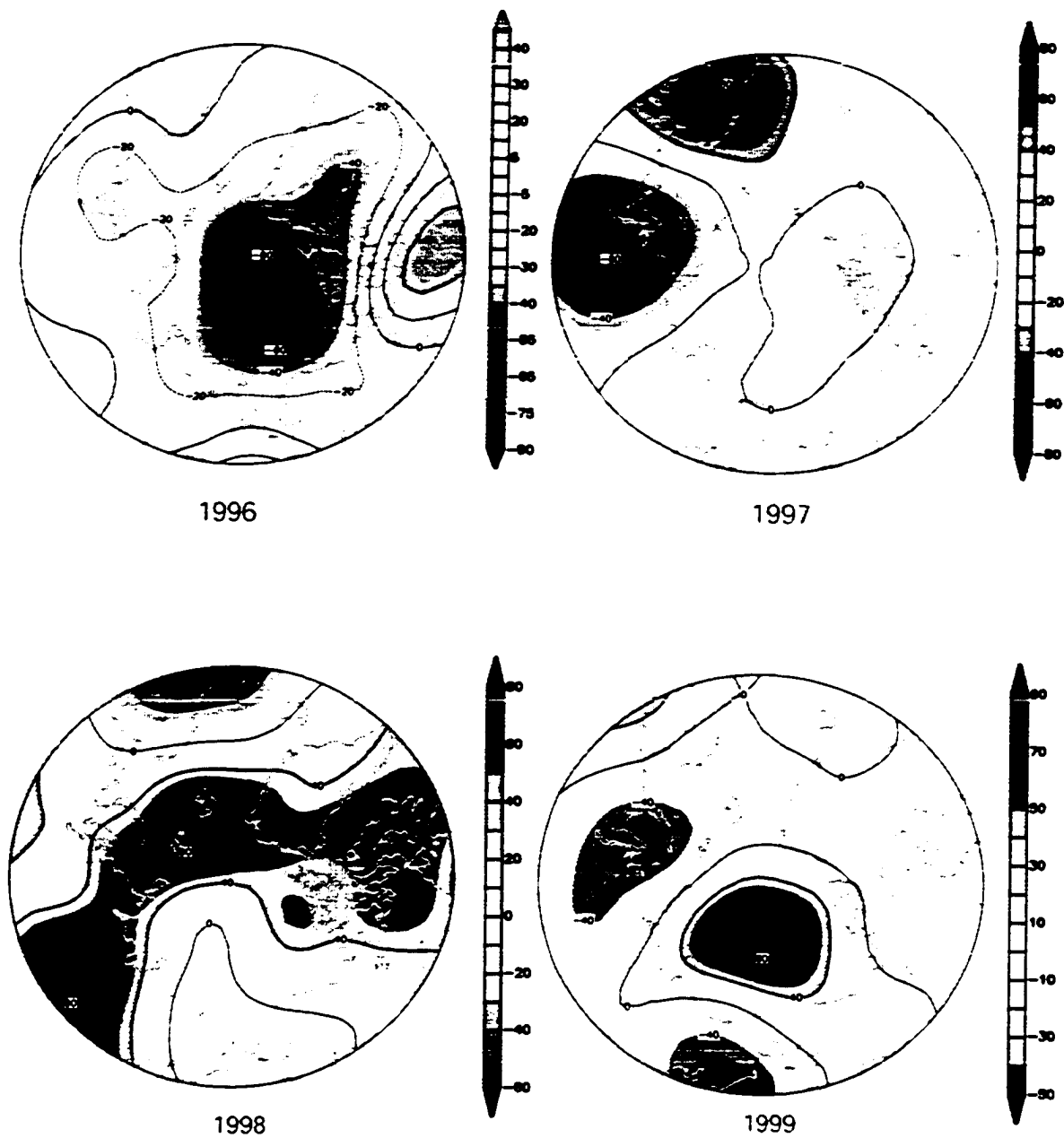
Figure 4.11a. Polar stereographic projections (60°N to 90°N) of annual summer (JJA) 500 mb geopotential height anomalies. 1996-1999.

111
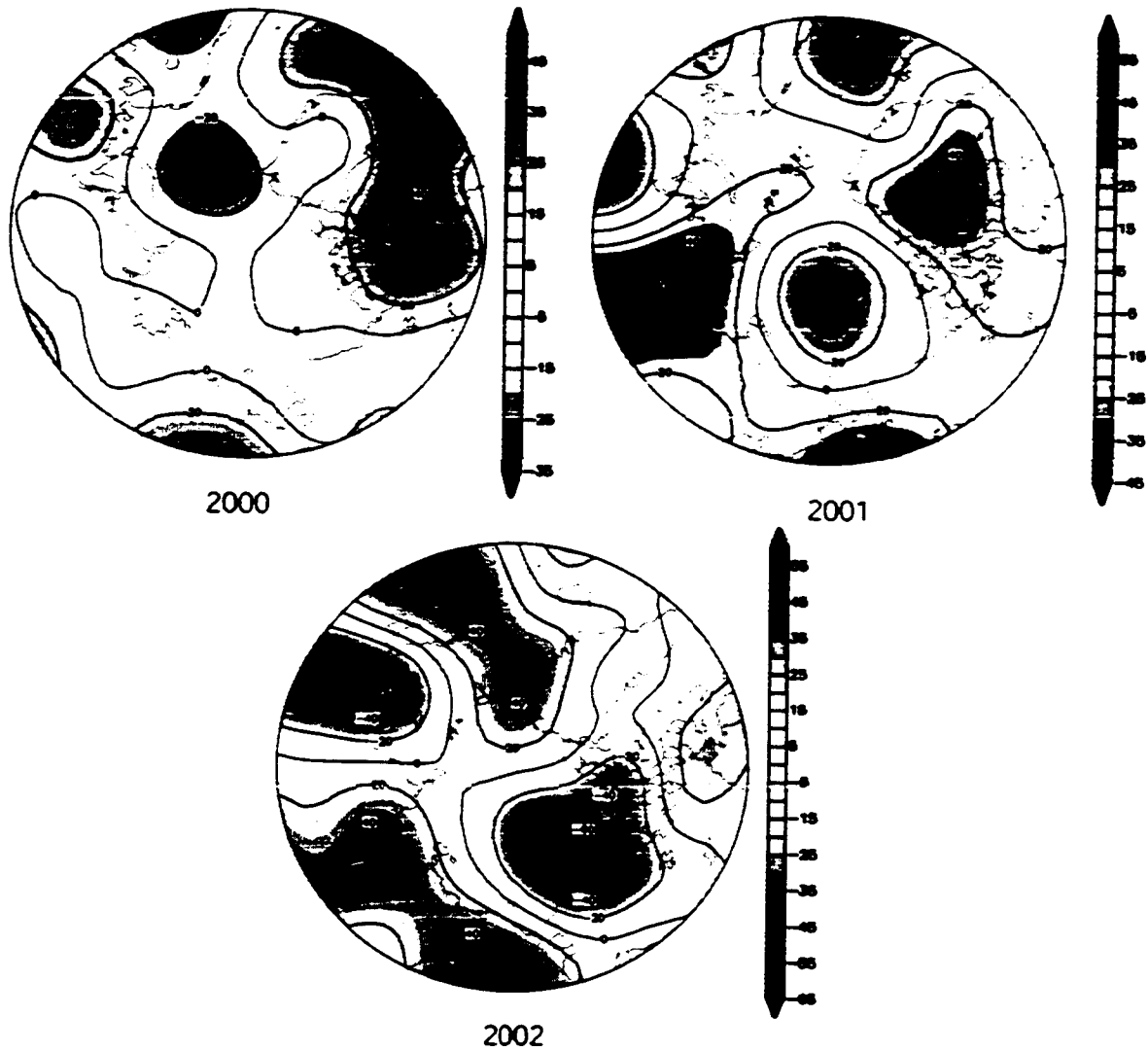
Figure 4.11b. Polar stereographic projections (60°N to 90°N) of annual summer (JJA) 500 mb geopotential height anomalies. 2000-2002.

JJA 1996

JJA 1997

JJA 1998

JJA 1999

JJA 2000

JJA 2001

JJA 2002
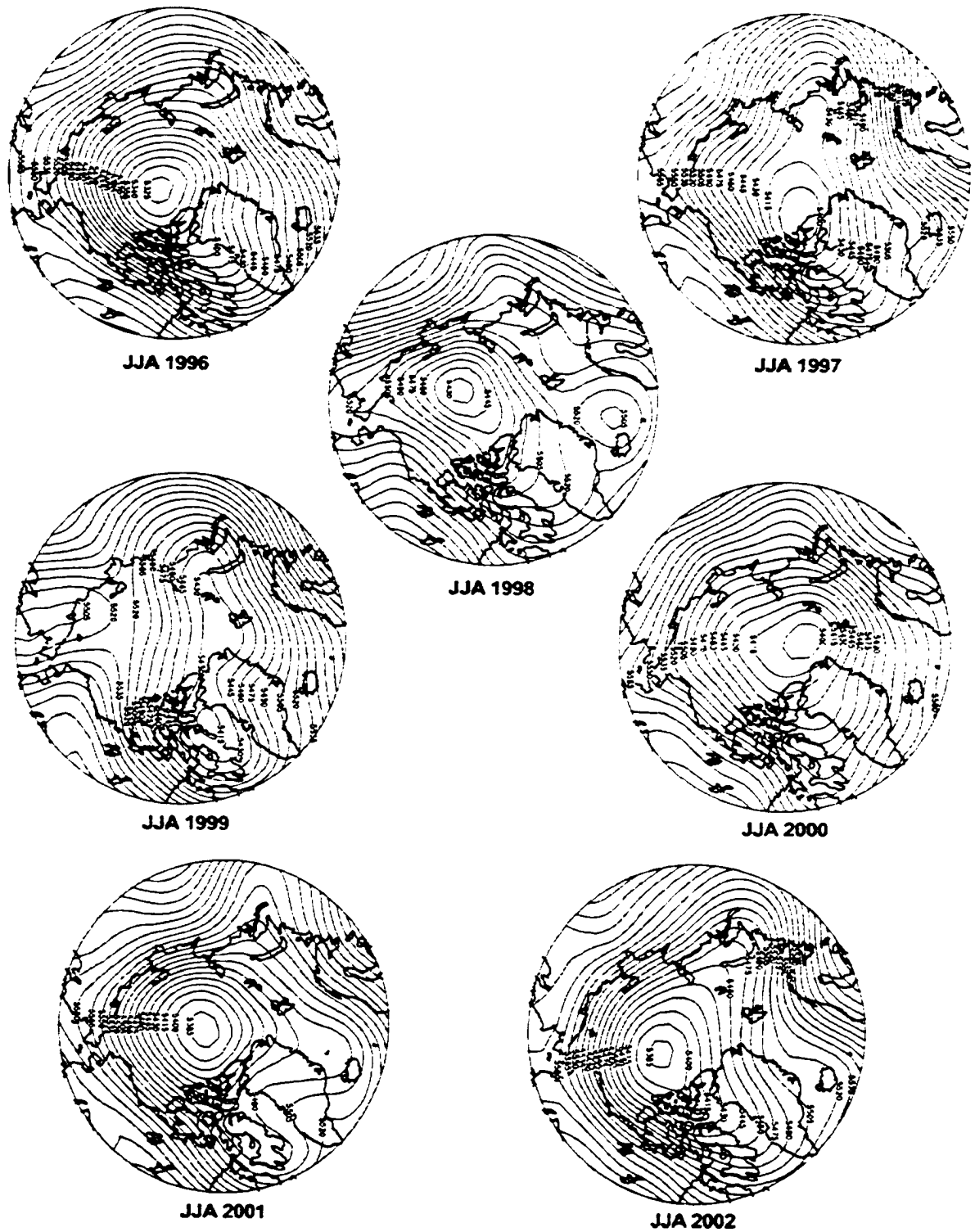
Figure 4.12. Polar stereographic projections (60°N to 90°N) of annual summer (JJA) synoptic configurations at 500 mb geopotential height.

113

CHAPTER 5.

MODELLED RESPONSE OF THE MELT, RUNOFF AND MASS BALANCE OF AN ARCTIC GLACIER TO CLIMATE CHANGE

5.1. Introduction

Anthropogenically induced climate warming is predicted to be greatest in northern high latitudes, especially in winter and spring (Boer et al., 2000; Holland and Bitz, 2003), and there is an increasing amount of evidence to indicate that these changes may already be occurring (Serreze et al., 2000; Morison, 2000; Moritz et al., 2002). Such changes will significantly impact glacier melt and runoff production (Meier, 1990; Oerlemans and Fortuin, 1992).

Given the high cost of Arctic fieldwork, and the difficulty in physically monitoring all glaciers, glacier response to climate is often investigated using numerical models based on energy-balance or degree-day methods (Braithwaite and Oleson, 1987; Bøggild et al., 1994; Fleming et al., 1997; Jóhannesson, 1997; Braithwaite and Zhang, 1999). Energy-balance models (EBMs) are considered most accurate, as they incorporate all variables impacting melt at the glacier surface. However, they also require substantial input data and computational power when run at high space-time resolution in distributed form. Degree-day models (DDMs) require less input data and computational power, and are therefore most useful when available meteorological datasets are limited, and/or where MB must be determined on a large scale (i.e., for a large glacier or ice sheet).

DDMs rely on a simple linear relationship between air temperature and ablation (Braithwaite, 1984; Braithwaite, 1995; Ohmura, 2001; Hock, 2003), where the factor of proportionality is the degree-day factor (DDF; in m WE d^{-1} °C), which varies according to surface type (snow or ice) (Hock, 1999; Singh et al., 2000). At the onset of the melt season, snowpack measured at a meteorological station is distributed over the glacier surface to simulate the end-of-winter (EOW) snowpack. Melt is then calculated for each modelled grid cell as a function of positive degree-days (PDDs; the sum of all positive temperatures extrapolated from the same meteorological station) and the DDF. As ice is exposed in each grid cell, the DDF is switched from a snow to an ice value, and melt is calculated accordingly. At the end of the balance year, the distributed winter

114

accumulation and calculated summer melt are summed to determine the annual net mass balance.

Two aspects of DDMs. however, are problematic. First, they follow two basic assumptions: (a) a constant surface air temperature lapse rate exists between a meteorological station and all points on a glacier (usually the moist adiabatic lapse rate (MALR): -6°C km^{-1}) (Jóhannesson. 1997: Greuell and Böhm. 1998: Braithwaite and Zhang. 2000): and. (b) a constant accumulation lapse rate exists between a meteorological station and all points on a glacier (usually increasing with elevation) (Jóhannesson. 1997: Hock. 2003). Field data from Arctic regions have shown that these assumptions are often untrue: the surface air temperature lapse rate during the summer melt season is often up to 4°C km^{-1} lower than the MALR. and is highly variable (Boon and Sharp. in review: Marshall et al.. in review). EOW accumulation often decreases – rather than increases – with elevation due to snow sublimation and redistribution during winter wind scour events at higher elevations (Koerner. 1966: Box and Steffen. 2001: Boon and Sharp. in review).

Second, spatial and temporal variability in melt, runoff and MB are driven not only by melt processes. but by accumulation caused by summer snowfalls (Fujita and Ageta. 2000: Boon and Sharp. in review) and refreezing processes (superimposed ice (SI) formation and internal accumulation: Pfeffer et al.. 1991: Janssens and Huybrechts. 2000: van der Veen. 2002)). Several modelling studies have therefore attempted to improve DDM simulations by incorporating these processes (e.g.. Woodward et al.. 1997: Arendt and Sharp. 1999). although it is unclear how well these new parameterizations represent actual field conditions.

Given that model output is used to determine climate impacts and assist in policy decisions (e.g.. Houghton et al.. 2001). it is imperative to quantify the impact of these problems on model performance. The goal of this research is to drive a DDM with field data from a high Arctic glacier and determine first the sensitivity of model output to parameter values. and then the possible response of glacier melt. runoff (melt produced following the end of the SI formation/internal accumulation period) and MB to predicted climate change.

115

5.2. The degree-day model

The DDM was created by Arendt (1997), and requires as input a digital elevation model (DEM) of the glacier surface, daily values of air temperature (°C), and daily snowfall amounts (metres water equivalent: m WE). The DDM can be run as a full grid simulation, or for a single point. For this paper, the DDM is run only at single points.

The end-of-winter (EOW) snowpack is distributed to points distant from the input meteorological station by specifying the accumulation at sea level (in m WE), and the lapse rate of accumulation with elevation (m WE m^{-1}). Summer air temperature and summer accumulation are distributed to points distant from the input meteorological station via a specified air temperature lapse rate (in °C m^{-1}) and accumulation lapse rate (in m WE m^{-1}). When the model is used to simulate conditions at the point at which meteorological data are collected, the EOW snowpack (from field measurements or other data) can be inserted into the input file as the first 'snowfall' (in m WE), and summer air temperature and accumulation lapse rates are not required.

The model can be parameterized with a constant DDF, where DDF$_{snow}$ and DDF$_{ice}$ are set to specific values used by the model as each surface is exposed. The model can also be parameterized with a variable DDF (Arendt and Sharp, 1999):

$$DDF = M\alpha + B \tag{1}$$

where M and B are the slope and intercept, respectively, and α is the surface albedo.

Surface albedo in Equation (1) is parameterized using an algorithm developed by van de Wal and Oerlemans (1994). This algorithm uses a series of fixed values to represent the α of fresh snow, old snow, superimposed ice, glacier ice, and water, then applies exponential functions to these values to calculate the time-dependent transition between each α phase. For example, following a new snowfall, α is set to the prescribed value for fresh snow. The fresh snow α then decays over time towards the α of old snow or, once all snow has been removed, towards the α of superimposed ice and then glacier ice. Free water at the surface forms as a function of snow or ice ablation, and forces α towards the value for water.

116

This algorithm requires the user to specify α values for five different surface types (new snow, old snow, superimposed ice, glacier ice, and water), as well as the water runoff time (the time in days for melt to run out of a grid cell). Thus the model calculates α at a given time step, and uses that value in Equation (1) to calculate a DDF based on the specified values of M and B. In order to select appropriate values of M and B, Equation (1) is solved for a known DDF and α value.

In the model, SI formation can be parameterized using one of two methods. The first is the temperature method (Ward and Orvig, 1953; Woodward et al., 1997), in which SI formation is dependent on the 14 m ice temperature, which is often assumed equivalent to the mean annual air temperature (MAAT; Hooke, 1976). SI thickness (X) is calculated as:

$$X = 2A\sqrt{at} \tag{2}$$

where a is the thermal diffusivity of ice (0.011 cm^2 s^{-1}), t is the SI formation period in seconds, and A is a constant calculated as:

$$A\,e^{A^2} = \frac{c\theta_0}{L\sqrt{\pi}} \tag{3}$$

where c is the specific heat capacity of ice at 0°C (2097 J kg^{-1} °C^{-1}), L is the latent heat of fusion of ice (333.5 KJ kg^{-1}), and θ_0 is the MAAT. Using a 10-day period of SI formation based on measurements by Wolfe (1995), Woodward et al. (1997) solved Equations (2) and (3) to define X as:

$$X = -0.69\theta_0 + 0.0096 \tag{4}$$

This method is problematic, however: assuming that the 14 m ice temperature is equivalent to the MAAT fails to account for the warming of near-surface glacier ice due to latent heat release during refreezing (e.g., McCall Glacier, Alaska: Wakahama et al., 1976; White Glacier, Canadian Arctic: Blatter, 1987).

117

The second SI parameterization is the PMAX method. in which the proportion of the snow water equivalence (SWE) of the EOW snowpack that forms SI is specified prior to running the model (Reeh. 1991). Thus SI thickness is calculated as:

$$X = \text{PMAX}d \qquad (5)$$

where PMAX is a proportion (e.g.. 0.60). and d is the end of winter snowpack thickness in m WE. This method is much coarser than the SLT method. due to the large range of measured and modelled values of PMAX (Reeh. 1991: Wolfe. 1995: Fujita et al.. 1996: Bugnion and Stone. 2002).

When run as a point simulation. the model outputs daily values of α and the DDF. as well as daily values of snowpack thickness. SI thickness. melt. MB. and cumulative MLT (all in m WE). When run as a grid simulation. the model outputs annual specific mass balances for each elevation band of the glacier. as well as a cumulative glacier-averaged mass balance (in m WE).

5.3. Study site

John Evans Glacier (JEG) is a large valley glacier on the east coast of Ellesmere Island. Canada (79° 40' N and 74° 00' W: Fig. 5.1). The main trunk of the glacier is 15 km long. covers approximately 160 km^2. and ranges in elevation from 100 to 1500 m a.s.l. (Arendt. 1997). The glacier is polythermal. with cold-based ice in the accumulation area and at the glacier margins where ice is thin. and warm-based ice throughout much of the ablation zone (Copland and Sharp. 2001). Ice thickness reaches a maximum of ~400 m close to the long-term equilibrium line (~750-800 m a.s.l.). and is ~100–200 m in the lower 4 km of the glacier.

Meteorological data have been collected year-round at JEG since June 1996 (Fig. 5.1) (Boon and Sharp. in review). The upper weather station (UWS) is at 1183 m a.s.l. in the long-term accumulation zone. the middle weather station (MWS) is at 824 m a.s.l. near the long-term equilibrium line altitude. and the lower weather station (LWS) is at 261 m a.s.l. in the ablation area.

118

5.4. Methods

We first perform a two-stage sensitivity test using point model runs to simulate conditions at the LWS. The first stage examines model sensitivity to: (a) temperature values used in the temperature-based SI parameterization (SI_{SLT}); and (b) values used for the constant DDF and variable DDF parameterizations. The second stage examines model sensitivity to: (a) proportion values used in the PMAX SI parameterization (SI_{PMAX}); and (b) values of the winter accumulation lapse rate (WALR), and the summer temperature and accumulation lapse rates (STLR and SALR, respectively).

Prior to each stage of sensitivity tests, the model is manually optimized and calibrated to approximately simulate measured 2002 conditions, and is then validated with 2001 data to ensure the use of realistic (i.e., transferable between years) parameter values in the baseline run.

We then examine the short-term (2000-2029) static response of JEG melt, runoff, and MB to climate change scenarios predicted by general circulation models (GCMs) (Walsh et al., 2002), by running the model for a single point within each glacier elevation band and calculating glacier-averaged results. The four scenarios tested are: (1) increased summer air temperature; (2) increased winter precipitation; (3) increased summer precipitation; and, (4) concurrent increases in air temperature and winter precipitation. Our interpretation of the results is constrained by the previously determined sensitivity of model output to parameter values.

5.4.1. Input data

The DEM of John Evans Glacier has a grid cell size of 25 m, with a point elevation accuracy of ±10 m (see Arendt, 1997: p. 128). Comparison of surface elevations from the DEM with measurements taken in the field in 1999 indicated good correspondence between the two (~10 m; Copland, 2001). This is appropriate for this study, as the model is never run for the entire DEM grid. Thus the DEM is used mainly to calculate glacier hypsometry for the climate change scenarios.

For the first stage of sensitivity tests, the model uses 2002 data from the LWS for optimization and calibration, as this season had the most extensive field datasets of both meteorological and snowpack conditions, thereby providing both model input and

119

measured data against which to assess model performance. 2001 data from the LWS are used for validation. For the second stage of sensitivity tests, model sensitivity to temperature and accumulation lapse rates is tested, thus input data from the MWS are used to simulate conditions at the LWS. 2002 data from the MWS are used for optimization and calibration, for the same reasons stated above, and 2001 data from the MWS are used for validation. All model runs simulate conditions at the LWS. as this station has the longest continuous summer season meteorological record against which to compare simulated output.

Air temperature was measured at the LWS using a Vaisala HMP35CF Temperature/ Relative Humidity sensor placed in a Gill radiation shield. When 2002 values were compared with values collected at a shielded HOBO air temperature data logger also located on the LWS. they were 0.1-2.0°C (average 0.75°C) higher (Fig. 5.2). Given that the difference between the sensors is greatest during the afternoon period. we assume it is caused mainly by inadequate ventilation of the Vaisala sensor. A 2 m composite air temperature record was therefore created for the LWS for both 2001 and 2002. by averaging measurements from two HOBOs located along the glacier centreline (200 and 300 m a.s.l.) with the Vaisala air temperature record. Although the HOBO record from the LWS was too short to incorporate into the composite record. the selected method maintains the seasonal air temperature cycle measured at the LWS. but lowers the values during the period of greatest difference to ones more comparable with the surrounding temperatures.

Air temperature values measured at the MWS in 2001 and 2002 using the same instrumentation may have a similar problem: however. we do not have a HOBO air temperature record at this station against which to compare the Vaisala record. We therefore use the air temperature measured by the Vaisala as the 2 m input air temperature record for the MWS in the second stage of sensitivity tests.

The air temperature sensor at each meteorological station was not consistently maintained at 2 m above the ice surface: the distance of each station from the base camp. and the distances between stations themselves. resulted in variations in servicing frequency. Sensor height above the ice surface therefore varied between 1-2 m. which

120

may result in lower air temperatures when the sensor was closer to the ice surface, and vice versa.

For the first stage of sensitivity tests, the initial snowfall amount for the input file was set to the snow water equivalence (SWE) of the EOW snowpack as determined from snow pit measurements. Subsequent summer snowfall amounts were calculated from measurements taken by an ultrasonic depth gauge (Campbell Scientific UDG), and verified with field observations. Snowfall events recorded by the UDG were multiplied by snow density (from Paterson, 1994: p. 9) to determine snowfall amounts in m WE. Each snowfall that occurred following ice surface exposure was assigned a density of wet new snow (350 kg m^{-3}) based on field observations of wet snow: this value corresponds well with wet snow densities measured in snow pits prior to snow cover removal. Because the model will not recognise an input snowfall if the corresponding air temperature is >0°C, any positive temperatures during snowfalls were set to zero.

For the second stage of sensitivity tests, the model calculates EOW snowpack thickness using specified values for sea level snow depth and the winter accumulation lapse rate. Thus, the initial snowfall value in the input file was set to zero, rather than the SWE of the EOW snowpack. Summer snowfalls were calculated using the methods already described, although the first summer snowfall was assigned a dry snow density of 90 kg m^{-3} based on field measurements, while all remaining snowfalls were assigned a wet snow density (350 kg m^{-3}).

For the second stage of sensitivity tests, the model requires additional values for accumulation and air temperature lapse rates. The winter accumulation lapse rate was calculated as the rate of change of snowpack depth per meter increase in elevation, using 2002 values of EOW snowpack (m WE) from the LWS and MWS. The average snow depth at sea level was determined using this lapse rate and the measured EOW snow depth at the LWS. The summer accumulation lapse rate was calculated as the average rate of change in snowfall depth per meter increase in elevation between the LWS and MWS, using all summer snowfalls recorded in 2002 at the LWS and MWS. The summer air temperature lapse rate was calculated as an average of the 2002 daily rate of change of air temperature per meter increase in elevation between the LWS and MWS. The same calculations were repeated for 2001 data.

121

5.4.2. Measured field data

The 2002 and 2001 albedo records at the LWS were calculated using daily average values of 10 s readings of incoming and reflected solar radiation recorded by a Kipp & Zonen and LI200S Li-Cor pyranometer, respectively. Values greater than 0.95 are often caused by either a low sun angle or fresh snow on the sensor, and were therefore removed: this accounted for 13% of days in the 2002 season, and 2% in the 2001 season.

Snow depth at the LWS was calculated by using daily UDG measurements (surface elevation in mm) to determine daily surface elevation change (m). In 2002, snow pit measurements of snow water equivalence (SWE: in m WE) were collected at the LWS five times between Day 159 (8 June) and Day 174 (23 June). These data provide a representative sample of SWE evolution prior to ice surface exposure, as surface lowering (and subsequent snow densification) following the last spring snowfall began on Day 158, and the ice surface was exposed on Day 178. Comparison of UDG-measured and manually measured snow depths indicates good correspondence ($r^2 = 0.91$: p < 0.05), thus the UDG record was used to derive a linear relationship between snow depth (d: in m) and snow pit SWE (m WE):

$$SWE = 0.28d \qquad (6)$$

The intercept was forced through zero, as zero d is equivalent to zero SWE. This relationship is statistically significant ($r^2 = 0.89$: p < 0.05). Comparison of the resulting continuous SWE curve with point SWE measurements taken from snow pits indicates good correspondence overall, although Equation (6) underestimates SWE just prior to ice surface exposure, when the snowpack is highly saturated (Fig. 5.3). This is because measured SWE is high during this time period, as it includes pore water stored in the snowpack. The model, however, calculates SWE by successively removing increments of snow from the EOW snowpack, and assumes pore water runs off rather than remaining in the snowpack. Thus the difference between simulated and measured SWE prior to ice exposure is an estimate of the snow water content: 93%. Following snowpack removal, daily SWE was calculated as the sum of each new snowfall multiplied by its assigned density (see above), or set to zero when the ice surface was exposed.

122

In 2001. snow pit measurements of SWE were not available at the LWS. SWE was therefore calculated using the linear relationship defined for 2002 in Equation (6). Comparison of the resulting continuous SWE record with two snow pits from 200 m a.s.l. (60 m down-glacier from the LWS) shows an approximate 0.06 m WE overestimation of SWE.

UDG measurements from 2002 and 2001 were also converted into daily melt amounts (m WE d^{-1}). During the snow covered period. daily melt was calculated by subtracting SWE (calculated with Equation (6)) on the previous day from SWE on the present day. with negative values indicating melt. Following snowpack removal. the measured albedo record indicates the exposure of SI (Fig. 5.4). Thus daily melt was calculated by multiplying the daily amount of surface elevation drop from the UDG (in m) by the density of SI (600 kg m^{-3}: Wadham and Nuttall. 2000). Once the SI was removed and glacier ice exposed. daily melt was calculated by multiplying the daily amount of surface elevation drop from the UDG (in m) by the density of glacier ice (873 kg m^{-3}: Paterson. 1994. p. 9).

In the case of a summer snowfall. daily melt was set to zero on the day(s) of the snowfall. following which melt was calculated by multiplying the daily surface lowering from the UDG (in m) by the snowfall density (350 kg m^{-3}). If the daily surface lowering was equivalent to the removal of both snow and underlying ice. melt was calculated by summing the depth of snow removed multiplied by the snow density. and the depth of ice removed multiplied by SI density. The duration of SI exposure was determined from the albedo record. Once glacier ice was re-exposed. daily surface lowering was again multiplied by glacier ice density.

Due to the high spatial and temporal variability of SI formation. we do not have continuous field measurements of SI formation and removal from either 2002 or 2001 against which to compare the simulated data. We therefore rely on SI exposure extracted from the albedo record. bi-weekly spot measurements of SI thickness. and field observations of SI formation and evolution. to assess model performance.

Cumulative melt for both 2002 and 2001 was calculated as a running total of daily melt. The measured MB record for each year was calculated beginning with the SWE of the EOW snowpack. with each timestep either removing melt or adding snowfall. In

123

order to incorporate SI into the MB record in the absence of field SI measurements. daily melt was set to zero for the period of SI formation (determined from model output). to indicate mass redistribution (i.e., meltwater refreezing) rather than ablation. This allows us to determine if differences between simulated and measured MB are due to errors other than the failure to incorporate SI.

5.4.3. Model performance

To assess model performance. graphs of simulated and measured daily albedo. SWE. SI. daily melt, cumulative melt and MB were compared qualitatively: simulated and measured daily melt were also compared quantitatively.

Quantitative measures for melt comparison included:

(1) coefficient of efficiency (Nash and Sutcliffe. 1970). often used in assessing model performance:

$$R^2 = 1 - \frac{\sum_{i=1}^{n}(MLT_m - MLT_s)^2}{\sum_{i=1}^{n}(MLT_m - \overline{MLT_m})^2}$$ (7)

(2) modified coefficient of efficiency (Hock. 1999). which emphasises low melt conditions by minimising the impact of high residuals during peak melt:

$$R_{ln}^2 = 1 - \frac{\sum_{i=1}^{n}\left[\ln(MLT_m) - \ln(MLT_s)\right]^2}{\sum_{i=1}^{n}\left\{\ln(MLT_m) - \left[\frac{1}{n}\sum_{i=1}^{n}\ln(MLT_m)\right]\right\}^2}$$ (8)

(3) coefficient of determination (Burt and Barber. 1996). which is the square of the correlation coefficient. and describes the proportion of the total variance in simulated daily melt that is explained by the regression of measured daily melt on simulated daily melt.

124

$$r^2 = 1 - \frac{\sum_{i=1}^{n}\left(MLT_s - \overline{MLT_m}\right)^2}{\sum_{i=1}^{n}\left(MLT_m - \overline{MLT_m}\right)^2} \qquad (9)$$

In Equations (7) – (9), n is the number of time steps calculated. MLT_m is the measured daily melt. MLT_s is the simulated daily melt. and $\overline{MLT_m}$ is the average measured daily melt.

5.5. Sensitivity Test Stage 1: SI$_{SLT}$, constant DDF, variable DDF

5.5.1. Parameter selection for calibration run

The model was manually optimized/calibrated by running it with 2002 data from Day 152 (1 June) – Day 210 (27 July), and varying parameter values in each run until the best fit between measured and simulated data was obtained (determined using the measures described in Section 5.4.3). Parameters determined using this method were used in subsequent model runs (Table 5.1).

We used the variable DDF parameterization by solving Equation (1) for DDF$_{snow}$= 0.003 m WE d^{-1} °C^{-1} and DDF$_{ice}$ = 0.007 m WE d^{-1} °C^{-1}. and measured albedos (α) of 0.95 and 0.25, respectively. This results in M = -0.0057 and B = 0.0084 (Table 5.1). The selected DDFs fall within the reasonable range measured on glaciers worldwide (Braithwaite and Zhang. 1999). and compare favourably with DDFs calculated at JEG in 1996 and 1998 (Arendt and Sharp. 1999). Values of α for specific surface types (new snow, old snow, superimposed ice, glacier ice, water) were selected based on 2002 field measurements (Fig. 5.4). The water runoff time was used as a tuning parameter to maximize correspondence between simulated and measured melt.

The SI$_{SLT}$ parameterization was used. as SI$_{PMAX}$ is tested in Sensitivity Test Stage 2. Although MAAT was not measured at JEG in 2001-2002. data are available from 1997 (Woodward et al.. 1997). Comparison of MAAT in 1997 and 2002 at Alert and Eureka shows that 2002 was 1.6°C warmer. We applied this value to the measured 1997 value from JEG to obtain a MAAT for 2002.

125

5.5.2. Calibration results

Comparison of the simulated and measured albedo records (Fig. 5.5a) shows that. while the two have the same base level and follow similar patterns. there are two main problems: (1) fresh snowfalls are automatically assigned an albedo of 0.95. which is not always true. as fresh snow albedo is affected by snow grain size and the radiative properties of the underlying surface (Brock et al.. 2000): and. (2) the initial albedo value is too high. as it is read from the input file as new snowfall. In reality. the surface is old snow from the EOW snowpack. which has a lower albedo. These limitations in the model reduce melt due to the high surface albedo. but have surprisingly little impact on overall model output.

Comparison of simulated and measured daily SWE indicates good correspondence (Fig 5.5b). SWE is overestimated at the onset of the summer season. when the albedo is set too high. It is then underestimated just prior to snow cover removal. which may be due to a high snow water content (see Section 5.4.2). Later in the season. the model alternately leaves fresh snowfall on the ground too long (Day 178 instead of 177) due to the high simulated albedo of the snowfall. or removes it too early (Day 194 instead of 195).

The simulated SI record shows SI formation on Day 160 and removal by Day 184 (Fig. 5.5b). which compares well with field measurements of SI formation on Day 159 and removal by Day 182. However. following the Day 192 snowfall. the simulated record allows SI to persist until Day 198. but field measurements indicate SI removal by Day 196. Subsequently. the model underestimates melt during this period. as it assumes a higher surface albedo. Total SI thickness may not be well simulated. as comparison of available manual measurements with model output shows some overestimation. Given the lack of a comprehensive series of manual SI measurements at the LWS. however. we are unable to improve the simulation.

Total simulated melt is only 0.02 m WE less than measured total melt (Fig. 5.6a) due to slight model underestimation of melt at the beginning and end of the season. Daily simulated and measured melt correspond well over the simulation period. but not on a day-to-day basis (r^2 = 0.68: p < 0.05) (Table 5.2: Fig. 5.5c). This could be due to the formation of a weathering crust (Munro. 1990). A weathering crust builds on the glacier

126

surface during ablation as the porosity of the subsurface increases. Meltwater runs off. but the surface elevation hardly changes: thus measured melt based on UDG data is underestimated. Eventually the porosity approaches 100%. and there is an abrupt drop in surface elevation. leading to an overestimation of melt by the UDG.

For example. from Day 178-182. measured melt is lower than simulated melt. possibly due to weathering crust formation. Then. from Day 185-189. rainy weather removed the weathering crust. but didn't create a significant volume of melt. Because the UDG measured a substantial drop in surface elevation. however. measured melt is higher than simulated melt. The removal of a weathering crust is corroborated by the slight increase in measured albedo on Day 187 (Fig. 5.4). corresponding with exposure of a relatively smooth ice surface below the weathering crust.

Given this error. the melt records compare best at low melt rates ($R_{in}^2 > R^2$: Table 5.2). To reduce the day-to-day variability in melt rate. the measured and simulated melt records were smoothed to a 3-day average. Each day's melt was calculated as the average of daily melt on that day. the previous day. and the next day. This improves the correspondence between the two records ($r^2 = 0.81$; $p < 0.05$) (Table 5.2: Fig. 5.5d).

Dividing daily melt into snow and ice melt shows that the model is marginally better at predicting ice melt (Table 5.3). although it consistently under predicts it – especially during the period of weathering crust removal. Dividing the 3-day melt record into individual snow and ice melt records gives the same results. although somewhat improved. While this could indicate that DDF values calculated by the model. using specified M and B values and the albedo parameterization. are inaccurate. altering these values did not improve model output. This indicates that other processes – such as the formation and removal of the weathering crust – are affecting ice melt simulation.

Simulated cumulative MB is only 0.004 m WE greater than measured cumulative MB (calculated with melt set to zero during periods of SI formation) (Fig. 5.6b). This indicates that the failure to incorporate SI into the measured MB record accounts for the majority of the difference between the two records. although the differences between the two records from Day 179 – 190 are due to the weathering crust effect.

127

5.5.3. Model validation

The model was validated with 2001 data from Day 151 (31 May) – Day 210 (29 July) using the parameter values determined in the optimization/calibration (Table 5.1). This allows us to examine the interannual applicability of the parameters used in the 2002 model run.

Visual and statistical comparisons of measured and simulated datasets from 2001 show good correspondence (Tables 5.2-5.3: Figs. 5.7-5.8). Melt and SWE are simulated as well as they were in the calibration run, although low melt conditions are more poorly simulated, and calculation of 3-day average melt does not improve correspondence between simulated and measured records as much as in the calibration run. Separate snow and ice melt are simulated much better than in the calibration run, although ice melt is again consistently underestimated. Given that total melt is underestimated by 0.22 m WE. and that the cumulative MB records also indicate underestimation of ice melt (Fig. 5.8), it is possible that the DDF_{ice} is slightly too low. However, running the model again with different values of M and B (based on a higher DDF_{ice}) does not improve output, indicating that the model parameters (Table 5.1) are at their optimum values. Thus we assume that they are appropriate for use in other years. 2001 is therefore used as the baseline run against which to assess the sensitivity of model parameters.

5.5.4. Sensitivity tests

Table 5.4 lists the model parameters and the range of values for which sensitivity tests were conducted, the source of the values, and the test results. All sensitivity test output is compared with output from the 2001 baseline run.

In the absence of probability density functions describing the range of plausible values for each model parameter (e.g.. van der Veen. 2002). model sensitivity to parameter values cannot be defined absolutely. We therefore use a qualitative measure for sensitivity. based on model response to the selection of both extreme high and low parameter values. relative to model response to average parameter values.

128

5.5.4.1. Parameter: SI_{SLT}

Model output shows low sensitivity to the MAAT (or 14 m ice temperature) value used in the SI_{SLT} parameterization (avg. MB change = 0.007 m WE per °C) (Fig. 5.9). The response is stepped, as SLT must change by 2°C to produce a change in SI formation. Higher mean SLT results in thinner SI and a greater likelihood of early SI removal, although SI is removed only one day early relative to the baseline run. Changes in SI formation impact MB by altering the total amount of internal accumulation: they have no effect, however, on melt.

5.5.4.2. Parameter: Constant DDF

Model output is highly sensitive to the values used for the constant DDF_{snow} (avg. MB change = 0.0355 m WE per 0.0005 m WE d^{-1} °C^{-1}) (Fig. 5.10), impacting snowpack removal, melt, SI formation, and MB. As DDF_{snow} increases, both snowmelt and SI formation begin earlier, and the snowpack is removed sooner. Between the lowest and highest DDF, there is a 10-day difference in the date of snowpack removal. With higher values of DDF_{snow}, SI grows thicker, reaches maximum thickness, and is exposed and removed more quickly. After the summer snowfall, however, higher values of DDF_{snow} result in lower maximum SI thickness, although SI is still removed sooner. Higher values for DDF_{snow} also result in higher melt: daily melt amounts at the highest value of DDF_{snow} are up to double the melt with the lowest DDF_{snow} value. The impact on MB is substantial, up to 0.040 m WE per 0.0005 change in DDF_{snow}. However, the MB impact is lowest between values of 0.005 and 0.0055 m WE d^{-1} °C^{-1} – only 0.011 m WE: this indicates that MB sensitivity is also a function of the specific DDF_{snow} value.

Model output is also sensitive to the values used for the constant DDF_{ice} (MB change = 0.0363 m WE per 0.0005 m WE d^{-1} °C^{-1}) (Fig. 5.11). DDF_{ice} only affects melt during the period of glacier ice exposure, thus the change in melt is constant between DDF_{ice} values (0.036 m WE). Because no other variables are affected, the annual MB change is also constant.

5.5.4.3. Parameter: Variable DDF

(a) Water runoff time

129

Model output is somewhat sensitive to the selection of the water runoff time within the albedo parameterization routine of the variable DDF parameterization (MB change = 0.012 m WE per 0.5 day) (Fig. 5.12). The greater the runoff time. the more meltwater accumulates at the glacier surface. This decreases surface albedo. subsequently impacting the DDF calculation. SI forms sooner and more thickly from the accumulated meltwater. but is removed sooner due to the lower albedo. Following summer snowfalls. higher water runoff times remove SWE more quickly. and subsequently allow SI to form earlier. be removed sooner. and reach reduced thickness.

(b) Surface albedos

The albedo of each surface type used in the albedo parameterization (sub-component of the variable DDF parameterization) was altered individually to test model response. Model output is somewhat sensitive to changing these values. but the impact depends largely on the duration of exposure of each surface type. and the air temperature during that period.

The model is insensitive to the old snow albedo: changing its value has no impact on model output, suggesting an error internal to the model. The model is least sensitive to the water albedo (avg. MB change = 0.001 m WE per 0.02 albedo). likely due to the small range of acceptable values. Sensitivity increases with the superimposed ice albedo (avg. MB change = 0.003 m WE per 0.02 albedo). with lower albedo values resulting in slightly thinner SI. earlier SI removal and subsequent glacier ice exposure. The model is equally sensitive to the glacier ice albedo (avg. MB change = 0.015 m WE per 0.05 albedo). with greater model sensitivity the longer glacier ice is exposed (Fig. 5.13). The model is most sensitive to the new snow albedo (avg. MB change = 0.012 m WE per 0.02 albedo). with higher albedo values resulting in greater MB. due to the impact on SI formation: a higher albedo results in snowpack of longer duration. providing a longer period in which SI can form.

(c) *M* and *B*

Sensitivity of model output to changing values of M and B in the variable DDF parameterization was tested as follows: Equation (1) was solved for the range of DDF_{snow} values and a new snow albedo of 0.95. while holding DDF_{ice} constant at the value selected in the calibration (0.007 m WE d^{-1} °C^{-1}). Equation (1) was then solved again for

130

the range of DDF_{ice} values and a glacier ice albedo of 0.25, while holding DDF_{snow} constant at the value selected in the calibration (0.003 m WE d^{-1} $°C^{-1}$).

Model output is highly sensitive to values of DDF_{snow} (as also seen with the constant DDF) used to calculate M and B values (avg. MB change = 0.037 m WE per 0.0005 m WE d^{-1} $°C^{-1}$) (Fig. 5.14). Changing DDF_{snow} significantly affects snowpack removal, melt, SI and MB. Each increase in DDF_{snow} results in snowpack removal one day earlier, increases daily melt by a maximum of 0.007 m WE, and changes the thickness and duration of SI. Even a small change in DDF_{snow} values can result in SI removal three days earlier following the summer snowfall. These changes subsequently have a large impact on annual MB.

The model is more sensitive to changing the values of DDF_{ice} used to calculate M and B (avg. MB change = 0.048 m WE per 0.0005 m WE d^{-1} $°C^{-1}$) (Fig. 5.15). This is likely due to the fact that, when calculating M and B, B changes by 0.0007 for each iterative change in DDF_{ice}, as opposed to only 0.0002 for each iterative change in DDF_{snow}. As B values have the largest impact on the DDF calculation (see Equation (1)), this change significantly impacts both ice and snow melt. The rate of snowpack removal is increased; SI is thinner and is removed more quickly with higher DDF_{ice} values, and daily melt increases by a maximum of 0.012 m WE. These impacts are greatest during the snow-free portion of the melt record, with the SI and melt impacts resulting in the high avg. MB change.

5.6. Sensitivity Test Stage 2: SI_{PMAX}, WALR, STLR and SALR

5.6.1. Parameter selection for calibration run

The model was manually optimized/calibrated a second time, using 2002 MWS data from Day 152 (1 June) – Day 201 (20 July) to simulate conditions at the LWS. This allowed us to test model sensitivity to PMAX values (SI_{PMAX}), and values for the winter accumulation lapse rate (WALR), and the summer accumulation and air temperature lapse rates (SALR and STLR, respectively). Parameter values were varied in each run until the best fit between measured and simulated data was obtained (determined using the measures described in Section 5.4.3). Parameters determined using this method were used in subsequent model runs (Table 5.5).

The variable DDF parameterization was used as outlined in Section 5.5.1. The SI_{PMAX} parameterization was used instead of SI_{SLT}, with a value of 0.60 (Reeh. 1991; Wolfe. 1995). The WALR and average sea level snow depth were calculated from 2002 field data. The average SALR was calculated as 0.000004 m WE m^{-1}, with a range of – 0.000025 – 0.000028 m WE m^{-1}. The large range is due to the fact that a snowfall may occur at one station but not the other; additionally, the SALR may change sign depending on the direction of travel of the air mass bringing the snowfall (i.e., moving up- or down-glacier). The average STLR was calculated as –0.0015°C m^{-1}, with a range of –0.0076 – 0.0056°C m^{-1}. Due to changes in overlying air mass characteristics, the daily STLR frequently changes sign (Boon and Sharp. in review; Marshall et al.. in review).

5.6.2. Calibration results

Comparison of simulated and measured albedo shows that simulated albedo fails to decay with time as the EOW snowpack is removed (Fig. 5.16a). While the model does read the summer snowfalls, the first snowfall occurs a day late. As mentioned in Section 5.5.2, the initial albedo is too high, and assigning a 0.95 albedo to all new snowfalls ignores secondary impacts on snow albedo; thus the albedo of each new snowfall is overestimated.

Comparison of simulated and measured SWE indicates model difficulties in distributing new snowfalls, largely because of the wide range in SALRs (Fig. 5.16b). The rate of EOW snowpack removal is initially too steep, and is further exacerbated by model failure to calculate the appropriate thickness of the fresh snowfall on Day 158. These two errors result in snowpack removal two days too early. In addition, the thickness and duration of the later summer snowfalls are either under- or overestimated by the SALR.

Comparison of simulated and measured SI shows reasonable correspondence (Fig. 5.16b): field measurements indicate SI formation beginning on Day 159 and removal on Day 182, with a second episode of SI formation after the second snowfall terminating on Day 196. The model simulates the second SI episode appropriately; however, the duration of the first episode is overestimated, with SI formation from Day 152-184. This could be because the model doesn't differentiate between ice layer formation either within or at the bottom of the snowpack. Field measurements do, however, thus we

132

observe SI formation after ice lenses have already formed within the snowpack. This may account for the discrepancy between modelled and observed data.

Total melt is simulated well, with only 0.001 m WE difference between the simulated and measured records (Fig. 5.17a). Comparison of the daily melt records, however, indicates coarse correspondence between the two ($r^2 = 0.54$; $p < 0.05$) (Table 5.6; Fig. 5.16c). Some of the day-to-day variability between simulated and measured melt can be attributed to the weathering crust phenomenon described in Section 5.5.2. In addition, the measured STLR averaged for this time period was 0.00009 m WE m^{-1} – much higher than the -0.0015°C m^{-1} used as the input parameter. Air temperature extrapolated from the MWS down to the LWS was therefore overestimated, exaggerating simulated melt. The records were therefore smoothed to a 3-day average, which significantly improves the correspondence between simulated and measured data ($r^2 = 0.69$; $p < 0.05$) (Table 5.6; Fig. 5.16d).

Dividing both the daily melt and the 3-day melt comparisons into snow and ice melt shows that the model is much better at predicting ice melt (Table 5.7). Simulated cumulative MB is only 0.004 m WE greater than measured cumulative MB (calculated with melt set to zero during periods of SI formation) (Fig. 5.17b). This indicates that the failure to incorporate SI into the measured MB record accounts for the majority of the difference between the two records, although the differences between the two records from Day 170 – 191 show the impact of the early simulated snowpack removal, and the weathering crust effect.

5.6.3. Model validation

In order to determine the portability of the selected parameters between years, the model was validated using 2001 data from the MWS for Day 157 (6 June) – Day 207 (26 July), and the parameters in Table 5.5, to simulate conditions at the LWS.

Comparison of the simulated and measured datasets indicates poor SWE correspondence and only broad-scale melt correspondence ($r^2 = 0.58$; $p < 0.05$), with ice melt consistently underestimated (Tables 5.6-5.7; Figs. 5.18-5.19). In comparison with the calibration, the validation simulated measured SWE worse, and melt conditions almost the same, although low melt conditions were more poorly simulated (Table 5.6).

133

Separate snow and ice melt simulations are better ($r^*_{val} > r^*_{cal}$) than the calibration. and total melt is simulated well (0.007 m WE difference). However. simulated MB is 0.169 m WE lower than measured MB (calculated with melt set to zero during periods of SI formation) (Fig. 5.19b). due mainly to the initial underestimation of EOW snowpack thickness and its subsequent early removal. as well as to errors in the STLR later in the season (around Day 204).

These results indicate that the parameter values used in the calibration cannot be successfully applied to a separate dataset due to interannual variations in the WALR and STLR. We therefore ran the model again for 2001 using the parameter values from Table 5.5. but lapse rates specific to 2001 (Table 5.8). As the output dataset from this run improved the correspondence between simulated and measured data (Figs. 5.20-5.21: Table 5.9). it was used as the baseline run for the following sensitivity tests.

5.6.4. Sensitivity tests

Table 5.4 lists the model variables and the range of values for which sensitivity tests were conducted. the source of the values. and the test results. As described in Section 5.5.4. we use a qualitative measure for sensitivity. based on model response to the selection of both extreme high and low parameter values. relative to model response to average parameter values.

5.6.4.1.   Parameter: SI$_{PMAX}$

Modelled SI and MB are highly sensitive to changing PMAX values (avg. MB change = 0.017 m WE per 0.1 PMAX) (Fig. 5.22). Simulated albedo is slightly affected. dropping from SI to glacier ice values one day earlier as PMAX is decreased. As these changes occur for only a short time period. however. melt is hardly affected. SI forms more thickly and has a longer duration with higher PMAX values. significantly increasing MB.

5.6.4.2.   Parameter: WALR

The model is highly sensitive to changes in the WALR (avg. MB change = 0.015 m WE per 0.000025 m WE m^{-1}). which extrapolates winter accumulation from sea level up to the LWS. EOW snowpack is consistently thicker the greater the lapse rate. remaining

134

on the ground 1-2 days longer for each iterative increase (Fig. 5.23a). SI thickness and duration also increase as WALR increases (Fig. 5.23b), because SI is a function of EOW snowpack thickness. Melt is slightly affected due to surface albedo change after SI removal, but the largest impact is on MB.

5.6.4.3. Parameter: STLR

The model is extremely sensitive to STLR values (avg. MB change = 0.27 m WE per 0.002°C m^{-1}), which extrapolate air temperature from the MWS down to the LWS. A more positive STLR decreases air temperature at the LWS, resulting in longer snowpack duration, from 11 days duration at -0.009°C m^{-1} to 51 days (the entire season) between 0.003 and 0.007°C m^{-1} (Fig. 5.24a). More positive STLRs also result in decreased SI thickness, but substantially increase SI duration (Fig. 5.24b), due to colder temperatures at the LWS reducing melt. The increased snowpack and SI duration subsequently have a significant impact on MB.

5.6.4.4. Parameter: SALR

Model sensitivity to values of SALR, which extrapolates summer snowfalls from the MWS down to the LWS, is dependent on whether SALR is positive or negative (avg. MB change = 0.011 m WE per 0.000005 m WE m^{-1}). The model is more sensitive to negative values of SALR, likely because it results in more snowfall at the LWS (Fig. 5.25a). With a negative SALR, the EOW snowpack is thicker and lasts two days longer, as the model is able to distribute the early season snowfalls measured at the MWS. This results in thicker SI of one day longer duration (Fig. 5.25b), and ultimately reduces total melt and increases MB (when compared with LR = 0°C m^{-1}). The model is less sensitive to positive values of SALR (Fig. 5.25a). The later summer snowfall is thinner and of shorter duration (1 day), while SI shows no change (Fig. 5.25b).

It is important to note that, were the model to simulate conditions at the MWS with data from the LWS, several snowfalls at the MWS would be missed. This is a major problem when extrapolating summer snowfalls to higher elevations from a low elevation station: often a snowfall at higher elevations falls as rain at lower elevations. Even with

135

the correct lapse rate. there must be a snowfall at the lower station before it can be distributed.

5.7.   Discussion of sensitivity test results

The model is most sensitive to changes in the WALR and STLR, and to negative values of SALR. It is evident that interannual variability in lapse rates will significantly affect model output. It is therefore inadvisable to: (a) assume a constant lapse rate for all model runs (e.g., MALR); (b) assume a positive lapse rate for accumulation, as it can often be negative, in which case model sensitivity is increased; and, (c) assume lapse rates derived for a single season are applicable to other seasons. When extrapolating summer snowfalls up-glacier from a low elevation site, not all higher elevation snowfalls can be represented, as they often occur as rain at low elevations.

The next most sensitive parameter is the variable DDF. The model is most sensitive to changing M and B values caused by altering DDF_{ice} values. This sensitivity increases the longer the period of glacier ice exposure, significantly affecting MB. The model is to a lesser extent sensitive to changing M and B values caused by altering DDF_{snow} values, which affects SI thickness and date of removal, EOW snowpack rate and date of removal, total melt, and subsequently MB.

Model sensitivity to the variable DDF parameterization is increased by its incorporation of the albedo parameterization (described in Section 5.2). Model output is most sensitive to changing new snow albedo values, as the rate of decay of the new snowpack is a function of several other variables, including water runoff time, days following new snowfall, and glacier ice albedo. Model output is therefore also sensitive to glacier ice albedo values, which directly impact melt during the snow free portion of the melt season. An accurate value is especially important when glacier ice is exposed for long time periods, as it significantly impacts both total melt and MB. The range of acceptable glacier ice albedo values is, however, relatively large due to seasonal and interannual variations in ice debris content (Paterson, 1994; Greuell and Genthon, 2004). Model output is also highly sensitive to the water runoff time, as it is a significant variable in the daily albedo calculation. Selection of an appropriate value can be difficult, especially when running the model for a grid, due to the spatial variability of the runoff

136

time (i.e., accumulation zone, firn zone, superimposed ice zone, ablation zone), and the temporal variability in runoff time depending on the stage of the melt season (Fountain, 1996).

Model output is also sensitive to values used in the constant DDF parameterization. The model is equally sensitive to constant vs. variable DDF_{snow} values, but less sensitive to constant vs. variable DDF_{ice} values. A major complication for constant DDFs is that the value should change for different snow types (new, old, wet, etc.), but is instead fixed. Selection of the appropriate DDF_{snow} value is complicated by the factors mentioned in Section 5.5.2 for snow albedo, especially given the wide range of measured values (Braithwaite and Zhang, 1999).

The model is most sensitive to values of PMAX selected for the SI_{PMAX} parameterization, thus knowledge of the appropriate PMAX value is most important when simulating MB using this parameterization. Model sensitivity to values of MAAT (or 14 m ice temperature) used in the SI_{SLT} parameterization is minimal, indicating that as long as the selected value is within a degree of the actual one, model output will remain unaffected.

5.8. Climate change response

5.8.1. Methods

We examine the static (i.e., ice geometry remains fixed) response of JEG melt, runoff and MB to short-term climate change by running the model for four climate scenarios: (1) increased summer air temperature; (2) increased winter precipitation; (3) increased summer snowfalls; and, (4) concurrent increases in summer air temperature and winter precipitation (Janssens and Huybrechts, 2000; Walsh et al., 2002).

The climate scenarios are derived from composited output from eight coupled atmosphere-ocean-ice GCMs (Table 5.10; Walsh et al., 2002). The model runs used to create the composite were forced with the IPCC's B2 scenario, which assumes slower population growth and greater environmental protection than the business-as-usual scenario, thus producing lower CO_2 emissions and less warming (Houghton et al., 2001). The composite output gives the temperature and precipitation increase for 2000-2029 relative to the 1961-1990 average (Walsh et al., 2002).

137

When run as a grid simulation. the DDM outputs only annual data. In order to create daily output for the entire glacier. therefore. the model is run for a single point within each glacier elevation band. and the resulting daily values are manually multiplied by the number of grid cells within each band. The daily totals from each elevation band are then summed. and divided by the total number of grid cells glacier-wide (0-1200 m a.s.l.). This effectively provides a daily glacier-averaged value of each output variable. weighted by the area of each elevation band.

Output from each climate scenario is compared with output from a baseline run using LWS data from 1 June – 31 August. 2001 (Fig. 5.26). As 2001 is within the 2000-2029 period simulated by the GCMs. it is necessary to determine its suitability as the baseline year. Comparison of 2001 mean summer (JJA) air temperature with observed 1961-1990 mean summer air temperature at Alert and Eureka indicates that summer 2001 is less than half a standard deviation warmer than the 30 yr average (0.5°C. Alert: 0.4°C. Eureka). As only JJA air temperatures are used in the climate sensitivity test. these results support the use of 2001 as the baseline year.

In Section 5.6.3. it was determined that there is good correspondence between measured and simulated data from June and July. 2001. when using the parameters in Table 5.8: it is therefore assumed that this relationship also holds for August. Given model sensitivity to WALR. STLR and SALR. all lapse rates were re-calculated for 2001 to incorporate August data (Table 5.11). Note that two values are used for each lapse rate parameter: one for conditions between the LWS and MWS (used for 100-900 m elevation bands). and a second for conditions between the LWS and UWS (used for 900-1200 m elevation bands). Given model sensitivity to SI$_{PMAX}$ values. the SI$_{SLT}$ parameterization was used instead. Although the model is relatively sensitive to the variable DDF parameterization. it provides more realistic output than the constant DDF. We therefore use the variable DDF parameterization. with values previously shown to give good correspondence between measured and simulated datasets. and also to compare well with values measured at JEG.

It is important to note that model performance was tested (in Sensitivity Test Stages 1 and 2) by simulating conditions in the ablation zone. at a low elevation on JEG: model performance for perennially snow-covered areas at higher elevations on JEG has not been

138

tested. However. it is assumed that model performance during snow covered periods at the LWS is an indicator of how well the model will perform at higher elevations. When using 2001 data as input and the parameter values in Table 5.8. the model simulated snow melt reasonably well ($r^2 = 0.46$; $p < 0.05$); the 3-day averaged snow melt record was even better ($r^2 = 0.58$; $p < 0.05$). We also compare simulated output from the 800-900 m elevation band with measured data from the MWS. and simulated output from the 1100-1200 m elevation band with measured data from the UWS. to ensure that model output is realistic.

5.8.1.1. Climate scenarios

Composite output from the eight GCMs predicts a monthly average air temperature increase for 2000-2029 (relative to the 1961-1990 average) of 1.0°C for June. 1.4°C for July. and 1.6°C for August in the JEG region (Walsh et al.. 2002) (Fig. 5.27). These temperature changes were applied to the input dataset (2001) for the air temperature scenario.

The composite GCM output also predicts an average precipitation increase of approximately 0.2 mm d^{-1} during the winter (Sep – May) period. However. modelled precipitation data show much higher spatial variability than modelled air temperature data. and simulations of both historical (1961-1990) and future (2000-2029) conditions can be overestimated by up to 52% (Walsh et al.. 2002). To avoid these problems. we instead use the assumption that precipitation will increase ~5% for every 1°C increase in air temperature (Bøggild et al.. 1994; Janssens and Huybrechts. 2000). Although this assumption has been questioned. as precipitation change is likely a function of altered atmospheric circulation rather than air temperature (van der Veen. 2002). the results maintain the low snowfall amounts that occur in the Arctic from Dec – Feb. by calculating the precipitation increase as a proportion of the original amount. rather than adding an absolute value.

Based on predicted monthly air temperature change from the composite GCM output. we calculate an average 15.3% (0.03 m WE for 2001) increase in winter precipitation. which is relatively similar to the 0.02 m WE increase calculated from the GCM output.

139

The 15.3% increase was applied to the 2001 EOW snowpack parameter for the winter precipitation scenario.

Given the precipitation increase expected with an increase in temperature. due to the warming atmosphere and its enhanced ability to retain moisture. there may also be an increase in summer precipitation. Although it is unclear if this will manifest as rain or snow. we test glacier response to increased summer snowfalls by adjusting the input record to include two additional summer snowfalls of the same thickness and duration as the recorded 2001 snowfall. The first test incorporates these snowfalls near the beginning of the input record. during two periods of negative air temperature (Day 153-155: Day 161-163). Since July and August temperatures are expected to increase more than June temperatures. we can assume that precipitation will increase the most in August. Thus the second test incorporates the snowfalls near the end of the input record. during two periods of <1.5°C air temperature (Day 210-212: Day 233-235): air temperature during the snowfalls was artificially set to 0°C. to ensure that the model would read them.

As changes in air temperature and precipitation will not occur independently. a final model run incorporates both the air temperature and the winter precipitation change to determine to what degree increased winter precipitation offsets changes caused by increased summer air temperature.

Output from each climate response run is compared with output from the 2001 baseline run to determine how the prescribed climatic changes impact glacier melt. runoff and MB.

5.8.2. Climate response results

5.8.2.1. Increased summer temperature

The increased summer air temperature results in a longer melt season. with shorter duration snowpack and SI. leading to a 111% increase in total melt and a subsequent 292% decrease in MB (Fig. 5.28a: Table 5.12). Because the EOW snowpack is actually removed. as the equilibrium line altitude rises above the UWS (1183 m a.s.l.). glacier-averaged SI reaches peak thickness 18 days early and is also removed during the season. This exposes the glacier ice surface for a longer period relative to the baseline run. leading to the increase in melt. Runoff begins earlier and lasts for 20 days longer than the

140

baseline run, and is 149% greater than baseline values. These changes lead to the significant decrease in annual MB.

5.8.2.2. Increased winter precipitation

The increase in EOW snowpack depth increases maximum SI thickness by 0.008 m WE. Glacier-averaged SI duration, however, remains unchanged, lasting the entire season. The increased SI thickness decreases total melt by 5% relative to the baseline run, although the actual melt duration remains unchanged (Fig. 5.28b: Table 5.12). Runoff, however, begins a day later, and is decreased by 9%. These changes result in a 29% increase in total MB.

5.8.2.3. Increased summer snowfalls

For the early-season snowfall test, additional snowfalls result in 0.012 m WE thicker SI that lasts – as in the baseline run – the entire melt season (Fig. 5.28c: Table 5.12). Consequently, although the melt period is the same length as in the baseline run, total melt is reduced by 8%. The runoff period is shortened by two days, and total runoff is reduced by 15%, ultimately leading to a 46% increase in MB.

The late-season snowfall test experiences the same amount of decrease in total melt and runoff as the early-season snowfall test (Fig 5.28d: Table 5.12). However, total MB increases by 58%. This is due to a two additional periods of SI formation later in the melt season: after the 210-212 and 233-235 snowfalls. These result in the runoff period being shortened by 11 days. Thus although the maximum SI thickness is the same as in the baseline run, the additional periods of SI formation result in reduced melt and runoff, and increased MB.

These SI episodes could, however, be an artefact of the model, as the DDM assumes that the ice surface has cooled to the MAAT when the snow falls, which is probably not the case in mid-melt season. It is more likely that the snow falls on ice that is near the pressure melting point, thus SI is not formed. If the snowfall is accompanied by relatively low air temperatures, however, the ice surface may cool sufficiently to allow some SI formation. In reality, therefore, the change in SI formation episodes probably lies somewhere in between the simulated output and observed conditions.

141

5.8.2.4. Concurrent increases in air temperature and winter precipitation

Results from the first three scenarios suggest that glacier response to concurrent temperature and precipitation changes should be driven mainly by the air temperature change. While EOW snowpack and SI duration are reduced by 33 and 29 days, respectively, relative to the baseline run. SI thickness increases by 0.013 m WE due to the thicker EOW snowpack providing melt for SI formation (Fig. 5.29; Table 5.12). The SI peak is reached 17 days earlier relative to the baseline run, thus the runoff period is lengthened by 19 days. Runoff is also increased because the EOW snowpack is entirely removed and glacier ice exposed, which doesn't occur in the baseline run. Total melt and runoff increase by 105% and 138%, respectively, resulting in a 267% decrease in MB.

5.8.3. Discussion of climate response results

It is apparent that changes in either air temperature or precipitation will have a significant impact on melt, runoff, and MB at JEG. Increased air temperatures have the largest impact on MB, especially in July (average increase of 1.4°C), when air temperatures are consistently above zero. The impact of an increase in air temperature is hardly moderated by a concurrent increase in winter precipitation, and results in the ELA rising above the UWS, exposing both SI and glacier ice to melt.

In order to compare results with other studies, we calculate the sensitivity of glacier melt, runoff and MB to a 1°C air temperature or 15% precipitation increase. For the first 1°C increase in air temperature, melt and runoff increase by 0.52 and 0.54 m WE, respectively, and MB decreases by 0.54 m WE. Glacier response to increased precipitation is more complex, depending on the timing of the increased precipitation. With a 15% increase in EOW snowpack, melt and runoff decrease by 0.03 and 0.04 m WE, respectively, while MB increases by 0.07 m WE. We don't calculate MB sensitivity to increased summer snow, as the values used in the analysis were not based on predicted precipitation increases, but were designed mainly to examine the impact of increased summer snowfalls on glacier processes.

MB sensitivity results are similar to those from Jóhannesson (1997), who calculated a MB decrease of $0.50 - 0.80$ m WE °C^{-1} on three Icelandic glaciers, and Fleming et al. (1997), who calculated a decrease of 0.70 m WE 1.5°C^{-1} at two glaciers in Spitsbergen.

142

Results also compare with the work of Oerlemans and Reichert (2000), who found that White Glacier (Canadian Arctic), responds solely to summer air temperature increases, and is relatively unaffected by precipitation changes. Results are higher than those reported by Braithwaite and Zhang (1999), where the MB sensitivity of sub-polar glaciers is listed as only 0.20 m WE °C^{-1}. The difference likely reflects regional variations in MB response, as well as the more detailed data available for this particular modelling study.

Precipitation sensitivity values are more difficult to compare with other research, as the majority of studies examine only air temperature-induced change, or coupled air temperature-precipitation induced change.

It is important to note that we have applied the monthly average temperature increase directly to each day, rather than predicting the distribution of daily air temperatures around the increased monthly mean. This results in temperatures above the 0°C threshold required for snow, particularly below 700 m, thereby reducing snowfalls at lower elevations. However, even under global warming conditions, days with sub-zero temperatures should still occur at lower elevation. In addition, because summer snowfalls at higher glacier elevations were extrapolated from conditions at the LWS (on the lower glacier), it is likely that some snowfalls were missed, as they may have occurred only on the upper glacier, while the lower glacier experienced rain. This problem likely underestimates total MB, by underestimating summer accumulation at higher elevations.

Climate changes will likely also result in changes to the WALR, STLR and SALR, as changing atmospheric circulation patterns alter the characteristics of the air masses transported to JEG (van der Veen, 2002). Our climate simulations, however, do not alter lapse rates between scenarios: we assume the impacts are minimal given the short timescale of the test.

These results are strongly constrained by the model sensitivity to lapse rate and variable DDF parameter values. While we are confident that variable DDF parameter values used successfully in calibration runs for 2002 can be transferred to other years (i.e., 2001: Sections 5.5.3, 5.6.3), it is important to determine how lapse rates will change under climate change conditions when examining longer-term climate response. The potential exists for associating specific lapse rates with larger-scale synoptic types (e.g., Marshall et al., in review), which would allow modellers to use synoptic indices (e.g.,

143

cyclonic vs. anticyclonic circulation) as additional input information to assist in selecting appropriate lapse rates. This area of research requires further study.

5.8.4. Climate change impacts on glacier runoff and hydrology

Given the modelled response of JEG melt, runoff and MB to predicted climate change, we can estimate the subsequent impacts on glacier hydrology. Results suggest that an increase in winter precipitation will not reduce the impact of a concurrent increase in air temperature. Melt season length is not reduced, as warmer temperatures simply increase the rate of snowpack removal. Additionally, there is no increase in meltwater refreezing within the snowpack at the end of the melt season, as the increased air temperature increases the equilibrium line altitude, reducing the snow-covered area in which refreezing could occur.

SI formation stores a small portion (0.007 m WE) of the increase in meltwater production with increased air temperature: however, the total volume of melt increase is so great that it cannot be entirely buffered by SI formation.

These climate change scenarios will also likely impact seasonal drainage system development. In 2001 (baseline run), the subglacial outburst was observed on JD 180 (29 June). Model output indicates that 0.10 m WE of melt had been produced by this date. Assuming that this is the approximate threshold melt amount required to initiate drainage system development, we can compare this value between climate scenarios to determine when this threshold is reached, and subsequently when the subglacial outburst may occur.

Under the increased air temperature scenario, the threshold is reached between JD 163-164: 16-17 days earlier than the baseline run. Under the increased EOW snowpack and both summer snowfall scenarios, the threshold is reached on the same day as the baseline run (JD 180). Under the increased air temperature and EOW snowpack scenario, however, the threshold was reached on JD 175: 5 days earlier than the baseline run.

These results suggest that an increase in air temperature results in early drainage system development due to increased early-season melt production. Thus the drainage system has a longer season in which to develop and, provided meltwater inputs are sustained, may therefore develop more extensively. This is corroborated by data from 2000, when the outburst was observed relatively early, on JD 174. Drainage system

144

development was unusually extensive in this year (Bingham et al., in review), due to the maintenance of high melt inputs for a lengthy period following the outburst.

Contrary to what may be expected, an increase in winter precipitation or early season snowfalls does not delay the onset of seasonal subglacial drainage. Unless the increased precipitation occurs concurrently with a decrease in air temperature, the drainage system will reach the melt storage threshold at the same time as the baseline run and, provided meltwater inputs are sustained following opening, drainage development should remain unchanged.

5.9. Conclusion

The DDM developed by Arendt (1997) is most sensitive to lapse rate and DDF parameter values, especially for the variable DDF parameterization, suggesting that these variables must be clearly defined and correspond well with field data to have confidence in model output. Lapse rates used in the model must be specific to the study site, and to the year(s) for which the model is run, while the components of the variable DDF algorithm should either be corroborated with field data, or be selected from only a small range of plausible values (measured and/or modelled) for a given site. The DDM is also relatively sensitive to SI_{PMAX} values: as previous studies have resulted in a large range of plausible values (e.g., Reeh, 1991; Wolfe and English, 1995; Fujita et al., 1996; Woodward et al., 1997; Bugnion and Stone, 2002), the SI_{SLT} parameterization should be used in the absence of field measurements of PMAX. Because this parameterization is less sensitive to selection of MAAT (or 14 m ice) values, it will have less of an impact on model output than inappropriate values of PMAX.

Melt, runoff and MB at JEG are most affected by future (2000-2029) air temperature increases predicted by GCMs, due in large part to the temperature increase during July, when the majority of days already experience positive air temperatures. Melt will increase, runoff will increase, and MB will substantially decrease: these impacts would be only minimally offset by a concurrent increase in winter precipitation. This is largely because the rate of snowpack removal increases with higher air temperatures. Melt, runoff and MB at JEG are also strongly affected by an increase in late-summer snowfalls.

145

which have the effect of reducing melt later in the season. increasing the number of SI formation episodes. and subsequently decreasing runoff and increasing MB.

Increases in melt production due to increased air temperatures will likely not be buffered by increased SI formation. as the magnitude of the melt increase will far exceed the increase in SI formation. Glacier hydrology has the potential to be substantially impacted by changes in glacier melt and runoff. as increased air temperatures will result in more melt production earlier in the melt season. allowing the supraglacial system to reach threshold values sooner. Thus the establishment of a surface to bed connection is expected to occur sooner with increasing air temperature.

While the climate response tests do not incorporate changes in lapse rates expected to occur under climate change conditions. static values are assumed appropriate for short timescale simulations. Discussion of the response of glacier runoff to climate change would be enhanced by examining more closely the role of surface meltwater storage in delaying runoff from the glacier. These processes occur annually on JEG and other polythermal glaciers (Skidmore and Sharp. 1999: Boon and Sharp. 2003). Changes in meltwater/runoff input to these storage locations will have a cascade effect on glacier dynamics and subsequent MB response (Zwally et al.. 2002: Parizek and Alley. 2004: Bingham et al.. in review). and could be studied by routing meltwater output from the DDM into a hydrological model (e.g.. Flowers and Clarke. 2002) coupled to a glacier dynamics model. This would give some understanding of the dynamic response of JEG to climate change. although it would be limited by the present uncertainties in models of glacier dynamics.

5.10. References

Arendt. A.A. 1997. Approaches to modelling the mass balance of High Arctic glaciers. M.Sc. thesis. University of Alberta. 222 pp.

Arendt. A.. M.J. Sharp. 1999. Energy balance measurements on a Canadian high Arctic glacier and their implications for mass balance modelling. International Association of Hydrological Sciences 256: 165-172.

146

Bingham. R.G.. P.W. Nienow. M.J. Sharp. L. Copland. **In review** Propagation of high-velocity events in the ablation zone of a High Arctic polythermal glacier: relation to seasonal changes in subglacial drainage system structure. Journal of Geophysical Research - Earth Surface.

Blatter. H. 1987. On the thermal regime of an Arctic valley glacier: a study of White Glacier. Axel Heiberg Island. NWT. Canada. Journal of Glaciology 33(114): 200-210.

Boer. G.J.. G. Flato. D. Ramsden. 2000. A transient climate change simulation with greenhouse gas and aerosol forcing: projected climate to the 21st century. Climate Dynamics **16:** 427-450.

Bøggild. C.E.. N. Reeh. H. Oerter. 1994. Modelling ablation and mass-balance sensitivity to climate change of Storstrømmen. Northeast Greenland. Global and Planetary Change **9:** 79-90.

Boon. S.. M. Sharp. 2003. The role of hydrologically-driven ice fracture in drainage system evolution on an Arctic glacier. Geophysical Research Letters 30(18): 1916. DOI: 10.1029/2003GL018034.

Boon. S.. M. Sharp. **In review.** A 6-year meteorological record from a high Arctic glacier: implications for mass balance modelling. Global and Planetary Change.

Box. J.E.. K. Steffen. 2001. Sublimation on the Greenland ice sheet from automated weather station observations. Journal of Geophysical Research – Atmospheres **106**(D24): 33.965-33.981.

Braithwaite. R.J. 1984. Calculation of degree-days for glacier-climate research. Zeitschrift fur Gletscherkunde und Glazialgeologie **20:** 1-8.

Braithwaite, R.J. 1995. Positive degree-day factors for ablation on the Greenland ice sheet studied by energy-balance modelling. Journal of Glaciology 41: 153-160.

Braithwaite, R.J., O.B. Olesen. 1987. Calculation of glacier ablation from air temperature, West Greenland. In Glacier Fluctuations and Climatic Change. J. Oerlemans, ed. Dordrecht: Kluwer Academic Publishers, p. 219-233.

Braithwaite, R.J., Y. Zhang. 1999. Modelling changes in glacier mass balance that may occur as a result of climate changes. Geografiska Annaler 81A(4): 489-496.

Braithwaite, R.J., Y. Zhang. 2000. Sensitivity of mass balance of five Swiss glaciers to temperature changes assessed by tuning a degree-day model. Journal of Glaciology 46: 7-14.

Brock, B.W., I. Willis, M. Sharp, N. Arnold. 2000. Modelling seasonal and spatial variations in the surface energy balance of Haut Glacier d'Arolla, Switzerland. Annals of Glaciology 31: 53-62.

Bugnion, V., P.H. Stone. 2002. Snowpack model estimates of the mass balance of the Greenland ice sheet and its changes over the twenty-first century. Climate Dynamics 20: 87-106.

Burt, J.E., Barber, G.M. 1996. Elementary Statistics for Geographers. New York: Guilford Press, 640 pp.

Copland, L. 2001. Polythermal Glacier Hydrology and Ice Flow Dynamics. Ph.D. thesis. University of Alberta, 138 pp.

Copland, L., M. Sharp. 2001. Mapping hydrological and thermal conditions beneath a polythermal glacier with radio-echo sounding. Journal of Glaciology 47(157): 232-242.

148

Fleming, K.M., J.A. Dowdeswell, J. Oerlemans. 1997. Modelling the mass balance of northwest Spitsbergen glaciers and responses to climate change. Annals of Glaciology 24: 203-210.

Flowers, G.E., G.K.C. Clarke. 2002. A multicomponent coupled model of glacier hydrology: 1. Theory and synthetic examples. Journal of Geophysical Research – Solid Earth 107(B11): 2287, doi: 10.1029/2001JB001122.

Fountain, A.G. 1996. Effect of snow and firn hydrology on the physical and chemical characteristics of glacial runoff. Hydrological Processes 10: 509-521.

Fujita, K., K. Seko, Y. Ageta, P. Jianchen, Y. Tandong. 1996. Superimposed ice in glacier mass balance on the Tibetan Plateau. Journal of Glaciology 42(142): 454-460.

Fujita, K., Y. Ageta. 2000. Effect of summer accumulation on glacier mass balance on the Tibetan Plateau revealed by mass-balance model. Journal of Glaciology 46(153): 244-252.

Greuell, W., R. Böhm. 1998. 2 m temperatures along melting mid-latitude glaciers, and implications for the sensitivity of the mass balance to variations in temperature. Journal of Glaciology 44(146): 9-20.

Greuell, W., C. Genthon. 2004. Modelling land ice surface mass balance. In Mass balance of the cryosphere: Observations and modelling of contemporary and future changes. J.L. Bamber and A.J. Payne, eds., Cambridge: Cambridge University Press, 662 pp.

Haas, C., J. Bareiss, M. Nicolaus. 2002. The surface energy balance and its importance for superimposed ice formation (SEBISUP). Report for the LSF project NP-9/2001, 16 pp.

149

Hock. R. 1999. A distributed temperature-index ice- and snowmelt model including potential direct solar radiation. Journal of Glaciology 45(149): 101-111.

Hock. R. 2003. Temperature index melt modelling in mountain areas. Journal of Hydrology 282(1-4): 104-115.

Holland. M.M.. C.M. Bitz. 2003. Polar amplification of climate change in coupled models. Climate Dynamics 21: 221-232.

Hooke. R.L. 1976. Near-surface temperatures in the superimposed ice zone and lower part of the soaked zone of polar ice sheets [Abstract]. Journal of Glaciology 16(74): 302-304.

Houghton. J. T.. Y. Ding. D.J. Griggs. M. Noguer. P.J. van der Linden and D. Xiaosu. eds. 2001. Climate Change 2001: The Scientific Basis. Contribution of Working Group I to the Third Assessment Report of the Intergovernmental Panel on Climate Change (IPCC). Cambridge: Cambridge University Press. 944 pp.

Janssens. I.. P. Huybrechts. 2000. The treatment of meltwater retention in mass-balance parameterizations of the Greenland ice sheet. Annals of Glaciology 31: 133-140.

Jóhannesson. T. 1997. The response of two Icelandic glaciers to climatic warming computed with a degree-day glacier mass-balance model coupled to a dynamic glacier model. Journal of Glaciology 43(143): 321-327.

Koerner. R.M. 1966. Accumulation on the Devon Island Ice Cap. Northwest Territories. Canada. Journal of Glaciology 6(45): 383-392.

Marshall. S.J.. M.J. Sharp. D.O. Burgess. F.S. Anslow. In review. Surface temperature lapse rate variability on the Prince of Wales Icefield. Ellesmere Island. Canada: Implications for regional-scale downscaling of temperature. Journal of Climate.

Meier, M. 1990. Role of Land Ice in Present and Future Sea-Level Change. In Sea-Level Change. M.A.R. Geophysics Study Committee - Commission on Physical Sciences. Washington: National Academy Press. p. 171-184.

Morison, J., K. Aagaard, M. Steele. 2000. Recent environmental changes in the Arctic: a review. Arctic 53(4): 359-371.

Moritz, R.E., C.M. Bitz, E.J. Steig. 2002. Dynamics of recent climate change in the Arctic. Science 297: 1497-1502.

Munro, D.S. 1990. Comparison of melt energy computations and ablatometer measurements on melting ice and snow. Arctic and Alpine Research 22(2): 153-162.

Nash, J.E., J.V. Sutcliffe. 1970. River flow forecasting through conceptual models. Part 1: A discussion of principles. Journal of Hydrology 10(3): 282-290.

Oerlemans, J., J.P.F. Fortuin. 1992. Sensitivity of glaciers and small ice caps to greenhouse warming. Science 258(5079): 115-117.

Oerlemans, J., B.K. Reichert. 2000. Relating glacier mass balance to meteorological data by using a seasonal sensitivity characteristic. Journal of Glaciology 46(152): 1-6.

Ohmura, A. 2001. Physical basis for the temperature-based melt-index method. Journal of Applied Meteorology 40(4): 753-761.

Oke, T. 1978. Boundary Layer Climates. London: William Clowes & Sons Ltd., 372 pp.

Parizek, B.R., R.B. Alley. 2004. Implications of increased Greenland surface melt under global-warming scenarios: ice-sheet simulations. Quaternary Science Reviews 23: 1013–1027.

151

Paterson, W. 1994. The Physics of Glaciers. Boston: Butterworth-Heinemann. 480 pp.

Pfeffer, W.T., M.F. Meier, T.H. Illangasekare. 1991. Retention of Greenland runoff by refreezing: implications for projected future sea level change. Journal of Geophysical Research – Oceans 96(C12): 22,117-22,124.

Reeh, N. 1991. Parameterization of melt rate and surface temperature on the Greenland Ice Sheet. Polarforschung 59(3): 113-128.

Serreze, M.C., J.E. Walsh, F.S. Chapin III, T. Osterkamp, M. Dyurgerov, V. Romanovsky, W.C. Oechel, J. Morison, T. Zhang, R.G. Barry. 2000. Observational evidence of recent change in the northern high-latitude environment. Climatic Change 46: 159-207.

Singh, P., N. Kumar, M. Arora. 2000. Degree-day factors for snow and ice for Dokriani Glacier, Garhwal Himalayas. Journal of Hydrology 235: 1-11.

Skidmore, M.L., M.J. Sharp. 1999. Drainage system behaviour of a high Arctic polythermal glacier. Annals of Glaciology 28: 209-215.

van der Veen, C.J. 2002. Polar ice sheets and global sea level: how well can we predict the future? Global and Planetary Change 32: 165-194.

van de Wal, R.S.W., J. Oerlemans. 1994. An energy balance model for the Greenland ice sheet. Global and Planetary Change 9: 115-131.

Wadham, J.L., A.M. Nuttall. 2000. Impact of Superimposed Ice on the Mass Balance of Northwest Spitsbergen Glaciers. Report, Scott Polar Research Institute. 47 pp.

152

Wakahama, G., D. Kuroiwa, T. Hasemi, C.S. Benson. 1976. Field observations and experimental and theoretical studies on the superimposed ice of McCall Glacier, Alaska. Journal of Glaciology 16(74): 135 -149

Walsh, J.E., V.M. Kattsov, W.L. Chapman, V. Govorkova, T. Pavlova. 2002. Comparison of Arctic climate simulations by uncoupled and coupled global models. Journal of Climate 15: 1429-1446.

Ward, W.H., S. Orvig. 1953. The glaciological studies of the Baffin Island Expedition. 1950. Part IV: The heat exchange at the surface of the Barnes Ice Cap during the ablation period. Journal of Glaciology 2(13): 158–168.

Wolfe, P.M. 1995. Hydrometeorological investigations on a small glacier in the Sawtooth Range, Ellesmere Island, Northwest Territories. M.Sc. thesis. Wilfrid Laurier University, 192 pp.

Woodward, J., M.J. Sharp, A. Arendt. 1997. The influence of superimposed-ice formation on the sensitivity of glacier mass balance to climate change. Annals of Glaciology 24: 186-190.

Zwally, H.J., W. Abdalati, T. Herring, K. Larson, J. Saba, K. Steffen. 2002. Surface melt-induced acceleration of Greenland ice-sheet flow. Science 297: 218-222.

5.11. Tables

Table 5.1. Parameter values used in Sensitivity Test Stage 1 (calibration and validation).

Summer air temperature and accumulation lapse rate	N/A	
Winter snow accumulation	*Read from input file*	
Degree day factor	*Slope*	-0.0057
	Intercept	0.0084
	Albedo	0.95 – new snow
		0.79 – old snow[1]
		0.42 – superimposed ice
		0.25 – glacier ice
		0.10 – water
		3 days – water runoff time
Superimposed Ice	*Temperature method*	-15.8°C – mean annual sea level temperature

[1]The selected value is higher than the minimum 'old snow' value in Figure 5.4. and therefore represents the upper limit of old snow albedo values.

Table 5.2. Values of statistical comparison criteria for Sensitivity Test Stage 1 (calibration and validation).

	Melt			3-day average melt		
	R^2	R_{ln}^2	r^2	R^2	R_{ln}^2	r^2
Calibration						
1 Jun - 27 Jul 2002	0.68	0.93	0.69	0.80	0.83	0.81
Validation						
31 May - 29 Jul 2001	0.70	0.78	0.76	0.76	0.75	0.84

R^2 = coefficient of efficiency; R_{ln}^2 = modified coefficient of efficiency; r^2 = coefficient of determination

Table 5.3. Coefficient of determination (r^2) and regression equation for separate snow and ice melt: Sensitivity Test Stage 1 (calibration and validation).

	Snow melt	Ice melt	3-day snow melt	3-day ice melt
Calibration	0.58	0.64	0.72	0.81
	$MLT_i =$	$MLT_i =$	$MLT_i =$	$MLT_i =$
1 Jun-27 Jul 2002	$1.03 MLT_m$	$0.64 MLT_m$	$1.40 MLT_m$	$0.70 MLT_m$
Validation	0.79	0.70	0.85	0.78
	$MLT_i =$	$MLT_i =$	$MLT_i =$	$MLT_i =$
31 May-29 Jul 2001	$0.91 MLT_m$	$0.62 MLT_m$	$1.01 MLT_m$	$0.67 MLT_m$

155

Table 5.4. Sensitivity test input and results for all model parameters. Columns indicates change in output value per iterative change. *Max SI 1* = maximum SI thickness following EOW snowpack removal; *Max SI 2* = maximum SI thickness following summer snowfall; *Initial SWE 1* = snow depth (m WE) at beginning of model run; *Max SWE 2* = snow depth (m WE) for summer snowfall.

VARIABLE	RANGE OF VALUES	ITERATIVE CHANGE	TOTAL MLT	TOTAL MB	MAX SI 1	MAX SI 2	INITIAL SWE 1	MAX SWE 2
SI algorithms SI_{SLT}[A]	-19.4 to -14.4°C	1°C	0.000-0.003	0.000-0.016	0.000-0.013	0.000-0.013	0	0
SI_{PMAX}[B]	20-75%	10%	0.000-0.004	0.009-0.027	0.009-0.024	0.009-0.024	0	0
Constant DDF (in m WE d^{-1} °C^{-1})								
snow	0.003-0.0055	0.0005	0.026-0.071	0.011-0.055	0.000-0.012	0.001-0.059	0	0
ice	0.006-0.0075	0.0005	0.036	0.036	0	0	0	0
Variable DDF (in m WE d^{-1} °C^{-1})								
Water runoff time[C]	1-3 days	0.5 days	0.011-0.024	0.003-0.020	0.002-0.004	0.002-0.037	0	0
Albedo of surface type								
water[D]	0.03-0.10	0.02	0.002	0.0008	0.0008	0.0007	0	0
glacier ice[E]	0.20-0.35	0.05	0.015	0.015	0	0	0	0
superimposed ice[F]	0.35-0.45	0.02	0.003-0.005	0.002-0.005	0	0.001	0	0
old snow[G]	0.65-0.85	0.05	-	-	-	-	-	-
new snow[H]	0.85-0.95	0.02	0.003-0.023	0.001-0.021	0.002	0.003-0.027	0	0
M & B								
snow[I]	0.003-0.0055	0.0005	0.023-0.067	0.013-0.071	0.008	0.003-0.038	0	0
ice[I]	0.006-0.0075	0.0005	0.033-0.060	0.031-0.058	0.002-0.008	0.002-0.025	0	0
Lapse rates WALR[H]	-0.000104 to 0.000046 m WE m^{-1}	0.000025 m WE m^{-1}	0.000-0.023	0.002-0.044	0.00-0.014	0.00-0.014	0.007	0.007
SALR[H]	-0.00001 to 0.00001 m WE m^{-1}	0.000005 m WE m^{-1}	0.00-0.035	0.003-0.031	0.00	0.00-0.011	0	0.003
STLR[B]	-0.009 to 0.007°C m^{-1}	0.002°C m^{-1}	0.072-0.382	0.030-0.431	0.001-0.034	0.00-0.065	0.000-0.003	0.000-0.055

[A]measured values from Eureka and LWS; [B]Reeh, 1991; Wolfe, 1995; Fujita et al., 1996; Woodward et al., 1997; Bugnion and Stone, 2002; [C]Arendt, 1997; [D]Oke, 1978; [E]Paterson 1994; [F]Haas et al., 2002; field data; [G]Paterson, 1994; Arendt, 1997; field data; [H]field data; [I]Arendt 1997; Arendt and Sharp, 1999.

Table 5.5. Parameter values used for Sensitivity Test Stage 2 (calibration).

Parameter	Variable	Value
Melt season lapse rates	*Air temperature*	-0.00149 °C m^{-1}
	Accumulation	0.000004 m WE m^{-1}
Winter snow accumulation regression	*Sea level winter accum*	0.0972 m WE
	Slope	0.0000265 m WE m^{-1}
Degree day factor	*Slope*	-0.0057
	Intercept	0.0084
	Albedo	0.95 – new snow
		0.79 – old snow
		0.42 – superimposed ice
		0.25 – glacier ice
		0.10 – water
		1 day – water runoff time
Superimposed Ice	*PMAX method*	0.60 – fraction of initial SWE that refreezes

Table 5.6. Values of statistical comparison criteria for Sensitivity Test Stage 2 (calibration and validation).

	Melt			3-day average melt		
	R^2	R_{ln}^2	r^2	R^2	R_{ln}^2	r^2
Calibration						
1 Jun - 10 Jul 2002	0.49	0.88	0.54	0.67	0.84	0.69
Validation						
6 Jun - 26 Jul 2001	0.54	0.79	0.58	0.66	0.66	0.67

R^2 = coefficient of efficiency; R_{ln}^2 = modified coefficient of efficiency; r^2 = coefficient of determination

157

Table 5.7. Coefficient of determination (r^2) and regression equation for separate snow and ice melt: Sensitivity Test Stage 2 (calibration and validation).

	Snow melt	Ice melt	3-day snow melt	3-day ice melt
Calibration[2]	0.23	0.40	0.27	0.60
	$MLT_s =$	$MLT_s =$	$MLT_s =$	$MLT_s =$
1 Jun-10 Jul 2002	$0.68MLT_m$	$0.60MLT_m$	$0.84MLT_m$	$0.75MLT_m$
Validation	0.28	0.60	0.45	0.68
	$MLT_s =$	$MLT_s =$	$MLT_s =$	$MLT_s =$
6 Jun-26 Jul 2001	$0.89MLT_m$	$0.73MLT_m$	$1.3MLT_m$	$0.82MLT_m$

Table 5.8. Parameter values for Sensitivity Test Stage 2. second validation (using 2001-specific lapse rates).

Melt season lapse rates	*Air temperature*	$-0.001 \,°C \, m^{-1}$
	Accumulation	$0.000005 \, m \, WE \, m^{-1}$
Winter snow	*Sea level winter accum.*	$0.1976 \, m \, WE$
accumulation regression	*Slope*	$-0.000079 \, m \, WE \, m^{-1}$
Degree day factor	*Slope*	-0.0057
	Intercept	0.0084
	Albedo	$0.95 -$ new snow
		$0.79 -$ old snow
		$0.42 -$ superimposed ice
		$0.25 -$ glacier ice
		$0.10 -$ water
		$1 \, day -$ water runoff time
Superimposed Ice	*PMAX method*	$0.60 -$ fraction of initial SWE that refreezes

158

Table 5.9. Sensitivity Test Stage 2 (second validation): (a) statistical comparison criteria: and, (b) coefficient of determination (r^2) and regression equation for separate snow and ice melt.

(a)

	Melt			3-day average melt		
	R^2	R_{ln}^2	r^2	R^2	R_{ln}^2	r^2
Validation (second)						
6 Jun - 26 Jul 2001	0.63	0.75	0.67	0.71	0.44	0.75

R^2 = coefficient of efficiency; R_{ln}^2 = modified coefficient of efficiency; r^2 = coefficient of determination

(b)

	Snow melt	Ice melt	3-day snow melt	3-day ice melt
Validation (second)	0.46	0.58	0.58	0.66
	$MLT_c =$	$MLT_c =$	$MLT_c =$	$MLT_c =$
6 Jun-26 Jul 2002	$0.67MLT_m$	$0.69MLT_m$	$0.90MLT_m$	$0.77MLT_m$

Table 5.10. Global circulation models (GCMs) used to create the composite output used for the climate response test.

Research centre	Model name	Country
Centre for Climate Research Studies	CCSR/NIES	Japan
Canadian Climate Centre	CGCM1	Canada
Commonwealth Science and Industrial Research Organisation	CSIRO Mk2	Australia
Max Planck Institute/ Deutsches Klimaechenzentrum	ECHAM4/OPYC3	Germany
Deutsches Klimaechenzentrum	ECHAM3/LSG	Germany
Geophysical Fluid Dynamics Laboratory	GFDL_R15_a	United States
Hadley Centre	HadCM3	United Kingdom
National Centre for Atmospheric Research	NCAR DOE PCM	United States

Table 5.11. Parameter values used for climate response tests (lapse rates calculated specifically for JJA 2001). Note the use of two lapse rates: L-M (elevation bands 100-900 m) and L-U (elevation bands 900-1200 m).

Melt season lapse rates	*Air temperature*	$-0.0029\ °C\ m^{-1}$ (L-M)
		$-0.0030\ °C\ m^{-1}$ (L-U)
	Accumulation	$-0.000005\ m\ WE\ m^{-1}$ (L-M)
		$0.000008\ m\ WE\ m^{-1}$ (L-U)
Winter snow accumulation regression	*Sea level winter accum.*	$0.2079\ m\ WE$ (L-M)
		$0.1996\ m\ WE$ (L-U)
	Slope	$-0.000071\ m\ WE\ m^{-1}$ (L-M)
		$-0.000050\ m\ WE\ m^{-1}$ (L-U)
Degree day factor	*Slope*	-0.0057
	Intercept	0.0084
	Albedo	0.95 – new snow
		0.79 – old snow
		0.42 – superimposed ice
		0.25 – glacier ice
		0.10 – water
		1 day – water runoff time
Superimposed Ice	*SLT method*	-15.8 – mean annual air temp.

160

Table 5.12. Results of climate response test: *SWE* = duration of EOW snowpack; *SI* = duration of SI following EOW snowpack removal; *MLT* = duration of melt from first to last day of continuous (>1 day) melt (>0.001 m WE); *Runoff* = duration of runoff period (following maximum SI); *MLT Total* = total melt during melt period; *Runoff Total* = total runoff during runoff period; *MB Total* = final MB at end of run; *Snowfall* = duration of each summer snowfall; *SI Max Day* = day of maximum SI thickness; *SI Max* = maximum SI thickness.

| CLIMATE TEST	SWE	SI	MLT	RUNOFF	MLT TOTAL*	RUNOFF TOTAL*	MB TOTAL*	SNOW FALL	SI MAX DAY	SI MAX
Baseline	151-243	159-243	164-240	196-240	0.61	0.47	-0.24	184-186; 242-243	196	0.0967
Air temp.	151-199	152-209	159-242	178-242	1.29	1.17	-0.94	184-186; 242-243	178	0.1034
EOW snowpack	151-243	159-243	164-240	197-240	0.58	0.43	-0.17	184-186; 242-243	197	0.1049
Early summer snow	151-243	159-243	164-240	198-243	0.56	0.40	-0.13	153-155; 161-163; 184-186; 242-243	198	0.1088
Late summer snow	151-243	159-243	164-240	196-212; 216-233	0.56	0.40	-0.10	184-186; 210-212; 233-235; 242-243	196	0.0966
EOW snowpack and air temp.	151-201	152-214	159-242	179-242	1.25	1.12	-0.88	184-186; 242-243	179	0.1095

*in m WE

5.12. Figures
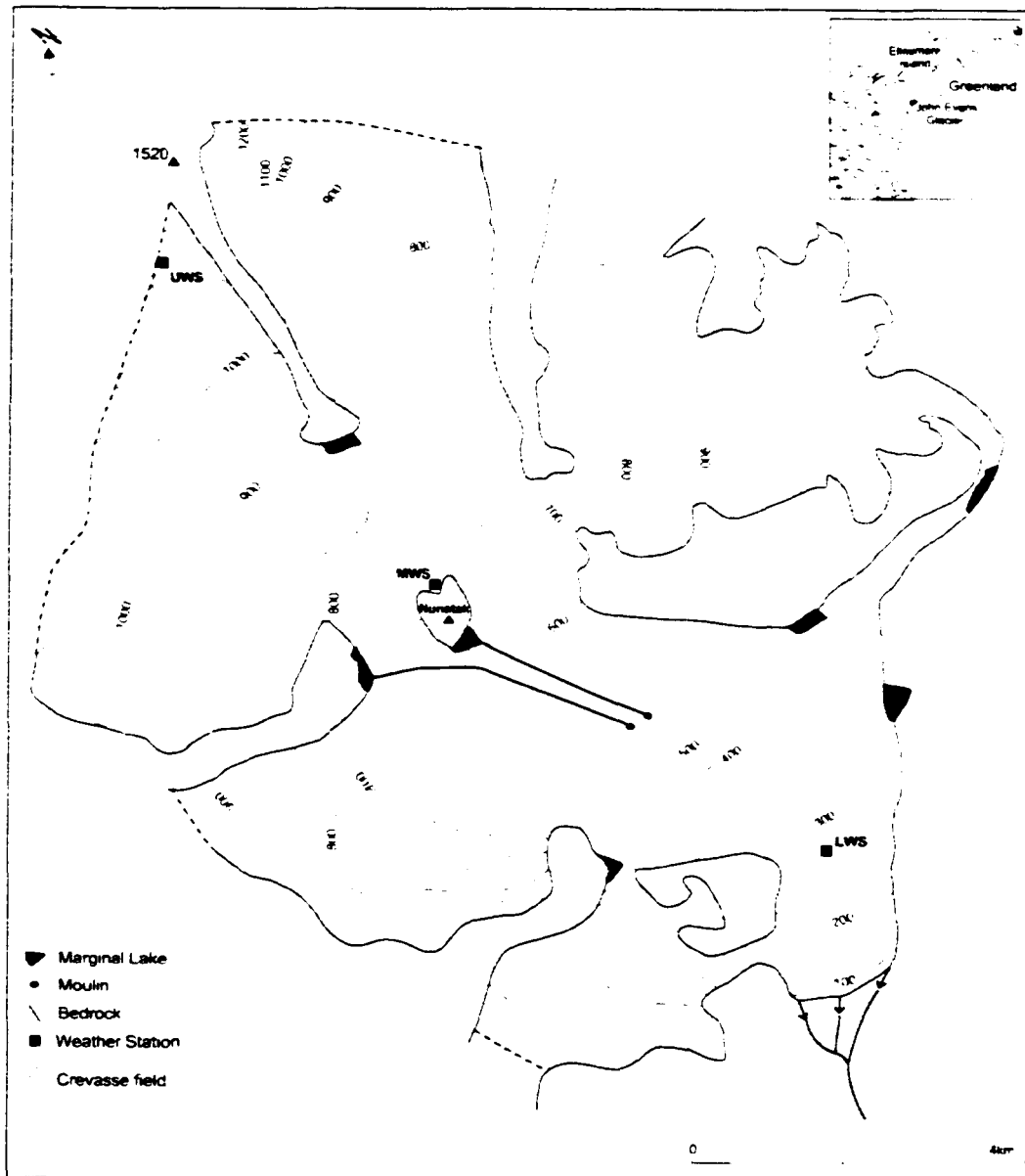
Figure 5.1. John Evans Glacier study site: note locations of meteorological stations.

162
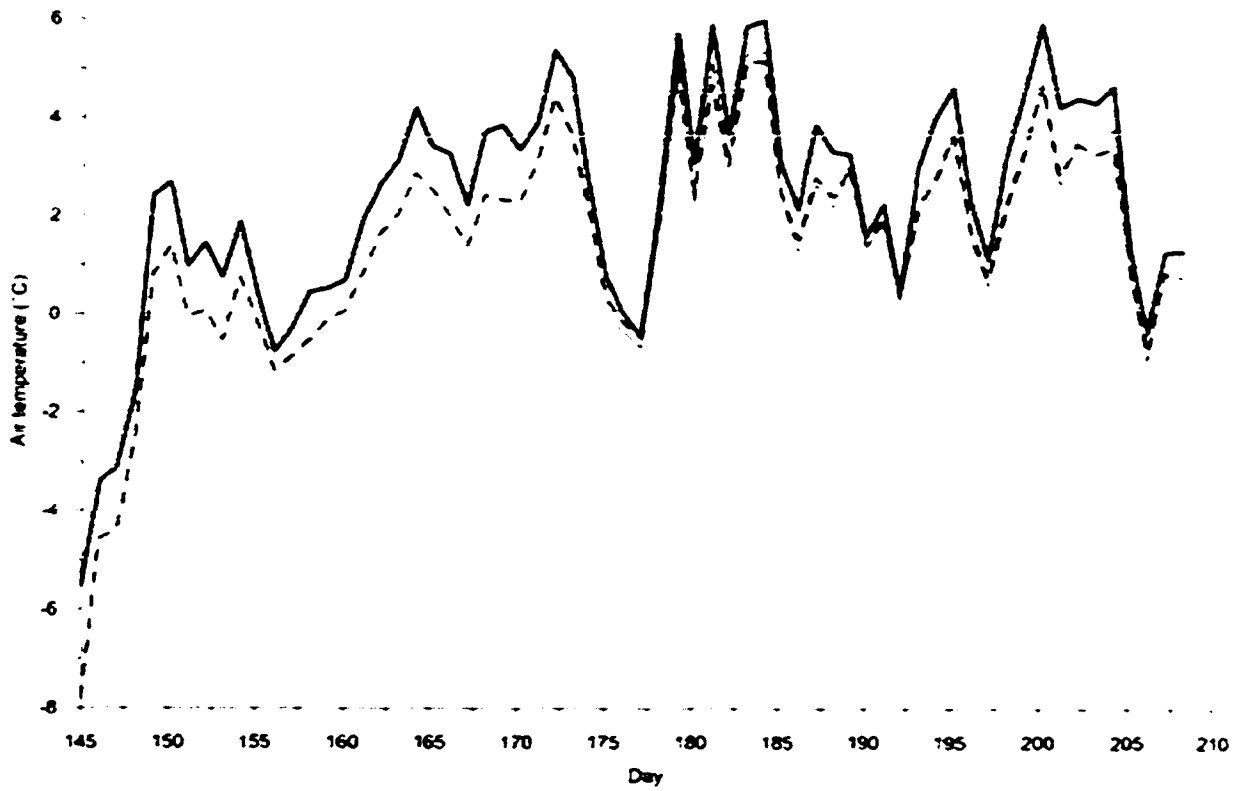
Figure 5.2. Air temperature measured at LWS with Vaisala HMP35CF sensor (bold black) and with HOBO sensor (grey); average air temperature calculated from Vaisala and HOBOs at 200 and 300 m a.s.l. (dashed).

163
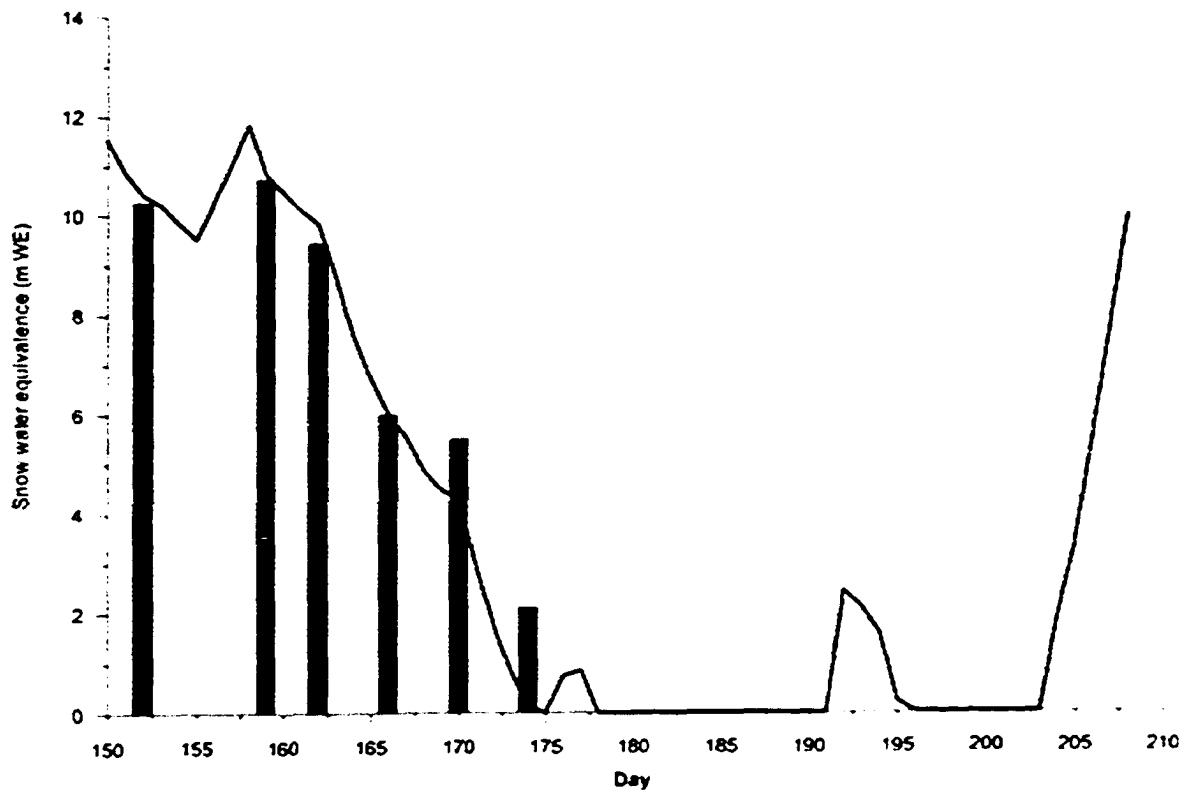
Figure 5.3. Snow water equivalent (SWE) measured in snow pits (solid bars) and continuous record calculated from UDG using Equation (6) (solid line).
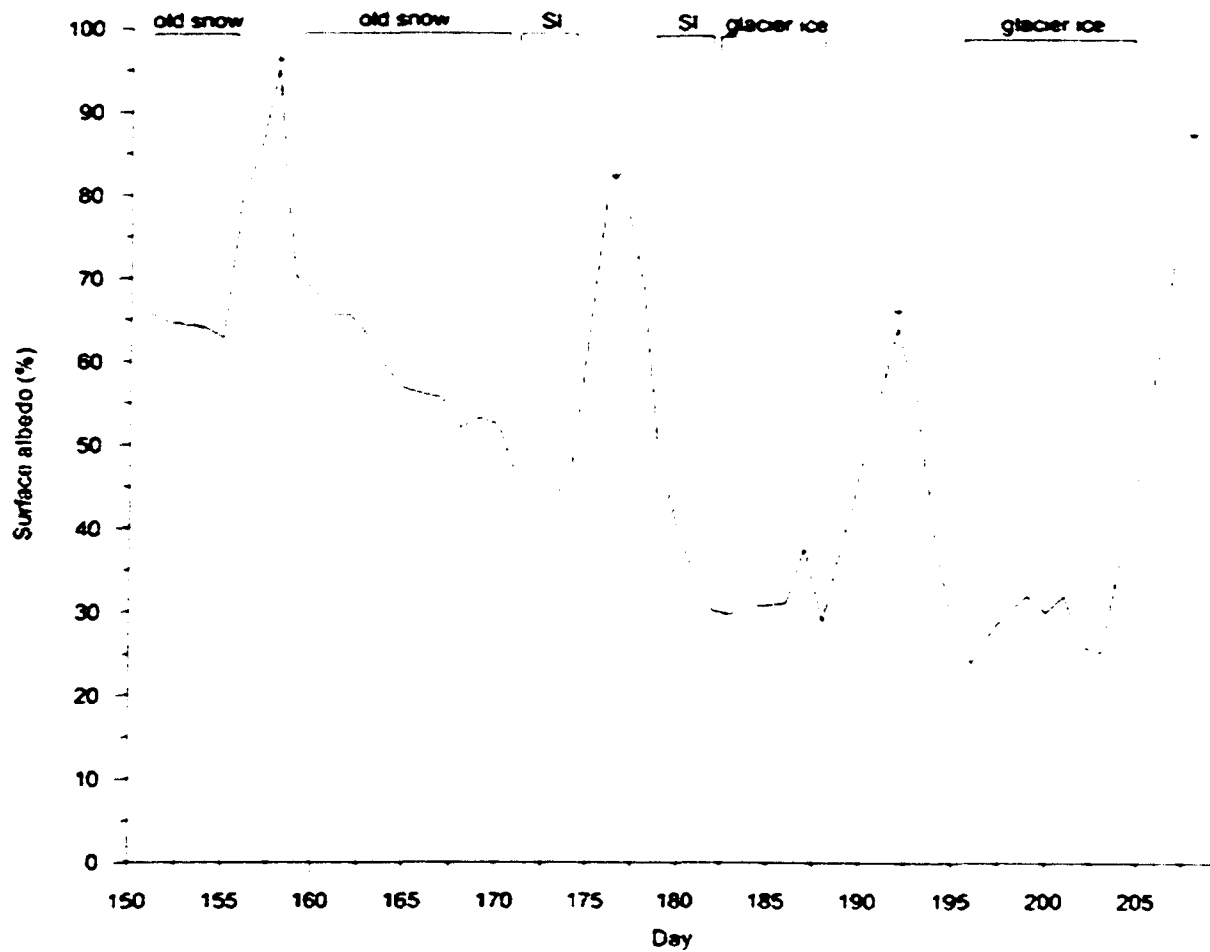
Figure 5.4. Calculated albedo from solar radiation measurements at LWS in 2002. Note different surface types: arrows indicate fresh snowfalls (SI = superimposed ice).

165
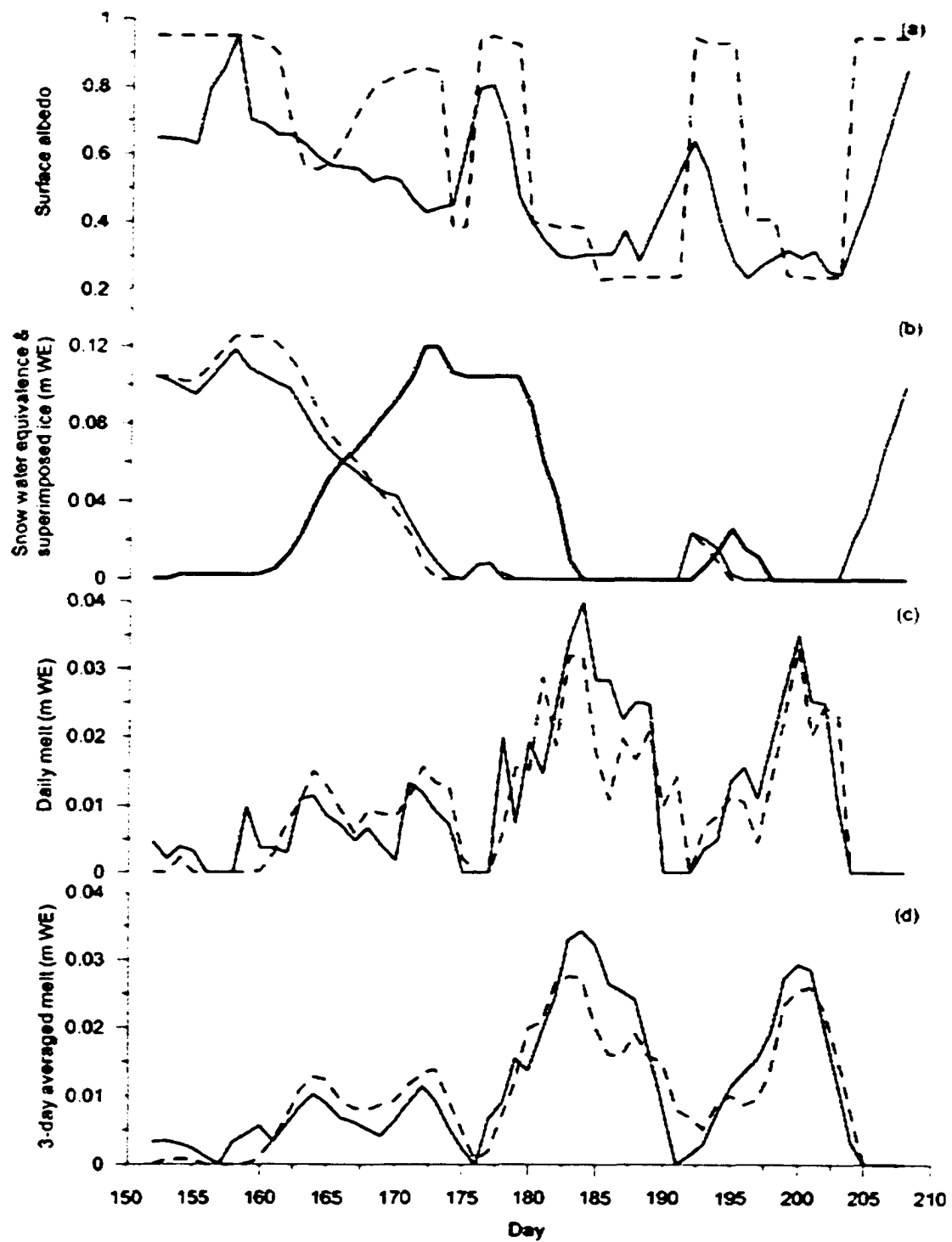
Figure 5.5. Measured (solid) and simulated (dashed) data Sensitivity Test Stage 1 (calibration: 1 June – 27 July. 2002): (a) albedo: (b) SWE and SI (solid bold): (c) melt: and, (d) 3-day averaged melt.

166
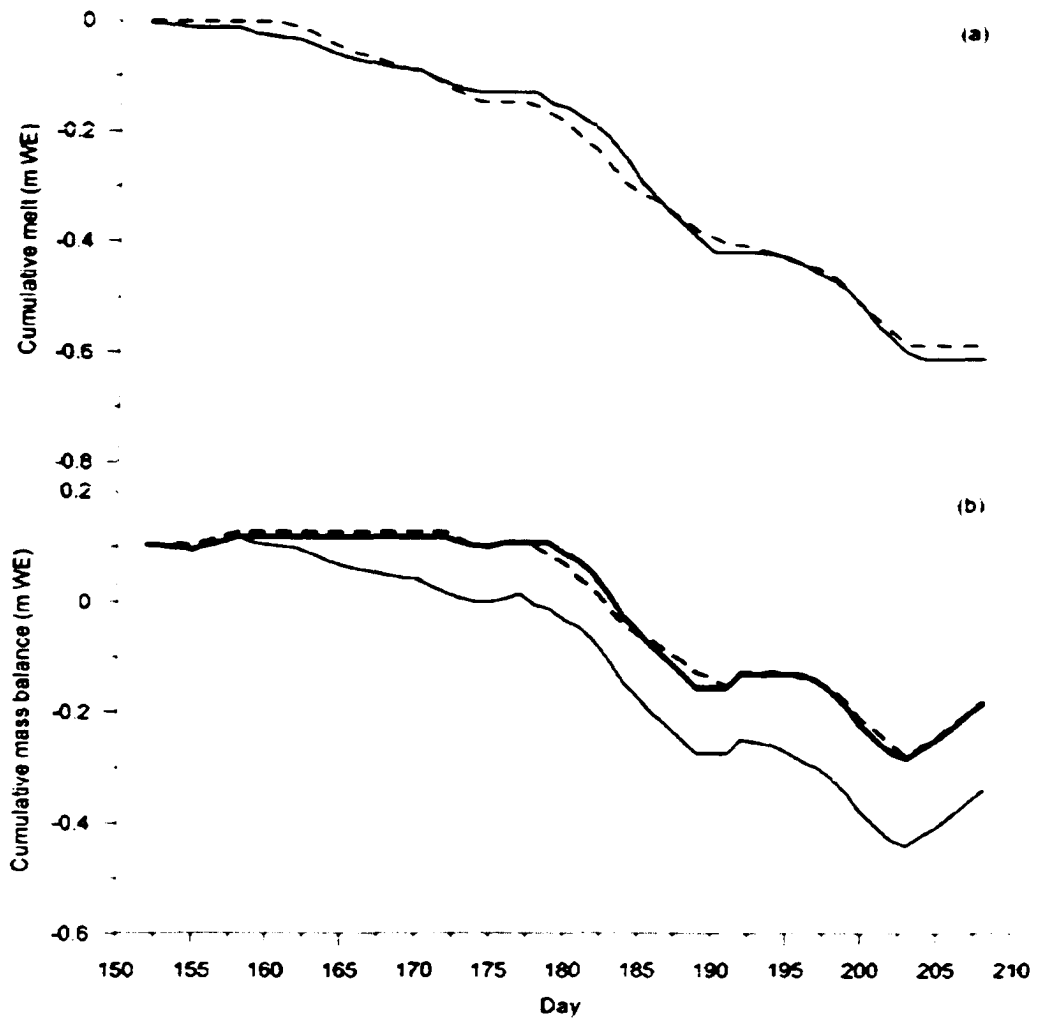
Figure 5.6. Measured (solid) and simulated (dashed) data for Sensitivity Test Stage 1 (calibration: 1 June – 27 July, 2002): (a) cumulative melt; and, (b) cumulative MB. Bold solid line in (b) is the measured MB adjusted after the simulation, to incorporate SI formation.
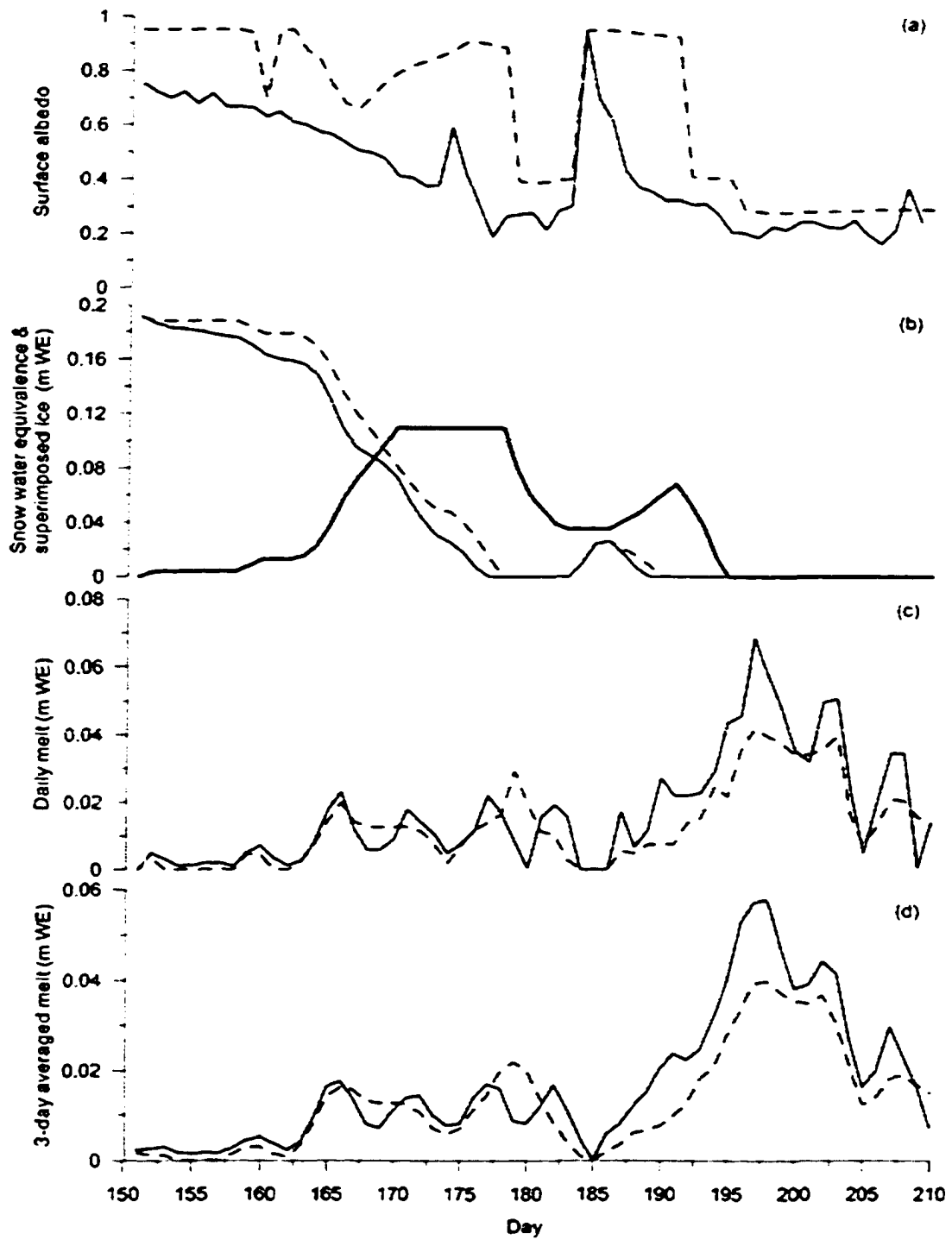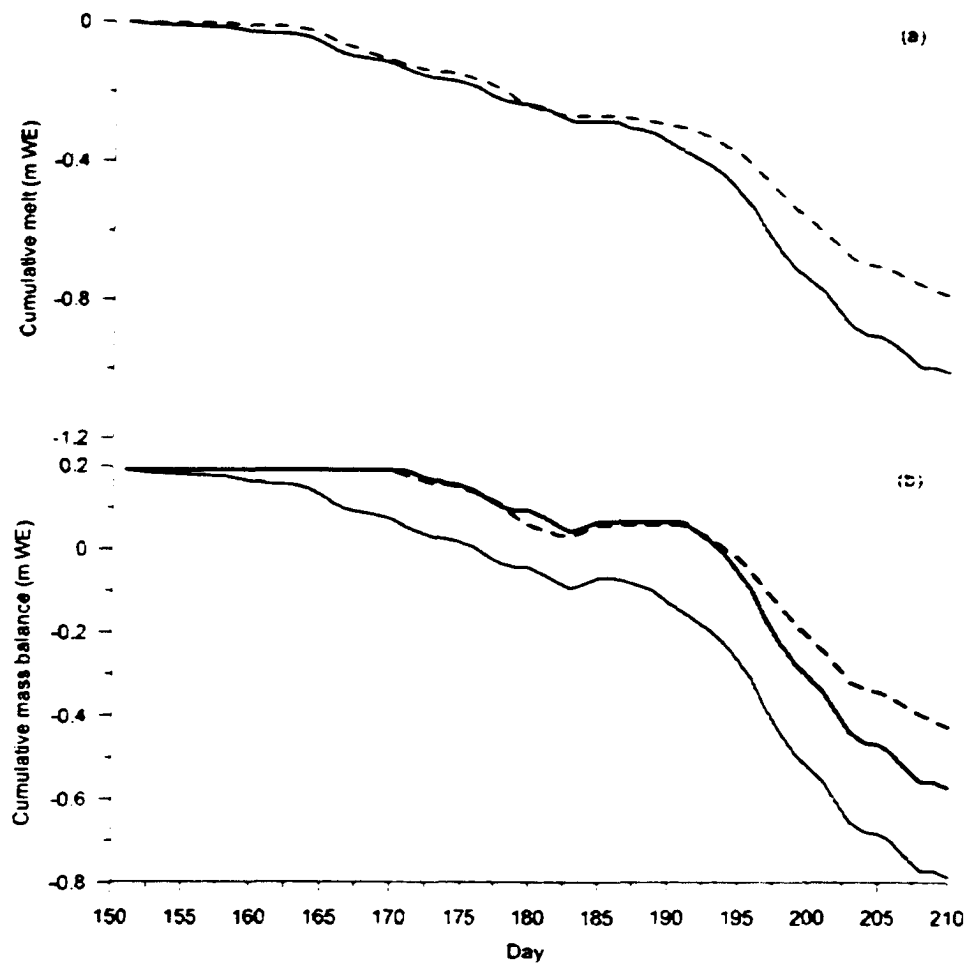
Figure 5.7. Measured (solid) and simulated (dashed) data for Sensitivity Test Stage 1 (validation: 31 May – 29 July, 2001): (a) albedo: (b) SWE and SI (solid bold): (c) melt: and, (d) 3-day averaged melt.
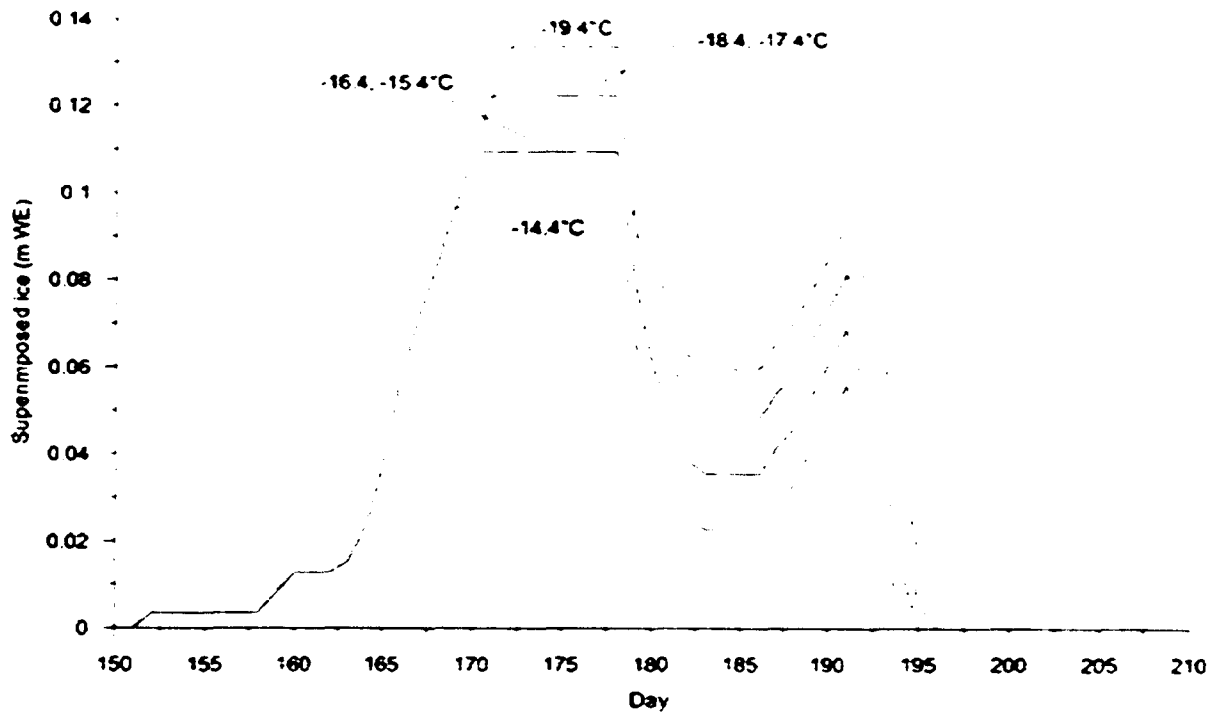
168

Figure 5.8. Measured (solid) and simulated (dashed) data for Sensitivity Test Stage 1 (validation: 31 May – 29 July, 2001): (a) cumulative melt; and, (b) cumulative MB. Bold solid line in (b) is the measured MB adjusted after the simulation, to incorporate SI formation.

169

Figure 5.9. SI$_{SLT}$ sensitivity test output. Labels indicate SLT values used in each run: in cases where two values are indicated. model output was the same for each value.
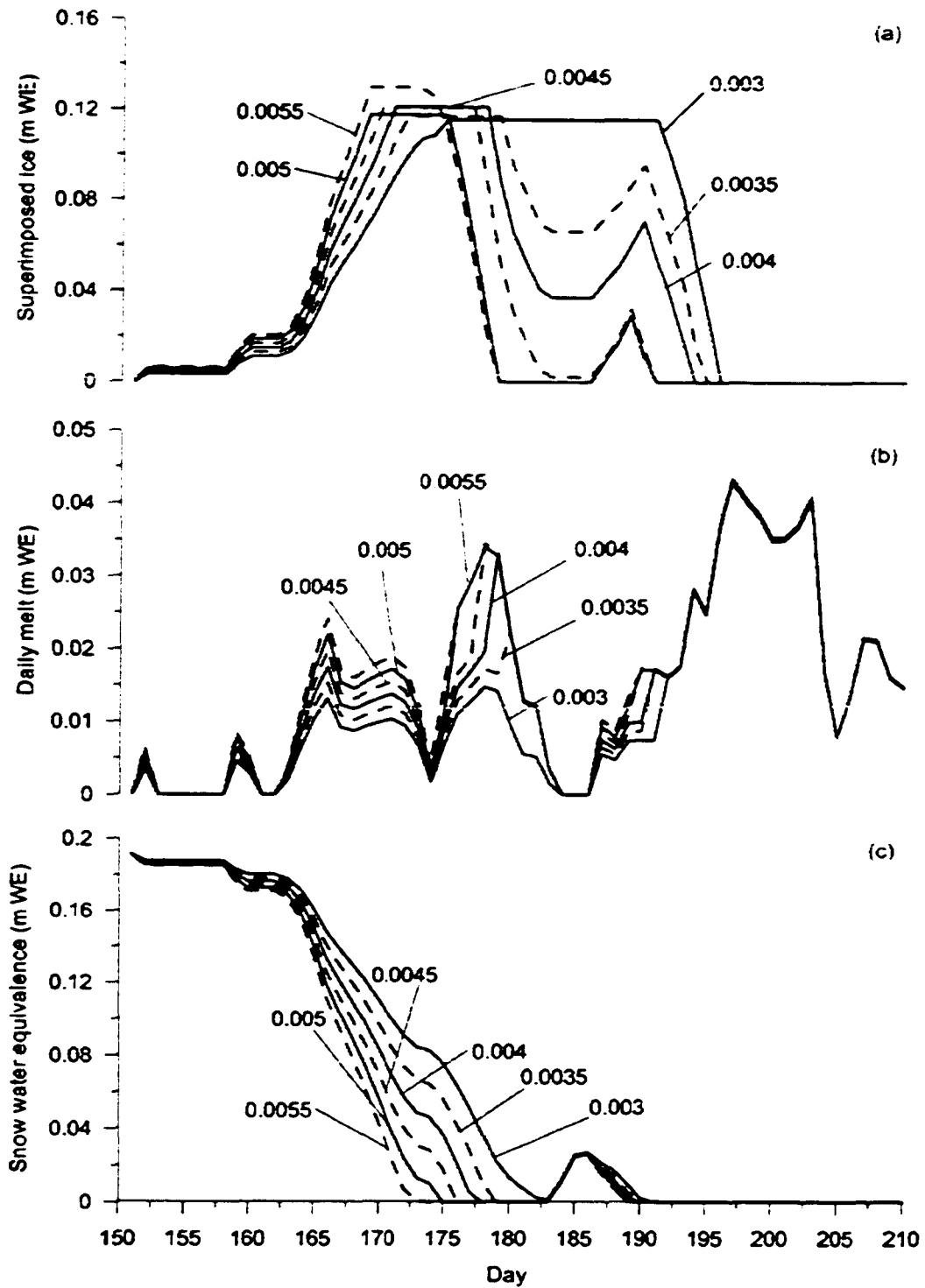
Figure 5.10. Sensitivity test of constant DDF$_{snow}$: (a) SWE: (b) SI: and (c) melt. Labels indicate values of DDF$_{snow}$ used in each run.
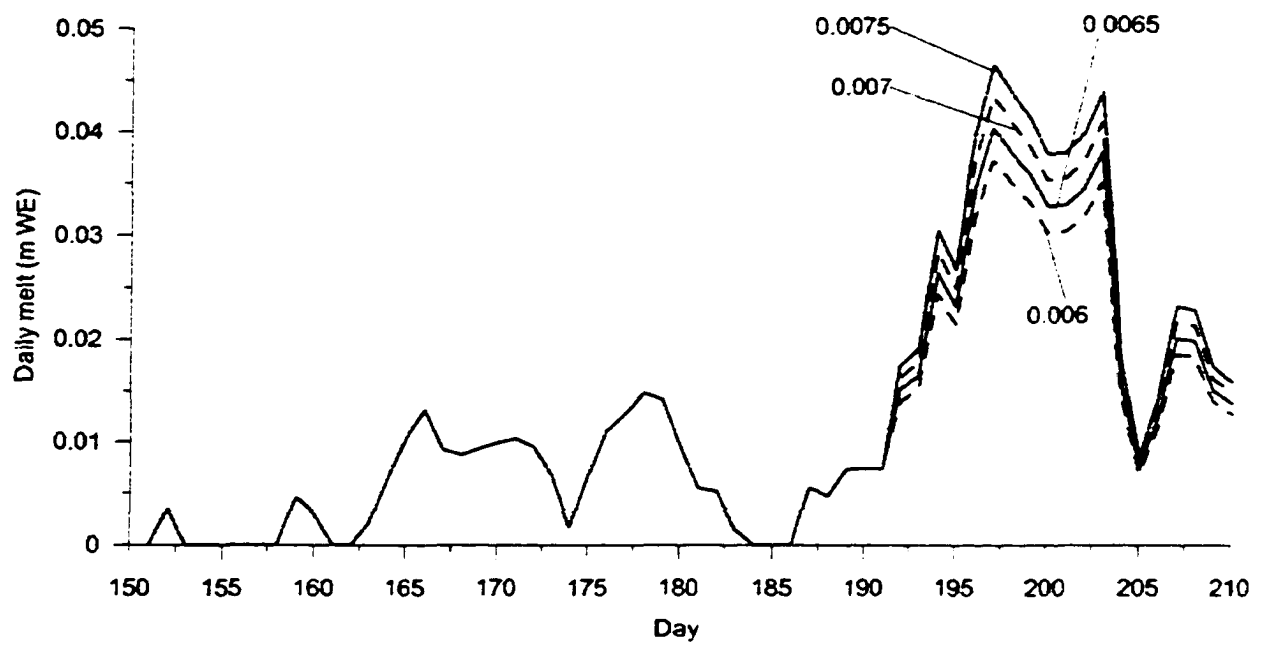
Figure 5.11. Sensitivity test of constant DDF_{ice}: melt output. Labels indicate values of DDF_{ice} used in each run.
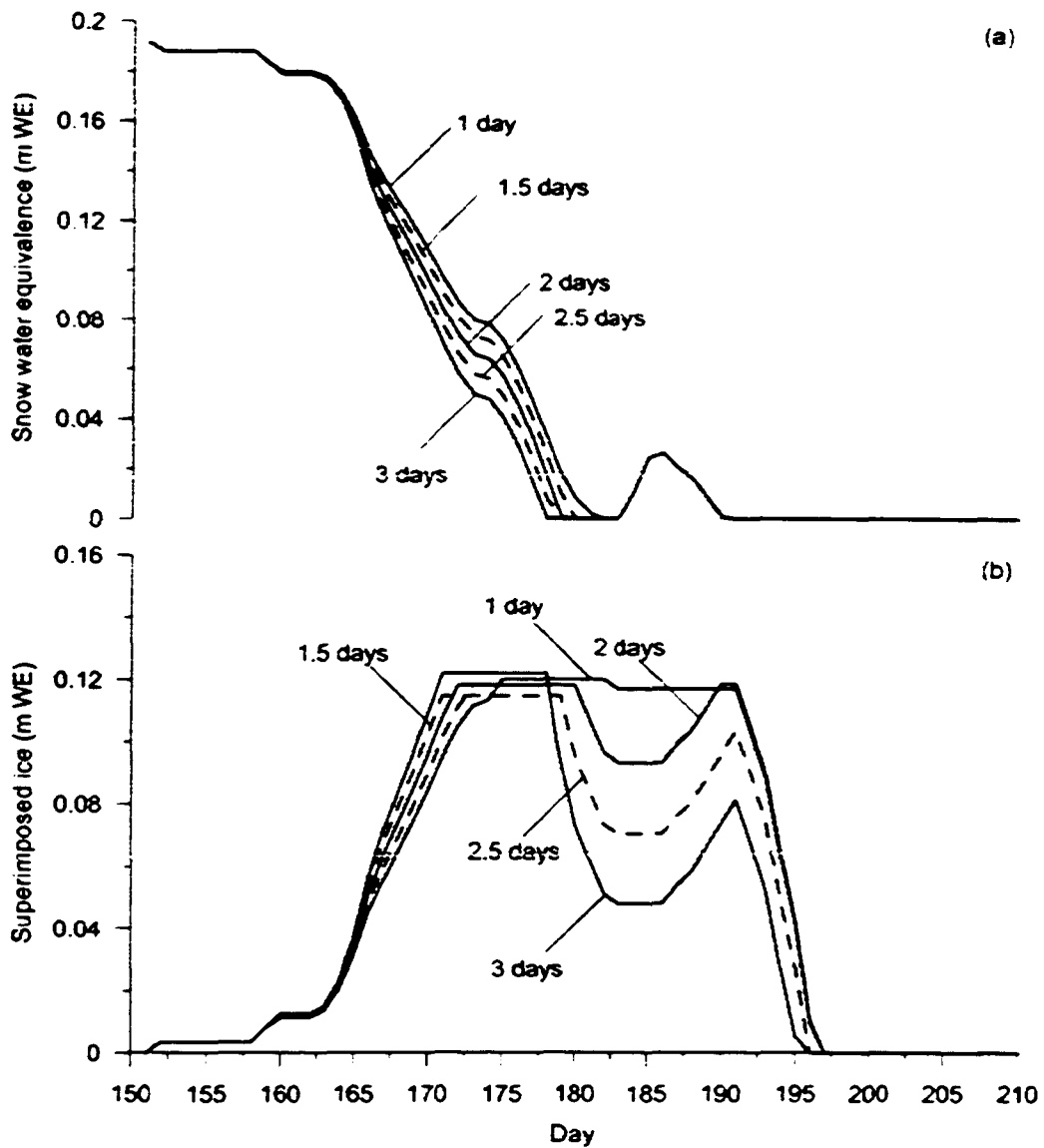
Figure 5.12. (a) SWE. and (b) SI output from sensitivity test of water runoff time (variable DDF parameterization). Labels indicate values of runoff time used in each run.
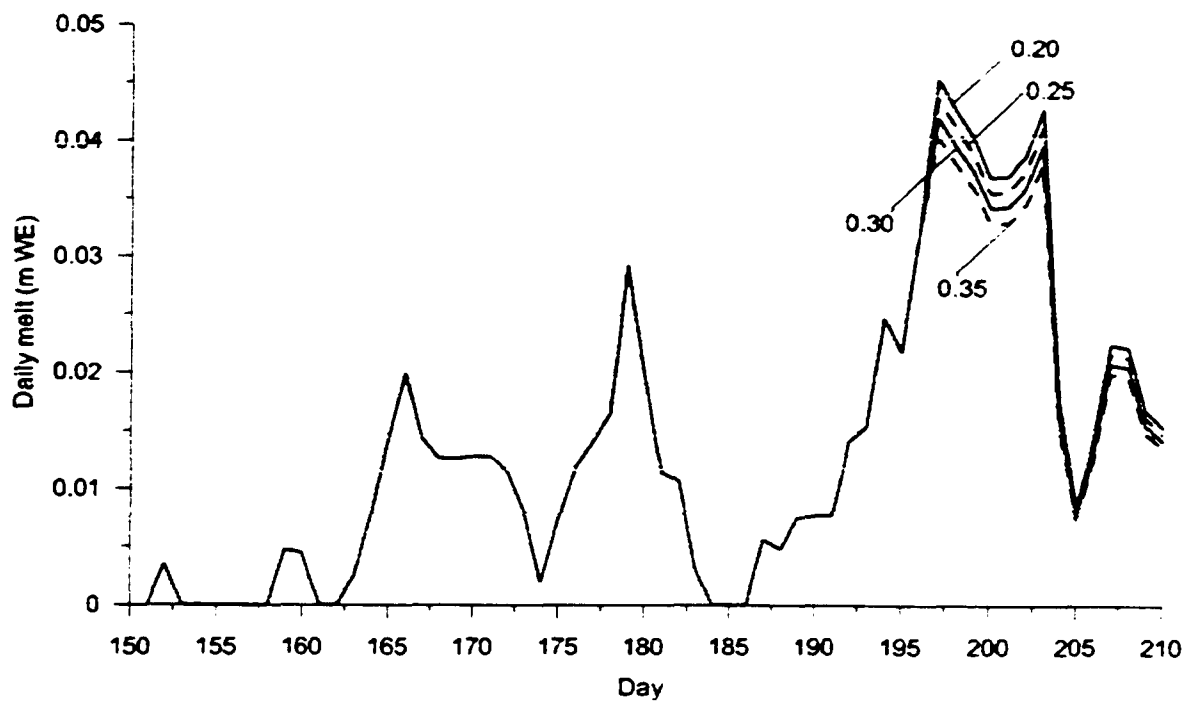
Figure 5.13. Melt output from sensitivity test of glacier ice albedo (variable DDF parameterization). Labels indicate values of glacier ice albedo used in each run.

174
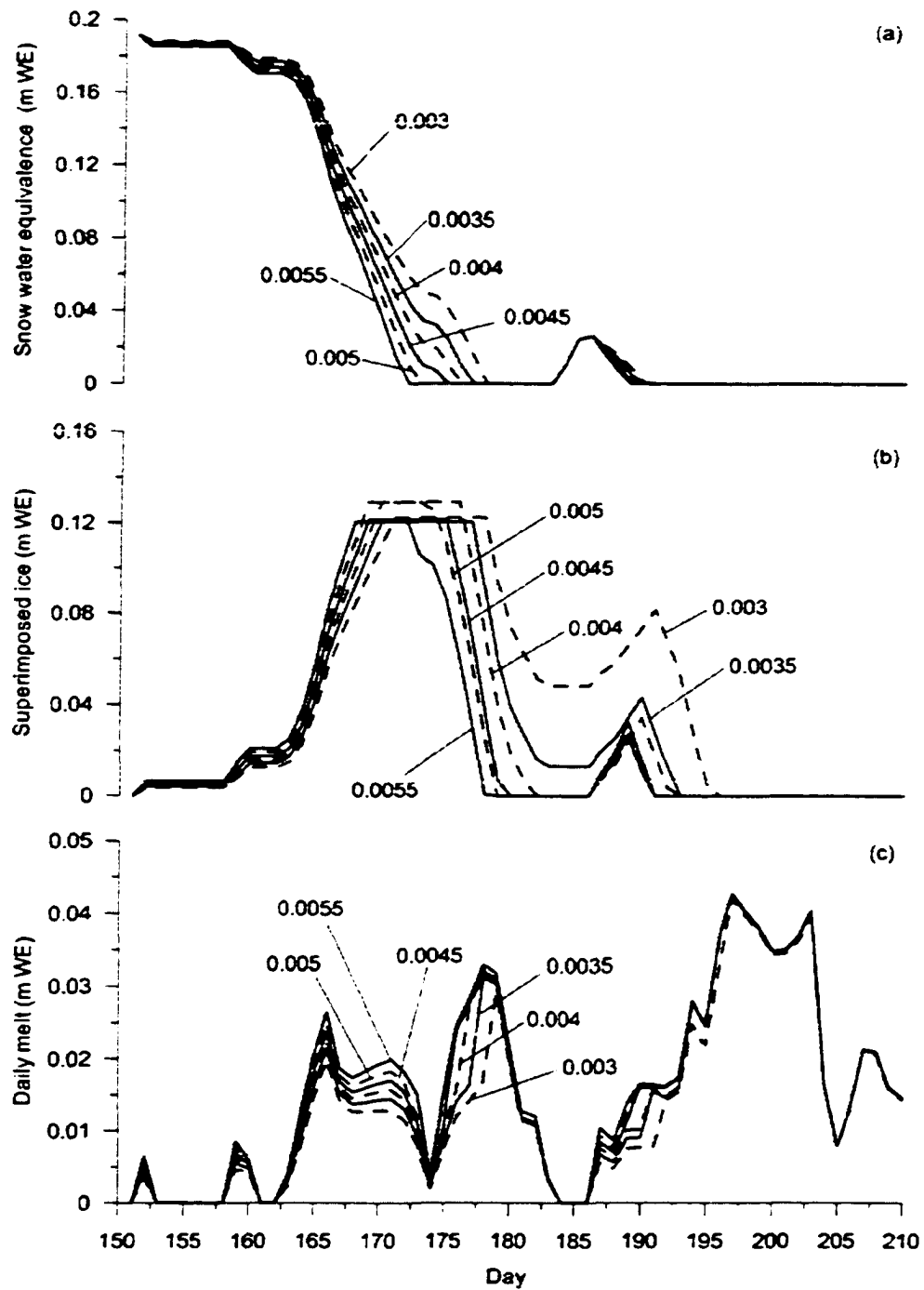
Figure 5.14. Sensitivity test of variable DDF_snow: (a) SWE; (b) SI; and, (c) melt. Labels indicate values of DDF_snow used to calculate M and B of Equation (1) for each run.
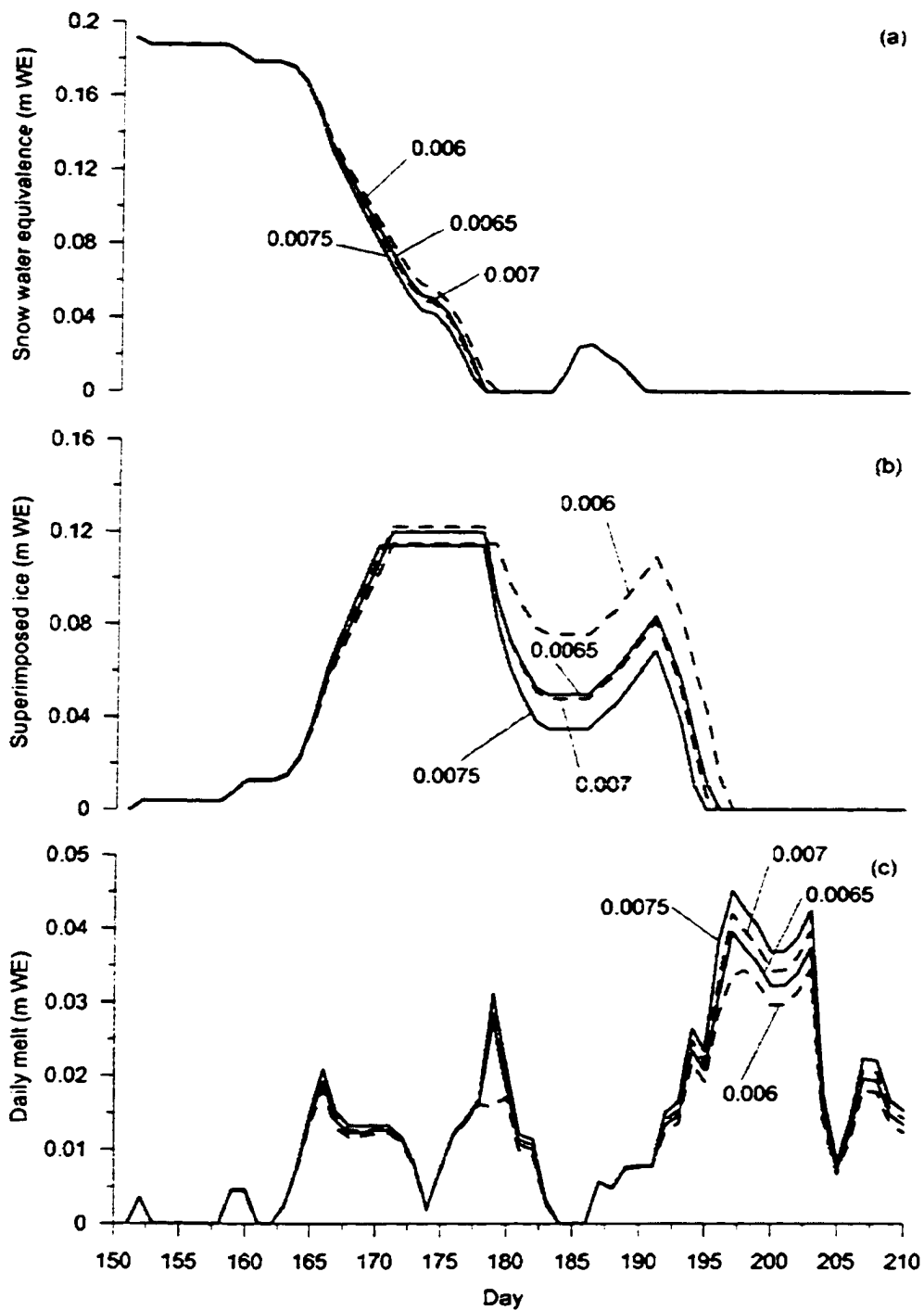
Figure 5.15. Sensitivity test of variable DDF$_{ice}$: (a) SWE: (b) SI: and. (c) melt. Labels indicate values of DDF$_{ice}$ used to calculate M and B of Equation (1) for each run.

176
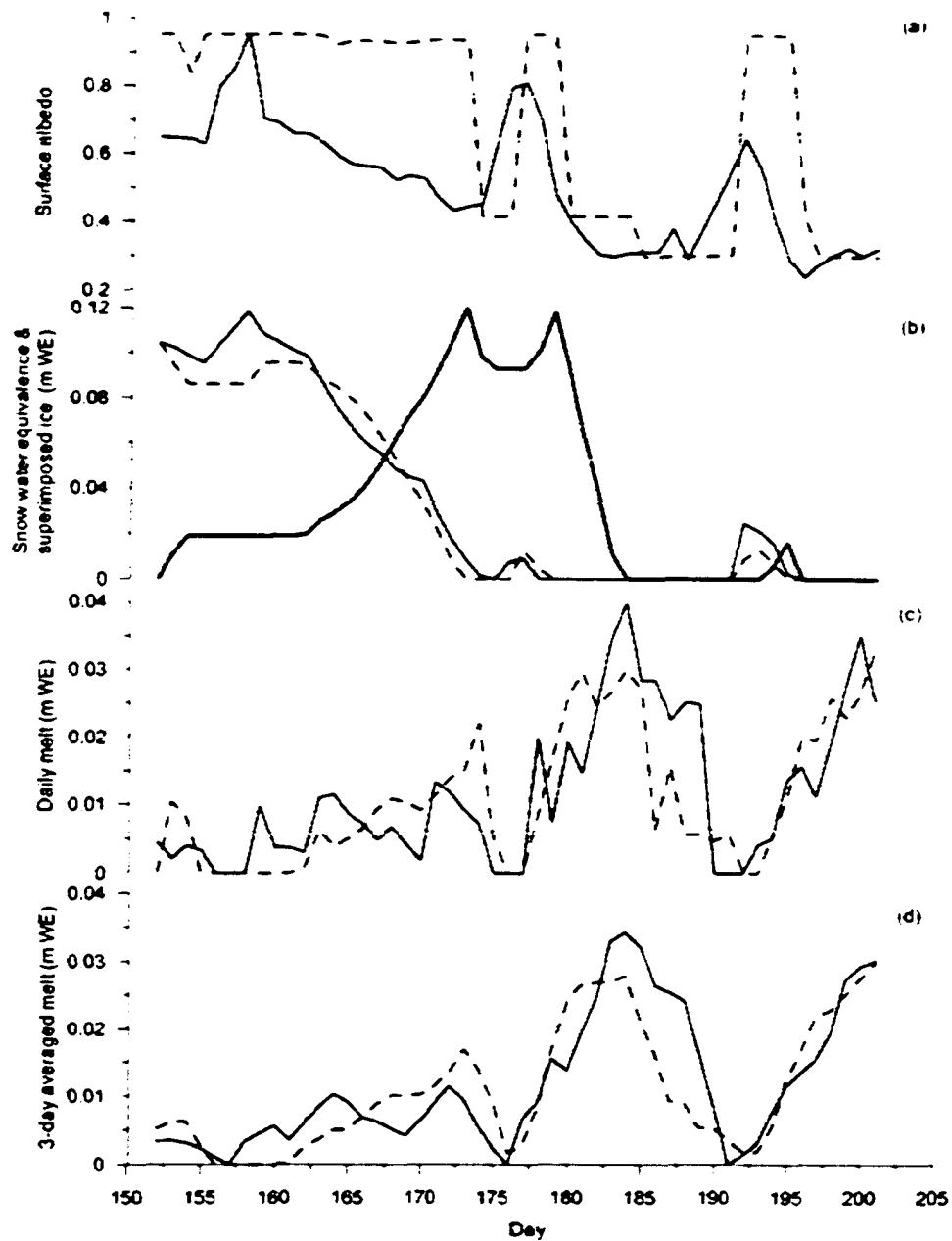
Figure 5.16. Measured (solid) and simulated (dashed) data for Sensitivity Test Stage 2 (calibration: 1 June – 10 July, 2002): (a) albedo: (b) SWE and SI (solid bold): (c) melt: and, (d) 3-day averaged melt.

177
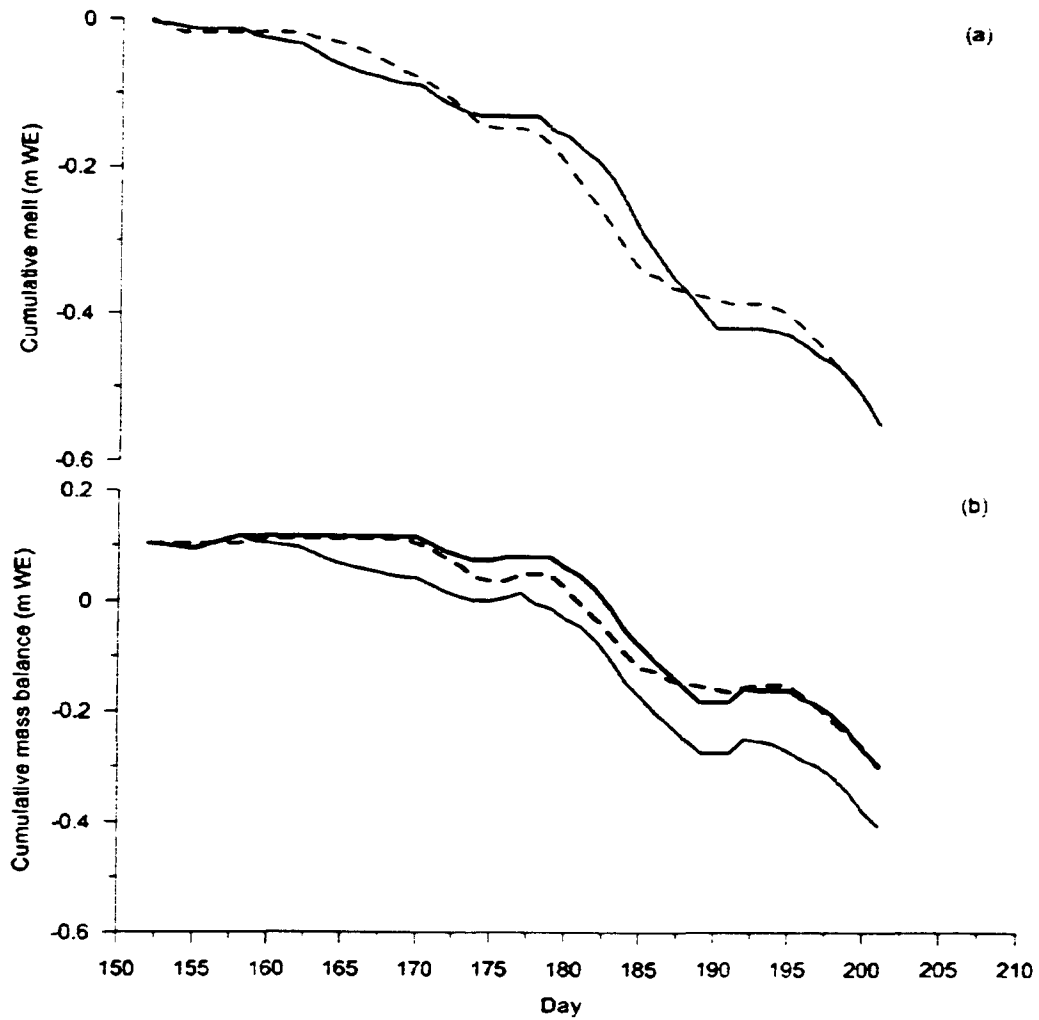
Figure 5.17. Measured (solid) and simulated (dashed) data for Sensitivity Test Stage 2 (calibration: 1 June – 10 July, 2002): (a) cumulative melt; and, (b) cumulative MB. Bold solid line in (b) is the measured MB adjusted after the simulation to incorporate SI formation.
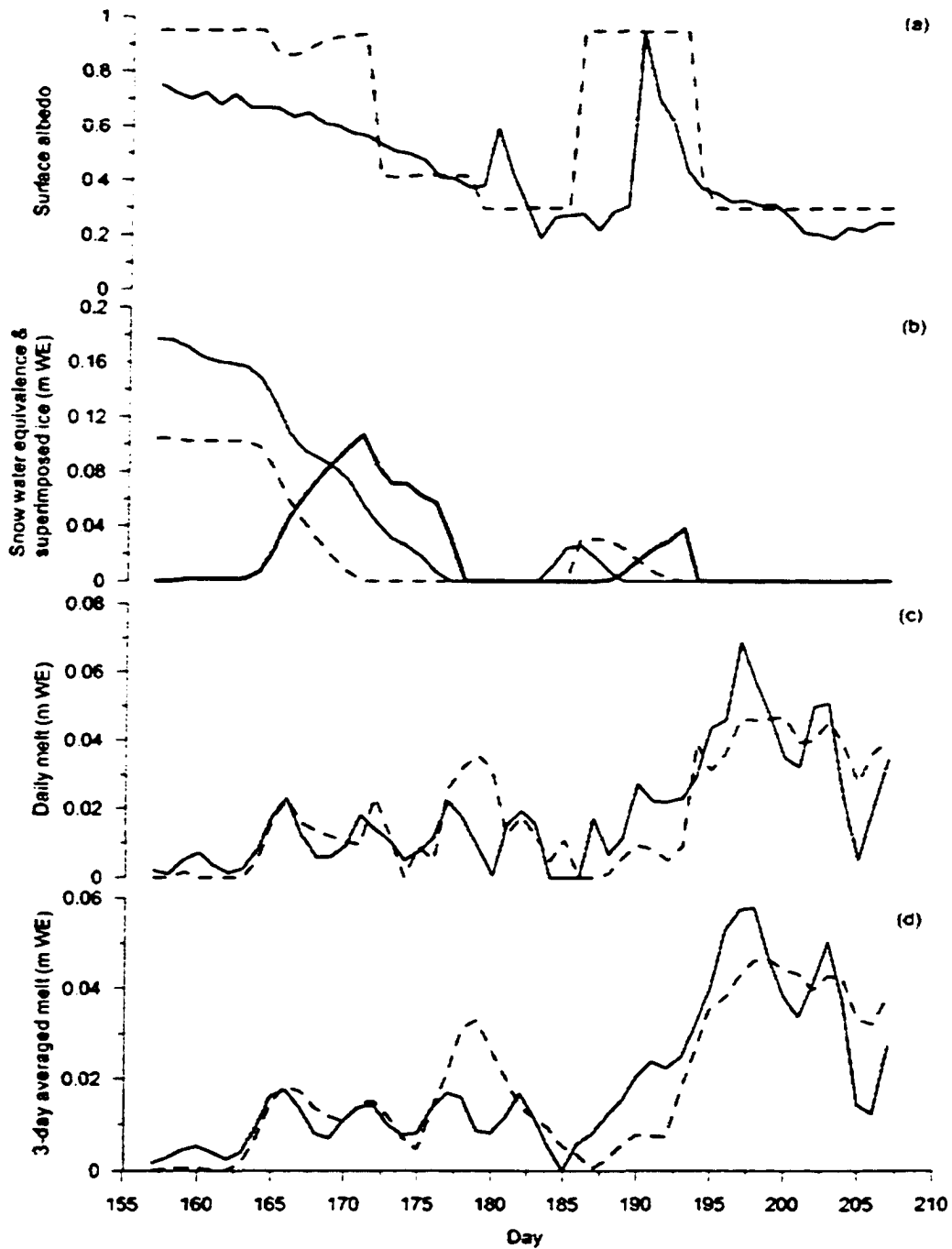
Figure 5.18. Measured (solid) and simulated (dashed) data for Sensitivity Test Stage 2 (validation: 6 June – 26 July, 2001): (a) albedo; (b) SWE and SI (solid bold); (c) melt; and, (d) 3-day averaged melt.

179
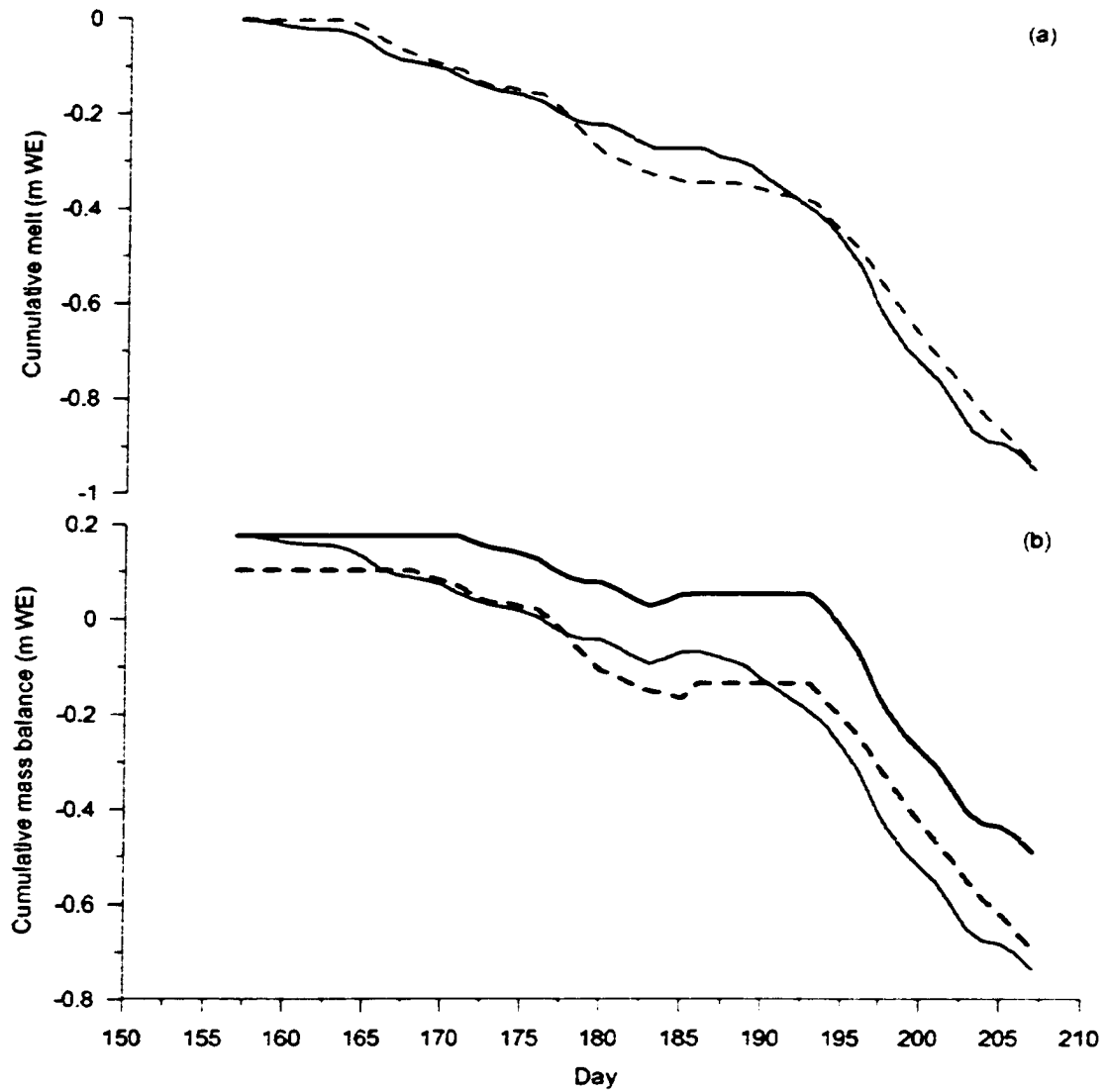
Figure 5.19. Measured (solid) and simulated (dashed) data for Sensitivity Test Stage 2 (validation: 6 June – 26 July. 2001): (a) cumulative melt; and. (b) cumulative MB. Bold solid line in (b) is the measured MB adjusted after the simulation. to incorporate SI formation..

180
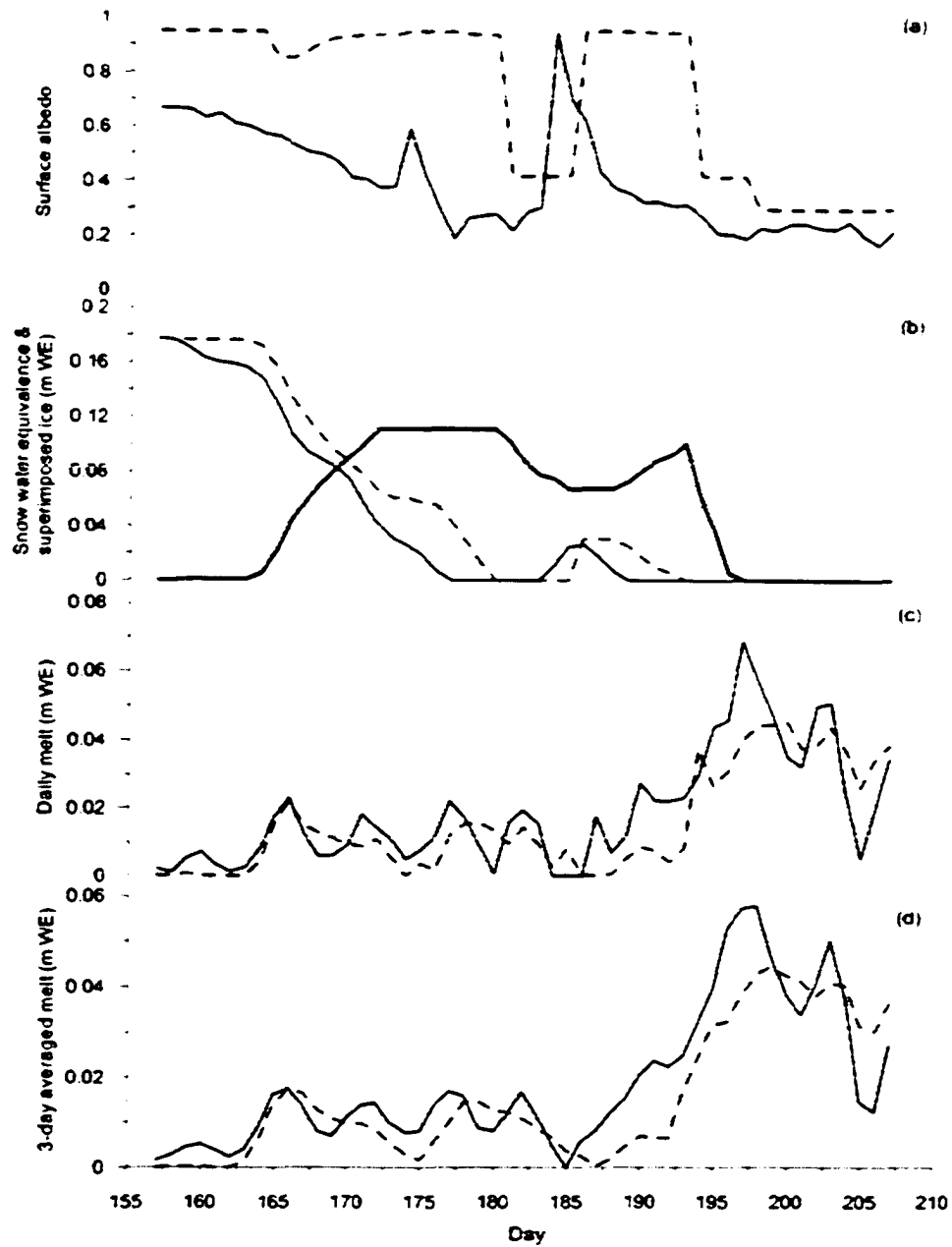
Figure 5.20. Measured (solid) and simulated (dashed) data for Sensitivity Test Stage 2 (second validation, using 2001-specific lapse rates: 6 June – 26 July, 2001): (a) albedo; (b) SWE and SI (solid bold); (c) melt; and. (d) 3-day averaged melt.

181
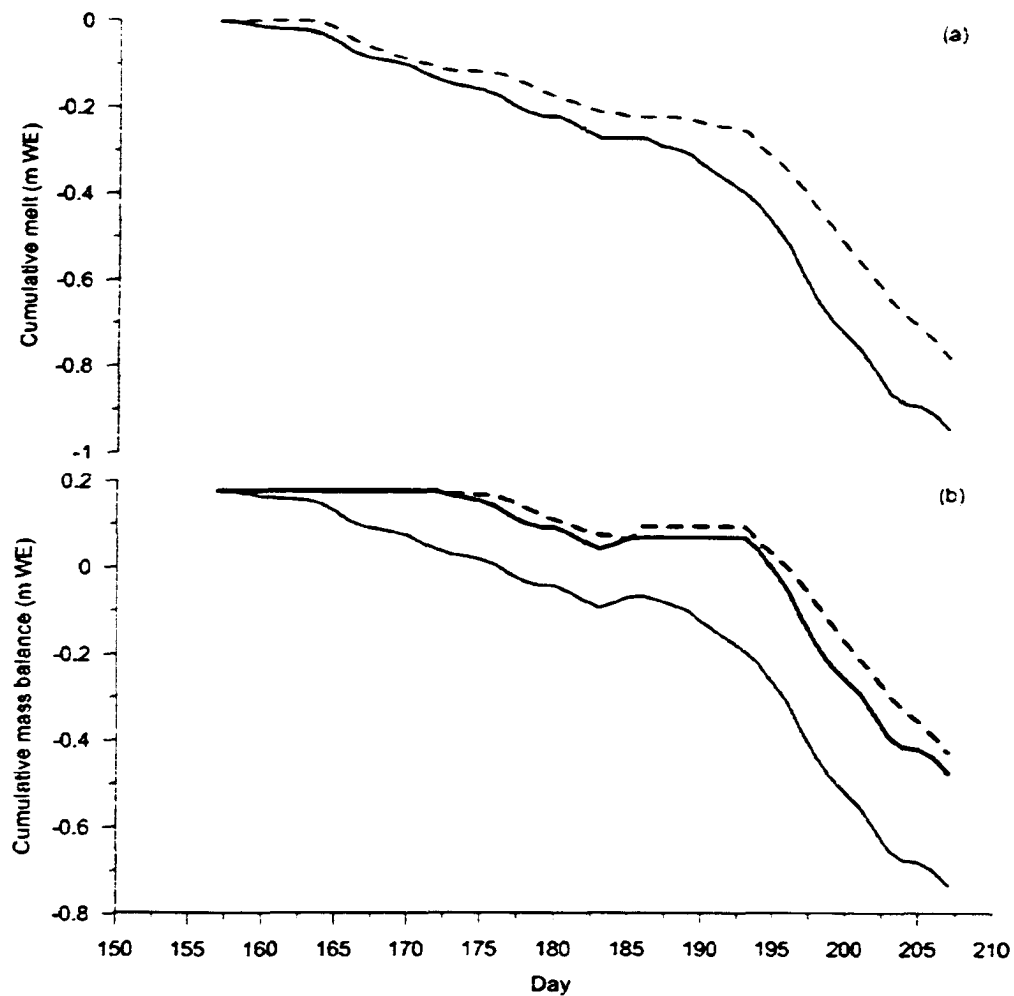
Figure 5.21. Measured (solid) and simulated (dashed) data for Sensitivity Test Stage 2 (second validation: 6 June – 26 July, 2001): (a) cumulative melt: and, (b) cumulative MB. Bold solid line in (b) is the measured MB adjusted after the simulation, to incorporate SI formation.

182
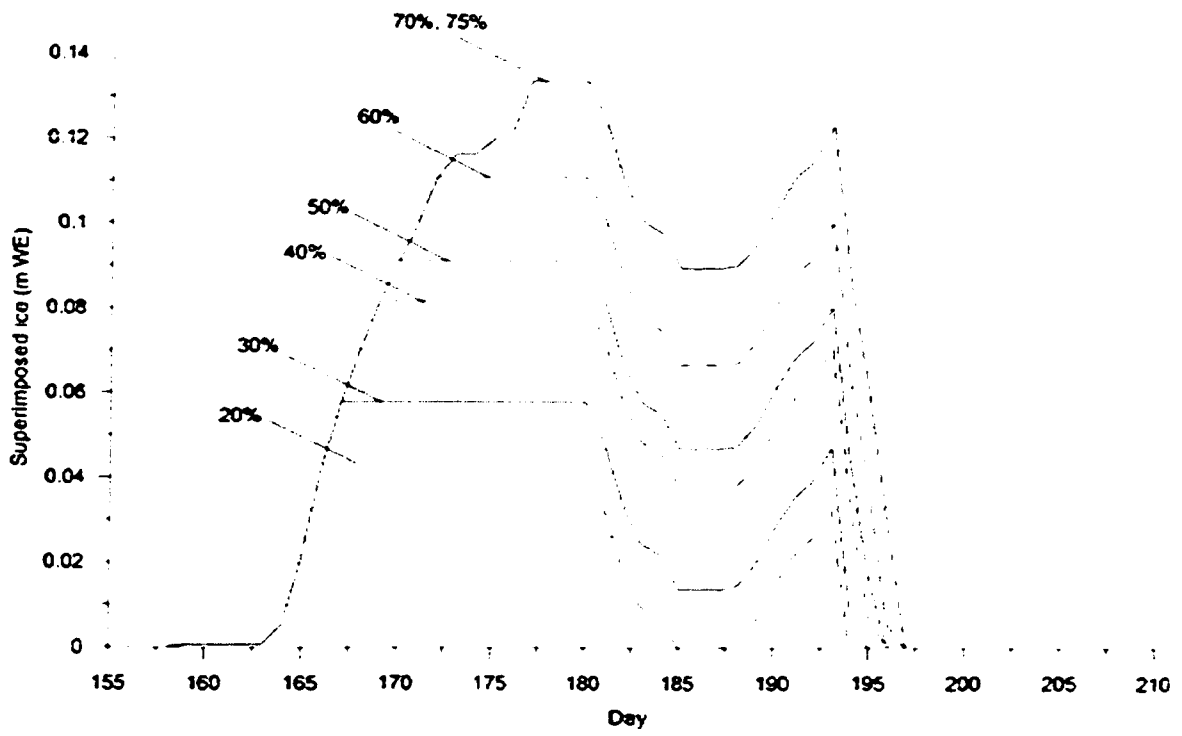
Figure 5.22. SI$_{PMAX}$ sensitivity test. Labels indicate values of PMAX used for each run.

183
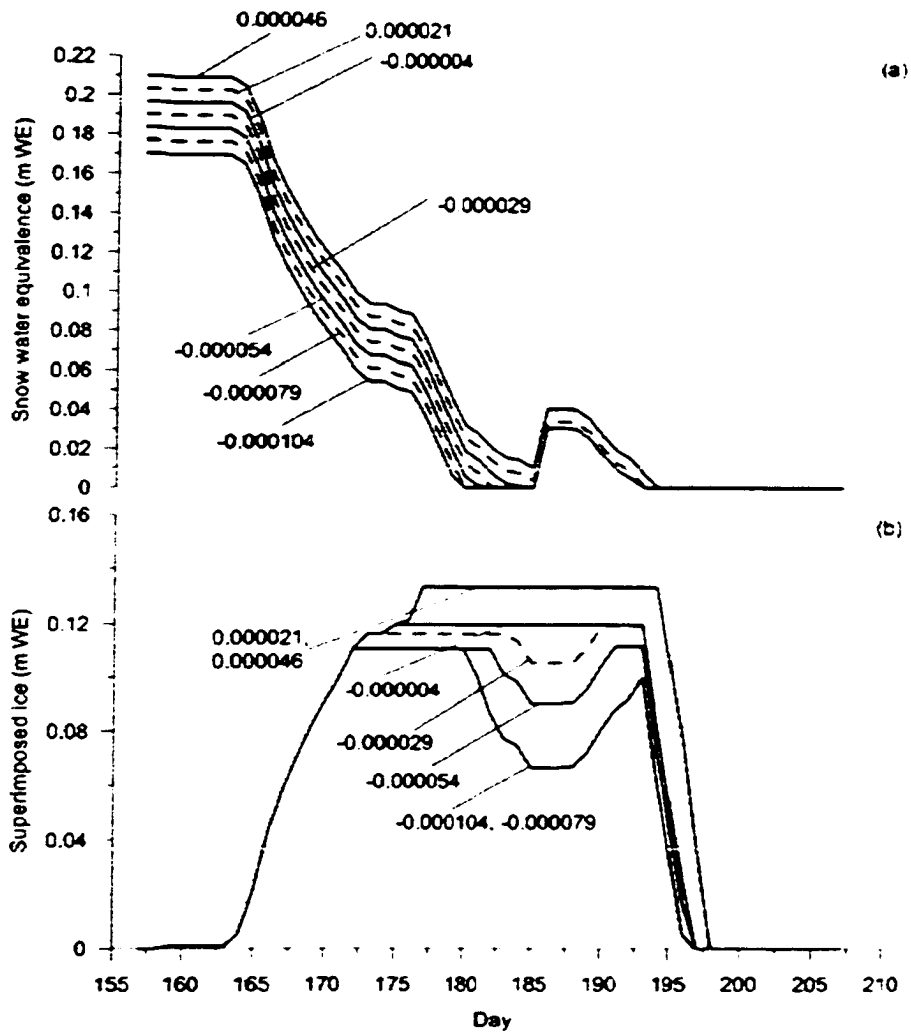
Figure 5.23. WALR sensitivity test: (a) SWE: and. (b) SI. Labels indicate WALR values in m WE m⁻¹ used for each run.
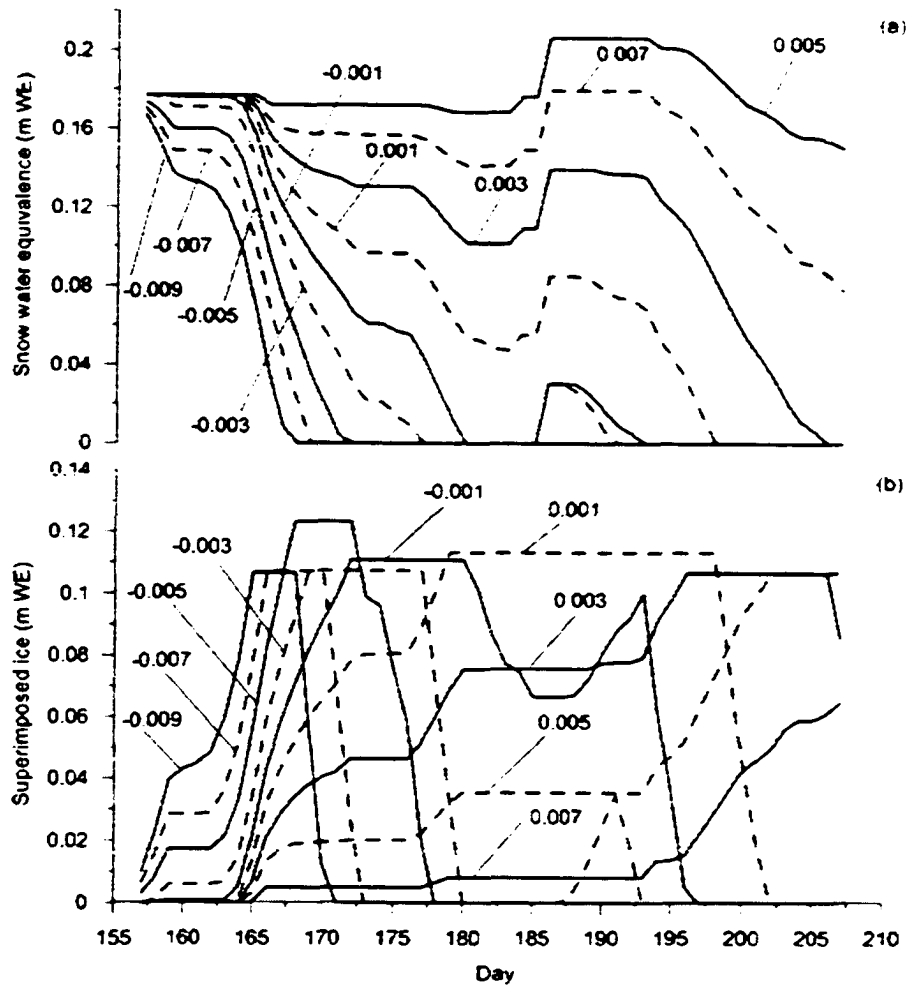
Figure 5.24. STLR sensitivity test: (a) SWE: and. (b) SI. Labels indicate STLR values in °C m⁻¹ used for each run.
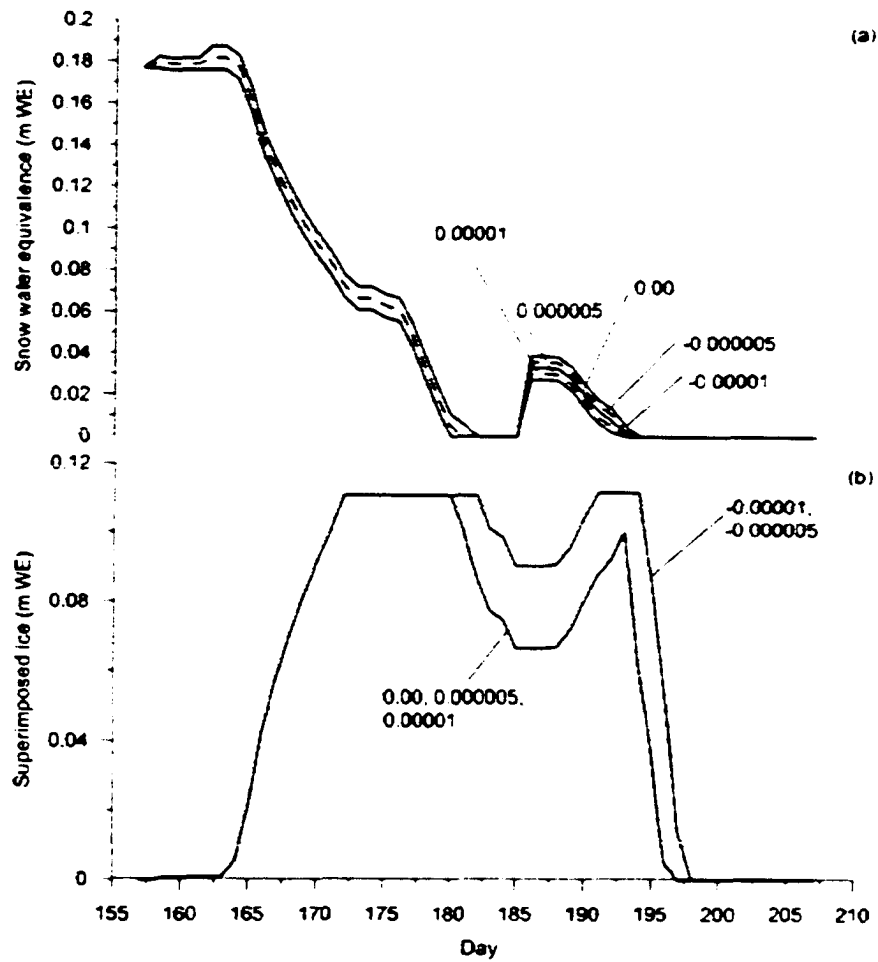
Figure 5.25. SALR sensitivity test: (a) SWE; and. (b) SI. Labels indicate SALR values in m WE m⁻¹ used for each run.

186
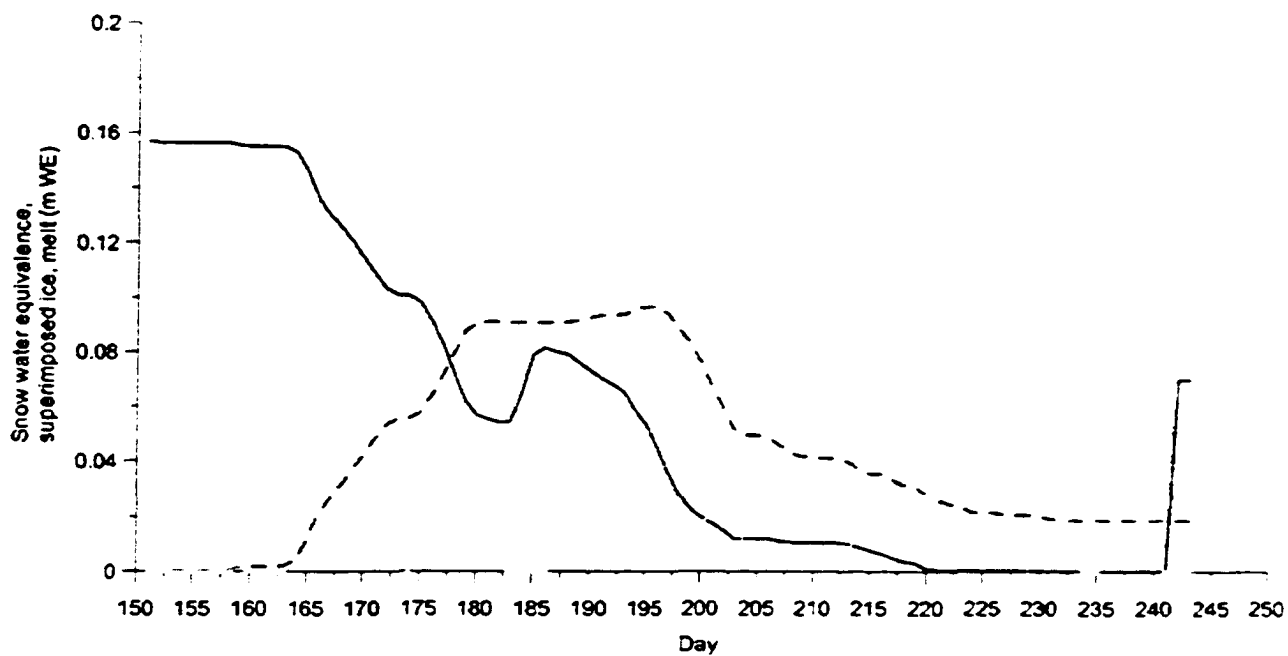
Figure 5.26. Simulated SWE (solid black). SI (dashed) and melt (grey) for climate response test: 2001 baseline run (1 June – 31 August). Note that glacier-wide SWE can reach zero if the equilibrium line altitude (ELA) rises above 1100 m a.s.l.

187
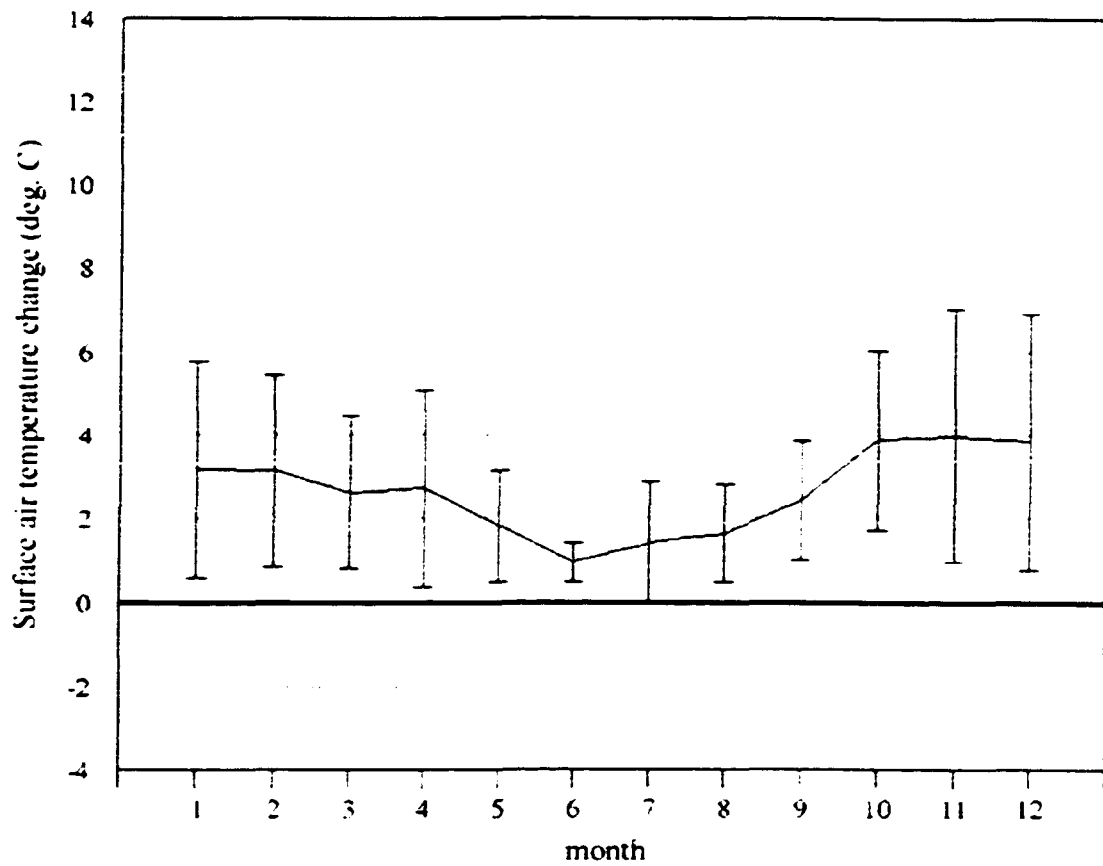
Figure 5.27. Composite GCM-projected change in surface air temperature at 291.80°E. 80.71°N (JEG) between 1961-1990 and 2000-2029 (*from:* http://faldo.atmos.uiuc.edu/FINGERPRINT/IMAGEMAP/seasonality.index.html).

188
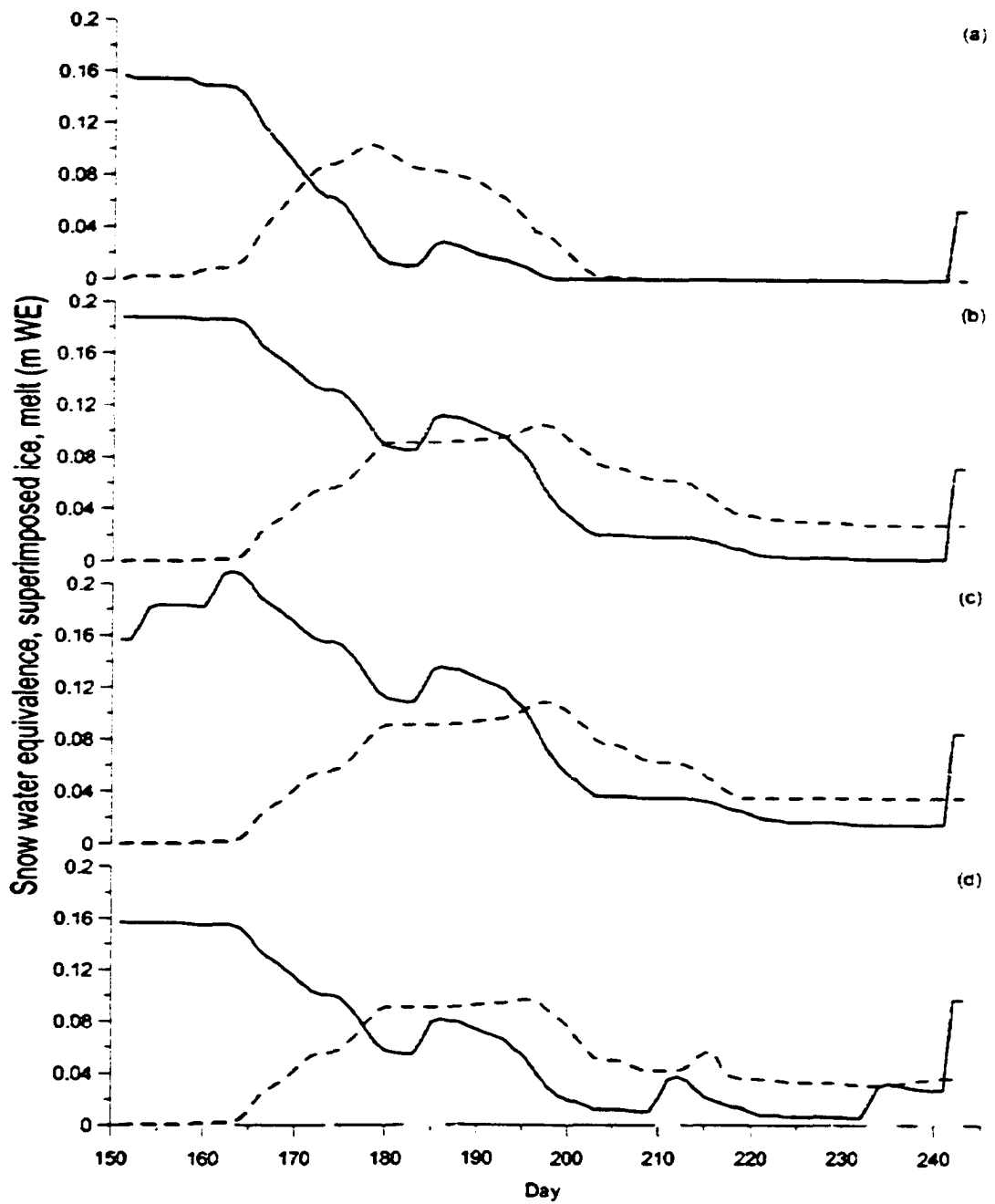
Figure 5.28. SWE (solid black). SI (dashed) and melt (grey) output from climate response tests: (a) air temperature increase: (b) EOW snowpack increase: (c) early summer snowfall: and. (d) late summer snowfall. Note that glacier-wide SWE can reach zero if the equilibrium line altitude (ELA) rises above 1100 m a.s.l.

189

Figure 5.29. SWE (solid black). SI (dashed) and melt (grey) output from concurrent air temperature and winter precipitation increase climate response test. Note that glacier-wide SWE reaches zero when the equilibrium line altitude (ELA) rises above 1100 m a.s.l.

CHAPTER 6.

THESIS CONCLUSIONS

6.1. Thesis goal and objectives

As stated in Chapter 1. the purpose of this research was to use field studies of a polythermal high Arctic glacier (John Evans Glacier (JEG). Ellesmere Island. 79° 40´ N. 74° 30´ W) to investigate Arctic glacier melt, runoff. and mass balance response to climate change.

My research objectives were:

(a) to determine the importance of surface meltwater storage and subsequent drainage system evolution in modulating the relationship between water entering and exiting the glaciohydrological system;

(b) to determine glacier melt response to local meteorological conditions by assessing the role of extreme events in overall melt and mass balance. and identifying the role of specific seasonal conditions in enhancing/suppressing melt; and.

(c) to use the information from *(b)* in a degree-day model (DDM) to investigate glacier melt, runoff. and mass balance response to climate change.

This chapter outlines the results of the thesis. and discusses the implications of the thesis for research in this field. as well as areas requiring further research.

6.2. Summary

Thesis results indicate that seasonal development of the glacier drainage system is characterized by sudden periodic shifts in the melt-runoff relationship. Prior to runoff production. initial melt is delayed within the snowpack and firn (Fountain. 1996). where it forms superimposed ice and internal accumulation (Pfeffer and Humphrey. 1996). A small proportion of melt produced following the ripening of the snowpack may go directly to runoff. but the majority is further delayed in supraglacial and ice-marginal storage (stream ponds. crevasses. lakes) (Boon and Sharp. 2003). Progressive interconnection of these storage locations. followed by catastrophic englacial drainage via the hydrofracture process. provides the impetus for opening the subglacial

191

hydrological system (Boon and Sharp. 2003). However. meltwater is again delayed within the subglacial system, behind a cold ice dam at the glacier terminus (Skidmore and Sharp. 1999; Heppenstall, 2001; Bingham. 2003). Once subglacial water has breached this dam, and provided sufficient meltwater inputs are maintained. the delay in the melt-runoff response is significantly reduced (Bingham. 2003). As the melt season progresses and continued meltwater inputs are directed into the drainage system. meltwater is transported more efficiently. thus further reducing the delay between melt and runoff production (Bingham et al.. in review).

It is clear that surface melt is the impetus behind seasonal development of the supra-and subglacial drainage systems, with the storage-release behaviour of the supraglacial system driving subglacial drainage system development. As surface melt is driven in turn by local meteorological conditions. it is clear that meteorology will also significantly impact seasonal drainage system development.

Extreme meteorological events that affect glacier melt subsequently impact glacier runoff and mass balance (Boon et al.. 2003). An extreme melt event on 28-30 July. 2000 brought a combination of high winds and high air temperatures to JEG. producing approximately 15% of total seasonal melt on the middle glacier. and 30% on the upper glacier. although the event itself occupied only 6% of the melt season. The contribution of the event to total seasonal runoff is estimated at approximately 18% on the middle glacier and 35% on the upper glacier.

The timing of such events is crucial. determining their impact on the timing and magnitude of summer melt and runoff. and the development of the en-/subglacial component of the glacier drainage system. Prior to the initiation of subglacial outflow (early season: early- to mid-June). extreme melt events may increase the rate of snowline retreat on the lower glacier. increasing total seasonal melt and potentially advancing the dates on which runoff and subglacial outflow are initiated (Fountain. 1996). Events occurring around the time when subglacial outflow is initiated (mid-season: late June to early July) could provide a major impetus for the establishment and initial growth of englacial and subglacial drainage passageways (Kamb. 1987; Kavanaugh and Clarke. 2001). Events occurring when subglacial outflow has already begun (late season: mid-July to early August) would have a much stronger runoff impact than earlier events. but a

192

weaker impact on glacier drainage. as en- and subglacial channels would likely already have formed in response to runoff earlier in the season. In some cases. however. creation of new englacial connections between the supraglacial and subglacial systems might occur. resulting in upglacier expansion of the subglacial network (Nienow et al.. 1998: Flowers and Clarke. 2002).

Variability in the occurrence of these extreme events may also be a significant factor in inter-annual variability and longer-term changes in the mass balance of high Arctic glaciers. and needs to be considered when evaluating the likely response of mass balance to climate change. Given that such events can account for a large fraction of summer melt in a relatively short period. they may play an important role in determining the sensitivity of mass balance and runoff to climate changes. It is therefore important to investigate the relationship between the incidence of such events. longer-term climate trends and characteristic modes of climate variability

I therefore examined the long-term (1996-2002) meteorological record from John Evans Glacier to determine the spatial and temporal variability in processes impacting annual glacier mass balance (end-of-winter snowpack. summer air temperature. summer wind events. summer snowfalls). Results indicate that. while extreme events occur only rarely. they do have a significant impact on long-term MB. However. meteorological conditions at JEG are highly spatially and temporally variable. with the processes important for MB varying in significance both spatially and interannually.

End-of-winter snow depth decreases with elevation on the glacier due to increased wind speeds and wind scour events at higher elevations. Summer surface lowering (melt) and net annual elevation drop are greatest lower on the glacier. and decrease with elevation. Surface air temperature decreases with elevation in the summer months. although not at a constant lapse rate. and not at the moist adiabatic lapse rate (MALR: -6°C km^{-1}). In the winter months. however. a temperature inversion often occurs. Air temperature thus increases with elevation. with steeper positive lapse rates on the upper part of the glacier than the lower.

Although the upper weather station (1183 m a.s.l.) is usually located in the accumulation area. it experienced net elevation loss over the recording interval due to the anomalously warm years of 1998 and 1999. The middle weather station (824 m a.s.l.)

193

experienced net surface elevation loss in 1998-2000. while the lower weather station (261 m a.s.l.) experienced net surface elevation loss in all years. Net surface elevation change at the UWS and LWS is driven mainly by summer conditions. while the position of the MWS near the fluctuating equilibrium line results in net elevation change being affected by both winter and summer conditions.

The climate-mass balance relationship in remote areas and for large ice sheets is often studied using numerical models that incorporate energy-balance or degree-day (temperature index) methods (Braithwaite and Oleson. 1990: Bøggild et al.. 1994: Fleming et al.. 1997: Jóhannesson. 1997: Braithwaite and Zhang. 1999). While energy-balance models are considered more accurate. degree-day models require fewer input data and less computational power. This is because they are highly simplified. relying on a linear relationship between glacier melt and air temperature (Braithwaite. 1984: Braithwaite. 1995: Ohmura. 2001: Hock. 2003). with the factor of proportionality being the degree-day factor (DDF: in m WE d^{-1} °C^{-1}) (Hock. 1999: Singh et al.. 2000).

DDMs are. however. based on two assumptions that this thesis has shown to be unfounded: (a) snow depth increases with elevation at a specified accumulation lapse rate (Jóhannesson. 1997: Hock. 2003): and. (b) summer surface air temperature decreases with elevation at the moist adiabatic lapse rate (MALR: -6.0°C km^{-1}) (Jóhannesson. 1997: Greuell and Böhm. 1998: Braithwaite and Zhang. 2000).

In addition. the DDF is used to incorporate all information regarding surface conditions (albedo. roughness. etc.) and meteorological conditions other than air temperature (e.g.. wind. precipitation. etc.). DDMs are thus unable to represent specific events such as summer snowfalls and summer wind events (e.g.. the 2000 event). despite their significant impact on mass balance (Woodward et al.. 1997: Arendt and Sharp. 1999: Hock. 1999). It would be useful. therefore. to vary DDFs for the summer melt season to incorporate the reduction of melt due to increased surface albedo both during and following summer snowfalls. the duration of which is highly dependent on local meteorological conditions (Fujita and Ageta. 2000: Oerlemans and Klok. 2003). DDFs could also be increased for periods when wind events are known to occur. While these adjustments may reduce some of the advantages of using DDMs (i.e.. more input data

194

required). Arctic glacier MB and its sensitivity to climate change cannot be accurately modelled without taking these issues into consideration.

Since analysis of the long-term meteorological record revealed that certain assumptions on which DDMs are based, as well as their representation of given processes, are problematic, my next step was to determine the sensitivity of DDM output to parameterization of these variables (winter accumulation lapse rate, summer air temperature lapse rate, summer accumulation lapse rate, degree-day factor, and method of determining superimposed ice production). I then determined the possible response of JEG to climate change, taking into account both the model sensitivity to parameterization, and our understanding of glacier hydrology at JEG.

Results indicate that the DDM I used (Arendt, 1997) is most sensitive to the parameterization of lapse rates and DDFs, especially the variable DDF. This indicates that these variables must be clearly defined and correspond well with field data in order to have confidence in model output. Lapse rates (winter accumulation, summer air temperature and accumulation) used in the model must be specific to the study site, and to the year(s) for which the model is run. The components of the variable DDF algorithm should either be corroborated with field data, or be selected from only a small range of plausible values for a given site.

The DDM is also relatively sensitive to the parameterization of superimposed ice using the PMAX algorithm. As previous studies have resulted in a large range of plausible values for PMAX (e.g., Reeh, 1991; Wolfe and English, 1995; Fujita et al., 1996; Woodward et al., 1997; Bugnion and Stone, 2002), superimposed ice formation should be parameterized using the mean annual air temperature method in the absence of field measurements of PMAX.

Results of the climate response scenarios indicate that melt, runoff and MB at JEG are most sensitive to future (2000-2029) air temperature increases predicted by GCMs (Houghton et al., 2001). This is largely due to the temperature increase in July, which has the greatest number of positive degree-days. Melt will increase, runoff will increase, and MB will substantially decrease; these impacts will be only minimally offset by a concurrent increase in winter precipitation. Melt, runoff and MB at JEG are also relatively sensitive to an increase in late-summer snowfalls, which have the effect of

195

reducing melt during the period of ice exposure, increasing the number of superimposed ice formation episodes, and subsequently decreasing runoff and increasing MB. The climate response scenarios do not incorporate changes in lapse rates and DDFs expected to occur under climate change conditions, as static values are assumed appropriate for short timescale simulations.

6.3. Research implications

This research has shown that there is a strong link between glacier melt production and subsequent drainage system evolution, and also between glacier melt production and glacier mass balance. Given these relationships. Arctic glaciers are highly sensitive to meteorological variability and climate change.

In the thesis introduction. I listed several areas of uncertainty in the general Arctic climate change scenario of increased sea level rise, increased sea ice formation, and changes in ocean circulation, should freshwater runoff from glaciated regions increase. These uncertainties include: (1) the relative contribution of small glaciers such as John Evans Glacier to sea level rise (Meier, 1984: 1990: Oerlemans and Fortuin. 1992): (2) the role of meltwater refreezing and surface meltwater storage in absorbing a portion of the increased meltwater production, thereby limiting meltwater input to the ocean system (Pfeffer et al.. 1991: Woodward et al.. 1997: Janssens and Huybrecht. 2000): (3) the relationship between increased air temperature and increased precipitation, and whether an increase in precipitation will offset warmer temperatures and mitigate glacier response to climate change (Oerlemans et al.. 1998: van der Veen. 2002): and. (4) the dynamic response of glaciers to climate change, and whether this will accelerate or decelerate the climate change response (Zwally et al.. 2002: Bingham. 2003).

Although this thesis does not address the relative contribution to sea level rise of glaciers like JEG. it does address several other uncertainties. Meltwater refreezing as superimposed ice will, to some extent, limit the increase in meltwater input to the ocean system. However, given the magnitude of the increase in melt, this buffer will be relatively small. In addition, meltwater storage in supraglacial features, rather than mitigate meltwater inputs to the ocean system, will likely increase them. This is because threshold storage values will likely be reached sooner under enhanced melt conditions.

resulting in earlier formation of connections between the glacier surface and bed. and thus a longer period during which glacier outflow enters the ocean. This thesis also indicates that the predicted increase in air temperature is unlikely to be offset by the predicted concurrent increase in winter precipitation. Higher air temperatures will likely increase the rate of snowpack removal. providing increased meltwater for the ocean system. In addition. higher temperatures will likely move the long-term equilibrium line up-glacier. thus there will be a smaller snow-covered area in which meltwater could refreeze at the end of the melt season.

As regards the dynamic response of glaciers to climate change. the hydrofracture process provides a mechanism whereby meltwater could reach the bed of large ice sheets and create a dynamic response to climate (Arnold and Sharp. 2002: Zwally et al.. 2002). However. to fully determine the dynamic glacier response to climate change requires a melt model coupled to both a glacier hydrological model and a glacier dynamics model.

This thesis has also shown that synoptic maps may be a useful way to improve mass balance modelling studies by increasing input data without requiring additional field data. Examination of synoptic maps may be a useful way of tying together meteorological conditions and their mass balance/hydrology response.

6.4. Areas for further research

The results of this thesis raise additional research questions that may be addressed in future studies:

(1) What is the physical structure of the en- and subglacial drainage system at JEG. and how does the structure change as a result of variations in surface meltwater input – specifically that caused by crevasse hydrofracture events? By drilling a series of boreholes at JEG from the glacier surface to the glacier bed (e.g.. Gordon et al.. 1998). we can determine how well predicted drainage patterns (Copland and Sharp. 2001: Bingham et al.. in review) compare with actual drainage patterns. Instrumenting these boreholes with pressure transducers would provide further information regarding the impact of hydrofracture events on the subglacial drainage system. by allowing monitoring of subglacial water pressure during the period of drainage development (e.g.. Hubbard et al.. 1995).

197

(2) Are the meteorological processes important for mass balance at JEG similar for other glaciers and ice caps in the region. or are they site-specific? Previous studies have indicated that glaciers in a given region often experience the same controls on mass balance (e.g.. Pacific Northwest: Yarnal. 1984: Bitz and Battisti. 1999: McCabe et al.. 2000: Rasmussen and Conway. 2004). While meteorological controls on mass balance have been studied at Meighen Ice Cap in the western Arctic (Alt. 1979: Alt. 1987). analysis of long-term meteorological records from the Devon Ice Cap (Koerner. 1970) and the Prince of Wales Ice Cap (Marshall et al.. in review) could assist in determining the presence of an eastern Arctic trend in processes important for mass balance.

(3) It is clear that. despite the critical role of the Arctic in moderating global climate change response. there are still gaps in our understanding of Arctic glacier-climate interactions. We could increase our knowledge in this area by improving modelling techniques in three main ways.

(a) Information on synoptic climatology can be a useful additional data source in mass balance modelling. In order to incorporate summer snowfalls. monthly-averaged synoptic maps could be examined to determine the presence or absence of a specific synoptic 'type' associated with a relatively high number of snowfalls (e.g.. 2002). This could follow the same methods used to determine the previous occurrence of extreme melt events such as the 2000 event (Boon et al.. 2003: Keimig. unpublished). Synoptic datasets could also be examined to determine their correspondence with local air temperature lapse rates. This has already been attempted on the Prince of Wales Ice Cap (Marshall et al.. in review). and while it shows some promise. should be studied more closely.

(b) Second. given that DDFs used in DDMs have already been successfully parameterized as a function of albedo (Arendt and Sharp. 1999: Brock et al.. 2000) and solar radiation (Hock. 1999). it is feasible to assume that the DDF could also be parameterized as a function of wind speed. Models could therefore be improved by incorporating the effects of wind for areas where wind events are significant (e.g.. Alps: Hock. 2003: Canadian Arctic: Courtin and Labine. 1973: Boon and Sharp. in review). While this would reduce some of the advantage of

198

DDMs by increasing the input data required to run them, it could also address the problems inherent in failing to incorporate enhanced melt due to wind. As wind speed variations may also affect air temperature lapse rates, it may be useful to model katabatic winds and their impact on air temperature.

(c) Finally, van der Veen (2002) has suggested that model performance can be tested and improved by using probability density functions (PDFs) of input parameter values to examine model parameterization sensitivity. This approach would not only require determination of PDFs for relevant model parameters at John Evans Glacier, but could also be applied to the DDM used in the thesis to provide a more quantitative measure of parameterization sensitivity.

(4) How accurate are climate sensitivity test results? Climate sensitivity of glacier mass balance can be tested through several methods, such as applying a given climate change scenario and determining the results (e.g., this thesis; Jóhannesson, 1997)), or applying a range of air temperature and precipitation changes (both positive and negative), often beginning with a 1K air temperature change or 5% precipitation change and moving up or down in 1K or 5% increments (e.g., Oerlemans et al., 2000). When the given climate change is applied to the input dataset, a constant daily air temperature or precipitation change is assumed, which is a highly unrealistic climate response. Our understanding of the climate sensitivity of JEG mass balance could be improved by using PDFs of air temperature and summer snowfalls as input data (van der Veen, 2002), and perturbing these functions by the predicted climate change. This would simulate a more realistic glacier response to climate change by maintaining the seasonal distribution of temperature and accumulation, rather than applying a constant change to each day. Additionally, we could determine PDFs associated with specific synoptic types, and experiment with changing the frequency or seasonality of different synoptic types, and examining their impact on model output.

(5) Finally, how can we gain a more integrated understanding of Arctic glacier response to climate change? This thesis has examined the mass balance response of JEG to climate change, as well as basic hydrological responses. However, glacier mass balance, hydrology and ice dynamics are strongly linked (Iken and Bindschadler,

199

1986: Fahnestock et al., 2001; Copland et al., 2003; Bingham et al., in review) thus, changing hydrology under climate change conditions will subsequently impact mass balance and dynamics. The impact of changes in meltwater input to supraglacial storage locations could be studied by routing meltwater output from the DDM into a hydrological model (e.g., Flowers and Clarke, 2002) coupled to a model of glacier dynamics.

Successful modelling of glacier hydrology, however, requires a reliable measured record of water outflow from the glacier. Photogrammetric techniques have proven useful in previous studies of glacier processes (e.g., surface albedo: Corripio, 2004), and may also be useful at JEG, as land-based measurements of proglacial stream flow have in the past been compromised by the nature of the proglacial stream system, which experiences substantial channel migration and aggradation, making it difficult to monitor discharge and/or water level. Time-lapse photographs from 2001 and 2002 monitored changes in glacier hydrology from the ice surface, and may be useful in calculating the volume of water exiting the glacier, thereby providing a dataset against which to verify hydrological model output.

In addition, glacier dynamics models remain poorly constrained, due in large part to our limited understanding of processes occurring at the glacier bed. Modellers have yet to develop a reliable glacier sliding law for use in these models; many researchers doubt that water pressure is the sole linking variable, as water storage and glacier bed properties are also important.

6.5. References

Alt, B. 1979. Investigation of summer synoptic climate controls on the mass balance of Meighen Ice Cap. Atmosphere-Ocean 17(3): 181-199.

Alt, B. 1987. Developing synoptic analogs for extreme mass balance conditions on Queen Elizabeth Island ice caps. Journal of Climatology and Applied Meteorology 26(12): 1605-1623.

Arendt. A.A. 1997. Approaches to modelling the mass balance of High Arctic glaciers. M.Sc. thesis. University of Alberta. 222 pp.

Arendt. A.. M.J. Sharp. 1999. Energy balance measurements on a Canadian high Arctic glacier and their implications for mass balance modelling. International Association of Hydrological Sciences **256:** 165-172.

Arnold. N.S.. M.J. Sharp. 2002. Flow variability in the Scandinavian ice sheet: modelling the coupling between ice sheet flow and hydrology. Quaternary Science Reviews **21(4-6):** 485-502.

Bitz. C.M.. D.S. Battisti. 1999. Interannual to decadal variability in climate and glacier mass balance in Washington. Western Canada. and Alaska. Journal of Climate **12:** 3181-3196.

Bøggild. C.E.. N. Reeh. H. Oerter. 1994. Modelling ablation and mass-balance sensitivity to climate change of Storstrømmen. Northeast Greenland. Global and Planetary Change **9:** 79-90.

Bingham. R.G. 2003. The hydrology and dynamics of a high Arctic glacier. Ph.D. thesis. University of Glasgow. 254 pp.

Bingham. R.G.. P.W. Nienow. M.J. Sharp. S. Boon. **In review.** Subglacial drainage processes at a High Arctic polythermal valley glacier. Journal of Glaciology.

Bingham. R.G.. P.W. Nienow. M.J. Sharp. L. Copland. **In review.** Propagation of high-velocity events in the ablation zone of a High Arctic polythermal glacier: relation to seasonal changes in subglacial drainage system structure. Journal of Geophysical Research - Earth Surface.

Boon. S.. M. Sharp. 2003. The role of hydrologically-driven ice fracture in drainage system evolution on an Arctic glacier. Geophysical Research Letters 30(18): 1916 DOI: 10.1029/2003GL018034.

Boon. S.. M.J. Sharp. P.W. Nienow. 2003. Impact of an extreme melt event on the runoff and hydrology of a High Arctic glacier. Hydrological Processes 17(6): 1051-1072.

Braithwaite. R.J. 1984. Calculation of degree-days for glacier-climate research. Zeitschrift fur Gletscherkunde und Glazialgeologie 20: 1-8.

Braithwaite. R.J. 1995. Positive degree-day factors for ablation on the Greenland ice sheet studied by energy-balance modelling. Journal of Glaciology 41: 153-160.

Braithwaite. R.J.. O.B. Olesen. 1990. Increased ablation at the margin of the Greenland ice sheet under a greenhouse-effect climate. Annals of Glaciology 14: 20-22.

Braithwaite. R.J.. Y. Zhang. 1999. Modelling changes in glacier mass balance that may occur as a result of climate changes. Geografiska Annaler 81A(4): 489-496.

Braithwaite. R.J.. Y. Zhang. 2000. Sensitivity of mass balance of five Swiss glaciers to temperature changes assessed by tuning a degree-day model. Journal of Glaciology 46: 7-14.

Brock. B.W.. I.C. Willis. M.J. Sharp. 2000. Measurement and parameterisation of albedo variations at Haut Glacier d'Arolla. Switzerland. Journal of Glaciology 46(155): 576-688.

Bugnion. V.. P.H. Stone. 2002. Snowpack model estimates of the mass balance of the Greenland ice sheet and its changes over the twenty-first century. Climate Dynamics 20: 87-106.

Copland. L.. M. Sharp. 2001. Mapping hydrological and thermal conditions beneath a polythermal glacier with radio-echo sounding. Journal of Glaciology 47(157): 232-242.

Corripio. J.G. 2004. Snow surface albedo estimation using terrestrial photography International Journal of Remote Sensing. **in press**.

Courtin. G.M.. C.L. Labine. 1977. Microclimatological studies on Truelove Lowland. In Truelove Lowland, Devon Island, Canada: A High Arctic Ecosystem. L.C. Bliss. ed. Edmonton: University of Alberta Press, p. 73-106.

Fahnestock. M.. W. Abdalati. I. Joughin. J. Brozena. P. Gogineni. 2001. High geothermal heat flow. basal melt. and the origin of rapid ice flow in central Greenland. Science **294**: 2338-2342.

Fleming. K.M.. J.A. Dowdeswell. J. Oerlemans. 1997. Modelling the mass balance of northwest Spitsbergen glaciers and responses to climate change. Annals of Glaciology **24:** 203-210.

Flowers. G.E.. G.K.C. Clarke. 2002. A multicomponent coupled model of glacier hydrology: 2. Application to Trapridge Glacier. Yukon. Canada. Journal of Geophysical Research – Solid Earth **107**(B11): 2288. DOI:10.1029/2001JB001124

Fountain. A.G. 1996. Effect of snow and firn hydrology on the physical and chemical characteristics of glacial runoff. Hydrological Processes **10**: 509-521.

Fujita. K.. K. Seko. Y. Ageta. P. Jianchen. Y. Tandong. 1996. Superimposed ice in glacier mass balance on the Tibetan Plateau. Journal of Glaciology **42**(142): 454-460.

Fujita. K.. Y. Ageta. 2000. Effect of summer accumulation on glacier mass balance on the Tibetan Plateau revealed by mass-balance model. Journal of Glaciology **46**(153): 244-252.

Gordon. S., M. Sharp, B. Hubbard. C.C. Smart. B. Ketterling. I. Willis. 1998. Seasonal reorganization of subglacial drainage inferred from measurements in boreholes. In Glacier Hydrology and Hydrochemistry. M. Sharp, K. Richards and M. Tranter, eds. Chichester: John Wiley and Sons, p. 239-267.

Greuell. W.. R. Böhm. 1998. 2 m temperatures along melting mid-latitude glaciers. and implications for the sensitivity of the mass balance to variations in temperature. Journal of Glaciology 44(146): 9-20.

Heppenstall. K.E. 2001. Chemical Weathering in a Glaciated Carbonate Catchment. Canadian High Arctic: Implications for Subglacial Hydrology. M.Sc. thesis. University of Alberta. 118 pp.

Hock. R. 1999. A distributed temperature-index ice- and snowmelt model including potential direct solar radiation. Journal of Glaciology 45(149): 101-111.

Hock. R. 2003. Temperature index melt modelling in mountain areas. Journal of Hydrology 282(1-4):104-115.

Houghton. J. T.. Y. Ding. D.J. Griggs. M. Noguer. P.J. van der Linden and D. Xiaosu.. eds. 2001. Climate Change 2001: The Scientific Basis. Contribution of Working Group I to the Third Assessment Report of the Intergovernmental Panel on Climate Change (IPCC). Cambridge: Cambridge University Press. 944 pp.

Hubbard. B.. M. Sharp. I. Willis. M.K. Nielsen. C.C. Smart. 1995. Borehole water-level variations and the structure of the subglacial hydrological system of Haut Glacier d'Arolla. Valais. Switzerland. Journal of Glaciology 41(139): 572-583.

Iken. A.. R.A. Bindschadler. 1986. Combined measurements of subglacial water pressure and surface velocity of Findelengletscher. Switzerland: conclusions about drainage system and sliding mechanism. Journal of Glaciology 32 (110): 101-119.

Jóhannesson. T. 1997. The response of two Icelandic glaciers to climatic warming computed with a degree-day glacier mass-balance model coupled to a dynamic glacier model. Journal of Glaciology 43(143): 321-327.

Kamb. B. 1987. Glacier surge mechanism based on linked cavity configuration of the basal water conduit system. Journal of Geophysical Research – Solid Earth 92 (B9): 9083-9100.

Kavanaugh. J.L.. G.K.C. Clarke. 2001. Abrupt glacier motion and reorganization of basal shear stress following the establishment of a connected drainage system. Journal of Glaciology 47(158): 472-480.

Koerner. R.M. 1970. The mass balance of the Devon Island Ice Cap. Northwest Territories. Canada. 1961-1966. Journal of Glaciology 9 (57): 325-336.

Marshall. S.J.. M.J. Sharp. D.O. Burgess. F.S. Anslow. In review. Surface temperature lapse rate variability on the Prince of Wales Icefield. Ellesmere Island. Canada: Implications for regional-scale downscaling of temperature. Journal of Climate.

McCabe. G.J.. A.G. Fountain. M. Dyurgerov. 2000. Variability in winter mass balance of Northern Hemisphere glaciers and relations with atmospheric circulation. Arctic. Antarctic. and Alpine Research 32(1): 64-72.

Nienow. P.W.. M.J. Sharp. I.C. Willis. 1998. Seasonal changes in the morphology of the subglacial drainage system. Haut Glacier d'Arolla. Switzerland. Earth Surface Processes and Landforms 23 (9): 825-843.

Oerlemans. J.. B. Anderson. A. Hubbard. P. Huybrechts. T. Jóhannesson. W.H. Knap. M. Schmeits. A.P. Stroeven. R.S.W. van der Wal. J. Wallinga. Z. Zuo. 1998. Modelling the response of glaciers to climate warming. Climate Dynamics 14(4): 267-274.

Oerlemans. J.. E.J. Klok. 2003. Effect of summer snowfall on glacier mass balance. Annals of Glaciology **38**. in press.

Ohmura, A. 2001. Physical basis for the temperature-based melt-index method. Journal of Applied Meteorology **40**(4): 753-761.

Pfeffer. W.T.. N.F. Humphrey. 1996. Determination of timing and location of water movement and ice-layer formation by temperature measurements in sub-freezing snow. Journal of Glaciology **42**: 292-304.

Rasmussen. L.. H. Conway. 2004. Climate and glacier variability in western North America. Journal of Climate **17**(9): 1804-1815

Reeh. N. 1991. Parameterization of melt rate and surface temperature on the Greenland Ice Sheet. Polarforschung **59**(3): 113-128.

Singh. P.. N. Kumar. M. Arora. 2000. Degree-day factors for snow and ice for Dokriani Glacier. Garhwal Himalayas. Journal of Hydrology **235**: 1-11.

Skidmore. M.L.. M.J. Sharp. 1999. Drainage system behaviour of a high Arctic polythermal glacier. Annals of Glaciology **28**: 209-215.

van der Veen. C.J. 2002. Polar ice sheets and global sea level: how well can we predict the future? Global and Planetary Change **32**: 165-194.

Wolfe. P.M.. M.C. English. 1995. Hydrometeorological relationships in a glacierized catchment in the Canadian High Arctic. Hydrological Processes **9**: 911-921.

Woodward. J.. M.J. Sharp. A. Arendt. 1997. The influence of superimposed-ice formation on the sensitivity of glacier mass balance to climate change. Annals of Glaciology **24**: 186-190.

Yamal, B. 1984. Relationships between synoptic-scale atmospheric circulation and glacier mass balance in South-Western Canada during the International Hydrological Decade, 1965-74. Journal of Glaciology 30(105): 188-198.

Zwally, H.J., W. Abdalati, T. Herring, K. Larson, J. Saba, K. Steffen. 2002. Surface melt-induced acceleration of Greenland ice-sheet flow. Science 297: 218-222.

APPENDIX A

DETAILS OF LINEAR RESERVOIR MODEL USED IN CHAPTER 2

In Chapter 2. a linear reservoir model was used to simulate the role of the snowpack in delaying the transfer of melt calculated with an energy balance model (EBM) to a supraglacial channel (Oerter et al.. 1981; Baker et al.. 1982). This model has the advantage of simplicity, and adequately approximates processes occurring within the glacier snowpack during spring melt (Colbeck. 1983; Röthlisberger and Lang. 1987; Fountain. 1996).

The model linearity specifies that. at any time t. the runoff from the snowpack (reservoir). Q_t (in m^3 h^{-1}). is proportional to the volume of water stored in the snowpack. V_t (in m^3):

$$Q_t = \frac{V_t}{k} \tag{1}$$

where k is the storage coefficient of the snowpack in hours. Given that meltwater is flowing into the snowpack at a rate of M_t (in m^3 h^{-1}). then the time rate of change of the volume of water stored in the snowpack must satisfy:

$$\frac{dV}{dt} = M_t - Q_t \tag{2}$$

Substituting Equation (1) into Equation (2) gives:

$$\frac{dV}{dt} = M_t - \frac{V_t}{k} \tag{3}$$

208

Since the change in water volume stored in the snowpack between $t - 1$ and t is equivalent to $V_t - V_{t-1}$, and the volume stored in the snowpack at t is $V_{t-1} + M_t$, we can substitute into Equation (3) to get:

$$V_t = M_t + V_{t-1} - \frac{(V_{t-1} + M_t)}{k}$$

(4)

Combining Equations (1) and (4) gives the final equation used for each model timestep:

$$Q_t = \frac{\left[M_t + V_{t-1} - \dfrac{(V_{t-1} + M_t)}{k} \right]}{k}$$

(5)

Hourly EBM melt output (M, in m WE; Fig. 2.2), was converted to $m^3\ h^{-1}$ and fed into the linear reservoir model to create a simulated runoff (Q) curve. The results of a windowed cross-correlation analysis (CCA), and field observations of changing snowpack thickness and saturation, were used to generate temporally variable values of k. Values of k were varied to obtain an optimum fit between standardized (by maxima) time series of modeled Q, which drives water level (WL) change in a closed basin, and measured WL change. This approach maximizes the proportion of the variance in WL change that can be attributed to surface melt processes. The difference between the two standardized time series (modeled Q and measured WL change) thus highlights events that may be attributable to other processes, such as drainage into newly formed fractures (Fig. 2.4). A regression of the two standardized time series indicates that model output (Q) successfully simulates measured WL change ($r^2 = 0.87$, $p = 0.95$). Values of k used to obtain this relationship compare well with values calculated in previous studies (Table A.1).

Examination of M, k, V and Q records indicates five distinct phases of reservoir development (Fig. A1). Prior to 19 June (Day 170), k is relatively high (20–46 h). The high values reflect superimposed ice formation and/or internal accumulation, and the

effects of meltwater entering an unsaturated snowpack. both of which delay runoff substantially (Fountain. 1996: Flowers and Clarke. 2002). Variations in k are out of phase with respect to M. likely reflecting the effects of diurnal filling and draining on snowpack saturation. This is corroborated by the V record, which shows an increasing volume of water stored in the snowpack, with diurnal cycles indicating some overnight meltwater drainage. Periods of meltwater drainage correspond with increases in Q.

From 19-21 June (Day 170-172), continued M results in a rapid drop in k, while V loses its diurnal oscillations and decreases dramatically, draining (see Q) in two distinct pulses (~ midnight on 19 and 20 June). This suggests sudden removal of the snowpack and exposure of the ice surface, perhaps in the form of a slush flow, thereby quickening the melt-runoff response. Saturated snow and slush flows were observed at various locations on the glacier surface during this time period, corroborating model results.

From 21-23 June (Day 172-174), M increases substantially, as does V and k. The increase in V suggests that the increased meltwater is again backed up somehow, prior to being released suddenly on 23 June, as evidenced by a peak in Q and a concurrent drop in k. This backup could be a result of a channel blockage upstream from the monitoring site, given that the sudden decrease in k on 19 – 20 June was attributed to snowpack removal.

23 June marks the onset of a period of bad weather. M is relatively low, while k and V are increased and Q is minimal. This indicates meltwater storage in the snowpack, which was likely increased due to fresh snow on the glacier surface. This storage gradually drains throughout the poor weather period, until 27 June.

From 27 June until the end of the record, the onset of improved weather results in a significant rise in k and V as M increases, filling the unsaturated fresh snowpack. This leads to a sudden drop in k and V on 28 June, indicating sudden drainage of the snowpack into the supraglacial system. This final outflow event precipitated the hydrofracture process and, ultimately, crevasse drainage.

References

Baker. D.. H. Escher-Vetter. H. Moser. H. Oerter. O. Reinwarth. 1982. A glacier discharge model based on results from field studies of energy balance, water storage and flow. International Association of Hydrological Sciences **138:** 103-112.

Colbeck, S.C. 1983. Theory of metamorphism of dry snow. Journal of Geophysical Research – Oceans and Atmospheres 88(NC9): 5475-5482.

Flowers, G.E., G.K.C. Clarke. 2002. A multicomponent coupled model of glacier hydrology: 1. Theory and synthetic examples. Journal of Geophysical Research – Solid Earth 107(B11): 2287. doi:10.1029/2001JB001122.

Fountain, A.G. 1996. Effect of snow and firn hydrology on the physical and chemical characteristics of glacial runoff. Hydrological Processes 10: 509-521.

Hannah, D.M., A. Gurnell. 2001. A conceptual. linear reservoir runoff model to investigate melt season changes in cirque glacier hydrology. Journal of Hydrology 246: 123-141.

Oerter, H., D. Baker, H. Moser, O. Reinwarth. 1981. Glacial-hydrological investigations at the Vernagtferner Glacier as a basis for a discharge model. Nordic Hydrology 12: 335-348.

Röthlisberger, H. and Lang, H. 1987. Glacial Hydrology. In Glacio-Fluvial Sediment Transfer. A. Gurnell and M. Clark, eds. Toronto: John Wiley and Sons, p. 207-284.

Table A.1. Values of k for various studies: compare with values for this study of maximum 46 h for snow and minimum 4 h for ice.

Study	k snow (h)	k ice (h)
Baker et al., 1982	30 (firn/snow)	-
Oerter et al., 1981	28 (non-ice)	5
Hannah and Gurnell, 2001	2-9	25

212
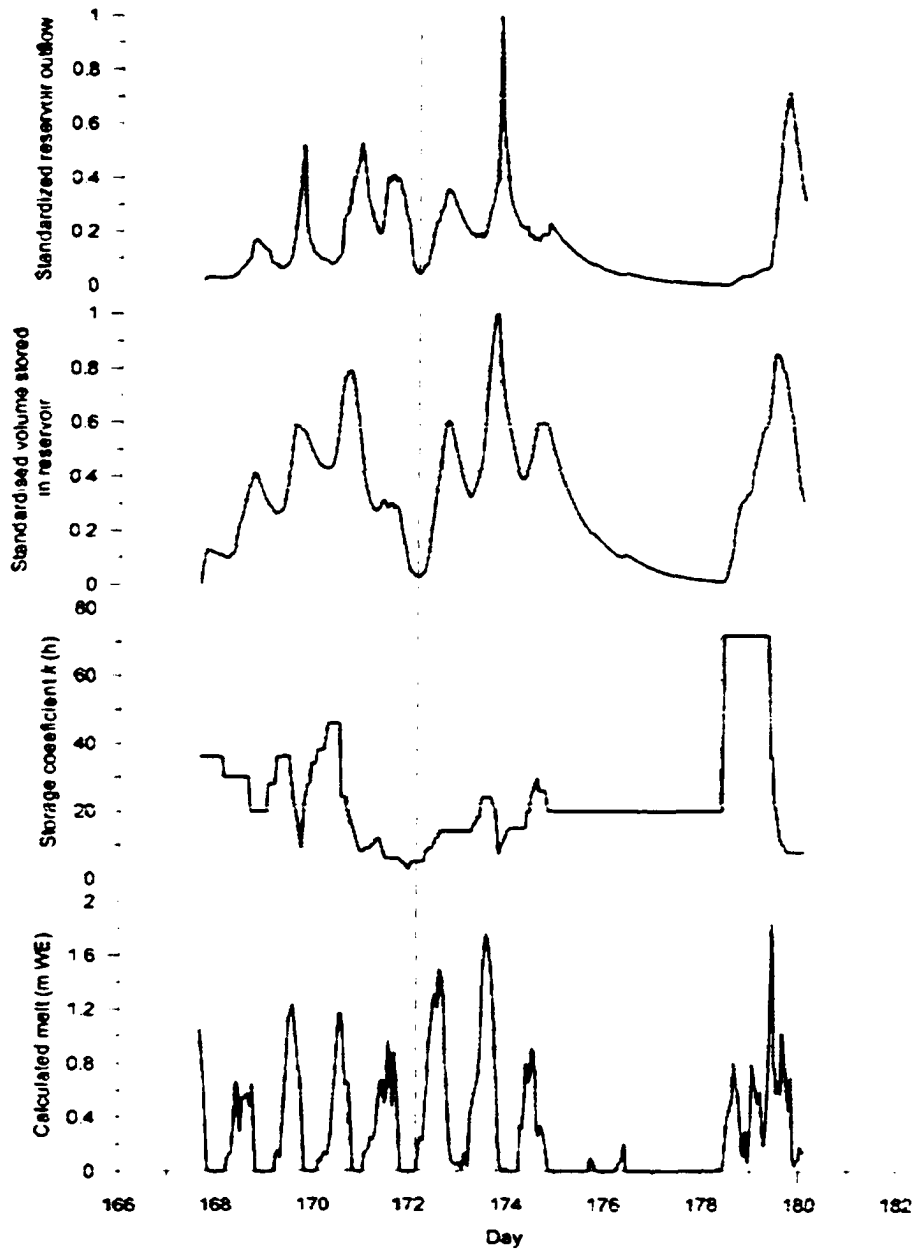
Fig. A.1. Variation of calculated melt (M). storage coefficient (k). standardized reservoir storage volume (V). and standardized reservoir outflow (Q) with time (2002). Dashed lines separate the five periods of meltwater production and storage within the snowpack.

213